ANL-6287

ANL-6287

Argonne National Laboratory

CHEMICAL ENGINEERING DIVISION SUMMARY REPORT

October, November, December, 1960

DISCLAIMER

Price $3.00 . Available from the Office of Technical Services, Department of Commerce, Washington 25, D.C.

ANL-6287
Chemical Separations Processes
for Plutonium and Uranium
(TID-4500, 16th Ed.)
AEC Research and
Development Report

ARGONNE NATIONAL LABORATORY
9700 South Cass Avenue
Argonne, Illinois

CHEMICAL ENGINEERING DIVISION SUMMARY REPORT

October, November, December, 1960

Stephen Lawroski, Division Director
R. C. Vogel, Associate Division Director
V. H. Munnecke, Assistant Division Director

March, 1961

Preceding Quarterly Reports:

ANL-6231	July, August, September, 1960
ANL-6183	April, May, June, 1960
ANL-6145	January, February, March, 1960

Operated by The University of Chicago
under
Contract W-31-109-eng-38

TABLE OF CONTENTS

		Page
SUMMARY		11
I.	CHEMICAL-METALLURGICAL PROCESSING	25
	A. Pyrometallurgical Development	32
	1. Melt Refining	32
	2. Liquid Metal Solvents Process Development	48
	B. Fuel Processing Facilities for EBR-II	78
	1. Design, Development, and Construction of Buildings and Equipment	78
	2. EBR-II Fuel Processing Mockup	89
	C. Pyrometallurgical Research	95
	1. Chemistry of Liquid Metal Solvents	95
	2. Calorimetry	120
II.	FUEL CYCLE APPLICATIONS OF VOLATILITY AND FLUIDIZATION TECHNIQUES	130
	A. Laboratory Investigations of Fluoride Volatility Processes	133
	1. Fluorine Chemistry and Fluoride Separation Studies	133
	2. The Reaction of Mixtures of Uranium Hexafluoride and Plutonium Hexafluoride with Bromine	143
	B. Engineering-scale Development	147
	1. Direct Fluorination of Uranium Dioxide Fuels	147
	2. Halogenation of Reactor Fuels	157
	C. Conversion of Uranium Hexafluoride to Uranium Dioxide	166
	1. Steam Hydrolysis of Uranium Hexafluoride	166
	2. Reduction of Uranyl Fluoride	167
III.	REACTOR SAFETY	168
	A. Metal Oxidation and Ignition Kinetics	170
	1. Ignition Studies of Uranium Powder by the Burning Curve Method	170
	2. Burning Propagation Studies	177
	B. Metal-Water Reactions	180
	1. Laboratory Studies: Condenser Method	180
	2. Laboratory Studies: Pressure-pulse Method	189
	3. Engineering Studies: In-pile Testing in the TREAT Reactor	193

TABLE OF CONTENTS

		Page
IV.	REACTOR CHEMISTRY	200
	A. Determination of Nuclear Constants	201
	1. Fast Neutron Cross Sections	201
	2. Capture and Fission in EBR-I, Mark III	201
	B. Reactor Decontamination	202
	1. Laboratory Investigations	202
	2. Loop Studies	206
V.	ROUTINE OPERATIONS	207
	A. Waste Processing	207
	B. High-level Gamma-irradiation Facility	207

LIST OF TABLES

No.	Title	Page
1.	Experimental Conditions for High-activity Level Melt Refining Experiment	33
2.	Fission Product Removal Effected in the Melt Refining of Highly Irradiated EBR-II Fuel	34
3.	Uranium and Molybdenum Material Balances for High-activity Level Melt Refining Experiment and for Reference Experiment with Unirradiated Fuel	35
4.	Fates of Selected Fission Products in the High-activity Level Melt Refining Experiment	36
5.	Rate Constants Determined at Various Temperatures for the Reaction of Nitrogen with Sodium-coated and Uncoated Uranium and Uranium-Five Percent Fissium Pins	43
6.	Calculated Values for the Uranium Dinitride Film Thickness	45
7.	Effect of Nitrogen Exposure and Various Pouring Techniques on Melt Refining Ingot Yield	47
8.	Skull Oxide Fractions Used in Magnesium Reduction Studies	51
9.	Survey of Fluxes for U_3O_8 Reduction	53
10.	Reduction of Plutonium Dioxide by Zinc-Magnesium in the Presence of Flux	57
11.	Results of Retorting Experiments	63
12.	Filtration of Magnesium Oxide from Zinc-10 Percent Magnesium Solution	64
13.	The Separation of Magnesium Oxide from Liquid Metal Phases	65
14.	Direct Reaction of Uranium Blanket Rods with Zinc to Form Uranium-Zinc Intermetallic	70
15.	Plutonium Stability in a Zinc-Magnesium Solution Contained in a Graphite Crucible at 750 C	72
16.	Plutonium Stability in a Magnesium Solution Contained in a Tantalum Crucible at 800 C	73
17.	Corrosion Tests of Various Materials in Zinc and Zinc-Magnesium Alloys	76

LIST OF TABLES

No.	Title	Page
18.	Container Materials to be Used in Solution Stability Tests . . .	77
19.	Comparison of Light Output at Various Integrated Gamma Exposures for Six Lamps . . .	81
20.	Comparison of Unirradiated Lamps . . .	82
21.	Roller Bearing Tests with Irradiated Greases . . .	86
22.	Solubility of Europium in Cadmium . . .	96
23.	Solubility of Gadolinium in Cadmium . . .	97
24.	Solubility of Dysprosium in Cadmium . . .	98
25.	Solubility of Erbium in Cadmium . . .	99
26.	Analyses of Zinc-Uranium Intermetallic Phases . . .	103
27.	Coprecipitation by $CeCd_{11}$ from Liquid Cadmium . . .	108
28.	Compilation of Distribution Data for the Bismuth-Zinc System . . .	109
29.	Comparison of Distribution Data for the Lead-Zinc and Bismuth-Zinc System . . .	111
30.	Experimental Data and Standard Free Energies for the System Uranium-Zinc . . .	117
31.	Molar Susceptibility of $CeCd_{11}$ . . .	118
32.	Standard Heat of Combustion of Tungsten and Sulfur in Oxygen . . .	122
33.	Heat of Combustion of Boron in Fluorine . . .	125
34.	Operating Times, Flow Rates and Plutonium Material Balance for the Fluorination of Plutonium Oxide . . .	135
35.	Recovery of Plutonium Hexafluoride from a Fluorine Stream after Passage through a Furnace Tube and a Thermal Gradient . . .	139
36.	Recoveries Obtained when Transferring Plutonium Hexafluoride in a Fluorine or Helium Stream, or by Vacuum Distillation . . .	141
37.	The Reaction of Plutonium Hexafluoride and Bromine . . .	143
38.	The Reaction of Bromine with Mixtures of Uranium Hexafluoride and Plutonium Hexafluoride . . .	144

LIST OF TABLES

No.	Title	Page
39.	Observed Gamma Spectrum of Plutonium Tetrafluoride.	145
40.	Fast Neutron Flux Measurements with Samples of Plutonium Tetrafluoride	146
41.	Summary of Uranium Dioxide Pellet Fluorination Runs	148
42.	Properties of Pellets Used in Fluorination Runs	149
43.	Radial Heat Transfer in a Packed Fluid Bed	158
44.	Fluid-Bed Reaction of 304 Stainless Steel and Chlorine	160
45.	Reaction of 304 Stainless Steel with Bromine and Carbon Tetrachloride	161
46.	Summary of Chlorination-Hydrofluorination Runs--Two-zone Process	164
47.	Effect of Heating Rate on Critical Height Values of -80 +100 Mesh Spherical Uranium Powder in Oxygen.	171
48.	Effect of Pre-oxidation on Ignition Temperature Behavior of -140 +170 Mesh Spherical Uranium Powder.	172
49.	Comparison of Experimental and Theoretical Ignition Temperatures for Uranium Powder	175
50.	Burning Propagation Studies at Elevated Ambient Temperatures	178
51.	Influence of Halogenated Hydrocarbons on the Temperature of an Electrically Heated Platinum Foil	179
52.	Zirconium-Water Reaction Data from High-pressure Condenser Discharge Apparatus	181
53.	Definition of Symbols Used in Equations (5) through (9).	184 & 185
54.	Results of the Reaction of Aluminum at 1000 C with Steam at 500 mm by the Pressure-pulse Method	192
55.	Results from Ninth Series of TREAT, Metal-Water Experiments	196
56.	Particle Size Data from Uranium Wire-Water Transients . . .	199
57.	Decontamination of Stainless Steel Type 304	203
58.	Decontamination of Stainless Steel Type 304 by the Alkaline Permanganate-Citrate Procedure	204

LIST OF TABLES

No.	Title	Page
59.	Decontamination of Stainless Steel Type 304 with Citric Acid.	205
60.	Summary of Liquid Radioactive Wastes Processed During the Year 1960	207
61.	Argonne High-Level Gamma Irradiation Facility	208

LIST OF FIGURES

No.	Title	Page
1.	Diametrical Expansion and Fission Gas Release during Heating of EBR-II-Type Alloy Pin -- Experiment FG-2.	40
2.	Diametrical Expansion and Fission Gas Release during Heating of EBR-II-Type Alloy -- Experiment FG-1	40
3.	Nitridation Rates of Uranium Pins.	42
4.	Nitridation Rates of Uranium-Five Percent Fissium Alloy Pins	43
5.	Temperature Dependence of Parabolic Rate Constants for Nitridation of Uranium Pins	44
6.	Temperature Dependence of Parabolic Rate Constants for Nitridation of Uranium-Five Percent Fissium Pins	44
7.	Photographs of Uranium-Five Percent Fissium Pins before and after Nitridation at 504 C	46
8.	Liquid Metal Process for Reclamation of Melt Refining Skull Material	49
9.	Reduction of Fissium Skull Oxide at 800 C with Magnesium-Zinc Solutions in Absence of Chloride Flux	55
10.	Reduction of Fissium Skull Oxide at 800 C with Magnesium-Zinc Solutions in Presence of Chloride Flux	56
11.	Leaching of Ruthenium from Fissium Skull Oxide with Zinc in the Presence of Dow 230 Flux	59
12.	Graphite (CS) Filter and Receiver Crucible Assembly.	60
13.	Uranium Isolated from Magnesium-rich Systems by Retorting	68
14.	Liquid Metal Process for Uranium Blanket Metal.	69
15.	Corrosion Capsule	74
16.	Rocking Furnace for Corrosion Tests	75
17.	Wall Periscope with Conventional Internal Shielding	85
18.	Wall Periscope with Internal Shielding and Double Offset Optical Path	85
19.	Variation of Density with Height of Norton Crucibles	90
20.	Fume Trap with Furnace in Tilted Position.	91

LIST OF FIGURES

No.	Title	Page
21.	Variation of Fume Trap Efficiency with Grams of Sodium Charged	92
22.	Various Component Parts for the M-6 Furnace	92
23.	M-6 Furnace Component Parts	93
24.	Assembled M-6 Furnace	93
25.	Inverted View of the Assembled M-6 Furnace	94
26.	Furnace Thermocouple	94
27.	Solubility of Europium, Gadolinium, Dysprosium, and Erbium in Liquid Cadmium	96
28.	Solubility of Manganese in Liquid Cadmium	100
29.	Solubility of Nickel in Liquid Cadmium	101
30.	(Due to circumstances beyond our control Figure 30 had to be deleted.)	
31.	Coprecipitation by $CeCd_{11}$ from Liquid Cadmium Solutions	108
32.	Effect of Temperature on the Distribution of Uranium between Bismuth and Zinc	110
33.	Mutual Solubilities of Aluminum and Cadmium	112
34.	Variation of Vapor Pressure of Zinc with Composition of the Alloy in the Uranium-Zinc System	115
35.	Vapor Pressure of Zinc over δ and ϵ Phases in Uranium-Zinc System	116
36.	Variation of $_{M}\chi_{Ce}^{-1}$ with Temperature	119
37.	Calorimeter Fluorine Tank with Toggle Valve Connection to Combustion Bomb	126
38.	Schematic Flow Diagram of Plutonium Fluorination System	134
39.	Cumulative Pressure Drop in the Fluorination System during the Fluorination of Plutonium Oxide	136
40.	Transfer of Plutonium Hexafluoride in a Fluorine Stream through a Thermal Gradient Flow System	137
41.	Gamma Spectrum of Plutonium Tetrafluoride	145

LIST OF FIGURES

No.	Title	Page
42.	Neutron Measurements with Plutonium Tetrafluoride	147
43.	Uranium Hexafluoride Collection Rate and Fluorine Utilization Efficiency during Fluorination of Uranium Dioxide Pellets	150
44.	Effect of Inlet Fluorine Concentration on Rate of Fluorination of Uranium Dioxide Pellets	151
45.	Effect of Pellet Bed Height on Fluorine Efficiency during Incomplete Fluorination of Uranium Dioxide Pellets	152
46.	Effect of Temperature on Concentration of Fines in Fluid Bed in Fluorination of Uranium Dioxide Pellets	153
47.	Comparison of Bed Pressure Drop for Hindered and Unhindered Fluidization	154
48.	Film Coefficient of a Small Heater in a Fluidized Bed as a Function of Gas Velocity	154
49.	Longitudinal Temperature Gradient in a Heated Fluidized Bed	155
50.	Heat Transfer Test: Thermocouple Locations in the Packed Fluid Bed	156
51.	Corrosion of Nickel and Inconel by Chlorine	162
52.	Chlorination of Uranium Dioxide Pellets	163
53.	Effect of Heating Rate on Ignition Temperature of -80 +100 Mesh Spherical Uranium Powder	170
54.	Experimental and Theoretical Ignition Temperatures of Spherical Uranium Powder as a Function of Specific Area	175
55.	Theoretical Curves Based on Equations of Murray, Buddery, and Taylor Showing Effect of Heating Rate on Ignition Temperature of Spherical Uranium Powder	176
56.	Results of Condenser Discharge Runs with 60-mil Zirconium Wires	182
57.	Diagram of Hot Metal Sphere Reacting with Liquid Water	183
58.	Computed Zirconium-Water Reaction	188
59.	Computed Zirconium Runs	189

LIST OF FIGURES

No.	Title	Page
60.	Diagram of Present Pressure-pulse System	190
61.	Reaction Between Aluminum at 1000 C and Steam, 500 mm Pressure	192
62.	Autoclave for In-pile Tests of Metal-Water Reactions	194
63.	Metal-Water Reactions TREAT Test Assembly	195
64.	Oscillograph Record from Transient CEN-46	196
65.	In-pile Uranium-Water Reactions	197
66.	Particle Size-Frequency Distribution Plot for Run CEN-44	197
67.	Particle Size-Frequency Distribution Plot for Run CEN-42	198
68.	Particle Size-Frequency Distribution Plot for Run CEN-45	198
69.	Particle Size-Frequency Distribution Plot for Run CEN-41	198
70.	Dependence of Extent of Uranium-Water Reaction on Surface Area	199
71.	View of Uranium Wire Fuel Cluster before and after Metal-Water Transient CEN-46	199
72.	Neutron Capture Cross Section of Uranium-236 as a Function of Neutron Energy	201

CHEMICAL ENGINEERING DIVISION
SUMMARY REPORT

October, November, December, 1960

SUMMARY

I. Chemical-Metallurgical Processing (pages 25 to 129)

The research and development work that is being done on pyrometallurgical processes is prompted by the considerable likelihood that the application of these processes to the recovery of nuclear reactor fuel may lead to a reduction in the cost of nuclear power. Of these pyrometallurgical processes, melt refining will be the first to be used on a plant scale. The process will be incorporated into the fuel-recovery cycle of the second Experimental Breeder Reactor (EBR-II). The reactor and the fuel-cycle facility are now under construction at the Reactor Testing Station in Idaho.

Final results on the first high-activity level demonstration of the melt refining process for EBR-II core fuel have been obtained. A 388-gram charge of uranium-five percent fissium fuel pins irradiated to a total atom burnup of about 0.6 percent was melt refined for three hours at 1400 C. Fission product removal was much as expected on the basis of earlier work with unirradiated material, tracers, and irradiated uranium. Rare earths, yttrium, cesium, barium, strontium, and iodine removals exceeded 99 percent. Approximately 95 percent of the tellurium and 9 percent of the zirconium were removed.

A second experiment on the release of fission product krypton and xenon from irradiated fissium fuel pins was completed. The amount of gas evolution appears to depend primarily on temperature rather than on the heating rate. The removal of krypton and xenon was complete at 1025 C within the limits of analytical accuracy.

Uranium and uranium-fissium alloy pins react with nitrogen in an argon atmosphere, forming uranium nitrides. The reaction follows a parabolic rate law, with approximately the same rate constants for uranium and the fissium alloy. In both cases, however, the rate is approximately doubled by the presence of metallic sodium coatings on the pins. Activation energies for the reaction, about 15 kcal/mole, are not affected significantly by the presence of fissium constituents in the uranium at five weight percent concentration, nor by sodium coatings on the uranium or the fissium alloy.

Various techniques are being investigated for increasing melt refining pouring yields under adverse circumstances. Certain mechanical devices, for example, are being evaluated as possible methods of puncturing oxide or nitride crusts on the surface of molten uranium.

Work was continued on the development of a process for recovery and suitable purification of fissionable material contained in crucible skull material remaining after melt refining operations. The processes under consideration utilize liquid metal solvents as media in which recovery and purification operations are conducted. To enable removal of skull material from a crucible, the material is first oxidized under controlled conditions to a free-flowing powder, which is readily poured from a crucible. The oxide is then reduced by magnesium dissolved in zinc. The reduced uranium appears in zinc solution. Two precipitations of uranium, first as a uranium-zinc intermetallic compound from the zinc solution, and then as uranium metal from a magnesium-rich solution, together with removal of the supernatant liquid metal phases provide purification of the uranium. It is then retorted to vaporize associated solvent metals and to effect consolidation of the uranium product.

This process was improved considerably during the past quarter through the use of one of several possible molten halide fluxes in conjunction with a magnesium-zinc reducing solution. In the presence of a suitable flux and by adequate mixing, quantitative reductions of both pure uranium oxides and skull oxides were consistently obtained within two hours, many within thirty minutes. Complete reduction of plutonium dioxide was similarly achieved. Another outstanding advantage of a flux is that it acts as a vehicle in which the magnesium oxide reaction product is suspended, thereby enabling a clean separation of this material from the metal phase. Physical removal of the magnesium oxide from a metal phase by filtration or through liquation of the magnesium oxide has been troublesome and unsatisfactory. A third advantage of the halide salt fluxes is that the reductions can, if desired, be conducted in an air atmosphere. Since unreduced uranium oxides are also suspended in the flux phase, a fourth potential benefit of a chloride flux arises from the possibility of reducing and leaching noble metals from the skull oxide with zinc prior to the reduction of uranium and the more stable fission product oxides with magnesium. The removal of ruthenium from skull oxides by this procedure was demonstrated during the past quarter.

A fairly extensive study of salt fluxes was undertaken in the past quarter to define those systems which produced the most rapid and quantitative reductions of U_3O_8 by a dilute magnesium-zinc alloy. The salt fluxes found beneficial were mixtures of alkali and alkaline earth element chlorides, the most rapid reductions occurring with the lighter cations. Magnesium chloride was a major ingredient in all fluxes that gave complete reduction within 30 minutes and is, therefore, presently regarded as an essential ingredient. Magnesium fluoride (5 mole percent) was also present in all fluxes because of its effectiveness in providing clean and rapid coalescence and separation of the salt and metal phases.

Studies of reduction in the absence of flux were conducted in both pure magnesium and dilute magnesium-zinc alloys. With a 10 percent magnesium concentration in zinc, reductions were fairly rapid and nearly quantitative, but became much slower at a five percent magnesium concentration. Reductions in pure magnesium were still slower and irreproducible. In this system, chloride fluxes are also beneficial. It is noteworthy that in pure magnesium-flux systems cerium (and, therefore, possibly other rare earths) remains in the flux phase. In dilute magnesium-zinc-flux system, rare earth oxides are quantitatively reduced and appear in the metal phase along with the uranium.

Preparations are now underway for medium-scale (200 grams of uranium) demonstrations of the skull reclamation process, shown in Figure 8, page 49, which utilizes salt fluxes. However, the step for removal of noble metals will not be incorporated until further laboratory studies have been made. A small-scale (15 grams of uranium) demonstration run showed good removals of cerium, molybdenum, and zirconium, the only elements followed, thus indicating that the process will provide adequate decontamination.

In retorting studies of uranium precipitated from magnesium-rich systems, a considerable portion of the product has been in the form of large agglomerated masses of uranium. Since these have been very easily handled, their formation appears desirable. The uranium agglomeration occurs during decomposition of uranium-zinc intermetallic compounds with magnesium. The factors responsible for their formation are not yet known, although stirring is believed to play a major role.

A possible simplification of the process for isolation of plutonium bred in the uranium blanket of the EBR-II reactor involves the direct low-temperature (450 C) reaction of uranium with zinc in slight excess of that required for stoichiometry to give an intermetallic ($UZn_{11.5}$) which would then be treated with magnesium to decompose the intermetallic and dissolve the plutonium. The low-temperature reaction was demonstrated in the past quarter with full-size blanket pins, 0.433 inch in diameter. Times of around 100 hours were required for completion of the reaction. It is hoped that these times can be appreciably shortened by further work.

In a 100-hour holding run, a plutonium-zinc solution at 800 C was stable in a graphite crucible. An initial loss of plutonium occurred from magnesium solutions held in tantalum crucibles at 800 C, after which the plutonium concentration stabilized. This loss is probably caused by a reaction with either solution or tantalum impurities and will be further investigated.

A program is underway for evaluating materials for containing liquid metal systems of interest. The very slight attack of tantalum by zinc at 850 C is reduced by the addition of magnesium. In preliminary

tests a tantalum-7.5 percent tungsten alloy has shown better resistance to attack by zinc than tantalum. Molybdenum is seriously attacked by zinc at 850 C, whereas graphite shows promise as an outstanding container material.

A direct-cycle fuel-reprocessing plant using pyrometallurgical procedures is being designed and constructed as part of the Experimental Breeder Reactor No. II (EBR-II) project. A Laboratory and Service Building is also included. Melt refining, liquid metal extraction, and processes involving fractional crystallization from liquid metal systems are being examined for the recovery and purification of EBR-II fuels. Based on these studies, process equipment is being designed and tested.

Installation of equipment in the Laboratory and Service Building has been completed, and shakedown testing has begun.

Construction of the Fuel Cycle Facility Building is continuing. The structure, which was 40 percent completed by September 6, 1960, was about 70 percent completed by December 6, 1960. Enclosure of the building has been completed and work is continuing inside during the winter.

The standard General Mills Model 300 manipulator arm has been successfully attached by remote means to the radiation stable electromechanical operating manipulator. This increases the versatility of the cell manipulator system. An order for 12 Model 8 manipulators for the Air Cell has been placed.

The switchboard and control cabinets for manipulators, cranes, and blister hoist have been tested and shipped to Idaho.

The final shipment of components for the Fuel Cycle Facility process cell windows has been received in Idaho.

The major lamp manufacturers have modified the design of the mercury lamps specified for use in the process cells. Tests show that the new lamps are very inferior for the proposed use as compared with the lamps previously manufactured. An adequate supply of lamps of the type formerly manufactured has been ordered.

Redesign of the small air lock and component parts is nearly completed. Kollmorgen Corporation was chosen to modify an existing wall periscope to make it suitable for use in the Air Cell by the addition of internal shielding. The installation drawings for the high-frequency power distribution system have been completed. Work continues on the drawings or installation packets of the melt refining off-gas system, the space radiation-monitoring system, the service plugs, and other equipment items for the Fuel Cycle Facility.

Three types of radiation-resistant greases have been irradiated and then tested in a roller bearing of a type used in the manipulator bridge. The tests indicate that the greases are adequate for the proposed use, but further tests are being conducted to determine the effects of radiation at levels below those used in the initial experiments.

An economical radiation-resistant end seal for MI cable is desirable for nonpermanent installations in the process cells. Several types have been tested and one type appears satisfactory. Flexible leads are also needed in the cells. Leads with four types of asbestos insulation have been irradiated and tested. Two of the types appear satisfactory.

The serious cracking problem previously noted with melt refining crucibles has been eliminated. This was accomplished by the modification made by the supplier in the manufacturing method and by the application of a set of acceptance standards devised and applied by this Division.

Tests have shown that the Fiberfrax fume trap will be adequate to handle the quantities of fumes evolved in the melt refining furnace. These experiments also show that a tight seal is not necessary between the crucible and the fume trap.

Twenty-four batches of enriched pin scrap were melted down into ingots for recasting of fuel pins for EBR-II.

Fundamental studies are being made in support of the process development activities. Data basic to the various liquid metal processes are the solubilities of those elements whose separations are being attempted. The solubilities of the rare earth elements europium, gadolinium, dysprosium, and erbium in liquid cadmium may be represented by the following empirical equations:

europium (330 to 500 C): $\log (\text{atom percent}) = 6.063 - 4210\ T^{-1}$

gadolinium (325 to 500 C): $\log (\text{atom percent}) = 3.217 - 3279\ T^{-1}$

dysprosium (325 to 630 C): $\log (\text{atom percent}) = 3.335 - 2447\ T^{-1}$

erbium (325 to 630 C): $\log (\text{atom percent}) = 6.309 - 6444\ T^{-1} + 1.485 \times 10^{6}\ T^{-2}$

The solubilities of manganese and nickel in liquid cadmium, which are important constituents of high-strength alloy steels, may be represented by the following empirical equations:

manganese (325 to 650 C): $\log (\text{atom percent}) = 3.263 - 3054\ T^{-1} + 0.4476 \times 10^{6}\ T^{-2}$

nickel (509 to 650 C): $\log (\text{atom percent}) = 1.954 - 740.8\ T^{-1}$

nickel (330 to 509 C): $\log (\text{atom percent}) = 6.722 - 5628\ T^{-1} + 0.9045 \times 10^{6}\ T^{-2}$.

Additional studies with the zinc-uranium system indicate the existence of two intermetallic compounds: a delta phase (phase richest in uranium) and an epsilon phase (phase richest in zinc). The epsilon phase was found, by thermal analysis, to decompose peritectically into the melt and delta phase at 844 C. Two contiguous intermetallic layers were found in diffusion tests made below 800 C, the outer layer being the epsilon phase and the inner layer the delta phase. A single layer of delta phase was found when diffusion tests were made at 875 C.

Measurements of the vapor pressure of the zinc-uranium system by the effusion method have confirmed the existence of two uranium-zinc intermetallic phases. The delta phase was found to have a constant vapor pressure, indicating a constant composition, the zinc-uranium ratio of this phase being approximately 8.4 to 1. The epsilon phase was found to have a vapor pressure which decreased with loss of zinc, indicating a range of composition. The limits of the composition of the epsilon phase are from $UZn_{11.2}$ to $UZn_{9.4}$.

Several additional observations have been made relative to the uranium-cadmium system. The temperature of the alpha-beta uranium transformation is unaffected by saturation with cadmium, indicating no appreciable solubility of cadmium in solid uranium. Similarly, no appreciable solubility of uranium in solid cadmium was found. The eutectic temperature at which equilibrium between cadmium, UCd_{11}, and melt exists was found to be 0.26 C below the freezing point of cadmium.

A systematic study is underway to ascertain the influence of atomic size, metallic valence, and electronic configuration on the coprecipitation of various metallic elements with the cerium-cadmium intermetallic phase $CeCd_{11}$. The following values for the coprecipitation coefficient, λ, defined

by the equation $\log\left(\frac{\text{tracer in solution}}{\text{total tracer}}\right) = \lambda \log\left(\frac{\text{carrier in solution}}{\text{total carrier}}\right)$, have been determined: sodium, $\lambda = 0$; lithium, $\lambda = 0$; potassium, $\lambda = 0$; yttrium, $\lambda = 0$; lanthanum, $\lambda = 1.49$; uranium, $\lambda = 0.13$; strontium, $\lambda = 0.10$; europium, $\lambda = 0.099$; and zirconium, $\lambda = 0.04$.

The distribution coefficient of representative fissile and fission product elements between the two immiscible liquids, zinc and bismuth, at 548 C have been determined. Values of the coefficient (weight percent in zinc phase/weight percent in bismuth phase) are palladium, 33.3; uranium, 0.17; cerium, 0.05; and strontium, 7.7×10^{-4}. The coefficient for uranium was found to vary from 0.078 at 447 C to 0.17 at 548 C.

The mutual solubilities of liquid aluminum and cadmium may be represented by the empirical equations

$$\log (\text{atom percent cadmium in aluminum}) = 3.479 - 2944\ T^{-1}$$

$$\log (\text{atom percent aluminum in cadmium}) = 3.702 - 2815\ T^{-1}$$

in the temperature range from 680 to 720 C.

The molar magnetic susceptibility of cerium in the intermetallic phase $CeCd_{11}$ may be represented by a Curie-Weiss equation [$\chi = C/(T-\Delta)$], with $\Delta = -2$ K and $C = 0.81$. The effective Bohr magneton number for this system is 2.55. This value is in good agreement with the value of 2.56 calculated for a free gaseous cerium ion in a $^2F_{5/2}$ ground state.

Experimental work on the study of the heat of formation of tungsten disulfide has been completed with the determination of the energy change of the reaction

$$W(c) + 2S(c) + 9/2\ O_2(g) + 4\ NaOH(aq) \longrightarrow WO_3(c) + 2\ Na_2SO_4(aq) + 2H_2O \quad .$$

The preliminary value for $\Delta E_c^0/M$ of the reaction is -2226.70 ± 0.88 cal per gram of tungsten-sulfur mixture (mole ratio of one to two).

Conditions for the combustion of uranium mononitride and zirconium hydride in oxygen in a bomb calorimeter have been determined. Calorimetric combustions of uranium mononitride are being carried out.

In the fluorine bomb calorimetry phase of the program, calorimetric studies are complete for the determination of the heats of formation of zirconium tetrafluoride, molybdenum hexafluoride, and boron trifluoride. Preliminary values for zirconium tetrafluoride and molybdenum hexafluoride were reported previously (ANL-6231, page 82). The preliminary value for the standard heat of formation of boron trifluoride gas is -269.97 ± 0.32 kcal/mole. Work is in progress on the determination of the heat of formation of

uranium hexafluoride and boron nitride. Because boron nitride reacts spontaneously with fluorine, a special reaction vessel was constructed for the study, which will be useful also for studies of other elements that react spontaneously with fluorine.

Work is continuing on the assembly of a 1500 C high-temperature enthalpy calorimeter and the design of a 2500 C furnace for studies at even higher temperatures.

II. Fuel Cycle Applications of Volatility and Fluidization Techniques (pages 130 to 167)

A direct fluorination volatility process has been proposed for the recovery of uranium and plutonium from irradiated nuclear reactor fuels. In this process advantage is taken of the volatilities of uranium and plutonium hexafluoride and of fluidization techniques. Attempts are being made to apply this process to uranium oxide and zirconium matrix fuels.

The proposed process for recovery of uranium and plutonium from spent uranium oxide, involves decladding by an appropriate reaction in a fluidized bed. Plutonium and uranium hexafluorides, which result from the reaction of the declad oxide fuel with fluorine, may be separated using a combination of the variability of the rates of fluorination of the plutonium and uranium compounds, and chemical reactivities of the hexafluorides.

The decladding step of the process for uranium dioxide fuels involves gas-metal reactions in the case of elements clad either with stainless steel or Zircaloy. The gas-metal reactions are carried out with the fuel elements submerged in an inert fluidized bed (calcium fluoride or alundum) which serves as a heat transfer medium. Dilute mixtures of hydrogen chloride in hydrogen fluoride or the separate gases have been successfully employed where zirconium decladding is necessary. In recent work chlorine has replaced the hydrogen chloride. In the case of stainless steel cladding, chlorine alone appears suitable as the decladding reagent based on results from pilot-plant studies.

The cladding reactions (referred to as primary) are being carried out in a two-zone fluid-bed reactor. Volatilization of the clad or alloying material occurs in the lower zone during the chlorination reaction. The volatile materials pass upward into the upper zone where hydrogen fluoride is admitted, thus effecting conversion to solid fluorides. The two zones are separated by an inverted conical baffle (other types may also be suitable) which reduces back-mixing of the gases and prevents the formation of gas mixtures that have been shown to affect these reactions adversely. The two-zone scheme appears attractive for reacting the cladding or alloying agent as well as for the chlorination of the sintered oxide fuel itself.

In pilot-plant studies the reaction of 304 stainless steel tube sections with chlorine has been investigated in a $1\frac{1}{2}$-inch diameter, two-zone fluid-bed reactor. Penetration rates ranged from 6 mils/hr at 570 C to 10.6 mils/hr at 590 C, using 100 percent chlorine as the primary (lower zone) reactant. Hydrogen fluoride was admitted to the upper reaction zone where the volatile ferric chloride is converted to the solid fluoride. The solid material deposits primarily on the surface of the bed particles, with a small fraction forming in the gas phase and remaining as fines. At 570 C, a three-hour experiment resulted in reaction of 75 percent of the 50-mil thick specimen. Other halogenating agents tested for decladding included bromine, carbon tetrachloride, and a mixture of carbon tetrachloride and water vapor, but none of these showed any promise. An equimolar ratio of chlorine and carbon tetrachloride gave a slightly lower rate of reaction than chlorine alone, 7.3 and 3.4 mils/hr at 600 and 577 C as compared with about 9.0 and 5.5 mils/hr.

After decladding has been achieved, a subsequent fluorination step is expected to provide the necessary separation of the fissile elements. The direct fluorination of dense uranium dioxide pellets is being examined in fluid-bed pilot-plant studies. A six-inch deep bed of $\frac{1}{4}$-inch inert-fired pellets was completely reacted in 6.5 hr, with satisfactory reaction control at 500 C and 20 percent inlet fluorine. In preliminary runs with hydrogen-fired pellets, overall fluorination rates appear lower by a factor of about 3 than with inert-fired pellets. In three-inch deep beds satisfactory fluorinations were carried out at 500 C with up to 40 percent inlet fluorine concentration. Analysis of runs to date shows a substantial effect on reaction rate and fluorine efficiency of the concentration of intermediate uranyl fluoride fines in the fluid bed.

Heat transfer tests are being continued in mockup systems similar to those encountered in fluorinations of uranium dioxide pellets, that is, with a fluidized medium in the voids of a nonfixed bed of heated pellets. Film coefficients for heat transfer from a single heater to a fluidized medium in the pellet voids obtained for $\frac{3}{8}$-inch pellets were 75 percent of those for fluidization without pellets. Heat transfer for this case appeared as good or better than in a similar system with $\frac{1}{2}$-inch pellets. Tests are in progress to determine the effective radial thermal conductivity of packed, fluidized beds in a system with an axial heater and a cooled column wall. Preliminary results show a conductivity of the order of 10 Btu/(hr)(sq ft)(F/ft). This value is very close to that for stainless steel type 347.

Spent oxide reactor fuels will contain both plutonium and uranium. Laboratory investigations are in progress to examine the problems involved in the steps of the Direct Fluorination Volatility Process, including those encountered in the quantitative transport of plutonium hexafluoride.

Two experiments have been performed on the fluorination of multigram quantities of plutonium dioxide, and 99 and 97 percent of the plutonium was accounted for in the volatile effluent.

Experiments have been made to demonstrate that plutonium hexafluoride produced in a laboratory fluorinator can be passed through heated sections of pipe and through thermal gradients with very good recovery of the compound. Trap-to-trap transport through laboratory equipment has demonstrated that 98 to 100 percent of the plutonium hexafluoride volatilized could be recovered.

It has also been demonstrated that a 38-gram sample of plutonium hexafluoride could be held at 60 C for 25.5 hours with no more decomposition than could be attributed to alpha radiation decomposition.

The reaction of bromine with plutonium hexafluoride, with and without the presence of uranium hexafluoride, has been investigated. Bromine is a satisfactory reagent for the reduction of plutonium hexafluoride to plutonium tetrafluoride and can be used to separate uranium and plutonium.

The gamma-ray spectrum of plutonium tetrafluoride has been investigated up to 2.0 Mev. Fast neutron flux measurements have been made on samples of plutonium tetrafluoride to assay the hazards connected with the α-n reaction.

A combined chlorination-fluorination process (Direct Chlorination Process) has been proposed as an alternate to the fluorination step. Accordingly, work was begun on the chlorination of sintered uranium dioxide pellets using chlorine, carbon tetrachloride, and mixtures of the two. Initial experiments conducted in a tube furnace on single pellets of dioxide (prepared at Mallinckrodt Nuclear Corp., with a density nearly 95 percent of theoretical) attained reaction rates of 370 to 780 mg/(sq cm)(hr), based on pellet weight loss data and the original surface area of the pellet. The highest rate reflects about 25 percent consumption of a pellet in one hour at 600 C. The chlorine-carbon tetrachloride mixture ($\frac{1}{3}$ each and $\frac{1}{3}$ nitrogen) proved best in the range from 500 to 600 C, although the difference in rate between this mixture and carbon tetrachloride alone narrowed at the higher temperature. These chlorination results suggest a Direct Chlorination Process as an alternate to the Direct Fluorination Process now being developed. This process would have the advantages of less costly reagents and lower heat load (lower heats of reaction).

Supporting corrosion studies on typical materials of construction being carried out in a one-inch tube-furnace showed nickel and Inconel sustained similar corrosion rates, about 20 mils/mo at 600 C, in chlorine-nitrogen stream (equimolar quantities), whereas the rate for Hastelloy-C was somewhat lower, being 12 mils/mo. At 550 C, the rate for nickel and Inconel was about 6 mils/mo.

Application of The Direct Fluorination Volatility Process to highly enriched, low uranium-Zircaloy alloy plate-type fuels has been reported previously (ANL-6183, pages 101 to 106 and ANL-6145, page 119). Application of a Direct Chlorination Process has been examined in pilot-plant studies. Appreciably higher rates of attack on uranium-Zircaloy-2 alloy plate assemblies were achieved with chlorine as the primary reactant instead of hydrogen chloride in the lower zone of the six-inch diameter, two-zone reactor; rates ranged from 274 to 417 g/hr of metal reacted as opposed to a maximum rate of 300 g/hr using hydrogen chloride at temperatures near 400 C. Also, much lower concentrations of chlorine were used, about 10 to 20 percent as compared with 60 to 90 percent hydrogen chloride. Analyses of several size fractions of the final bed indicate the uranium and zirconium are uniformly deposited on the particles in the upper zone during the course of the hydrofluorination reaction. No losses of these materials from the reactor have been experienced, as determined by analysis of the off-gas scrub solution, indicating that the two-zone scheme has high efficiency for "trapping" volatiles.

The reaction of chlorine and hydrogen fluoride with anhydrous ammonia in the gas phase followed by water scrubbing was found to be an effective method for efficient disposal of the excess reactants in these halogenation studies. Appreciable corrosion had been experienced previously in a recirculating caustic column. A three-inch diameter by three-foot long glass column (partially packed) was adequate for absorbing a combined flow of 12 mole/hr chlorine and 10 mole/hr hydrogen fluoride, using about 5 to 10 gal/hr water and 25 percent excess ammonia.

The conversion of uranium hexafluoride to uranium dioxide by a two-step fluid-bed process is currently being studied. The major problem in the first step, reaction of the hexafluoride with steam to form uranyl fluoride, continues to be one of control of particle size. A recycle stream of "seed" particles equivalent to about 15 percent of the feed is being employed. The present feed rate is equivalent to 174 lb uranium/(hr)(sq ft reactor cross section), and the column is being operated at 200 C.

An auxiliary three-inch reactor has been installed for work on the second step, reduction of the uranyl fluoride to dioxide with hydrogen or hydrogen-steam mixtures. The column has been designed so that both fluid and static or moving-bed experiments may be carried out. Preliminary data from runs at 600 and 650 C indicate that much better conversion is obtained with a hydrogen steam mixture than with hydrogen alone.

III. Reactor Safety (pages 168 to 199)

The oxidation, ignition, and combustion processes of uranium, zirconium, and plutonium are being studied to provide information to aid in minimizing the hazards associated with handling these metals.

Studies of the ignition of uranium powders by the burning curve method are continuing. Results have shown that an increase in heating rate caused an increase in ignition temperature for a -80 +100 mesh (d = 149 microns) powder. An increased heating rate, however, decreased the critical height of powder required to yield a constant ignition temperature. The critical height was shown previously to be nearly independent of container diameter. The effects of heating rate were shown to be consistent with the Frank-Kamenetskii theory of thermal explosions and the Murray, Buddery and Taylor ignition equation. Both treatments apply when a linear oxidation rate law prevails.

The effect of pre-oxidation on the ignition temperature of a -140 +170 mesh (d = 88 microns) uranium powder was investigated. The ignition temperature decreased as much as 25 C when the surface of the particles appeared to be fully covered by oxide nodules (20 percent reaction). Further pre-oxidation caused the ignition temperature to increase.

Ignition temperatures of uranium and uranium carbide powders were measured in air and compared to values obtained in pure oxygen. Ignition temperatures of both materials in air were within 20 C of those in oxygen.

Studies of the rate of burning propagation along uranium and zirconium foil strips is continuing. Propagation rates did not increase significantly with uranium when the ambient air temperature was increased to 300 C. Propagation rates increased about 40 percent at most in experiments with zirconium when the ambient air temperature was increased to 400 C.

Previous work has shown that the presence of certain halogenated hydrocarbons in air decreases the burning propagation rate along metal foils. An investigation into the causes of the decreased rates was initiated. Studies of the cooling of a heated platinum foil by various mixtures of trifluorobromomethane and dichlorodifluoromethane with air and argon indicated that increased heat removal was not responsible for the decreased burning rates.

The experimental program to determine rates of reaction of molten reactor fuel and cladding metals with water is continuing. The principal laboratory-scale method involves the rapid melting and dispersion of metal wires in a water environment by a surge current from a bank of condensers. A new high-pressure apparatus was described in the previous quarterly (see ANL-6231, page 155). The series of runs with 60-mil zirconium wires at pressures up to 1500 psi is continuing. More extensive and more rapid reaction was reported in the previous quarterly for runs in heated water. This trend was found to continue to higher metal temperatures. Up to 90 percent reaction occurred at an initial metal temperature of 2200 C.

A series of equations was derived to describe the behavior of heated metal spheres in a water environment. The derivations were similar to those reported in a previous quarterly (see ANL-6029, page 126), with the addition of equations to describe the gaseous diffusion process whereby water vapor diffuses through the hydrogen mantle surrounding reacting particles. Preliminary results of studies on the analog computer have led to a reasonable interpretation of the unusual pressure effect.

A second laboratory-scale method involves the rapid contact of steam with heated metal. In this method, the metal receives a "pressure pulse" of water vapor. A new apparatus was constructed which is entirely enclosed in a box heated to 105 C. Runs with one atmosphere of water vapor reacting with molten aluminum at 1000 C are reported. Preliminary results indicate that the oxide film is very protective at these temperatures.

A series of metal-water transient irradiation experiments in TREAT was made with uranium wires for which the rate of energy input was progressively changed. Ninety-three percent enriched uranium wires with diameters of 34 and 64 mils were used. Observation of the uranium after the reactor bursts indicated that, with an average energy of 44 megawatt-seconds (216 calories per gram uranium), a reactor period of 515 milliseconds did not melt the uranium. Reactor periods of 304 milliseconds or less resulted in melting of the wires. The uranium attained temperatures of about 1500 C and the process was accompanied by the extensive formation of particles. One run with a bundle of three uranium wires resulted in 12.9 percent reaction, accompanied by the fusing together of the three wires with the production of some fine particles. A plot of the amount of uranium-water reaction versus the reactor period indicated that the extent of reaction decreased as the period increased.

Particle size measurements were made on uranium wire which had been melted and dispersed under water by the TREAT reactor bursts. The particles of most frequent occurrence had diameters in the range 2 to 16 mils; this is to be compared with the original diameter of 64 mils. However, the presence of larger globules resulted in Sauter mean diameters (see Table 56 for definition) ranging from 17 to 78 mils. A correlation was observed between the extent of uranium-water reaction and the change in specific surface area; as the ratio of final area to initial area increased from 1.0 to 5.4, the percent of metal-water reaction increased from 0.4 to 17.2 percent.

IV. Reactor Chemistry (pages 200 to 206)

The neutron capture cross sections of uranium-236 have been determined at neutron energies ranging from 0.36 to 1.73 Mev. The cross sections varied from 0.27 barn at 0.36 Mev to <0.1 barn at 1.73 Mev, going through a

maximum of 0.32 barn at 0.97 Mev and a minimum of 0.25 barn at 0.47 Mev. Work has begun on the determination of the fast neutron capture cross sections of neptunium-237 for monoenergetic neutrons in the range from 0.4 to 1.7 Mev.

The Reactor Decontamination Program has two principal objectives: 1) to determine experimentally in pilot-plant equipment the degree of contamination to be expected in the steam phases of a boiling water reactor system in the event of fuel cladding failure, and 2) to find suitable methods of removing deposited activity from internal surfaces, should it be necessary because of excessive radiation levels. The pilot-plant equipment used for the first objective consists of a stainless steel type 304 loop that simulates the action of a boiling water reactor. Fuel ruptures are simulated by inserting tracer activities or irradiated metallic uranium. In a parallel effort, studies are being made in the laboratory to find suitable means of removing deposited activities.

In laboratory studies, scouting experiments indicated that oxalic or dilute sulfuric acids in conjunction with hydrogen peroxide have promising decontamination capabilities for stainless steel type 304 surfaces. Modifications of the second step of the alkaline permanganate-citrate decontamination procedure to reduce the corrosiveness on low alloy steels did not impair the ability to decontaminate stainless steel. The modifications consisted of upward pH adjustments or the addition of inhibitors. Citric acid alone was not very effective as a decontaminant; peroxide additions improved the results obtained. The addition of Delchem 2128A as a third step in conjunction with the alkaline permanganate-citrate procedure yielded somewhat improved decontamination over the conventional two-step procedure.

Two series of reproducibility runs were made with the stainless steel type 304 pilot-plant loop. In the first series of three runs, stainless steel type 304 sample strips were used, whereas SAE type 1018 mild steel strips were used in the second. Results are not yet available.

V. Routine Operations (pages 207 to 208)

The operation of the radioactive waste-processing facility and the gamma-irradiation facility continued without incident.

For the convenience of the reader, appropriate parts of this summary are repeated at the beginning of each of the first four sections of this report.

I. CHEMICAL-METALLURGICAL PROCESSING

The research and development work that is being done on pyrometallurgical processes is prompted by the considerable likelihood that the application of these processes to the recovery of nuclear reactor fuel may lead to a reduction in the cost of nuclear power. Of these pyrometallurgical processes, melt refining will be the first to be used on a plant scale. The process will be incorporated into the fuel recovery cycle of the second Experimental Breeder Reactor (EBR-II). The reactor and the fuel cycle facility are now under construction at the Reactor Testing Station in Idaho.

Final results on the first high-activity level demonstration of the melt refining process for EBR-II core fuel have been obtained. A 388-gram charge of uranium-five percent fissium fuel pins irradiated to a total atom burnup of about 0.6 percent was melt refined for three hours at 1400 C. Fission product removal was much as expected on the basis of earlier work with unirradiated material, tracers, and irradiated uranium. Rare earths, yttrium, cesium, barium, strontium, and iodine removals exceeded 99 percent. Approximately 95 percent of the tellurium and 9 percent of the zirconium were removed.

A second experiment on the release of fission product krypton and xenon from irradiated fissium fuel pins was completed. The amount of gas evolution appears to depend primarily on temperature rather than on the heating rate. The removal of krypton and xenon was complete at 1025 C within the limits of analytical accuracy.

Uranium and uranium-fissium alloy pins react with nitrogen in an argon atmosphere, forming uranium nitrides. The reaction follows a parabolic rate law, with approximately the same rate constants for uranium and the fissium alloy. In both cases, however, the rate is approximately doubled by the presence of metallic sodium coatings on the pins. Activation energies for the reaction, about 15 kcal/mole, are not affected significantly by the presence of fissium constituents in the uranium at five weight percent concentration, nor by sodium coatings on the uranium or the fissium alloy.

Various techniques are being investigated for increasing melt refining pouring yields under adverse circumstances. Certain mechanical devices, for example, are being evaluated as possible methods of puncturing oxide or nitride crusts on the surface of molten uranium.

Work was continued on the development of a process for recovery and suitable purification of fissionable material contained in crucible skull material remaining after melt refining operations. The processes under consideration utilize liquid metal solvents as media in which recovery and

purification operations are conducted. To enable removal of skull material from a crucible, the material is first oxidized under controlled conditions to a free-flowing powder which is readily poured from a crucible. The oxide is then reduced by magnesium dissolved in zinc. The reduced uranium appears in zinc solution. Two precipitations of uranium, first as a uranium-zinc intermetallic compound from the zinc solution, and then as uranium metal from a magnesium-rich solution, together with removal of the supernatant liquid metal phases provide purification of the uranium. It is then retorted to vaporize associated solvent metals and to effect consolidation of the uranium product.

This process was improved considerably during the past quarter through the use of one of several possible molten halide fluxes in conjunction with a magnesium-zinc reducing solution. In the presence of a suitable flux and by adequate mixing, quantitative reductions of both pure uranium oxides and skull oxides were consistently obtained within two hours, many within thirty minutes. Complete reduction of plutonium dioxide was similarly achieved. Another outstanding advantage of a flux is that it acts as a vehicle in which the magnesium oxide reaction product is suspended, thereby enabling a clean separation of this material from the metal phase. Physical removal of the magnesium oxide from a metal phase by filtration or through liquation of the magnesium oxide has been troublesome and unsatisfactory. A third advantage of the halide salt fluxes is that the reductions can, if desired, be conducted in an air atmosphere. Since unreduced uranium oxides are also suspended in the flux phase, a fourth potential benefit of a chloride flux arises from the possibility of reducing and leaching noble metals from the skull oxide with zinc prior to the reduction of uranium and the more stable fission product oxides with magnesium. The removal of ruthenium from skull oxides by this procedure was demonstrated during the past quarter.

A fairly extensive study of salt fluxes was undertaken in the past quarter to define those systems which produced the most rapid and quantitative reductions of U_3O_8 by a dilute magnesium-zinc alloy. The salt fluxes found beneficial were mixtures of alkali and alkaline earth element chlorides, the most rapid reductions occurring with the lighter cations. Magnesium chloride was a major ingredient in all fluxes that gave complete reduction within 30 minutes and is, therefore, presently regarded as an essential ingredient. Magnesium fluoride (5 mole percent) was also present in all fluxes because of its effectiveness in providing clean and rapid coalescence and separation of the salt and metal phases.

Studies of reduction in the absence of flux were conducted in both pure magnesium and dilute magnesium-zinc alloys. With a 10 percent magnesium concentration in zinc, reductions were fairly rapid and nearly quantitative but became must slower at a five percent magnesium concentration. Reductions in pure magnesium were still slower and irreproducible.

In this system, chloride fluxes are also beneficial. It is noteworthy that in pure magnesium-flux systems cerium (and, therefore, possibly other rare earths) remains in the flux phase. In dilute magnesium-zinc-flux system, rare earth oxides are quantitatively reduced and appear in the metal phase along with the uranium.

Preparations are now underway for medium-scale (200 grams of uranium) demonstrations of the skull reclamation process shown in Figure 8, page 49, which utilizes salt fluxes. However, the slip for removal of noble metals will not be incorporated until further laboratory studies have been made. A small-scale (15 grams of uranium) demonstration run showed good removals of cerium, molybdenum, and zirconium, the only elements followed, thus indicating that the process will provide adequate decontamination.

In retorting studies of uranium precipitated from magnesium-rich systems, a considerable portion of the product has been in the form of large agglomerated masses of uranium. Since these have been very easily handled, their formation appears desirable. The uranium agglomeration occurs during decomposition of uranium-zinc intermetallic compounds with magnesium. The factors responsible for their formation are not yet known, although stirring is believed to play a major role.

A possible simplification of the process for isolation of plutonium bred in the uranium blanket of the EBR-II reactor involves the direct low-temperature (450 C) reaction of uranium with zinc in slight excess of that required for stoichiometry to give an intermetallic ($UZn_{11.5}$) which would then be treated with magnesium to decompose the intermetallic and dissolve the plutonium. The low-temperature reaction was demonstrated in the past quarter with full size blanket pins, 0.433 inch in diameter. Times of around 100 hours were required for completion of the reaction. It is hoped that these times can be appreciably shortened by further work.

In a 100-hour holding run, a plutonium-zinc solution at 800 C was stable in a graphite crucible. An initial loss of plutonium occurred from magnesium solutions held in tantalum crucibles at 800 C, after which the plutonium concentration stabilized. This loss is probably caused by a reaction with either solution or tantalum impurities and will be further investigated.

A program is underway for evaluating materials for containing liquid metal systems of interest. The very slight attack of tantalum by zinc at 850 C is reduced by the addition of magnesium. In preliminary tests a tantalum-7.5 percent tungsten alloy has shown better resistance to attack by zinc that tantalum. Molybdenum is seriously attacked by zinc at 850 C, whereas graphite shows promise as an outstanding container material.

A direct-cycle fuel-reprocessing plant using pyrometallurgical procedures is being designed and constructed as part of the Experimental Breeder Reactor No. II (EBR-II) project. A Laboratory and Service Building is also included. Melt refining, liquid metal extraction, and processes involving fractional crystallization from liquid metal systems are being examined for the recovery and purification of EBR-II fuels. Based on these studies, process equipment is being designed and tested.

Installation of equipment in the Laboratory and Service Building has been completed, and shakedown testing has begun.

Construction of the Fuel Cycle Facility Building is continuing. The structure, which was 40 percent completed by September 6, 1960, was about 70 percent completed by December 6, 1960. Enclosure of the building has been completed and work is continuing inside during the winter.

The standard General Mills Model 300 manipulator arm has been successfully attached by remote means to the radiation stable electromechanical operating manipulator. This increases the versatility of the cell manipulator system. An order for 12 Model 8 manipulators for the Air Cell has been placed.

The switchboard and control cabinets for manipulators, cranes, and blister hoist have been tested and shipped to Idaho.

The final shipment of components for the Fuel Cycle Facility process cell windows has been received in Idaho.

The major lamp manufacturers have modified the design of the mercury lamps specified for use in the process cells. Tests show that the new lamps are very inferior for the proposed use as compared with the lamps previously manufactured. An adequate supply of lamps of the type formerly manufactured has been ordered.

Redesign of the small air lock and component parts is nearly completed. Kollmorgen Corporation was chosen to modify an existing wall periscope to make it suitable for use in the Air Cell by the addition of internal shielding. The installation drawings for the high-frequency power distribution system have been completed. Work continues on the drawings or installation packets of the melt refining off-gas system, the space radiation monitoring system, the service plugs, and other equipment items for the Fuel Cycle Facility.

Three types of radiation-resistant greases have been irradiated and then tested in a roller bearing of a type used in the manipulator bridge. The tests indicate that the greases are adequate for the proposed use, but further tests are being conducted to determine the effects of radiation at levels below those used in the initial experiments.

An economical radiation-resistant end seal for MI cable is desirable for nonpermanent installations in the process cells. Several types have been tested and one type appears satisfactory. Flexible leads are also needed in the cells. Leads with four types of asbestos insulation have been irradiated and tested. Two of the types appear satisfactory.

The serious cracking problem previously noted with melt refining crucibles has been eliminated. This was accomplished by the modification made by the supplier in the manufacturing method and by the application of a set of acceptance standards devised and applied by this Division.

Tests have shown that the Fiberfrax fume trap will be adequate to handle the quantities of fumes evolved in the melt refining furnace. These experiments also show that a tight seal is not necessary between the crucible and the fume trap.

Twenty-four batches of enriched pin scrap were melted down into ingots for recasting of fuel pins for EBR-II.

Fundamental studies are being made in support of the process development activities. Data basic to the various liquid metal processes are the solubilities of those elements whose separations are being attempted. The solubilities of the rare earth elements europium, gadolinium, dysprosium, and erbium in liquid cadmium may be represented by the following empirical equations:

europium (330 to 500 C): $\log (\text{atom percent}) = 6.063 - 4210\ T^{-1}$

gadolinium (325 to 500 C): $\log (\text{atom percent}) = 3.217 - 3279\ T^{-1}$

dysprosium (325 to 630 C): $\log (\text{atom percent}) = 3.335 - 2447\ T^{-1}$

erbium (325 to 630 C): $\log (\text{atom percent}) = 6.309 - 6444\ T^{-1} + 1.485 \times 10^{6}\ T^{-2}$.

The solubilities of manganese and nickel in liquid cadmium, which are important constituents of high-strength alloy steels, may be represented by the following empirical equations:

manganese (325 to 650 C): $\log (\text{atom percent}) = 3.263 - 3054\ T^{-1} + 0.4476 \times 10^{6}\ T^{-2}$

nickel (509 to 650 C): $\log (\text{atom percent}) = 1.954 - 740.8\ T^{-1}$

nickel (330 to 509 C): $\log (\text{atom percent}) = 6.722 - 5628\ T^{-1} + 0.9045 \times 10^{6}\ T^{-2}$.

Additional studies with the zinc-uranium system indicate the existence of two intermetallic compounds: a delta phase (phase richest in uranium) and an epsilon phase (phase richest in zinc). The epsilon phase was found, by

thermal analysis, to decompose peritectically into the melt and delta phase at 844 C. Two contiguous intermetallic layers were found in diffusion tests made below 800 C, the outer layer being the epsilon phase and the inner layer the delta phase. A single layer of delta phase was found when diffusion tests were made at 875 C.

Measurements of the vapor pressure of the zinc-uranium system by the effusion method have confirmed the existence of two uranium-zinc intermetallic phases. The delta phase was found to have a constant vapor pressure, indicating a constant composition, the zinc-uranium ratio of this phase being approximately 8.4 to 1. The epsilon phase was found to have a vapor pressure which decreased with loss of zinc, indicating a range of composition. The limits of the composition of the epsilon phase are from $UZn_{11.2}$ to $UZn_{9.4}$.

Several additional observations have been made relative to the uranium-cadmium system. The temperature of the alpha-beta uranium transformation is unaffected by saturation with cadmium, indicating no appreciable solubility of cadmium in solid uranium. Similarly, no appreciable solubility of uranium in solid cadmium was found. The eutectic temperature at which equilibrium between cadmium, UCd_{11}, and melt exists was found to be 0.26 C below the freezing point of cadmium.

A systematic study is underway to ascertain the influence of atomic size, metallic valence, and electronic configuration on the coprecipitation of various metallic elements with the cerium-cadmium intermetallic phase $CeCd_{11}$. The following values for the coprecipitation coefficient, λ, defined by the equation $\log\left(\frac{\text{tracer in solution}}{\text{total tracer}}\right) = \lambda \log\left(\frac{\text{carrier in solution}}{\text{total carrier}}\right)$ have been determined: sodium, $\lambda = 0$; lithium, $\lambda = 0$; potassium, $\lambda = 0$; yttrium, $\lambda = 0$; lanthanum, $\lambda = 1.49$; uranium, $\lambda = 0.13$; strontium, $\lambda = 0.10$; europium, $\lambda = 0.099$; and zirconium, $\lambda = 0.04$.

The distribution coefficient of representative fissile and fission product elements between the two immiscible liquids, zinc and bismuth, at 548 C have been determined. Values of the coefficient (weight percent in zinc phase/weight percent in bismuth phase) are palladium, 33.3; uranium, 0.17; cerium, 0.05; and strontium, 7.7×10^{-4}. The coefficient for uranium was found to vary from 0.078 at 447 C to 0.17 at 548 C.

The mutual solubilities of liquid aluminum and cadmium may be represented by the empirical equations

$$\log (\text{atom percent cadmium in aluminum}) = 3.479 - 2944\ T^{-1}$$

$$\log (\text{atom percent aluminum in cadmium}) = 3.702 - 2815\ T^{-1}$$

in the temperature range from 680 to 720 C.

The molar magnetic susceptibility of cerium in the intermetallic phase $CeCd_{11}$ may be represented by a Curie-Weiss equation[$(\chi = C/(T-\Delta)]$, with $\Delta = -2$ K and $C = 0.81$. The effective Bohr magneton number for this system is 2.55. This value is in good agreement with the value of 2.56 calculated for a free gaseous cerium ion in a $^2F_{5/2}$ ground state.

Experimental work on the study of the heat of formation of tungsten disulfide has been completed with the determination of the energy change of the reaction

$$W(c) + 2S(c) + 9/2\ O_2(g) + 4NaOH(aq) \longrightarrow WO_3(c) + 2Na_2SO_4(aq) + 2H_2O \quad .$$

The preliminary value for $\Delta E^0_c/M$ of the reaction is -2226.70 ± 0.88 cal per gram of tungsten-sulfur mixture (mole ratio of one to two).

Conditions for the combustion of uranium mononitride and zirconium hydride in oxygen in a bomb calorimeter have been determined. Calorimetric combustions of uranium mononitride are being carried out.

In the fluorine bomb calorimetry phase of the program, calorimetric studies are complete for the determination of the heats of formation of zirconium tetrafluoride, molybdenum hexafluoride, and boron trifluoride. Preliminary values for zirconium tetrafluoride and molybdenum hexafluoride were reported previously (ANL-6231, page 82). The preliminary value for the standard heat of formation of boron trifluoride gas is -269.97 ± 0.32 kcal/mole. Work is in progress on the determination of the heat of formation of uranium hexafluoride and boron nitride. Because boron nitride reacts spontaneously with fluorine, a special reaction vessel was constructed for the study which will be useful also for studies of other elements that react spontaneously with fluorine.

Work is continuing on the assembly of a 1500 C high-temperature enthalpy calorimeter and the design of a 2500 C furnace for studies at even higher temperatures.

A. Pyrometallurgical Development

1. Melt Refining
(R. K. Steunenberg, L. Burris, Jr.)

The 50 percent enriched uranium fuel alloy used in the first EBR-II core loading will be recovered by the melt refining process. After decladding, the fuel pins are chopped and then melted in a zirconia crucible. The charge is held at about 1400 C for three or four hours. Volatilization of some of the fission products and selective oxidation by the crucible result in the removal of about two-thirds of the fission products. The purified metal is separated by pouring it into a graphite mold. (A supplementary process is required to recover the unpoured metal and oxide remaining in the crucible.) Development work has been continued on the following aspects of the melt refining process: (1) melt refining demonstration runs utilizing 400 grams of highly irradiated uranium-fissium alloy, (2) experiments on the evolution of fission product krypton and xenon during the heating and melting of highly irradiated fuel pins, (3) studies of the nitridation of sodium-coated pins in a nitrogen-argon atmosphere, and (4) investigations of modifications in melt refining pouring techniques.

a. High-activity Level Melt Refining Experiments
(V. G. Trice, W. H. Spicer)

Small-scale melt refining experiments using highly irradiated uranium-fissium fuel pins have been started to demonstrate the recovery and reconstitution of spent EBR-II fuel and to observe the physical behavior of the material during various phases of the melt refining process. The first experiment of the series has been completed. Physical observations, the most notable of which was the formation of a crust or film on the surface of the melt, were discussed in the previous report (ANL-6231, page 38).

In the first experiment, the highly irradiated alloy was melt refined for three hours at 1400 C. The experimental conditions are listed in Table 1. The purified metal product was removed from the crucible by top pouring. The resultant ingot was sampled at the top, middle, and bottom. To facilitate its removal, the skull remaining in the crucible after pouring was converted to a powder by air oxidation for $2\frac{1}{2}$ hours at 650 to 700 C. The oxidation was carried out in such a way that molybdenum was retained in the oxidized skull and not volatilized (ANL-6231, page 53). The resulting skull oxides were then treated with hydrogen at 700 C to reduce ruthenium oxide to the metal. Although the reduction of the oxides is not a part of the process, its use here avoids a troublesome analytical problem, since ruthenium oxide is not readily dissolved by aqueous solutions. After a five-minute grinding and blending treatment in an electric mortar ("Mixer-Mill"

manufactured by Spex Industries of Scotch Plain, New York), a homogeneous powder was produced, from which three random samples were obtained. The charge, ingot, and skull oxide samples were analyzed radiochemically for rare earths-yttrium, barium-strontium, tellurium, iodine, and cesium. The total molybdenum content of all samples was determined and the charge and ingot samples were analyzed for fission product ruthenium and zirconium.

Table 1

EXPERIMENTAL CONDITIONS FOR HIGH-ACTIVITY LEVEL MELT REFINING EXPERIMENT

Composition of alloy before irradiation, weight percent:

Uranium-238	84.00
Uranium-235	10.73
Molybdenum	2.59
Ruthenium	2.11
Rhodium	0.260
Palladium	0.186
Zirconium	0.118
Niobium	0.01

Charge Weight:	387.6 grams
Burnup:	0.58 percent of total atoms[a]
Cooling Time:	40 days
Melt Refined:	3 hours at 1400 C
Crucible:	Norton RZ5601 lime-stabilized zirconia crucible degassed at less than 25 microns for one hour
Atmosphere:	750 mm argon
Crucible Wetted Area:	35.7 sq cm (assuming an alloy density of 17 g/cc)
Metal-Skull Separation:	Top pouring

[a] Burnup determination by cesium-137 analysis.

The chemistry of the melt refining process has been investigated previously through experimentation with synthetic alloys containing unirradiated uranium, and uranium irradiated to 0.4 percent burnup and cooled for 380 days. These studies showed that the volatile constituents and the fission product elements more electropositive than uranium are removed by melt refining, while those elements more noble than uranium are retained in the refined metal product. The observations also showed that the reactive

fission product elements form an adherent layer of reaction products on the walls of the crucible, permitting an excellent separation of the purified metal by top pouring.

The experiment with highly irradiated uranium-fissium alloy completely verified the conclusions relating to the chemistry of the melt refining process based on the earlier experiments. Data comparing the fission product removals after melt refining are presented in Table 2.

Table 2

FISSION PRODUCT REMOVALS EFFECTED IN THE MELT REFINING OF HIGHLY IRRADIATED EBR-II FUEL

Element	Percent Removed[a]	Decontamination Factor[b]
Rare Earths and Yttrium	99.2+[c]	120+
Cesium	99.5	200
Tellurium	95.4	22
Barium-Strontium	>99.9	2.3×10^5
Iodine	99.8	680
Zirconium	9.2	1.1

[a] $\text{Percent removed} = \left[1 - \frac{\text{Concentration in product}}{\text{Concentration in charge}}\right] \times 100$.

[b] $\text{Decontamination Factor} = \frac{\text{Concentration in charge}}{\text{Concentration in product}}$.

[c] Analytical technique leaves significant amounts of other activities as contaminants in separated rare earth samples.

In previous work employing cerium as representative of the rare earth fission products, considerable information was developed correlating the extent of their removal by melt refining to parameters such as crucible dimensions and charge size (expressed in terms of wetted crucible area) and the melt refining conditions.[1] The data obtained in this experiment for total rare earth and yttrium removals are consistent with this correlation. Data for the other electropositive fission product elements show the occurrence of extensive removal, as anticipated. Although

[1] Chellew, N. R., Bennett, G. A. and Trice, V. G., The Melt Refining of Irradiated Uranium: Application to EBR-II Fast Reactor Fuel. VIII The Behavior of Rare Earths, Yttrium, Barium, Strontium and Cesium, Nuclear Sci. and Eng., 9, 64 (1961)

zirconium can be removed from fissium melts by liquation of zirconium carbide, the 22 ppm carbon which was found in the charge is not sufficient to explain the observed 9.2 percent removal of zirconium. The joint solubility of carbon and zirconium in uranium is such that at least 100 ppm carbon would be required (see ANL-5959, page 145) to effect the removal.

The sampling program employed in the experiment affords observations on the distributions of various elements between the ingot of purified metal and the skull retained in the crucible (see Tables 3 and 4).

Table 3

URANIUM AND MOLYBDENUM MATERIAL BALANCES FOR HIGH-ACTIVITY LEVEL MELT REFINING EXPERIMENT AND FOR REFERENCE EXPERIMENT WITH UNIRRADIATED FUEL

Melt Refining Conditions

Time: 3 hours
Temp: 1400 C
Crucible: lime-stabilized zirconia

		Irradiated Fuel	Unirradiated Fuel (Reference Experiment)
Relative weight of various fractions	Charge	1 00	1 0
	Ingot	0.724	0 867
	Oxidized skull	0 324	
Uranium concentration, weight percent	Charge	95	-
	Ingot	94	95
	Oxidized skull	82	79
Uranium accounted for, percent of charge	Ingot	72	87
	Oxidized skull	28	13[a]
	Total	100	100
Molybdenum concentration, weight percent	Charge	2 5	-
	Ingot	2 6	2 5
	Oxidized skull	1 8	1.6
Molybdenum accounted for, percent of charge	Ingot[b]	74	-
	Oxidized skull	23	-
	Total	97	-
Fate of uranium retained in crucible, percent of charge	Unpoured U	22	10
	Oxidized U	5 9 (±1.1)[c]	2.8
	Ratio of unpoured to oxidized U	3 8	3.8

[a] Value computed by difference

[b] Molybdenum Enrichment in Purified Metal =

$$100 \times \frac{\text{Mo Concentration in Ingot - Mo Concentration in Charge}}{\text{Mo Concentration in Charge}} = 3.42 \text{ percent.}$$

[c] Based on the precision (0.95 level) of the uranium and molybdenum analyses.

Table 4

FATES OF SELECTED FISSION PRODUCTS
IN THE HIGH-ACTIVITY LEVEL MELT
REFINING EXPERIMENT

Melt Refining Conditions

Time: 3 hours
Temp: 1400 C
Crucible: lime-stabilized zirconia

Element	Percent of amount charged	
	Ingot	Skull
Rare Earths and Yttrium	0.59	85
Tellurium	3.4	84
Cesium	0.37	0.024
Barium-Strontium	0.0032	2.0
Iodine	0.11	0.089
Total Metal	72.4	27.6[a]

[a]Computed by difference.

No attempt was made, however, to determine the extent of volatilization or penetration of the crucible walls by the elements present. In this respect, the information about material balance is incomplete. Nevertheless, pertinent data of process interest are given, namely, the compositions of the purified metal to be recycled to fuel fabrication and the skull to be treated further for uranium recovery.

In order to measure the removal of fission products, it is first necessary to know their concentrations in the charge material. The fuel employed in this experiment was irradiated in the CP-5 reactor in the form of 0.144-in. diameter, 14-in. long pins. Due to longitudinal flux variations in the reactor, the fuel burnup may have varied by as much as a factor of two over the length of the fuel pin. Therefore, it was necessary to select an irradiation monitor. Ruthenium, a fission product that is not removed from the fuel by the melt refining process, was chosen as the internal irradiation monitor.

Three random samples of the irradiated fuel were obtained and analyzed for the various fission product activities. Using the radio-ruthenium monitor, data obtained from the random samples providing local values of the fission product activities were corrected to yield the average concentration of the various fission products in the charge by the following procedure:

(1) The radioruthenium concentration in the ingot of melt refined metal, corrected for noble metal enrichment (calculated from total molybdenum concentrations in the charge and ingot as shown in Table 3), provided the average radioruthenium concentration in the charge, Ru_{av}.

(2) Multiplying the local values of fission product activities (FP_L), obtained from the random samples of the fuel, by the ratio of the average to local radioruthenium concentration, yields the average value of the fission product concentration in the charge, namely,

$$FP_L \times \frac{Ru_{av}}{Ru_L} = FP_{av} \quad .$$

The fates of the various fission product elements (see Table 4) were as expected from previous studies.[2] Cesium, barium-strontium, and iodine were apparently volatilized, since they were not present in the ingot or in the skull. Most of the rare earths-yttrium and tellurium were found in the skull. Of these activities, an amount between 6 and 16 percent was unaccounted for. This was not unexpected since previous melt refining studies with inactive uranium-fissium alloys containing cerium have shown that a cerium oxide layer formed on the walls of the crucible is not removed completely by the skull oxidation procedure. It has been suggested that tellurium is retained with the rare earths through the formation of rare earth tellurides.[1]

A further datum which can be derived from the molybdenum contents of the charge and the ingot is the noble metal enrichment in the ingot. Since the uranium is oxidized more readily than the fissium elements during melt refining, a small, but significant, uranium depletion occurs in the purified metal. Thus the fissium content of the purified metal is slightly higher than that of the charge. Assuming molybdenum to be representative of the noble metals, the calculation summarized in Table 3 shows the fissium or noble metal content of the purified metal ingot to be 3.4 percent greater than that of the charge.

In order to calculate the percentage of uranium appearing in the skull as unpoured metal, use was made of the following conclusions, which were based on previous experience: (1) uranium retained in the crucible as a component of the skull is present either as unpoured metal or

---

[2] Burris, L., et al., Developments in Melt Refining of Reactor Fuels, Proceedings of the Second United Nations International Conference on Peaceful Uses of Atomic Energy, Geneva, Switzerland (1958), Vol. 17, p. 401.

as oxidized metal; (2) molybdenum, a noble metal in the process, appears in the skull only in the unpoured metal; and (3) the unpoured metal has the same composition as the ingot. The percentage of uranium in the skull present as unpoured metal is then calculated as follows:

$U_S W_S$ = total uranium in the skull.

$\frac{U_I}{Mo_I} \times Mo_S W_S$ = uranium in the skull as unpoured metal.

$\frac{U_I}{U_S} \times \frac{Mo_S}{Mo_I} \times 100$ = percent of uranium in the skull present as unpoured metal.

U_S, U_I = uranium concentrations in the skull oxide and ingot, respectively.

Mo_S, Mo_I = molybdenum concentrations in the skull oxide and ingot, respectively.

W_S = weight of skull oxide.

The data, calculated by this procedure (see Table 3) for the high-activity level melt refining experiment and for a reference experiment with unirradiated alloy that immediately preceded the active run, indicated two significant facts. First, 5.9 percent of the uranium was oxidized in the hot run but only half as much, 2.8 percent, was oxidized in the cold run. Second, the ratio of unpoured to oxidized uranium, 3.8, was the same in both experiments. The relatively large amount of uranium that was oxidized may be the result of a radiation effect in the reaction kinetics or simply the result of atmospheric contamination. Replication of the experiment will provide the correct answer. The identical ratios of unpoured to oxidized uranium obtained in the two runs, if not fortuitous, show that the relatively low yield of 72.4 percent obtained in the hot run represents a reasonable pouring yield when the amount of oxidized uranium present is considered.

b. Fission Gas Release Studies
(N. R. Chellew, C. C. Honesty)

Experimental determinations of the release of noble fission gases and the swelling of fuel pins occurring when highly irradiated uranium-five weight percent fissium alloy is heated to melting were continued. An initial experiment (ANL-6231, page 42) indicated that, with a pin 0.143 inch in diameter heated slowly (~5.5 C per minute) to melting, the evolution of xenon and krypton became rapid at about 700 C and continued to about 1050 C. In the same temperature interval, swelling of the pin occurred until a diametrical increase of approximately 47 percent was observed at about 1000 C.

To evaluate the noble gas release and expansion behavior of the EBR-II type alloy under more realistic conditions, a second experiment was performed in which an irradiated pin was heated to melting under a time-temperature program simulating that contemplated for plant operation. This program was established on a tentative basis by experiments conducted in a prototype furnace for the EBR-II Fuel Cycle Facility

The alloy employed in the gas-evolution studies was prepared by irradiating in the CP-5 reactor, injection-cast pins of uranium-238 containing 10.7 weight percent uranium-235 and five weight percent fissium constituents. A pin, 0.143 ± 0.001 inch in diameter, was cut so as to yield charge and control samples which weighed 6.48 and 0.82 grams. Analyses of cesium-137 and uranium-235 in the control sample indicated the total atom burnup of the alloy to be 0.6 percent. The material was cooled for 106 days prior to the experiment.

The experimental procedure was as follows: (1) the charge pin, approximately 1.6 inches long, was placed on a tantalum holder and inserted in a tube furnace equipped with glass end ports for viewing and photographing the pin during the experiment by means of a cave-wall periscope; (2) the furnace and the charge were degassed at 120 C for 70 minutes at a pressure less than 40 microns; (3) high-purity argon, at a pressure of 680 mm, was introduced to the system and circulation of the atmosphere was begun at a constant rate of 183.3 cc per minute; (4) the pin was heated to a maximum temperature of 1138 C in 231 minutes, then cooled rapidly.

During the experiment, the noble gas activity which evolved to the continuously circulating atmosphere was passed through a seven-cc Pyrex bulb and was monitored by a gamma-ray spectrometer equipped with a 2 x 2-inch sodium iodide crystal. In a separate test, krypton-85 was injected into the furnace atmosphere under simulated run conditions to calibrate the flow-rate meter and to establish corrections for the time lag involved in transporting the activity from the irradiated pin to the counting assembly. These tests showed that the mixing of active and inactive gases was incomplete in the ten-minute period required to effect a complete gas cycle in the loop. The total activity in the recycled gas was, therefore, calculated as follows: In a given period of time, a certain fraction of the total gas in the system passed through the scintillation counter. The total activity in each fraction was determined by integrating the area under the activity peak observed by the counter. The activities in the fractions were then summed to give the total gaseous activity in the system at any particular time.

The conditions employed and the experimental results for the present experiment are reported in Figure 1. For comparison with these results data from the first fission gas release experiment are presented in Figure 2.

FIGURE 1
DIAMETRICAL EXPANSION AND FISSION GAS RELEASE DURING HEATING OF EBR-II-TYPE ALLOY PIN-EXPERIMENT FG-2
ALLOY COMPOSITION, URANIUM-5 WEIGHT PERCENT FISSIUM, LENGTH, ~1 6 in , DIAMETER, 0 143 in , TOTAL ATOM BURNUP, ~0 6 PERCENT, COOLING TIME, 106 DAYS
ATMOSPHERE HIGH PURITY ARGON (closed system), PRESSURE, 680 - 780 mm

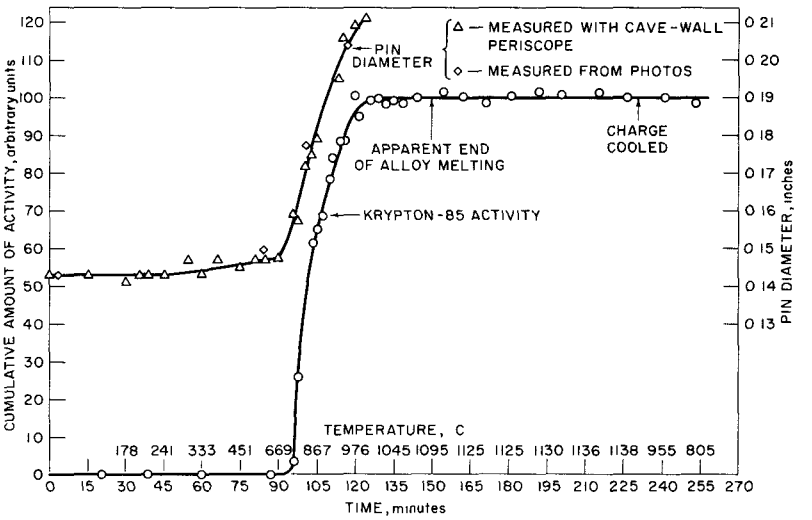

FIGURE 2
DIAMETRICAL EXPANSION AND FISSION GAS RELEASE DURING HEATING OF EBR-II-TYPE ALLOY PIN-EXPERIMENT FG-1
ALLOY COMPOSITION, URANIUM-5 WEIGHT PERCENT FISSIUM, LENGTH, 1 5 in , DIAMETER, 0 143 in , TOTAL ATOM BURNUP, ~0 6 PERCENT, COOLING TIME, 49 DAYS
ATMOSPHERE HIGH PURITY ARGON (closed system), PRESSURE, 685 - 790 mm

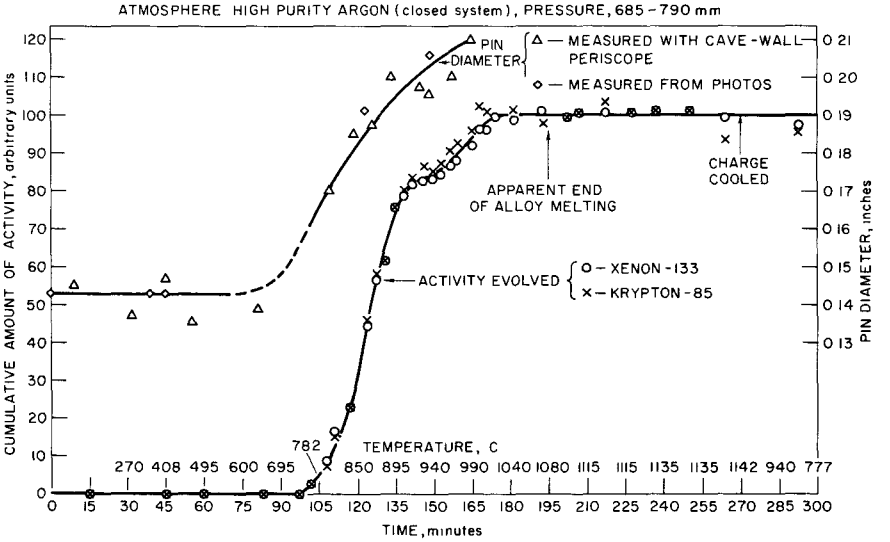

The first experiment was conducted in a similar manner except that the heating rate was slower. In both figures the arbitrary units of cumulative noble gas activity were adjusted to correspond to the percentage of the total amount of isotope evolved as functions of heating time and alloy temperature. The overall results of the experiments may be summarized as follows:

(1) Most of the krypton-85 and xenon-133 are released from the unrestrained fuel pins as they are heated over the temperature range of 700 to 1025 C. The temperature range in which rapid evolution occurred was not altered significantly by varying the heating rate. There was no observable release of gas when the molten alloy was allowed to cool rapidly.

(2) It was shown that essentially complete evolution of the noble gases had occurred when a temperature of 1025 C was attained in Experiment FG-2. The krypton-85 activity present in a sample of the gas in the system at the end of the experiment was compared with a sample of the gas evolved when the control pin was dissolved. Analyses of the samples indicated that 98.5 percent of the krypton activity was removed from the heated pin during the experiment. In consideration of the experimental errors involved, it is believed that the 98.5 percent value is indicative of complete removal of krypton.

(3) The rapid release of gas in both experiments was accompanied by an increase in diameter of about 47 percent as the alloy reached a temperature of 1000 C. At higher temperatures the pins no longer retained their cylindrical shape. The rough agreement of radial expansion as a function of temperature in the two experiments suggests that the heating rate has little effect on the ultimate expansion of the metal. The observations on expansion of the alloy during heating are in agreement with results reported by Monaweck and Sowa (ANL-6010, pages 29 to 31), which indicated that the dominant factor controlling unrestrained expansion of highly irradiated EBR-II-type fuel alloy (total atom burnup, 1.24 percent) was temperature. Their results showed that cast pins initially 0.144 inch in diameter, charged to a preheated furnace, attained maximum expansions to 0.183 inch at 871 C and 0.196 inch at 954 C within a few minutes. On further heating, no significant expansion occurred.

(4) In neither experiment did any spattering of metal occur as a result of expansion or rapid gas evolution. This observation was confirmed by a subsequent inspection of the aluminum boat used in the furnace assembly and by the recovery of 99.9 percent of the original weight of pins charged to the crucible.

(5) The temperature at which the alloy appeared to be fully molten, about 1080 C in Experiment FG-1 and 1095 C in FG-2, is in agreement with measurements made by Saller et al.,[3] which indicated that the completion of melting for a similar unirradiated alloy (except for the absence of ~0.01 percent niobium) was about 1081 C.

c. Nitride Formation on Sodium-coated Fuel Pins (J. P. LaPlante)

The purified argon atmosphere to be used in the EBR-II Fuel Cycle Facility is expected to contain nitrogen in concentrations up to five volume percent. It has been estimated that fission product decay heat will raise the temperature of the pins to 300 C during the various operations preceding the melt refining procedure. Since the formation of nitride shells on the fuel pins could prevent satisfactory coalescence of the metal in the melt refining step, the nitridation rates of metallic uranium under argon-nitrogen atmospheres are being investigated, with particular emphasis on the effects of fissium constituents, sodium coatings, and irradiation.

Nitridation rates of uranium and uranium-five percent fissium pins with and without sodium coatings in an argon atmosphere containing about five percent nitrogen were determined. The sodium coatings were prepared by subliming metallic sodium onto pins cleaned previously with a polishing wheel. The rates of nitridation were obtained from manometric measurements of the nitrogen consumed in a constant volume system.

FIGURE 3
NITRIDATION RATES OF URANIUM PINS

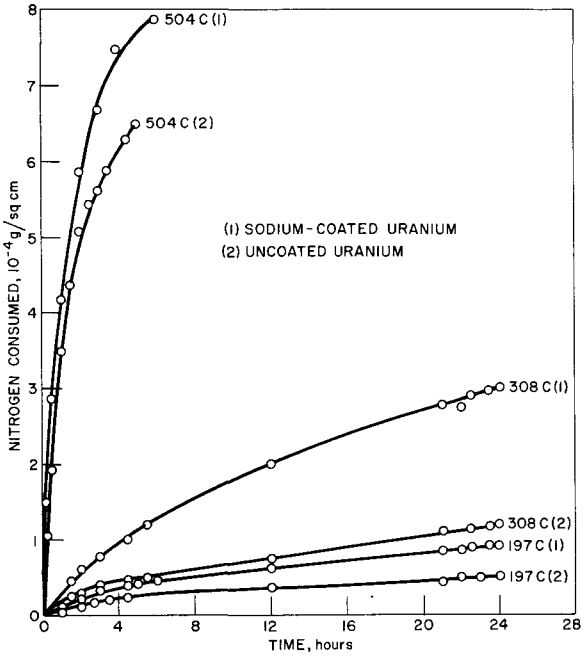

The nitrogen-uranium reaction followed a parabolic rate law at temperatures ranging from 197 to 504 C, with initial induction periods of less than 15 minutes. Since X-ray diffraction studies of uranium and uranium-five percent fissium pins show uranium oxide to be present as a very minor constituent, it is believed that a thin film of oxide may be responsible for the induction periods.

The amount of nitrogen consumed is plotted against time in Figures 3 and 4. If the logarithm of the

[3] Saller, H. A. et al., Properties of a Fissium-type Alloy, BMI-1123 August 3, 1956), pp. 20-21.

FIGURE 4
NITRIDATION RATES OF URANIUM-FIVE PERCENT FISSIUM ALLOY PINS

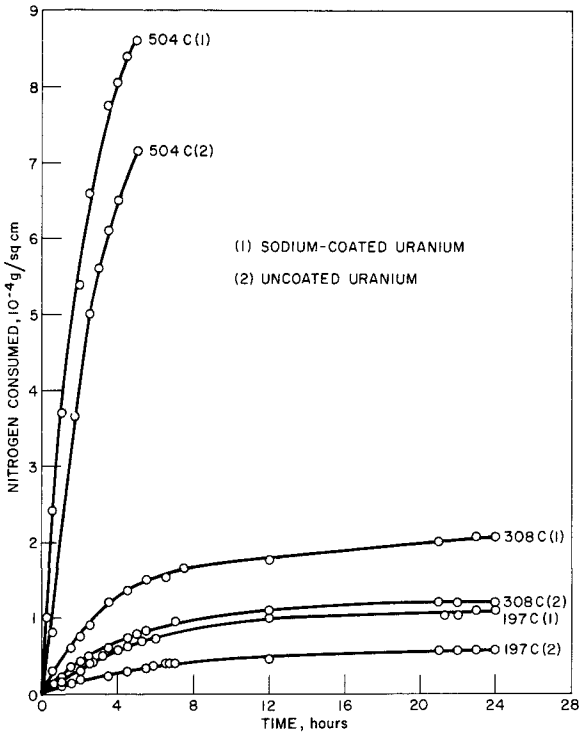

amount of nitrogen consumed is plotted against the logarithm of time, a straight line with a slope of approximately 0.5 is obtained, indicating that the parabolic rate law is applicable in this case. The experimental values for the slopes, along with rate constants calculated for each reaction by determining the slopes of lines resulting from plotting the square of the amount of nitrogen consumed per unit surface against time, are listed in Table 5.

Arrhenius plots of the rate constants (see Figures 5 and 6) show their temperature dependence. Experimental points from the four types of experiments fall on straight lines over the temperature range from 197 to 504 C when the logarithms of the rate constants are plotted against the reciprocal of absolute temperature.

Table 5

RATE CONSTANTS DETERMINED AT VARIOUS TEMPERATURES FOR THE REACTION OF NITROGEN WITH SODIUM-COATED AND UNCOATED URANIUM AND URANIUM-FIVE PERCENT FISSIUM PINS

Atmosphere: five percent nitrogen in argon

Sample Type	Coating	Slope of Log-Log Plot	Rate Constant, k x 10^{11} [(g/sq cm)^2/min] Temperature 197 C	308 C	504 C
Uranium	None	0 51	0.230	-	-
Uranium	None	0.55	-	5.00	-
Uranium	None	0 49	-	-	199 0
Uranium	Sodium	0.53	0 713	-	-
Uranium	Sodium	0.56	-	12.1	-
Uranium	Sodium	0.49	-	-	295 0
Fissium	None	0.52	0.236	-	-
Fissium	None	0 54	-	5 60	-
Fissium	None	0.50	-	-	186.0
Fissium	Sodium	0.53	0.938	-	-
Fissium	Sodium	0.56	-	15.2	-
Fissium	Sodium	0.54	-	-	325.0

FIGURE 5
TEMPERATURE DEPENDENCE OF PARABOLIC RATE CONSTANTS FOR NITRIDATION OF URANIUM PINS

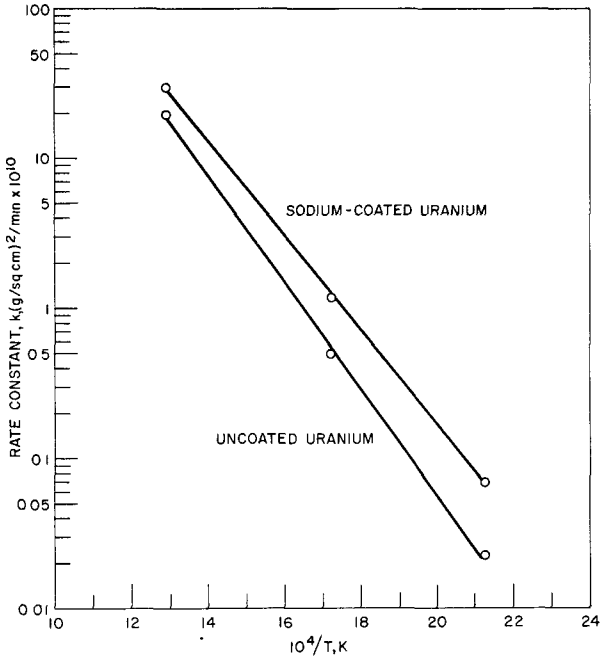

FIGURE 6
TEMPERATURE DEPENDENCE OF PARABOLIC RATE CONSTANTS FOR NITRIDATION OF URANIUM-FIVE PERCENT FISSIUM PINS

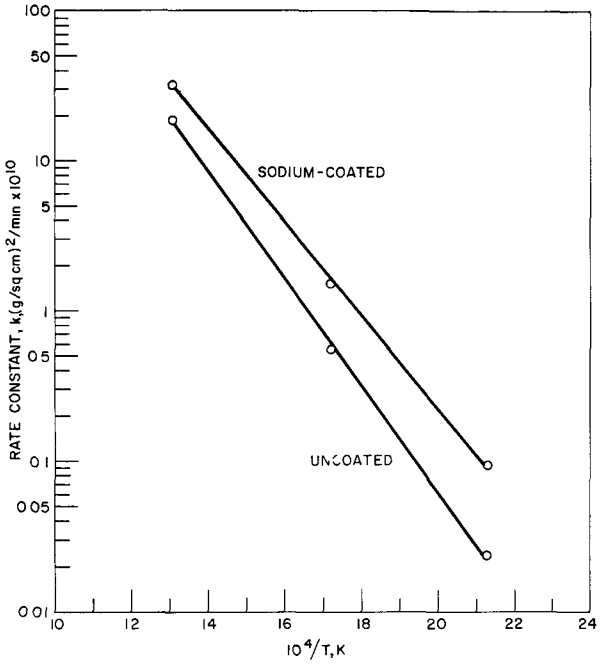

The Arrhenius-type equation,

$$k = A \exp(-\Delta E/RT) \quad ,$$

was determined for each line. The parabolic rate constants $[(g/sq\ cm)^2/min]$ for uranium and sodium-coated uranium pins were, respectively,

$$k = 6.29 \times 10^{-5} \exp(-16{,}000/RT)$$

and

$$k = 3.09 \times 10^{-5} \exp(-14{,}300/RT) \quad .$$

The activation energies for the reactions were 16.0 and 14.3 ± 2.0 kcal/mole. For the uranium-five percent fissium pins, without and with sodium coatings, the parabolic rate constants $[(g/sq\ cm)^2/min]$ were

$$k = 5.12 \times 10^{-5} \exp(-15{,}800/RT)$$

and

$$k = 2.58 \times 10^{-5} \exp(-13{,}800/RT) \quad .$$

The corresponding activation energies were 15.8 and 13.8 ± 2.0 kcal/mole. The probable error value for k is ±12 percent.

Extrapolation of the lines for uncoated pins in Figures 5 and 6 results in values of 5.2×10^{-9} $(g/sq\ cm)^2/min$ and 5.0×10^{-9} $(g/sq\ cm)^2/min$ for the parabolic rate constants of uranium and uranium-five percent fissium alloy,

respectively, at 600 C. The value for uranium at 600 C shows reasonable agreement with the value of 3.4×10^{-9} (ANL-5974, page 187) and with the values 8.0×10^{-9} and 4.0×10^{-9} $(g/sq\ cm)^2/min$ reported by Mallett and Gerds[4] and Adda,[5] respectively. The rate constant of 5.0×10^{-9} $(g/sq\ cm)^2/min$ for uranium-five percent fissium is comparable to the value of 5.4×10^{-9} $(g/sq\ cm)^2/min$ previously reported by J. G. Schnizlein (ANL-5974, page 187). An activation energy of 18.0 kcal/mole was reported by Adda[5] for the nitridation of uranium at temperatures between 350 and 660 C.

While the sodium-coated pins showed somewhat increased nitridation rates and slightly lower activation energies, the differences are not considered large enough to justify an investigation of differences in the mechanism of the reaction.

X-ray diffraction studies of the films formed through nitridation of the pins indicated that either U_2N_3 or UN_2 was present. It was not possible to distinguish between the two compounds by this method. Film thicknesses were calculated, assuming a uranium dinitride film to be distributed evenly over the pin with a density of 11.73 g/cc. The results are given in Table 6.

Table 6

CALCULATED VALUES FOR THE URANIUM DINITRIDE FILM THICKNESS

Atmosphere: 5 percent nitrogen in argon
Time: 24 hours

	Uranium Dinitride Film Thickness (μ) Temperature		
	197 C	308 C	504 C
Uranium pins	0.5	1.0	5.5
Uranium pins[a]	0.9	2.5	6.7
Fissium pins	0.5	1.0	6.1
Fissium pins[a]	1.0	1.8	7.3

[a] Sodium-coated.

[4] Mallett, M. W. and Gerds, A. F., Reaction of Nitrogen with Uranium, J. Electrochem. Soc., 102, 292 (1955).

[5] Adda, Y., Investigation of the Kinetics of the Reactions of Oxidation, Nitridation and Hydridation of Uranium, Gauthier-Villars, Editeur, Impriment Libraire, Paris (1958).

Photographs of the uranium-five percent fissium pins before and after nitridation are presented in Figure 7. The pins were sodium-coated prior to nitridation, and the sodium was removed after the experiment. The appearance of the unalloyed uranium pins was similar.

Figure 7

PHOTOGRAPHS OF URANIUM-FIVE PERCENT FISSIUM PINS
BEFORE AND AFTER NITRIDATION
At 504 C

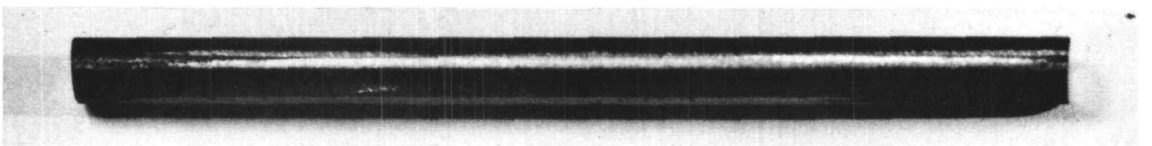

Before

After

d. Supplemental Melt Refining Pouring Techniques
(G. A. Bennett, W. A. Pehl)

It has been shown that under high-purity atmospheres the presence of sodium coatings on fissium pins has no significant effect on melt refining yields. In ANL-6231, page 49, a yield of 97.4 percent on a 2-kg scale was reported. This result was confirmed by a 96.5 percent yield in a duplicate run made in the past quarter. However, the nitridation of pins is possible through exposure for various lengths of time to the cell atmosphere of the Fuel Cycle Facility, which may contain up to five percent nitrogen. Melt refining yields may be affected adversely by these nitride coatings. Operating accidents, equipment failures, and other unexpected events may also result in lowered yields. Therefore, methods are being tested in the hope that they will enable the attainment of reasonably satisfactory yields under adverse circumstances.

The methods under consideration are limited to relatively simple techniques or devices which could be utilized in remote operation, e.g., application of vacuum to induce fracture of crusts or coatings by rapid evolution of dissolved gases, or application of simple mechanical devices. The investigations completed with this objective in mind are summarized in Table 7.

Table 7

EFFECT OF NITROGEN EXPOSURE AND VARIOUS POURING TECHNIQUES ON MELT REFINING INGOT YIELD

Experimental Conditions

Charge material: 5 percent fissium with cerium added
Charge quantity: ~2 kg
Coating material: none
Storage atmosphere: nitrogen at 40 mm pressure

Run No.	Charge Shape	Storage Conditions		Yield on Initial Pouring[a] (%)	Dross Appearance	Additional Pouring Technique	Total Yield after Additional Pouring (%)
		Temp (C)	Time (hr)				
290	Pins	300	47	91.9	Several pinshells only	None	91.9
277	Pins[b]	300[c]	66	70.0	Many pinshells	None	70.0
291	Pins	500	46	5.5	Numerous pinshells	Pinshells mashed	48.2
289	Massive metal	1200	17	0	Heavy crust	(1) Vacuum applied[d]	Very small (<5%)
						(2) Punctured crust at center	72
288	Massive metal	1200[e]	16.5	0	Heavy crust	Vacuum applied[d]	77
292	Massive metal	1200	16.5	0	Heavy crust	(1) Vacuum applied[d]	0
						(2) Punctured crust at pouring edge	47.5

[a] Yield obtained on pouring under one atmosphere of argon.

[b] Sodium-coated.

[c] Storage atmosphere for Run 277: 5 percent nitrogen-95 percent argon.

[d] Final vacuum: ~1 mm Hg.

[e] Storage atmosphere: 6 percent nitrogen-94 percent argon.

It should be pointed out that extreme conditions were chosen deliberately in order to produce pin coatings and crusts on the melts. Consequently, yield figures indicate in a qualitative manner only the extent of contamination and have no relation to expected plant yields. The difference between the yield on initial pouring and the total yield, given in Table 7, indicates the effectiveness of the supplemental pouring technique. The following preliminary conclusions may be drawn from these results:

(1) The reaction between bare uranium and nitrogen is slow at 300 C under practical process conditions, but is accelerated by an increase in temperature. The reaction also appears to be accelerated somewhat by the presence of sodium.

(2) The application of vacuum to effect a pour in the case of heavy crust formation is unreliable. The use of a "poker" to break through this crust into the molten metal beneath appears to be effective.

(3) The use of a mechanical "masher," in this case a tantalum cross attached to a tantalum rod, to break up pin shells and thereby allow drainage of molten metal from the inside, appears promising.

Future work will be undertaken to establish the effect of these devices under less severe conditions.

2. Liquid Metal Solvents Process Development
(L. Burris, Jr., R. K. Steunenberg)

Liquid metal processes are being developed for the recovery of fissionable material contained in the melt refining crucible skulls produced in the EBR-II fuel cycle and for the isolation of plutonium bred in blanket material. At the completion of the melt refining operation, approximately ten percent of the charge remains behind in the zirconia crucible in the form of a "skull" composed of metal and oxides. An auxiliary process is required to recover partially decontaminated uranium from the skull and return it to the melt refining process. Although complete fission product removal is not necessary, a substantial amount of each fission product element must be removed in order to maintain the proper fissium composition in the recycled fuel. The objective of the blanket process is to upgrade the plutonium concentration to a point sufficient for re-enrichment of the EBR-II fuel material (from 1 percent to about 50 percent plutonium in uranium).

Work on the skull reclamation process has led to the revised process flowsheet given in Figure 8. This process differs from the one presented in ANL-6183, page 41, in the following ways. A molten chloride salt flux is now being used in conjunction with a magnesium-zinc reducing

solvent. Since the magnesium concentration in this solvent is relatively low, the uranium appears in solution on reduction by the magnesium. The chloride flux markedly facilitates the reduction of oxides and acts as a vehicle for the suspension of and removal of the magnesium oxide reaction product. Quantitative reductions of skull oxide within two hours are reported for several flux compositions. Since the uranium is initially in zinc solution, the uranium, for purification purposes, is precipitated first as a uranium-zinc intermetallic and subsequently as uranium metal from a magnesium-rich solution. This order of precipitation is the reverse of the order reported in ANL-6183. In addition, the use of chloride flux permits consideration of noble metal removal by zinc reduction and leaching in a step preceding reduction of uranium oxides. Preliminary work indicates such a step to be effective.

FIGURE 8

LIQUID METAL PROCESS FOR RECLAMATION OF MELT REFINING SKULL MATERIAL

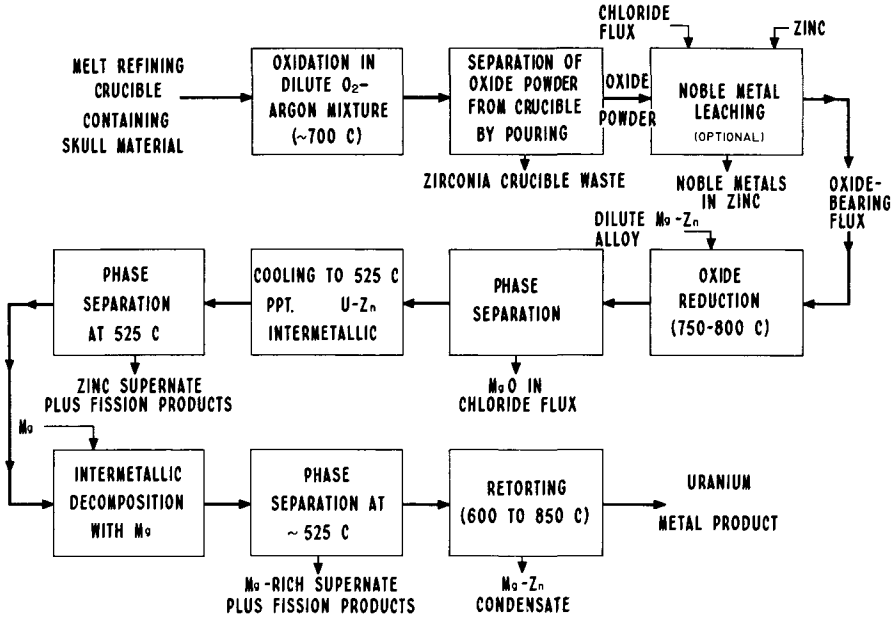

Work on the blanket process has included study of a potential process simplification involving the direct, low-temperature (~450 C) interaction of uranium and zinc to produce a uranium-zinc intermetallic. The plutonium present would be subsequently liberated and separated from uranium by decomposition of the intermetallic with magnesium in which the plutonium is soluble and the uranium is insoluble. The stabilities of various plutonium solutions in construction materials of interest were investigated.

a. Oxidation of Fissium Skulls
(R. D. Pierce, R. C. Cairns, L. F. Dorsey, R. Nowak)

Twenty-two crucible skulls containing cerium-uranium-fissium were oxidized to provide oxides for reduction studies. The oxidations were performed without difficulties at about 750 C in an atmosphere of 25 percent oxygen-argon at 800 mm total pressure. The success of these oxidations lends further confidence to this step of the skull recovery process.

Equipment has been constructed to study the behavior and methods of handling active volatiles formed during the skull oxidation step in the EBR-II skull reclamation process. Irradiation of 450 grams of uranium-fissium alloy, containing cerium, has been carried out in Argonne's CP-5 reactor.

b. Pyrometallurgical Reduction Studies

(1) Reduction of Skull Oxides by Magnesium
(T. R. Johnson, R. L. Christensen)

A possible method of reducing skull oxides from the EBR-II melt refining process is to contact the oxides with undiluted liquid magnesium. In previous experiments (ANL-6183, page 47), finely divided uranium dioxide (less than 100-mesh) was readily reduced to the metal by magnesium. The skull oxides, however, are expected to be considerably coarser than 100 mesh and to have varying compositions.

Several reductions of a typical skull oxide were conducted in undiluted liquid magnesium. The oxide was prepared by oxidizing a large melt refining crucible skull in an oxygen-argon atmosphere at 800 C. A screen analysis of the product is indicated in Table 8. It is interesting to note the variation in composition of the various screen fractions. The starting material for the reduction studies was prepared by recombining the screen fractions and quartering the material into eight 35-gram portions. Three of the portions were sampled by quartering and analyzed for uranium. The uranium contents of the three samples, 77.3, 76.6, and 77.5 percent, were consistent within the precision of the uranium analysis.

A 35-gram portion of the oxide was charged to a tantalum crucible, along with about 100 grams of magnesium and one gram of sodium. The sodium was added to improve wetting of the crucible by the liquid metal. Stirring was provided by a small propeller rotated at 1000 rpm, except in one run, where a large flat paddle was used. In both cases baffles were employed to provide efficient mixing. The reduction was conducted at 800 C in an argon atmosphere. Upon completion of the

run, sufficient zinc and magnesium were added to produce a final metal alloy containing 18 weight percent magnesium, 3 weight percent uranium, and 79 weight percent zinc. The system was then stirred at 300 rpm at 700 C.

Table 8

SKULL OXIDE FRACTIONS USED IN MAGNESIUM REDUCTION STUDIES

Mesh Size	Analysis (w/o) U	Ce	Mo	Ru	Zr	Percent in Original Skull Oxide	Percent in Charge Material[a]
+14	74.6	0.35	0.97	1.44	2	0.6	-
-14, +25	72.0	1.18	2.00	1.35	4	10.5	11.1
-25, +45	75.6	0.94	1.95	1.40	2	21.6	32.6
-45, +80	74.0	1.40	1.71	1.37	1	18.7	-
-80, +170	74.4	1.42	1.38	1.06	1	15.3	23.1
-170, +325	74.7	1.87	0.99	0.60	1	14.6	14.6
-325	74.1	2.60	0.86	0.32	1	18.6	18.6
Average	74	1.56	1.47	1.02	~2		

[a]Percentage of mesh size used in recombination of skull oxide.

The extent of the reaction cannot be determined from the uranium content of magnesium samples taken during the reduction, since the amount of metallic uranium that is present exceeds its solubility under these conditions. The addition of sufficient zinc dissolves the uranium and its concentration can then be determined by analyzing liquid metal samples drawn into tantalum tubes fitted with No. 60 graphite filters. It is possible, however, that a part of the reduction occurs after the zinc has been added to the system.

In general, the reduction yields achieved with undiluted magnesium were low, varying from 50 to 85 percent, and the reaction appeared to be sensitive to the conditions of the experiment. Grinding the skull oxide to a fine powder (-100 mesh) did not improve results appreciably. The large flat agitator blade appeared to provide slightly better stirring than the small twisted propeller. It has been concluded that the reduction of skull oxides by magnesium represents a potential alternative in the skull recovery process, but that zinc-low magnesium alloys are better suited to the purpose.

(2) The Use of Fluxes in the Reduction of U_3O_8 by Zinc-Magnesium Alloy
(J. B. Knighton, J. W. Walsh)

Both U_3O_8 and oxides of uranium-fissium alloy have been reduced successfully by magnesium and by zinc-magnesium alloy, with and without the use of Dow-230 flux (ANL-6231, page 56). The use of

a molten halide flux appears to be the most promising approach for reduction of this type. Advantages provided by such fluxes are (1) the reduction rates of uranium oxides are markedly increased by the proper choice of flux, (2) the magnesium oxide produced as a byproduct of the reaction is effectively collected in the flux and separated from the resulting zinc-magnesium-uranium alloy, and (3) the reductions can, if desired, be conducted in an air atmosphere, since the flux protects the alloy from oxidation.

In this study, the initial approach to the reduction problem consisted of defining those flux systems which cause the most rapid and quantitative reduction of U_3O_8 by zinc-magnesium alloy. Following this survey, studies can be made with the optimum flux composition to establish the most favorable operating conditions for rapid, complete reduction.

In the initial survey, the variable under study was the flux composition; all other variables were held constant. The chlorides of lithium, sodium, potassium, magnesium, calcium, strontium, and barium were employed as the major flux components. The bulk of the flux consisted of equimolar concentrations (47.5 mole percent each) of two chloride salts of the above-mentioned alkali and alkaline earth metals. The cations in the different fluxes were present in the same molar proportions. Five mole percent magnesium fluoride was added to all the fluxes to achieve a clean flux-metal interface.

All the experiments were performed in air atmosphere, using a tapered-wall alundum crucible supported in a resistance furnace. Mixing was accomplished by means of a quartz propeller-type agitator rotated at 800 rpm. About 400 grams of zinc-five weight percent magnesium and 200 grams of the selected flux were used to provide approximately equal volumes of the two phases. The uranium oxide was added to the flux phase in a quantity sufficient to produce a uranium concentration of 1.0 weight percent in the final ingot. Samples of the metal phase were withdrawn into Vycor tubes at various time intervals up to two hours and analyzed for uranium. Silicon and aluminum concentrations in the metal phase were less than 20 ppm, indicating that neither the quartz agitator nor the alundum crucible was attacked by the flux-metal system.

The process variables, i.e., mixing rate, temperature, final uranium concentration in the zinc, magnesium content of the zinc, uranium oxide source and particle size, quantity of flux and alloy, and geometry of the system, were arbitrarily fixed and maintained constant throughout the series of experiments. The effect of flux composition was then evaluated on the basis of rate and extent of reduction as a function of time.

The results of the survey study are given in Table 9.

Table 9

SURVEY OF FLUXES FOR U_3O_8 REDUCTION

Conditions:
- Temperature: 750 C
- Mixing: 800 rpm with quartz stirring rod
- Atmosphere: Air
- Crucible: Alumina
- Metal Charge: 400 grams zinc-5 w/o magnesium
- Flux Charge: 200 grams of selected flux
- U Conc: 1% uranium in metal at 100% reduction

Run No.	Flux Composition			Percent Reduction at Times of				
	47.5 m/o	47.5 m/o	5 m/o	10 min	20 min	30 min	60 min	120 min
UR 31	LiCl	$MgCl_2$	MgF_2	99.9+	99.9+	99.9+	99.9+	99.9+
UR 43	NaCl	$MgCl_2$	MgF_2	86.0	99.4	99.4	99.4	99.4
UR 44	KCl	$MgCl_2$	MgF_2	85.1	94.8	94.8	94.8	94.8
UR 32	LiCl	$CaCl_2$	MgF_2	26.7	44.0	56.0	86.0	99.8
UR 45	NaCl	$CaCl_2$	MgF_2	23.6	30.8	39.4	60.0	84.0
UR 46	KCl	$CaCl_2$	MgF_2	13.6	18.0	21.4	31.3	41.0
UR 33	LiCl	$SrCl_2$	MgF_2	25.4	42.0	59.4	95.0	96.0
UR 48	NaCl	$SrCl_2$	MgF_2	8.0	13.0	20.8	40.2	70.3
UR 36	KCl	$SrCl_2$	MgF_2	2.5	3.8	4.9	8.0	10.0
UR 35	LiCl	$BaCl_2$	MgF_2	12.5	21.6	26.0	52.0	85.0
UR 64	NaCl	$BaCl_2$	MgF_2	12.5	19.9	27.3	31.3	44.6
UR 49	KCl	$BaCl_2$	MgF_2	4.0	5.3	10.3	18.0	19.0
UR 39	LiCl	NaCl	MgF_2	5.7	9.0	8.8	13.3	23.4
UR 40	LiCl	KCl	MgF_2	4.0	3.0	3.0	6.0	7.0
UR 50	KCl	NaCl	MgF_2	2.1	3.0	3.0	6.0	12.8
UR 37	$CaCl_2$	$MgCl_2$	MgF_2	97.0	99.+	99.+	99.+	99.+
UR 41	$SrCl_2$	$MgCl_2$	MgF_2	99.0	99.0	99.0	99.0	99.0
UR 42	$BaCl_2$	$MgCl_2$	MgF_2	92.0	99.6+	99.6+	99.6+	99.6+
UR 51	LiCl	LiCl	LiF	10.0	11.0	12.0	17.0	23.1
UR 52	$MgCl_2$	$MgCl_2$	MgF_2	97.5	99.9+	99.9+	99.9+	99.9+

Several pertinent observations can be made from these data:

(1) Certain fluxes permit rapid and quantitative reduction of uranium oxides by zinc-five weight percent magnesium in simple equipment, under an air atmosphere.

(2) There is a definite correlation between the reducibility of a system and the atomic weights of the alkali and alkaline earth cations present in the molten chloride flux, the best reductions occurring with the lighter cations.

(3) When combinations of the Group I cations (lithium, sodium, and potassium) and Group II cations (magnesium, calcium, strontium, and barium) are used, the rate and degree of completion of the reduction decrease progressively in the order lithium, sodium, potassium and in the order magnesium, calcium, strontium, barium. For example, the following fluxes, each containing lithium chloride, are listed in decreasing order of effectiveness:

lithium chloride-magnesium chloride-magnesium fluoride

lithium chloride-calcium chloride-magnesium fluoride

lithium chloride-strontium chloride-magnesium fluoride

lithium chloride-barium chloride-magnesium fluoride

A similar trend is found for fluxes containing sodium chloride or potassium chloride in common. The only exception to the trend was the potassium chloride-barium chloride-magnesium fluoride system, which produced better reductions than the potassium chloride-strontium chloride-magnesium fluoride system.

Similar results were obtained when a common Group II cation was used and the Group I cation was varied. In all the combinations tested, the lithium chloride fluxes gave the best reduction and the potassium chloride fluxes gave the poorest.

(4) Systems containing 95 mole percent or more of Group I cations gave poor reductions.

(5) Systems composed entirely of Group II cations produced rapid and complete reductions.

(6) Magnesium chloride, in particular, was present as a major component (47.5 mole percent or more) in all experiments in which complete reduction was achieved within 30 minutes. Thus, magnesium chloride is considered to be an essential ingredient of any flux chosen for effective reduction of uranium oxides.

While the reduction of uranium oxides by zinc-magnesium alloy in the presence of flux is being investigated primarily as a potential step in the EBR-II melt refining skull recovery process, it has potential application in a much wider area. For example, the very low losses of uranium to the flux phase suggest its use for the direct production of uranium metal from the oxide. It also shows promise for application in other pyrometallurgical fuel reprocessing schemes, such as the processing of oxide or carbide fuels.

(3) Reduction of Fissium Skull Oxides with Magnesium-Zinc Solutions

(R. D. Pierce, L. F. Dorsey)

Studies, on a 200-gram-uranium scale, have been made of the reduction of fissium skull oxides at 800 C with solutions of magnesium in zinc, both in the presence and absence of a molten chloride salt flux. These reductions were conducted with sufficient zinc solvent to dissolve all the reduced uranium.

FIGURE 9
REDUCTIONS OF FISSIUM SKULL OXIDE AT 800 C WITH MAGNESIUM-ZINC SOLUTIONS IN ABSENCE OF CHLORIDE FLUX

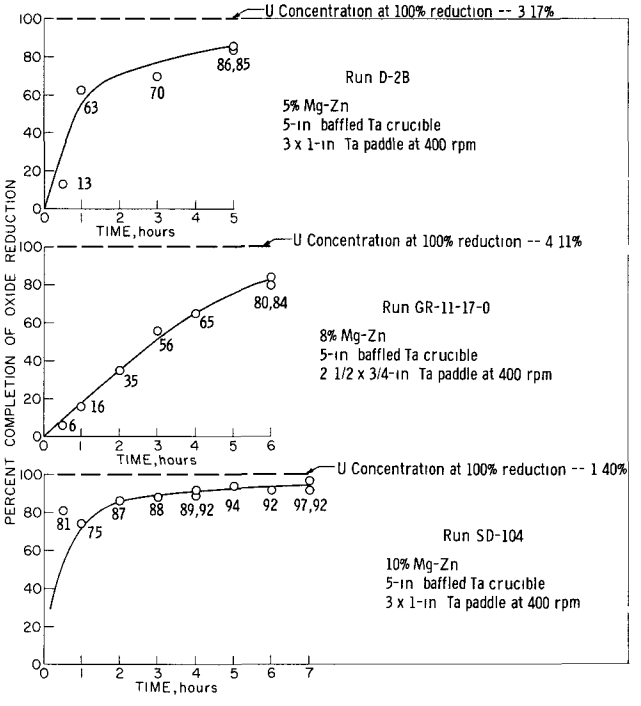

In the absence of a chloride flux, reductions of fissium skull oxides were rapid and nearly quantitative when a ten percent magnesium concentration was used, but were much slower at a five percent magnesium concentration (see Figure 9). The reductions without flux do not appear attractive for the skull recovery process because of the behavior of the magnesium oxide that is produced. This oxide clumps, principally at the liquid surface, and entraps some unreacted skull oxide. The magnesium oxide also retains large amounts of zinc solution despite attempts to transfer away this liquid phase by pouring, siphoning, or filtering. Although the uranium might be recovered from retained zinc by washing the magnesium oxide with fresh zinc, removal of the final waste magnesium oxide from the crucible appears extremely difficult. Consequently, no further reduction studies of this type are planned.

The use of a salt flux in these reductions has successfully eliminated the problems caused by magnesium oxide. Quantitative skull oxide reductions were obtained in the four runs that were made with 5 to 10 percent magnesium in zinc (see Figure 10). These reductions went to completion within two hours. Run SD-108 is especially interesting because large "clinkers" (0.4 to 1.2 cm) of oxidized skull were charged and were successfully reduced within a two-hour period. The other runs used the full range of oxide particle sizes that result from oxidation of a skull (see ANL-6231, page 55).

FIGURE 10

REDUCTIONS OF FISSIUM SKULL OXIDE AT 800 C WITH MAGNESIUM-ZINC SOLUTIONS IN PRESENCE OF CHLORIDE FLUX

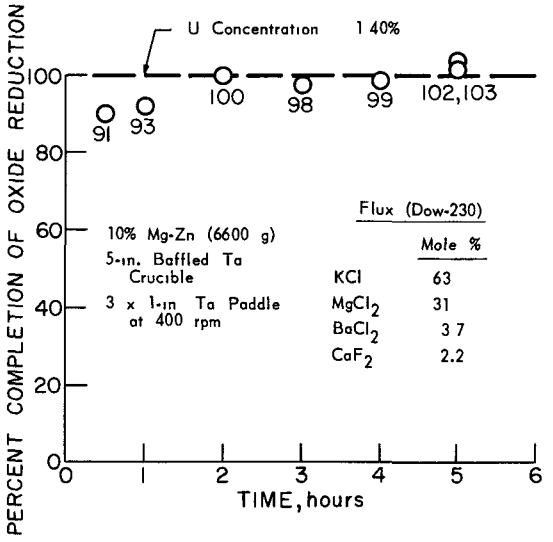

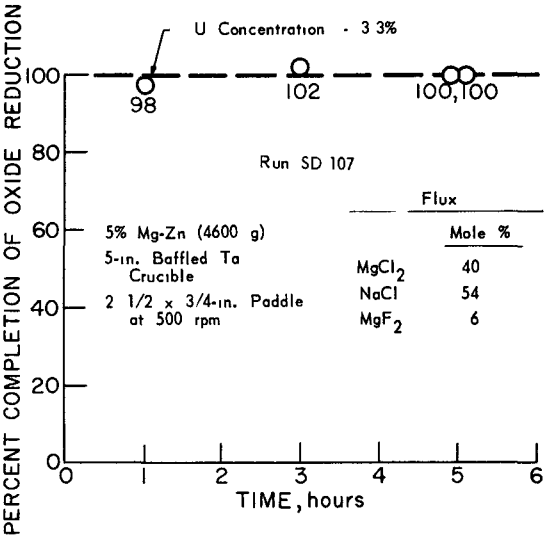

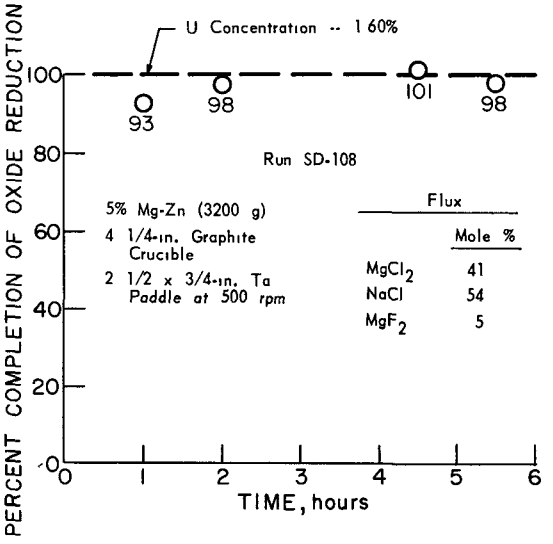

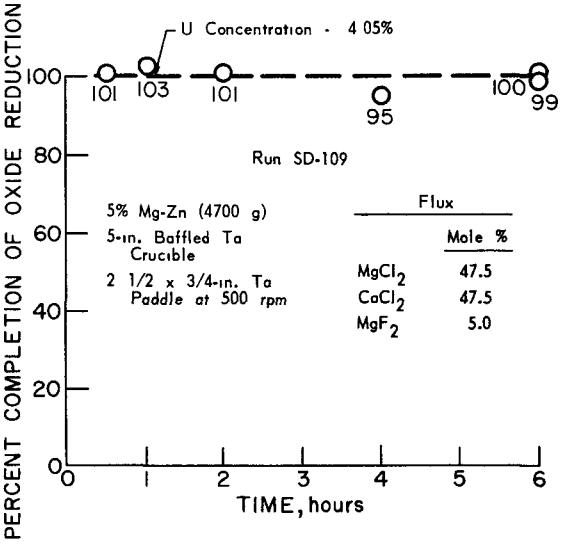

The fluxes used in Runs SD-107, -108, and -109 (listed in Figure 10) were those which, in laboratory studies, provided a sharp metal-salt interface and enhanced the reduction as well. While distribution of the magnesium oxide was not determined, the good quality of the zinc ingot and the results of studies on magnesium oxide distribution (see page 65) indicate that the magnesium oxide is in the salt phase.

(4) The Reduction of Plutonium Dioxide by Zinc-Magnesium Alloy in the Presence of Flux
(J. B. Knighton, I. O. Winsch, T. F. Cannon)

The effectiveness of molten salt fluxes in promoting the reduction of uranium oxides suggests the possibility of reducing plutonium dioxide in the same manner. An experiment was performed in which plutonium dioxide was reduced by a zinc-five weight percent magnesium alloy in the presence of a molten halide flux. The composition of the flux, expressed in mole percent, was calcium chloride, 47.5; magnesium chloride, 47.5; and magnesium-fluoride, 5.0. The reduction was conducted to 750 C under a helium atmosphere in a tantalum crucible. The system was agitated with a tantalum paddle stirrer. The duration of the run was two hours, and filtered samples of the metal phase were taken at 30-minute intervals. The sampling tubes were made of tantalum and fitted with graphite filters. Sufficient plutonium dioxide was added to yield a zinc-magnesium alloy containing 0.54 weight percent plutonium at complete reduction.

When the reduction was completed, the metal and flux were poured into a graphite mold. Upon cooling, the flux and metal were easily removed from the mold and separated with a very clean interface. The entire flux was submitted for plutonium analysis.

The preliminary results, given in Table 10, indicate that the reduction was essentially quantitative by the time the first 30-minute sample was taken.

Table 10

REDUCTION OF PLUTONIUM DIOXIDE BY ZINC-MAGNESIUM IN THE PRESENCE OF FLUX

Temperature: 750 C
Stirring: tantalum paddle, ~ 400 rpm
Container: tantalum
Atmosphere: helium

Sample	Time (min)	Plutonium Content of Metal Phase[a] (weight percent)	Sample	Time (min)	Plutonium Content of Metal Phase[a] (weight percent)
1	30	0.57	4	120	0.53
2	60	0.52	flux	120	0 0084
3	90	0.52			

[a] Theoretical value at complete reduction: 0.54 percent

Samples taken subsequently showed that the plutonium concentration in the zinc-magnesium alloy remained constant within the analytical uncertainty. The flux analysis showed only 0.015 gram of plutonium in the entire flux at the end of the run. Based on the flux analysis, the reduction was at least 99.8 percent complete.

(5) Removal of Ruthenium from Fissium Skull Oxide by Zinc Leaching
(J. C. Hesson, K. R. Tobias)

Although the solubility of ruthenium in liquid metal solutions of the skull reclamation process may be adequate for achieving the required separation, it became of interest to determine whether ruthenium (as oxides or metal) could be reduced and leached from fissium skull oxide by molten zinc. Other noble metals would be expected to behave similarly.

Two experiments were made in which skull oxide (100 grams containing 1.5 percent ruthenium) was contacted with zinc at about 775 C under an argon atmosphere. Zinc alone (578 grams) was used in one run, while in the other, both zinc (705 grams) and a Dow 230 chloride flux* (200 grams) were employed. Filtered metal samples indicated that in both experiments essentially all the ruthenium transferred to the zinc phase. In the absence of flux, ruthenium results were somewhat erratic and some exceeded the theoretical concentration. Analyses of the samples for uranium indicated no inclusion of uranium oxide. When a flux was employed, complete ruthenium transfer was effected in about nine hours (see Figure 11).

When no flux was used, the skull oxide was not wetted by the zinc nor incorporated into it. Consequently, separation of the zinc and oxide might be difficult. When flux was used, the skull oxide was in the flux phase.

c. Demonstration of Skull Recovery Process
(R. D. Pierce, T. R. Johnson, J. F. Lenc, J. C. Hesson, L. F. Dorsey, K. R. Tobias, M. A. Bowden)

Solidification of material in the transfer tube caused considerable experimental difficulty in the previous runs of the skull reclamation process (ANL-6183, page 42). The experimental equipment has been modified to avoid cold spots in the transfer tube.

---

*Dow 230 chloride flux has the following composition, expressed in mole percent: potassium chloride, 63; magnesium chloride, 31; barium chloride, 3.7; and calcium fluoride, 2.2.

FIGURE 11

LEACHING OF RUTHENIUM FROM FISSIUM SKULL OXIDE WITH ZINC IN PRESENCE OF DOW-230 FLUX

CONDITIONS:
SYSTEM AGITATED UNDER ARGON ATMOSPHERE AT 775C IN PRESENCE OF DOW-230 FLUX:

KCl - 63 mole % $BaCl_2$ - 3.7 mole %
$MgCl_2$ - 31 mole % CaF_2 - 2.2 mole %

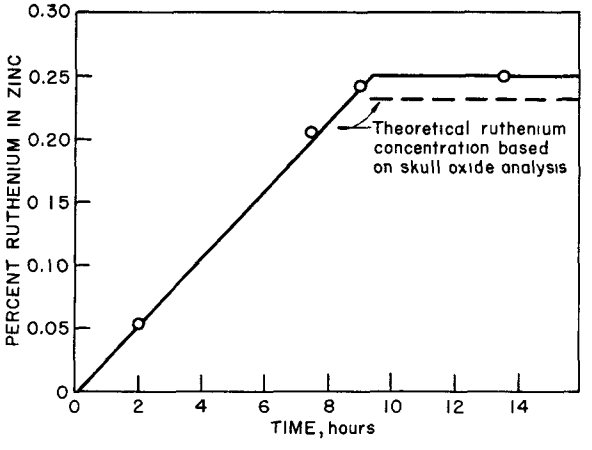

The modified equipment will be employed in a new series of runs to demonstrate the revised recovery process shown in Figure 8, page 49. The noble metal removal step probably will not be incorporated until laboratory studies of this step are further advanced.

The revised equipment has operated satisfactorily in preliminary tests. Two separations of salt and metal phases have been made without difficulty by successive pressure-siphon transfers. These separations were accomplished by forcing out liquid metal by means of pressure until the interface was $\frac{1}{8}$ inch from the bottom of the transfer tube in one run, and $\frac{1}{4}$ inch in the other. By tilting the furnace slightly, to bring the bottom of the transfer tube into the salt phase, a similar transfer of the salt phase was effected. The receiver bomb was opened after the metal transfer for insertion of a new receiver into which the salt was transferred.

Small-scale studies of the use of filtration as the method of separating precipitated uranium-zinc intermetallic or uranium metal phases have been made. In the course of this work, a complete small-scale demonstration run of the skull reclamation process was made employing filtration as the phase-separation procedure.

Filtration of Precipitated Metal Phases

The filter and receiver crucible assembly shown in Figure 12 was employed to test pressure filtration as a method of separating supernatant liquid metals from precipitated uranium phases.

FIGURE 12
GRAPHITE (CS)
FILTER AND RECEIVER
CRUCIBLE ASSEMBLY

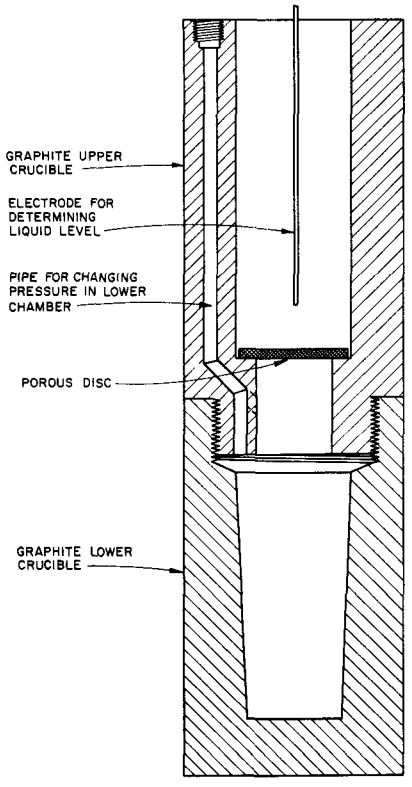

The precipitation of uranium from zinc solution by cooling to 550 C and a subsequent pressure filtration to remove the supernatant zinc phase were accomplished readily in two runs. Analyses of the zinc filtrates showed the concentration of uranium to be that of its solubility in zinc at 550 C (namely 0.05 per cent).

Subsequently, the intermetallic cakes were decomposed by adding magnesium to a concentration of about 50 weight percent in the available zinc. Filtration of the magnesium-rich supernatant liquid metal was also readily accomplished at 700 C. Stirring was shown to be essential, since, without stirring, a zinc-rich layer having a relatively high solubility for uranium remained near the bottom of the filter unit. The filtrate from an unstirred melt contained 2.2 percent uranium as contrasted with only 0.03 percent from a stirred melt. In one run the uranium cake was retorted to vaporize the solvent metals and later coalesced into a 10-gram metal button by arc melting.

Small-scale Demonstration Run

A small-scale (20 grams of skull oxide) demonstration run of the skull reclamation process was carried out stepwise by means of the relatively simple filtration equipment shown in Figure 12. The reduction step was carried out in the presence of a chloride flux (53 mole percent sodium chloride, 41 mole percent magnesium chloride, and 6 mole percent magnesium fluoride). Separation of the flux phase was accomplished at 800 C by forcing the uranium-zinc solution by means of pressure through the filter until a $\frac{1}{8}$-inch metal heel plus the flux remained. The upper filter chamber was cleaned out and the product ingot recharged for precipitation of a uranium-zinc intermetallic by re-solution of the uranium at 800 C and cooling. After filtering off the zinc, magnesium was added to the intermetallic cake and stirred at 700 C, thereby liberating uranium metal. The supernatant metal phase was forced through the filter by means of pressure, and the uranium cake was then retorted in place, removed, and analyzed.

In small-scale intermittent operations such as described above, losses, which would not occur in repetitive plant processing, are high, e.g., metal heels and metal adhering to stirrer, baffles, and crucible walls. Therefore, the yield of metal as uranium product was only

55 percent (8.3 grams out of 15 charged). However, process losses, as represented by uranium losses in the metal filtrates and the fused salt flux were low, amounting to only 2.7 percent of the uranium charged. The uranium material balance was 96 percent.

As compared to the initial material, fission product concentrations in the product uranium had been reduced by the following factors: cerium, 20; molybdenum, 20; and zirconium, 12. The bulk of the cerium was removed, as expected, in the magnesium-rich supernatant liquid resulting from decomposition of the uranium-zinc intermetallic. Most of the molybdenum was removed on the first filtration of the uranium-zinc product solution. Of the 0.2 gram of molybdenum initially present, 0.06 gram was present in the metal heel from this filtration (as expected because of the low solubility of molybdenum in zinc), 0.03 gram adhered to the stirrer and baffle, and 0.04 gram remained in the flux. The high molybdenum content of the salt flux is surprising and will be further investigated. The reasons for the good zirconium removal are not apparent. The level of ruthenium concentrations in this run was too low to be followed.

This small-scale run provides encouragement that adequate fission product removals can be achieved. Additional information on both uranium yield and fission product distribution will be provided by the forthcoming demonstration runs upon a larger scale.

d. The Removal of Magnesium Oxide from Liquid Metals

The objective of this work is the development of a practical method for the separation of magnesium oxide, formed during the reduction of uranium oxides by liquid magnesium or by liquid magnesium-zinc alloys, from the resulting uranium metal or uranium solution. This separation is necessary to avoid the carryover of magnesium oxide with the recycled uranium to the melt refining step, where it would cause difficulty in coalescence of the uranium with resultant low pouring yields.

(1) Separation and Identification of Magnesium Oxide (A. Schneider, G. Rogers, D. Knoebel*)

The reduction of uranium oxide by magnesium in liquid metal was reported previously (ANL-6183, page 50). In examining various possible methods for the removal of the magnesium oxide from the liquid metal, it was deemed desirable to characterize this oxide with regard to its composition, particle size, and specific gravity. The presence of magnesium oxide and alpha uranium in a residue resulting from the retorting of a reduction ingot was demonstrated by X-ray diffraction techniques. However, the

*Summer student employee.

separation of this oxide, for characterization purposes, from the associated uranium product is difficult. Therefore, pure magnesium oxide resulting from an oxidation-reduction reaction in a liquid metal was more conveniently prepared by contacting zinc oxide powder with a magnesium-cadmium melt, since all components, except magnesium oxide, in the reduction ingot (zinc, magnesium, and cadmium) can be removed quantitatively by vacuum retorting. The completeness of the reduction was ascertained by determining the zinc content of filtered samples withdrawn from the melt. The retorting residue was found to be pure magnesium oxide, its X-ray diffraction pattern being in excellent agreement with that of Swanson and Tatge.[6] The particles of the oxide ranged in size between 1 and 10 microns. The specific gravity of this material was about 3.5.

(2) The Quantitative Determination of Magnesium Oxide in Metal Ingots or Liquid Solutions
(A. Schneider, G. Rogers)

Before various separation schemes could be tested, it was necessary to develop reliable sampling and analytical methods for the determination of magnesium oxide. The following procedures were used in this work: (1) the determination of the relative magnesium oxide concentration in various locations of an ingot containing magnesium, uranium, and cadmium or zinc; and (2) the determination of the total amount of magnesium oxide present in an ingot.

The first procedure is useful in determining whether a separation method based on differences in specific gravity between magnesium oxide and the liquid metal solution can be applied to a particular system. The procedure consists of retorting fractions of an ingot, taken from several locations, to remove the volatile components. The residue, consisting of magnesium oxide, uranium, and uranium oxides, is dissolved in nitric acid and the magnesium content obtained by titration with ethylenediamine tetraacetic acid. The retortings were carried out in the still described in ANL-6183, page 47. The still was fitted with a tantalum liner to permit the distillation of zinc. The retorting efficiency was checked in several blank runs; the results obtained are given in Table 11. It is evident that the weight of the residue corresponded closely with the amount of magnesium oxide added.

In the second procedure, which is necessary for the evaluation of the efficiency of a given separation scheme, the magnesium oxide was first extracted from the liquid metal into a molten salt mixture; this was followed by a determination of the magnesium oxide content in the salt.

---

[6]Swanson, H. E., and Tatge, E., Standard X-ray Diffraction Patterns, NBS Circular 539 (1953).

Table 11

RESULTS OF RETORTING EXPERIMENTS

Charge (grams)					Residue	
Mg	MgO	Cd	Zn	U	Weight (gram)	Deviation of Weight from Theoretical (percent)
7.0483	-	-	-	-	0.0026	+0.03
-	-	4.9221	-	-	0.0014	+0.03
-	0.1890	-	-	-	0.1781	-5.6
1.8074	0.1628	5.3689	-	0.6072	0.7584	-1.5
4.0839	-	-	-	-	0.0193	+0.47
1.0983	-	-	7.4186	-	0.0143	+0.27

(3) The Separation of Magnesium Oxide from Reduced Uranium

Three methods have been considered for the separation of magnesium oxide formed during the reduction of uranium oxide:

a) filtration of a solution containing all the uranium;

b) liquation of the melt to induce the magnesium oxide to rise to the surface of the metal solution, with subsequent withdrawal of the bulk of this solution from below the surface; and

c) extraction of magnesium oxide with a molten salt mixture.

(a) Separation of Magnesium Oxide by Filtration (J. C. Hesson, K. R. Tobias)

Two runs were performed to examine filtration as a means of separating magnesium oxide from liquid magnesium-zinc solutions. Previous efforts to remove magnesium oxide from cadmium-magnesium solutions by filtration had been somewhat discouraging because the filters gradually became plugged (ANL-6068, page 61). In this earlier work, approximately 1-inch filter frits of graphite or steel were forced into fittings in the open end of a dip tube through which the metal solution was forced by pressure. The scale of operation was 500 to 1000 grams of metal per square centimeter of filter area.

In the two new runs, approximately 335 grams of a zinc-10 percent magnesium ingot from a reduction run were melted in each of two graphite crucibles, the one having a grade 40 and the other a

grade 60 graphite filter (69 and 33 micron pore sizes, respectively) in the bottom. Filtration of 50 grams of metal per square centimeter of filter area was readily achieved. Most of the residue in the crucible remained in the upper portion as a spongy mass so that a relatively small proportion of residue was actually on the filter.

Table 12 presents the conditions and results of these two experiments. The efficiency of magnesium oxide removal appeared to be good in the small-scale experiments. Filter plugging was not a problem with this small volume.

Table 12

FILTRATION OF MAGNESIUM OXIDE FROM ZINC-10 PERCENT MAGNESIUM SOLUTION

Filters: Grade 40 graphite in Run 137;
grade 60 graphite in Run 138

Charge: 332 grams in Run 137; 339 grams in Run 138

	Conditions of Filtration			Wt of Filter Cake (g)	Wt of Retorted Cake (g)	% Metal Vaporized from Cake	Minimum Efficiency of MgO Removal[a]
Run	Temp (C)	Time (min)	Pressure (psi)				
137	780	7	1.5	68.4	9.3	86	99
138	830	12	2.5	24.0	1.25	95[b]	94

[a]Based on retorting about 20 percent of filtrate and attributing the residue weight to magnesium oxide after deduction of uranium present in residue as obtained by analysis.

[b]Retorted cake contained 12 percent uranium. No analysis made in first run.

Two points should be made with regard to filtration. One is the large holdup of metal with the oxide residue in the filter crucible. In plant operation, this holdup of metal would necessitate a metal-washing operation to remove the contained uranium. The second point is that a method of removal of magnesium oxide from the crucible must yet be found. For these reasons, filtration of magnesium oxide does not appear attractive.

(b) Separation of Magnesium Oxide by Liquation and Liquid Metal Removal
(A. Schneider, G. Rogers)

The separation of magnesium oxide by liquation and liquid metal removal appeared feasible for magnesium-zinc and magnesium-cadmium systems, which are considerably heavier than magnesium oxide, but was shown to be impractical for magnesium melts (ANL-6183, page 50). Several experiments were performed in which U_3O_8 was reduced by a five percent magnesium-zinc solution. The longitudinal distribution of magnesium oxide in the solidified ingot showed that migration of magnesium oxide in the molten material proceeds slowly. In one experiment, over 40 percent of the magnesium oxide was carried to the bottom of the ingot during solidification, probably by entrapment in the intermetallic compounds formed on cooling. As with filtration, it was also found that an appreciable quantity of metal remained associated with the magnesium oxide after pouring off the liquid metal from the crucible. The removal of the crucible residue could prove to be quite difficult. These observations indicate that this method is not promising. It was also found that some unreduced uranium oxide concentrated near the surface of the melt.

(c) Separation of Magnesium Oxide by Fused Salt Extraction
(A. Schneider, G. Rogers)

The removal of magnesium oxide by fused salt extraction was studied as a separate step following the reduction of uranium oxide or as a simultaneous process by carrying the reduction out in the presence of the molten flux. The results are shown in Table 13.

Table 13

THE SEPARATION OF MAGNESIUM OXIDE FROM LIQUID METAL PHASES

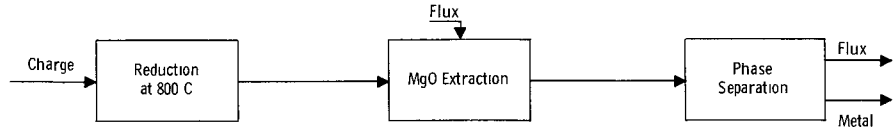

Exp No	Charge, grams			Time hrs	Reduction (w/o)[a]	Flux, grams					Final Reduction (w/o)[a]	MgO Partition, a/o	
	Zn	Mg	U_3O_8			$MgCl_2$	NaCl	KCl	NaF	CaF_2		Metal	Flux
10-19-0	4000	350	220	5	88 to 90	-	335	426	38	-	-	1	93 ± 3
11-3-0	577	30	10	7	92	15	-	61	-	4	100	0	95 ± 5
11-17-0	4008	354	220	6	84	150	-	610	-	40	97	2	100
12-7-0[b]	-	99	30	4	100	28	72	-	4	-	-	8	92

[a]Reduction yield based on uranium contents of filtered metal samples, except in Exp 12-7-0, where yield was determined by hydriding method (see ANL-6183, p. 46) In Exp 10-19-0, lower yield obtained from decrease of magnesium content of melt.

[b]Reduction carries out in presence of flux at 728 C no separate extraction step.

The composition of the flux was governed by the desired melting range (generally above that of the metal phase) and its stability when contacted by a solution containing uranium and magnesium. The flux used in Experiment 10-19-0 was found to be unstable in a blank run, as evidenced by the decrease in uranium and magnesium contents of the molten metal, by the appearance of some magnesium in the flux, and by the volatilization of sodium.

Fluxes containing magnesium chloride were found to be stable and were used in subsequent experiments. The results in Table 13 show that a high (over 90 percent) removal of magnesium oxide was accomplished by fused salt extraction. Since it has also been found that the presence of suitable fluxes enhances the reduction rate of uranium oxides in liquid metals, this is considered to be the preferred method for the removal of magnesium oxide.

For reductions in pure magnesium (Experiment 12-7-0), the solidified ingot consisted of two separate metal phases, located at the top and bottom of the ingot, and embedded in the flux phase. The bulk of the magnesium was in the upper metal phase. The heavier metal phase consisted of the reduced uranium wetted by a small amount of magnesium. The uranium content of the flux was very low. The fact that the uranium metal separated from the bulk of the magnesium may provide a convenient method for the separation of the uranium product from the magnesium oxide.

e. Retorting of Uranium Concentrates
(J. F. Lenc, M. A. Bowden)

The objective of the retorting step of the skull reclamation process is to isolate a uranium product in high yield from accompanying liquid metals. The uranium product must be in a form easily removable from a suitable crucible in order to permit remote handling and must be sufficiently free of impurities (such as oxide and carbide) to enable suitable incorporation with other fuel material on recycle to the melt refining process. In previous retorting studies, uranium has been present initially as a precipitated intermetallic compound of uranium and zinc or uranium and cadmium. Upon retorting, the uranium product has retained skeleton characteristics of the original intermetallic compound. Because the uranium precipitation steps have been reversed in the revised flowsheet (see page 49), the uranium before retorting is present as precipitated uranium within a magnesium-rich matrix instead of as a uranium-zinc intermetallic compound. Therefore, three retorting runs were made during the past quarter to ascertain the character of the product which results from retorting such systems.

The charges for these runs were prepared by magnesium decomposition of uranium-zinc intermetallic concentrates formed by direct reaction of uranium and zinc as described on page 69 in connection with

blanket processing studies. Sufficient magnesium was added to produce a 46 percent magnesium-zinc alloy. The first charge consisted of 2.1 kg of the material produced in Run 4 (Table 14, page 70) and 1450 grams of magnesium. The second charge consisted of 2.4 kg of material from the first three runs given in Table 14 and 1850 g of magnesium. These were heated to 700 C in graphite crucibles contained in a reaction tube furnace and stirred mechanically for 4 to 5 hours (400 rpm in Run 1 and 700 rpm in Run 2). In the first run, stirring was continued as the temperature was slowly reduced over a subsequent 4-hour period to 380 C. In the second run, stirring was discontinued before cooling.

Examination of the ingots after cutting and acid-etching showed a sharp line of demarcation between the uranium layer, which occupied the bottom quarter of the ingot, and the overlaying magnesium-rich alloy layer. In the first run in which stirring had been continued during cooling, the uranium was in the form of tiny globules (maximum diameter of $\frac{1}{8}$ inch) within the zinc-magnesium matrix. An X-ray diffraction analysis of one of the globules showed alpha uranium to be a major constituent and the magnesium-zinc eutectic alloy to be a minor constituent. In the second run, in which stirring was not continued during cooling, the bulk of the uranium had agglomerated into rough spherical masses ranging between $\frac{1}{4}$ inch and 1 inch in diameter.

The tops of the ingots were cut away from the precipitated uranium phases and subjected to retorting in a tantalum crucible to isolate the uranium. The cutting of the ingots was substituted for the removal of supernatant liquid phases by pressure siphoning. The retorting cycles were as follows:

	Temp Range (C)	Time (hr)	Pressure Range (mm Hg)
Material	500 to 560	4	<1.0 to 0.02
from	670 to 725	5	0.03 to 0.01
Run 1	825 to 840	2	0.01
Material	510 to 575	4	0.12 to 0.02
from	690 to 730	2.5	0.02 to 0.01
Run 2	750 to 845	5	0.01

The product from the first run was in the form of a flat, dense sinter cake, weighing 340 grams, which was readily dumped from the crucible. About 20 grams of unreacted pin fragments were found in the retorted material. The product from the second run was still largely in the form of the roughly spherical-shaped masses present in the ingot before retorting (See Figure 13). The remainder of the uranium was in a compact layer about $\frac{1}{8}$-inch thick. The entire material was also readily removed from the crucible.

FIGURE 13

URANIUM ISOLATED FROM MAGNESIUM-RICH SYSTEMS BY RETORTING

Another run was carried out in a $3\frac{5}{8}$-inch diameter, grade CS graphite crucible (density of 1.89 g/cc). In this run magnesium (1 kg) was added to a dilute uranium-zinc solution (1.3 kg) to precipitate the uranium from solution. The solution was stirred (700 rpm) at 750 C for five hours, after which it was solidified in the graphite crucible. The crucible and charge were then transferred to the retorting furnace. Retorting conditions were about the same as for the two runs described previously. The major portion of the product again had formed into a dense ball (86 grams). A remaining 21 grams adhered firmly to the crucible bottom, and on removal a layer of graphite came away with it. Other more dense grades of graphite will be tested.

The variation in the character of the retorted uranium products is attributed to the variations in agitation employed in decomposition of the uranium-zinc intermetallic. Quantitative formation of relatively large coalesced masses of uranium could be very desirable from the standpoint of providing a readily handled product. This possibility will be carefully pursued.

f. Large-scale Cadmium Distillation Equipment
(P. A. Nelson, R. C. Cairns, J. DeKany)

The installation of equipment for large-scale distillation of cadmium is proceeding. In addition to experience on large-scale

distillation and retorting, this apparatus will afford operating experience on liquid metal transfer, on liquid level, pressure and temperature measurement and control, and on other operations associated with liquid metal processing.

Installation of the piping and instrumentation is the only major work remaining before completion of the equipment.

g. Development of a Process for Recovery of Plutonium from EBR-II Blanket Material
(I. O. Winsch, T. F. Cannon)

The liquid metal blanket processes under consideration for separation of plutonium from uranium are based on the relatively high solubility of plutonium in magnesium-rich zinc or cadmium alloys and the contrasting low solubilities of uranium in these alloys. As shown in Figure 14, a magnesium-rich solution may be achieved by several methods, following dissolution of the fissile elements in a suitable liquid metal. The currently favored procedure involves dissolution in zinc, precipitation of a uranium-zinc intermetallic compound, removal of the supernatant zinc, and decomposition of the intermetallic by the addition of sufficient magnesium. After separating the magnesium-rich solution containing the plutonium from the precipitated uranium, the plutonium may be recovered by vaporization of the magnesium and zinc.

FIGURE 14

LIQUID METAL PROCESS FOR URANIUM BLANKET METAL

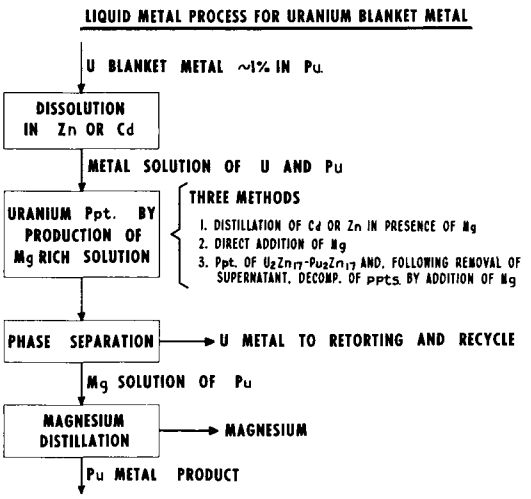

(1) Direct Formation of Uranium-Zinc Intermetallic Compound

A possible simplification of the above blanket process is the direct reaction of blanket uranium material with a quantity of zinc which is only slightly in excess of the stoichiometric amount required to form the intermetallic compound $UZn_{11.5}$. As compared with the dissolution step, this would reduce substantially the amount of zinc required and would eliminate a phase separation. Experimental work by A. Martin of this Division has indicated that, at a temperature of around 430 C, the reaction between uranium and zinc to form an intermetallic presumed to be $UZn_{11.5}$, using 0.25-inch diameter pins, was complete after 20 hours. Higher temperatures reduced the reaction rate. It postulated that at the

lower temperature fine crystals of the intermetallic are formed and break away from the surface, allowing further reaction. At higher temperatures, the intermetallic layer becomes more dense and adherent, making it difficult for the zinc to penetrate to the uranium surface.

Five experiments were completed in the past quarter in attempts to produce $UZn_{11.5}$ at 430 C. The conditions and results of these experiments are shown in Table 14. The experiments were carried out in a graphite crucible contained in a secondary stainless steel furnace in which an argon atmosphere was maintained. Uranium rods, having the same dimensions as EBR-II inner blanket rods, 0.433 inch in diameter, were cut into 1.5-inch lengths and spaced in the crucible to allow a maximum contact area with the zinc. Agitation by a motor-driven tantalum agitator was attempted in the first three runs and was found to be impractical because of the high viscosity of the slurry and the physical interference of the uranium rods. Agitation was not attempted in the last two runs.

Table 14

DIRECT REACTION OF URANIUM BLANKET RODS WITH ZINC TO FORM URANIUM-ZINC INTERMETALLIC

Run No.	Total Time (hr)	Temp (C)	Charge			Uranium-Zinc Ratio[a]	Uranium Reacted (% of Initial Charge)
			Uranium (g)	Zinc (g)	Magnesium (g)		
1	30	500 to 550	1000	3500	5.2	0.29	20
2A	24	430	965	2525	5	0.38	50
2B	48	430	965	3725	5	0.26	60
3A	28	430	481	2000	-	0.24	50
3B	48	430 to 800	481	2000	-	0.24	60
4[b]	27	435 to 445	477	2000	-	0.24	50
5[b]	80	435 to 445	474	1500	-	0.32	87
6	81	438 to 440	477	2000	-	0.24	98

[a] The stoichiometric ratio for formation of $UZn_{11.5}$ is 0.32.

[b] No agitation in these runs. In the first three runs mechanical agitation was employed during about the first 12 hours, after which it was discontinued because of the high viscosity of the system.

The reaction temperature was 430 to 445 C in all runs except the first (500 to 550 C) and the last portion of the third, in which the temperature was cycled between 430 and 800 C. The reaction rate was low, as indicated by times exceeding 80 hours before the reaction approached completion. Cycling the temperature between 430 and 800 C (Experiment 3B) was not

helpful. As noted previously, mechanical agitation was tried in the first three runs and found impractical. However, Aeroprojects, Inc. has indicated that reaction rates may be appreciably accelerated by ultrasonic mixing.[7]

The direct reaction of uranium and zinc as a first step in a blanket process has been demonstrated. Although required reaction times in a quiescent system are long (at least 80 hours), practical methods of reducing the reaction time, such as ultrasonic mixing, may be found. However, a reaction time of 80 hours may not be judged excessive in view of the process simplification which is realized. It should also be realized that the process does not depend on the success of this step, since the sequence of a direct dissolution of uranium and a subsquent phase separation of precipitated intermetallic crystals is a practical operation and has been demonstrated many times.

(2) Decomposition of Uranium-Zinc Intermetallic with Magnesium

Two runs have been completed to demonstrate the decomposition of the uranium-zinc intermetallic compound and subsequent precipitation of uranium from solution by addition of magnesium to form the zinc-46 weight percent magnesium eutectic alloy. Inasmuch as this is a step in both the blanket and skull reclamation process (for plutonium separation in the former and rare earth separation in the latter), the precipitated uranium phase was retorted to demonstrate uranium recovery. This work is discussed in the section on retorting, page 66. It is sufficient to record here that the intermetallic decomposition was easily achieved.

This work will continue with cerium-uranium alloys, cerium being used as a stand-in for plutonium, to demonstrate the expected liberation of cerium on magnesium decomposition of the uranium-zinc intermetallic compound. If no difficulties are encountered, plutonium-uranium alloys will be employed later.

(3) Plutonium Stability in Liquid Magnesium and Zinc Solutions

A number of proposed flowsheets for processing reactor fuels and blanket materials require the use of zinc and magnesium in recovering the final plutonium product. The fate of plutonium dissolved in magnesium or magnesium-zinc solutions contained in tantalum or graphite crucibles is important processing information. Plutonium-magnesium solutions in graphite have previously been shown to be unstable (ANL-5820, page 121). Additional necessary pieces of information are the stabilities of a plutonium-magnesium solution in tantalum and of a plutonium-zinc solution

[7] Winchester, R., Aeroprojects, Inc., private communication.

having a low magnesium concentration in graphite. Three long-term stability experiments, each of two weeks duration, have been completed with magnesium-plutonium solutions in tantalum, and a zinc-plutonium solution in graphite.

Plutonium-(3 percent magnesium-zinc) solutions in graphite appear to have good stability, as indicated by the expected and fairly constant plutonium concentrations found throughout the run (Table 15).

Table 15

PLUTONIUM STABILITY IN A ZINC-MAGNESIUM SOLUTION CONTAINED IN A GRAPHITE CRUCIBLE AT 750 C

Conditions

Charge:	2.23 g plutonium; 1930 g zinc; 58.0 g magnesium
Crucible:	graphite
Agitator:	tantalum
Sampling Tube:	tantalum with graphite frit
Atmosphere:	helium at 10 psig

Sample No.	Time (hr)	Percent of Plutonium in solution[a,b]	Sample No.	Time (hr)	Percent of Plutonium in solution[a,b]
1	0	107	6	98	110
2	2	100	7	190	98
3	4	(134)[c]	8	242	98.5
4	46	103	9	334	108
5	50	98			

[a] Analyses by alpha counting.

[b] Based on 0.32 g zinc and magnesium volatilized/hr.

[c] Questionable value.

The variation in concentrations is higher than desirable and results from the volatilization of zinc and magnesium which occurred throughout the run. The extent of this at any particular sampling time was unknown, except for the first sample, when it would have been negligible, and the last sample, after which it was measured. Condensation took place on the crucible lid, and this condensate could occasionally have dropped back into the melt spontaneously or could have been dislodged during sampling. The material found on the lid of the crucible at the end of the run was assumed to have been deposited at a uniform rate (0.32 g/hr) throughout the run, and solution concentrations of the intermediate samples in Table 15 were corrected

accordingly. Although this served to bring the plutonium concentrations into line, the arbitrariness of the assumption should be realized. The greatest weight should be given to the first and last samples, and from these it appears that graphite is a satisfactory container material for zinc-plutonium alloys.

Equipment to determine solution stability is now being designed so that condensation will occur above the melting point, thereby promoting return of essentially all the condensate to the melt.

Two runs were made to investigate the stability of plutonium-magnesium solutions held at 800 C in a tantalum crucible. In the first of these, the dissolution of the plutonium in magnesium and the stability run which followed were made in the same crucible without interruption in heating. Constant agitation was effected by means of a motor-driven tantalum agitator. As indicated in Table 16, the theoretical plutonium concentration was not realized, about 95 percent appearing in solution. A plutonium concentration of about 90 percent prevailed for the duration of the experiment. It seems from these results that plutonium-magnesium solutions are stable, but there is the possibility, since not all of the plutonium appeared in solution, of an initial reaction with solution impurities or tantalum impurities (surface oxide or carbide deposits).

Table 16

PLUTONIUM STABILITY IN A MAGNESIUM SOLUTION CONTAINED IN A TANTALUM CRUCIBLE AT 800 C

Conditions for Run 2

Charge: 5.17 g plutonium; 979 g magnesium.
Crucible, agitator and sampling tube were tantalum. No filter frit was used in sampling tube.
Atmosphere: helium at 10 psig.

Conditions for Run 3

Final solution of Run 2 poured into new tantalum crucible. Other conditions were the same as in Run 2.

Run No.	Sample No.	Time (hr)	Percent of Plutonium in Solution	Run No.	Sample No.	Time (hr)	Percent of Plutonium in Solution
2	1	23	83	3	1	0.0	100
2	2	71	94.5	3	2	5.5	67
2	3	99	96.0	3	3	78	53.5
2	4	144	84.0	3	4	121	51.5
2	5	191	91.0	3	5	150	50.5
2	6	311	90.9	3	6	254	55.0
2	7	341	91 5	3	7	307.5	49.5
2	8[a]	343	89.0				

[a] Remelt of combined vaporized magnesium and magnesium-plutonium alloy.

The magnesium employed had a reported purity of greater than 99.95 percent. Spectrographic analysis of the magnesium showed no detectable impurity. The specifications for this material give maximum impurity concentrations of 5 ppm for lead, silicon, tin, manganese, copper, and iron.

Some indication that the source of impurities is not the magnesium was provided by a second experiment (Run No. 3) in which the plutonium-magnesium solution from the above run was poured into a new tantalum crucible. Experimental conditions were the same as those in the preceding run (Run No. 2). Within 70 hours, the plutonium concentration decreased to about 50 percent of the amount in solution at the end of the first run and thereafter remained essentially constant. Analyses were performed by alpha counting and corrections were made for magnesium volatilization.

These experiments indicate that further work is required on the stability of plutonium-magnesium solutions to determine the reasons for the initial plutonium loss in a tantalum crucible. Since carbon is known to precipitate plutonium from magnesium solution, particular care will be taken to eliminate, and, if necessary, to identify the source of this impurity.

h. Materials and Equipment Evaluation
(P. Nelson)

(1) Corrosion Studies
(P. Nelson, M. Kyle, J. Hepperly)

A program is underway to test the corrosion resistance of refractory metals, graphite, and ceramics to molten metals, particularly to zinc and zinc-magnesium solutions. In recent corrosion tests, coupons were enclosed in a welded tantalum capsule (1-inch diameter by 2 inches long) with 20 to 30 grams of the desired corrosive metal, as shown in Figure 15. The tantalum capsules were enclosed in welded stainless steel capsules to protect them from atmospheric attack. The capsules were loaded into a rocking furnace (see Figure 16) which was operated at positive argon pressure for further protection of the capsules. The furnace rotated 180 degrees in approximately one minute.

FIGURE 15
CORROSION CAPSULE

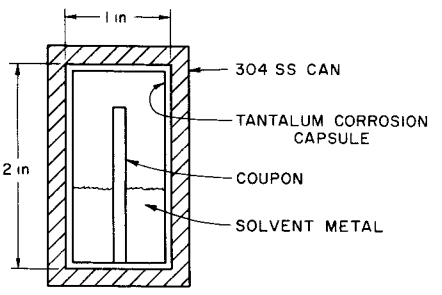

Runs were made using this procedure at 850 C to determine the corrosion resistance of various materials to zinc and zinc-magnesium alloys. This temperature is somewhat higher than those presently contemplated for the processes under development;

FIGURE 16
ROCKING FURNACE FOR CORROSION TESTS

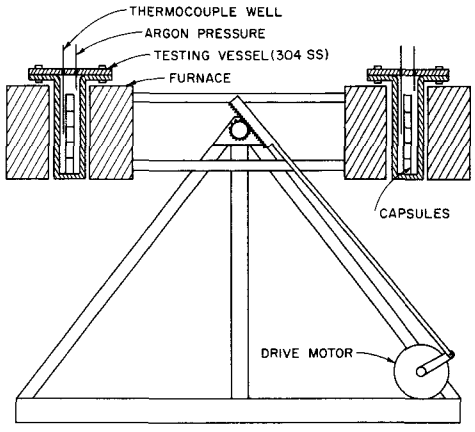

it was chosen to accelerate the possible effects and to provide a satisfactory margin in the choice of process temperatures. The results are tabulated in Table 17.

These preliminary test results lead to the following conclusions concerning the corrosion resistance of some materials to molten zinc and magnesium-zinc alloys at 850 C:

1. The addition of magnesium to zinc reduces the corrosiveness of zinc to tantalum, tantalum-7.5 percent tungsten, and molybdenum.

2. Tantalum-7.5 percent tungsten is more resistant to attack by zinc solutions than tantalum.

3. Molybdenum produced by powder metallurgy is more seriously attacked by zinc than is tantalum.

4. Graphite shows promise as an excellent container material.

Work is planned to obtain more complete information on the materials which have shown some promise as container materials for zinc and zinc-magnesium systems. At the present time, a program is planned to test various grades of tantalum obtained from commercial suppliers to determine if tantalum purity plays a significant role in corrosion resistance. A total of eight samples from various manufacturers will be tested.

Tantalum-tungsten alloys will also be tested in this program. These samples will be analyzed for impurities before tests begin. Welded (both electron beam and inert gas-arc welded) and unwelded coupons will be prepared for testing in zinc and zinc-magnesium alloys at 800 C. High-purity zinc and magnesium will also be obtained to determine the effect of purity on corrosion rates.

Work is in progress to determine the corrosion resistance of various steels and tantalum to alloys of the ternary system magnesium-zinc-cadmium. Alloys of this general type may have future process significance. A molten salt corrosion testing program is also being initiated. The test procedures will be similar to those used for the corrosive metals. The effect of moisture content of the flux on corrosion is considered to be of prime importance.

Table 17

CORROSION TESTS OF VARIOUS MATERIALS IN ZINC AND ZINC-MAGNESIUM ALLOYS

Conditions

Temperature: 850 C

Agitation: Capsule rotated end over end through 180° arc at 30 cycles per hour

Area of test coupon: Approximately 3 sq inches

Quantity of corrosive metal: 20 to 30 grams

Sample	Container Material	Corrosive Substance	Length of Run (hr)	Corrosion
A-1	Ta	Zn	100	Moderate attack with formation of 1 to 5-mil thick layer on tantalum surface.
C-2	Ta	Zn	300	Moderate attack with formation of layer on surface.
A-3	Ta	95% Zn- 5% Mg	100	Slight attack (less than 1 mil)
E-4	Ta	90% Zn-10% Mg	300	Slight attack (less than 0.5 mil)
E-5	Ta	85% Zn-15% Mg	300	None (did not wet container)
E-6	Ta	80% Zn-20% Mg	300	None (did not wet container)
A-7	Ta	70% Zn-30% Mg	100	None (did not wet container)
A-8	Ta	50% Zn-50% Mg	100	None (did not wet container)
E-9	Ta	Mg	300	None (did not wet container)
D-24	Ta	Mg	300	None (did not wet container)
B-10	Ta-7.5% W Alloy	Zn	100	Very slight attack (<0.5 mil) with formation of undetermined coating 2 mils thick
C-11	Ta-7.5% W Alloy	Zn	300	Very slight attack (<0.5 mil)
A-12	Ta-7.5% W Alloy	Zn-5% Mg	100	None
D-13	Ta-7.5% W Alloy	90% Zn-10% Mg	300	None
D-14	Ta-7.5% W Alloy	75% Zn-25% Mg	300	None
D-15	Ta-7.5% W Alloy	54% Zn-46% Mg	300	None
B-19	Mo[a]	Zn	100	Gross intergranular corrosion
C-20	Mo[a]	Zn	300	Complete disintegration of sample
C-21	Mo[a]	95% Zn- 5% Mg	300	Gross intergranular corrosion
E-22	Mo[a]	90% Zn-10% Mg	100	Intergranular corrosion to a depth of about 3 mils
D-23	Mo[a]	54% Zn-46% Mg	300	Slight intergranular corrosion
B-16	Pyrolytic graphite	Zn	100	None. Some flaking of graphite
C-17	Pyrolytic graphite	Zn	300	Approximately 2% weight loss by flaking
B-18	Al_2O_3	Zn	100	None

[a]The molybdenum used in these tests was a small drawn cup, $\frac{1}{2}$ inch diameter by 1 inch high. The material from which it was drawn was prepared by powder metallurgy.

The moisture content will be varied by utilizing various drying techniques from no drying of reagent grade anhydrous materials to very exacting drying and handling techniques which have been used by other investigators.[8,9]

(2) Solution Stability Experiments
(J. Wolkoff, J. DeKany, J. Pavlik)

Equipment is being assembled for experiments to determine the stability of uranium in various molten alloys and container material systems. These experiments will be conducted in agitated crucibles of approximately one-liter capacity. Samples will be taken at intervals over the total length of the runs, which will be 100 to 500 hours in length. A list of the crucible materials which will be tested is given in Table 18.

Table 18

CONTAINER MATERIALS TO BE USED IN SOLUTION STABILITY TESTS

1. Carbon and graphites
   - Grade CS[a] (medium grain)
   - Grade ATJ[a] (fine grain)
   - Grade ZTA[a] (dense fine grain)
   - Two grades of impregnated graphite
   - High-purity graphite
2. Tungsten
   - Unalloyed tungsten
   - Plasma-gum-deposited tungsten on graphite
   - Vapor deposited tungsten on graphite
3. Tantalum
4. Tantalum-10 percent tungsten
5. Vitreous magnesia

[a] Grades shown are National Carbon Company designations.

[8] Susskind, H. et al., Combating Corrosion in Molten Extraction Processes, Chemical Engineering Progress, 56(3), 57-63 (1960).

[9] Ginell, W. S., Oxidative Extraction of Lanthanide Metals from Molten Bismuth by Fused Salts, Ind. and Eng. Chem., 51, 185-190 (1959).

The first systems to be tested are graphite containers and zinc-magnesium-uranium solutions at 800 to 850 C. The results should provide experimental evidence of the effect of the uranium activity (varied by variation of the magnesium concentration) on the stability of uranium in solution.

B. Fuel Processing Facilities for EBR-II
(J. H. Schraidt, M. Levenson)

1. Design, Development, and Construction of Buildings and Equipment

The Fuel Cycle Facility and the Laboratory and Service Building are described in previous quarterly reports (ANL-5789 and ANL-5820). The former building will be used for the processing of EBR-II fuel and the latter will provide radiochemical analytical and related facilities for the entire Idaho Division of Argonne National Laboratory.

Contractors have completed installation of equipment in the Laboratory and Service Building. Shakedown testing of process equipment has started.

a. Status of Fuel Cycle Facility Building Design and Construction
(E. J. Petkus, H. L. Stethers)

The construction of the Fuel Cycle Facility continues. The Facility was about 70 percent completed as of December 6, 1960, as compared to 40 percent completion on September 6, 1960. The building has been enclosed so that work can continue throughout the winter. The Argon Cell liner has been erected, and the heavy aggregate concrete has been poured around the liner. The steel roof deck and most of the outside metal siding have been installed.

All the structural welds in the Argon Cell liner have been made and tested. The contractor has begun sandblasting and zinc metallizing* of the Argon Cell liner plate. Miscellaneous work, such as installation of brackets for lighting fixtures and grinding of liner welds, has been completed. In addition, most of the penetration sleeves have been installed.

The pouring of heavy aggregate shielding concrete has been completed for both the Argon and Air Cells. The concrete basement slab was completed in November. Since then, the contractor has been

*Metallizing is the application of a molten metal, such as zinc, to a base plate, usually steel.

installing major equipment items, such as the main exhaust fans and the Argon Cell gas refrigerator equipment. Electrical, piping, and ventilating work is proceeding in the basement area. The freight elevator was installed and the contractor will test it as soon as electrical power is available.

The concrete block for the outside of the building, and most of the metal siding, have been placed. The steel roof deck has been erected, and the contractor is now laying the roof. The erection of the stack was completed during October, and stack electrical work is now proceeding.

b. Cranes and Manipulators
(J. Graae, G. J. Bernstein)

The combination lifting beam for remote removal of either a crane trolley or a manipulator carriage has been completed and will be shipped to Idaho in the near future.

Manipulator refinements have been made. These include the addition of a remotely removable forearm assembly and the modification of an articulated General Mills Model 300 arm so that it may now be attached by remote operation to the cell manipulator in place of a hook or hand fixture. In making the attachment, all the necessary mechanical and electrical connections are made automatically. The ability to attach the arm to the cell manipulator greatly enhances its usefulness in emergency or nonroutine operations.

The Argon Cell manipulator bridge power inlet, consisting of receptacle, plug, and junction box, has been built and tested for mechanical functioning only. Based on these tests, efforts are being made to purchase the manipulator bridge power inlet.

Twelve Model 8 manipulators for the Air Cell have been ordered from Central Research Laboratories. These manipulators will be used for assisting in the disassembly of spent fuel subassemblies received from the Reactor Building. They will also be used for handling sealed fuel pins during pin inspection and reassembly of fuel subassemblies.

Control cabinets and switchboard for manipulators, cranes, and blister have been completed, inspected, tested, and shipped to Idaho. The testing was done by means of checkout equipment plugged into the top of the cabinets. This checkout equipment contains voltmeters, pilot lights, phase-sequence indicators, and switches. By means of a toggle switch control box (remote controller) in conjunction with the checkout equipment, the proper function of the various relay circuits and limit switch circuits

was checked and errors found and corrected. The checkout equipment is contained in two small boxes and will be sent to Idaho for initial checkout and subsequent maintenance and trouble shooting in the Fuel Cycle Facility.

c. Process Cell Windows
(T. W. Eckels)

In October it was reported from Idaho that most of the plexiglass oil-expansion tanks for the Junior Cave shielding windows (installed in the Laboratory and Service Building during June) were slowly seeping oil. Since these tanks are identical to those which were about to be delivered for the Fuel Cycle Facility windows, corrective measures were immediately taken. The design of the end caps for the plexiglass cylinders was modified. All the expansion tanks for the Fuel Cycle Facility windows have been reworked, and six additional tanks have been provided to replace those now installed on the Junior Cave windows.

The final shipment of components for the Fuel Cycle Facility shielding windows, including the tanks mentioned above, was received at the Idaho site during the first week of December. The work of installing the windows should begin early in 1961.

d. Process Cell Lighting
(T. W. Eckels)

The 1000-watt fluorescent mercury vapor lamps which had been specified for use in the Argon and Air Cell lighting had soft-glass envelopes. Recently, the major lamp manufacturers have changed from soft-glass to weather-resistant (borosilicate) glass envelopes; these have been found to darken readily on exposure to gamma irradiation.

Late in 1958, tests to determine the possible gamma-ray darkening of lamps were instituted in the Gamma Irradiation Facility at Argonne. The tests consisted of exposing operating lamps to irradiation. After irradiation, the light output of each lamp was reported as a percent of its output prior to irradiation, but after a 50-hour initial stabilization operating period. To get exposure rates of 10^5 to 10^6 rad/hr, the lamps irradiated had to be of a size to fit in the small irradiation urn in use at the facility. At the time of the tests the 175-watt size H22KF/W* was available with a soft (lime) glass envelope only. It is a small-scale version of the 1000-watt type specified for use in the Process Cells. This lamp gave results which were very favorable for the proposed use. Earlier this year the major manufacturers announced the H37-5KC/W (250-watt), H39-22KC/W (175-watt), and H34-12GW/W (1000-watt) lamps, all with a weather-resistant (borosilicate) glass envelope. Tests were reinstituted on the 175- and 250-watt types (they appear identical, both using a BT-28 size envelope). The results are given in Table 19.

*American Standards Association type designation.

Table 19

COMPARISON OF LIGHT OUTPUT AT VARIOUS INTEGRATED GAMMA EXPOSURES FOR SIX LAMPS

Gamma Exposure (rad)	Light Output after Irradiation - Percent of Original Intensity					
	175-watt Lamp		250-watt Lamp			
	H-22KF/W[a,e]	H39-22KC/W[b,e]	H37-5KB[c,f]	H37-5KC/C[d,e]	H37-5KC/W[b,e]	H37-5KC/W[b,f]
0	100	100	100	100	100	100
1×10^6	98	87	-	-	-	-
6×10^6	-	50	-	-	-	-
1×10^7	98	34	-	-	-	-
1×10^8	97	29.5	51	35	64	35
2×10^8	97	27				
4.5×10^8	-	23				
5×10^8	97	18.5				
6.6×10^8	-	16[g]				
8×10^8	85	-				
1×10^9	83.5	-				

[a] Soft-glass envelope with white phosphor coating (ANL-6068, page 31).

[b] Hard-glass envelope with white phosphor coating.

[c] Hard-glass envelope with no phosphor.

[d] Hard-glass envelope with color-improvement phosphor.

[e] Manufacturer A.

[f] Manufacturer B.

[g] Test terminated. Further irradiation considered unnecessary.

The somewhat better performance of the 250-watt lamps, as compared with the 175-watt lamp with the hard-glass envelope, can be attributed to higher envelope temperatures of the 250-watt lamps.

A separate study of four different types of lamps was made to determine the applicability of the lamps to the illumination of EBR-II process cells, where the illuminated objects will be viewed through shielding windows. Each lamp was operated for 100 hours without gamma irradiation to furnish baseline data before the tests were begun. The results of the tests are given in Table 20. Whereas the transmittance of the shielding window to the light emitted by the various lamps was nearly the same (about 15 percent), other properties differed sufficiently to indicate the advantage of the mercury vapor lamp with the white phosphor coating over the other lamps tested, namely, two mercury vapor lamps, one with a color-improvement phosphor coating and the other with a clear envelope. Color discrimination, based on observations made by human subjects, was excellent for the incandescent lamp, good for the mercury vapor lamps with the white and color-improvement phosphor coatings, and poor for the mercury vapor lamp with the clear envelope. Since color coding may be used within the process cells, good color discrimination is an important consideration in the choice of lamps for cell use. The efficiency (lumens/watt) of the mercury vapor lamp with the white phosphor coating (60 lumens/watt) was somewhat greater than the efficiency

of the lamp with a color-improvement phosphor coating (51 lumens/watt) and the clear mercury vapor lamp (54 lumens/watt), and was much greater than the efficiency of the incandescent lamp (~16 lumens/watt). Based on the results of these tests and the results obtained from the gamma-irradiation tests, which showed that soft-glass lamps were much more radiation resistant than hard-glass lamps, 1000-watt mercury vapor lamps with white phosphor-coated, soft-glass envelopes have been chosen for use in the process cells. An adequate supply of these lamps has been ordered.

Table 20

COMPARISON OF UNIRRADIATED LAMPS

	1000-watt Mercury Vapor Lamps			1500-watt Incandescent Lamp
	White Phosphor Coating	Color-improvement Phosphor Coating	Clear	Clear
Efficiency[a] (lumens/watt)	60	51	54	~16
Transmittance[b] of Shielding Window (percent)	14.9	15.0	14.8	14.9[c]
Color Discrimination[d] through Shielding Window	good	good	poor	excellent

[a] Manufacturers' values after 100 hours of operation. The light output became stabilized after this period of operation.

[b] Calculated values based on the spectral energy distribution of each lamp.

[c] Transmittance for Illuminant A measured through a completed window. The spectral energy distribution of the 1500-watt incandescent lamp is very similar to that of Illuminant A (2848 K color temperature).

[d] Four human subjects viewed variously colored objects directly under incandescent lighting and then through a prototype shielding window with the objects illuminated by means of the stated lamp.

e. Fuel Cycle Facility Equipment
(G. J. Bernstein, A. A. Chilenskas, L. F. Coleman, T. W. Eckels, R. H. Jahnke, M. A. Slawecki)

Components for the melt refining furnace off-gass system have been tested during the past year in the Chemical Engineering Division mockup area. The results, in general, have been satisfactory. Procurement of the melt refining furnace off-gas system of the Fuel Cycle Facility is being made, and installation instructions are being prepared. These instructions cover the installation of the piping, valves, instrumentation, and vacuum pump enclosures which are to be installed in the subcell of the Fuel Cycle Facility. The piping connects the vacuum pumps and argon supply to the melt refining furnaces. Drawings covering the installation of piping and instrumentation have been prepared. The vacuum pump enclosures have been designed and the drawings completed. Procurement of materials is underway.

Installation drawings for the high-frequency power-distribution system have been completed. These detail the interconnections between the induction generators, the capacitor work stations, and those service sleeves which transfer the high-frequency current to the two melt refining furnaces and the two pin-casting furnaces.

Preliminary installation drawings have been prepared for the space radiation monitoring system. This system consists of background radiation monitors located in potentially hazardous areas in the Fuel Cycle Facility. A recorder, located in the Operations Control Room, provides a record of the radiation level in each area. An alarm is sounded in the Control Room and in the affected area if the level exceeds a pre-set value.

Gas, vacuum, electrical, and other services for experimental equipment in the Argon Cell enter the cell through service plugs installed in service sleeves which are sealed in the cell floor. The design permits changing a plug without impairing the high-purity atmosphere in the cell or releasing radioactive contaminants. The sleeves are already installed. The design of the necessary types of plugs has been a cooperative effort of three Divisions (Metallurgy, Remote Control Engineering, and Chemical Engineering) at the Laboratory; final fabrication drawings are now being prepared. A model of the top portion of the electrical-thermocouple plug was made and tested in a mockup of the cell using the prototype operating manipulator. The fabrication and testing indicated the need for several minor design modifications. These are now being incorporated in the final drawings.

The degassing furnace shell will be fabricated by Krueger Fabricating Company, Inc. of Madison, Wisconsin. The complete furnace will be set up at ANL for performance testing before shipment to Idaho.

AMF Atomics has completed fabrication of the mechanical and electrical components of the transfer cell equipment. This equipment will be used in conjunction with the large transfer lock to transport material between the Air Cell and the Argon Cell. It consists basically of a steel platform which can be sealed to the bottom of the transfer lock. Hydraulic rams located below the lock and below a floor opening in the Air Cell are used to raise the platform into proper position. A cart running on rails carries the platform and its load between the two ram positions.

The specifications for the design and construction of coffins for interbuilding, storage pit, and scrap-handling use, have been released to the potential bidders. The bids are scheduled for return by December 23, 1960. The three coffins will be used to transfer highly radioactive materials between the Reactor Building and the Fuel Cycle Facility, and between the Fuel Cycle Facility and the storage or waste disposal sites.

Redesign of the small transfer lock is almost completed. This design will use a portion of the window shutter drive mechanism. Redesign of the track and carts that are used in the locks is proceeding.

A bid by the Kollmorgen Corporation to modify a five-foot wall periscope of their manufacture which the Chemical Engineering Division already owns has been accepted. The shielding of this periscope was designed for a lower level of radiation.

The modifications necessary (see Figures 17 and 18) to meet current specifications are the following:

(1) provide for the installation of a hemispherical glass protective dome to avoid radioactive contamination of the periscope;

(2) increase the length of the horizontal leg from 60 to 61 inches to permit attachment of the dome to the cell wall;

(3) rework the horizontal leg to incorporate necessary annular internal lead shielding; and

(4) provide near the midpoint of wall thickness a double offset in the horizontal optical path so that a 12-inch length of lead can be inserted to shield the central axis of the horizontal tube of the periscope.

The conventional Kollmorgen wall periscope with internal lead shielding in the horizontal leg has a straight-through optical path, of about $1\frac{5}{8}$-inch diameter, which remains unshielded. An externally mounted solid lead cylinder is available as an accessory to backstop this path.

FIGURE 17
WALL PERISCOPE WITH CONVENTIONAL INTERNAL SHIELDING

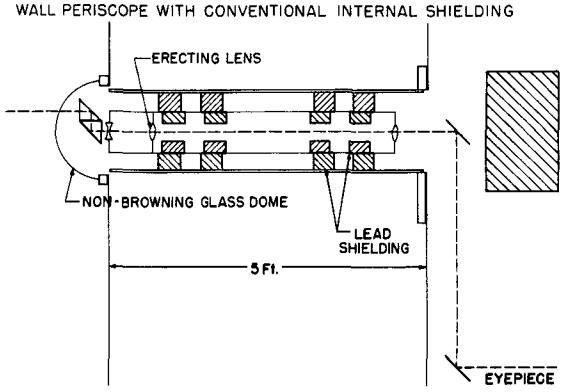

FIGURE 18
WALL PERISCOPE WITH INTERNAL SHIELDING AND DOUBLE OFFSET OPTICAL PATH

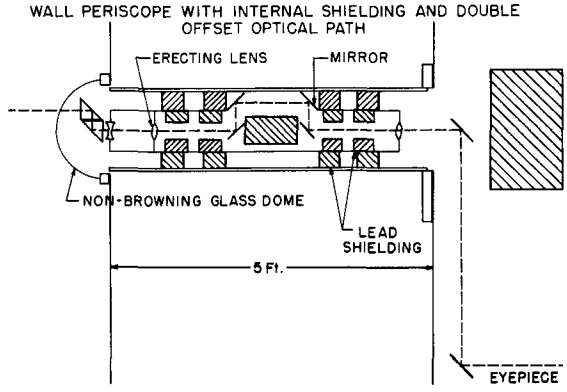

An experiment performed by the Reactor Engineering Division in 1958 demonstrated that for the level of gamma activity for which the Air Cell is designed, the backstop shield alone would be inadequate. The inadequacy was due to the scattering of otherwise unattenuated gamma rays streaming down the straight-through optical path. From calculations based on the experiment, it was concluded that exposure at the eyepiece of the periscope could be as high as 300 mr/hr, while at the top of the vertical leg (that is, at the point where the vertical leg intersects the horizontal axis) the rate could be as high as 5000 r/hr. This point is only seven feet above the floor and is completely outside the shielding wall.

The modification described in Item 4 above will reduce the exposure rate at the eyepiece to less than 0.1 mr/hr and should reduce the rate to less than 10 mr/hr along the horizontal axis. The added internal shielding will increase the weight of the periscope by about 50 pounds, to make the total weight of the periscope about 1400 pounds. An earlier modification which had been considered required a very heavy external lead shield to surround completely the juncture of the vertical and horizontal legs of the periscope. However, despite the great added weight (about 1000 pounds) of the shielding, this design would still allow from 200 to 300 mr/hr of scattered radiation to pass through the vertical leg. Although this radiation could be stopped by one or two inches of lead at the bottom of the vertical leg, no less than 0.25 mr/hr exposure would still be obtained at the eyepiece.

f. Materials Testing
(G. J. Bernstein, L. F. Coleman, J. Graae, M. Slawecki)

(1) Testing of Radiation-Resistant Greases

Testing of radiation-resistant greases is continuing. Particular attention is being given to a tapered roller bearing (Timken No. 432 cup - No. 438 cone) which will be incorporated in the manipulator bridges. These bridges are attached to the center pivot post in the Argon

Cell. Roller bearings are used in the truck assemblies which support the bridges as they revolve around the cell. Since the bridges and trucks cannot be removed for service, it is imperative that these bearings be suitable for maintenance-free operation for several years. It is anticipated that the radiation level in the area of the bearings will be approximately 10^5 rad/hr. Accordingly, lubricants that are suitable for use after a total radiation of more than 10^9 rad are needed.

Early tests (ANL-6145, page 28) showed that chromium alloy coating and molybdenum disulfide coating were unsatisfactory for the high rolling stresses developed in roller bearings. Three types of radiation-resistant greases which have been rated by their manufacturer at 3 to 5×10^9 rad are currently being tested. These greases are irradiated in bulk and then applied to clean new roller bearings. The bearings are being tested in a heavy-duty drill press under 800 lb axial load at 40 rpm. The load approximates the actual load which will be applied to the bearing in service. (The maximum operating speed of the bearing in service will be about six rpm. However, 40 rpm was the lowest speed readily available and for the purposes of these tests was felt to be an adequate approximation of service conditions.) Results of these tests to date are summarized in Table 21.

Table 21

ROLLER BEARING TESTS WITH IRRADIATED GREASES

Timken Bearing (No. 432 cup - No. 438 cone)
800 lb axial load at 40 rpm

Grease Type[a]	Irradiation[b] (rad)	Running Time (hr)	Remarks
NRRG-159	3×10^9	300[c]	Ran well. Run terminated voluntarily.
NRRG-235	5×10^9	52	Failed due to breakdown of jell and plating out of solid residual lubricants.
NRRG-335	5×10^9	250	Test still continuing. Squeak developed after 176 hr. Bearing not heating up. Grease looks fluid.

[a] Products of Standard Oil Co. of California.

[b] Irradiated to manufacturer's rated limit.

[c] Estimated to be equivalent to four years of actual operating time in the Fuel Cycle Facility.

Additional tests are underway to determine whether or not any of these greases will fail due to loss of consistency at radiation levels well below the rated limit.

(2) Testing of Radiation-resistant Insulation for Electrical Leads

The yearly radiation dose at locations where electrical leads will be used in the Air and Argon Cell will vary from approximately 10^7 to 10^{10} rad. This will impose severe limitations upon the types of insulation used. Although MI cable* provides the most promising radiation-resistant insulation, it is hygroscopic and must be provided with end seals, and it is not sufficiently flexible for all connections. Two general types of end seals for MI cable have been investigated and two types of flexible insulated conductors have been tested.

MI cable is used in all cases where a rigid conductor is practical. On all permanent installations, such as cables through the shielding wall, and on all installations where replacement would be very difficult, the MI cable is hermetically sealed with a ceramic end seal (see ANL-6068, pages 25 and 26, and ANL-6101, page 23). This end seal is very resistant to radiation damage, but is expensive and difficult to install. A substitute has been sought for applications for which replacement is comparatively simple, as in the replaceable service sleeve plugs used to provide services to the Argon Cell.

An ideal end seal would be completely moisture resistant at all times and provide good electrical insulation even after receiving a radiation dose of 10^{11} rad. Such requirements are not compatible with those of economy and simplicity. It was decided that a seal would be acceptable for replaceable cables if (1) the pre-irradiation moisture permeability was sufficiently low so that no appreciable change in resistance occurs, if (2) the electrical insulation resistance of a cable with such seals was greater than one megohm after radiation doses of 10^9 rad, and if (3) the insulation resistance after irradiation could be restored to approximately 200 megohms by a short period of heating, preferably at 100 C or less.

Several types of end seals have been tested. The most successful has been one using Temporell No. 741** as a potting compound (see ANL-6231, page 30). Samples of end seals with this potting compound

---

*Type MI Cable: One or more electrical conductors insulated with a highly compressed refractory mineral insulation and enclosed in a liquid-tight and gas-tight tube sheathing. Sheath and conductors are of electrolytic copper and the mineral insulation is magnesium oxide for the cable mentioned.

**A product of Orell, Inc.

have been irradiated to dosages of 6.1×10^9 rad over a period of ten months. They showed no insulation degradation during the first three months, even after a dosage of 2.2×10^9 rad. Subsequently the insulation resistance, which previously was greater than 200 megohms,* dropped as low as 3 megohms. Heating for six hours at 100 C restored the resistance to its former value. An attempt was made to increase the resistance of the seal to moisture by coating the seal with an insulating varnish; this showed no beneficial effect. The tests indicate that a seal with this potting compound will be satisfactory for the proposed use.

Some connections require a lead that is quite flexible during the initial installation, but which will remain fixed thereafter. Leads individually insulated with ceramic bead insulation are used for such cases, with overlapping fish-spines being the preferred type of bead. Connections to the ends of MI cable are a typical case (see ANL-6068, pages 25 and 26).

Other connections require a lead which is frequently flexed after installation. Asbestos-insulated wire has been investigated for such a lead. Wires of this type are normally used in construction where resistance to high temperatures or flameproofing is desired. It is available with single or multilayer insulation and with or without moisture-resistant impregnating agents. The use of multiple layers and impregnating agents increases the resistance to abrasion and reduces the loss of insulating material due to powdering.

Samples of copper wire with AI, AIA, and AA insulation** have been tested. A sample of a wire of heat-resistant alloy covered with asbestos insulation similar to type AA has also been tested. After doses of 2.3×10^9 rad the samples with type AI and type AIA became excessively brittle (see ANL-6183, page 28). Samples with type AA insulation have received a dose of 5.7×10^9 rad, and samples of the alloy wire with an insulation similar to type AA have received a dose of 1.4×10^{10} rad. Both these unimpregnated types of insulation still appear serviceable. Insulation resistance has dropped as low as 2 megohms, but slight heating restored it to a value greater than 200 megohms.

---

*Insulation tests were made with an instrument that impressed 500 volts DC upon the insulation. Readings were taken after a one-minute electrification period. The maximum value which could be read on the instrument was 200 megohms.

**Types AI, AIA, and AA-insulated wires: Type AI insulation is a felted asbestos insulation saturated with flame-, heat-, and moisture-resistant compounds. Type AIA is identical to type AI with the addition of a saturated asbestos braid outer covering. Type AA is identical to type AIA except for the absence of moisture-resistant compounds.

In a number of insulation tests, decreases in the insulation resistance measured after an irradiation period has been attributed to moisture sorption if the initial resistance could be restored by heating. Since radiation damage effects can also often be removed by heating, tests were undertaken to determine whether moisture was the actual cause of the decrease in resistance. A sample of the asbestos-covered alloy wire held in a closed vial containing a desiccant was irradiated. This sample had previously received a dosage of 1.35×10^{10} rad and had on six occasions shown the insulation degradation effect. After additional irradiation for one month (an incremental dose of 4×10^{8} rad) in the vial the insulation was greater than 200 megohms. This test will be repeated.

Results obtained thus far indicate that leads insulated with type AA or similar asbestos insulation will be satisfactory for in-cell use. Since some powdering of the insulation occurred, the need for multilayer insulation is indicated.

(3) Testing of Aluminum Paints

Irradiation of aluminum paint samples is continuing; the irradiation doses vary from 0.7 to 1.4×10^{10} rad. All paints are covering and only slight discoloration is seen. Some pitting and peeling has occurred.

2. EBR-II Fuel Processing Mockup

a. Manipulator and Manipulator Removal Blister
(D. C. Hampson, J. Graae)

The manipulator removal blister was removed from the mockup area. The roof plug was leak tested and the faulty weld seams were chipped out and rewelded. The equipment was carefully cleaned, painted, crated, and shipped to Idaho.

The pivot tower and power inlet for the Argon Cell was shipped to Idaho.

b. Melt Refining Furnaces
(D. C. Hampson, W. E. Miller, W. Holcomb)

(1) Equipment Performance

(a) Crucibles

Crucible behavior during melt refining runs has been reported previously (see ANL-6183, pages 29 to 32 and ANL-6231, page 34). Since the vendor changed methods of crucible manufacture

FIGURE 19
VARIATION OF DENSITY WITH HEIGHT OF NORTON CRUCIBLES

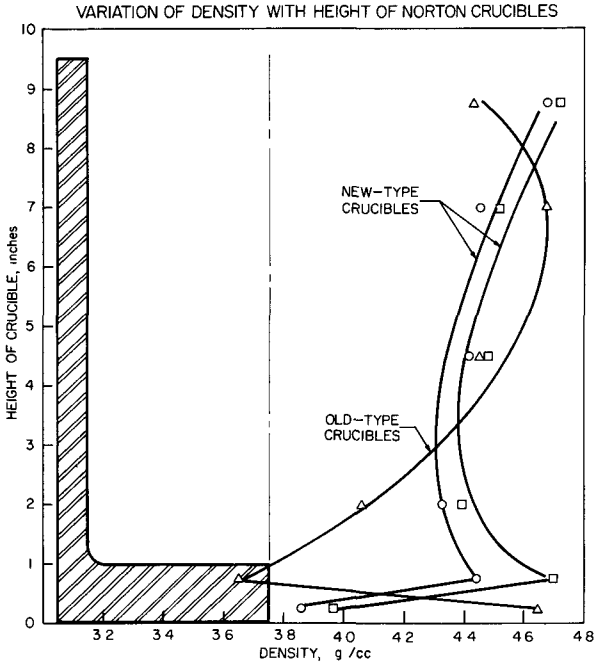

(ANL-6183, pages 29 to 32) and since a set of standards has been established as a guide to crucible acceptance, no serious cracking of crucibles has occurred. The acceptance standards are based on crucible dimensions, appearance, weight, and initial cracks. About 10 percent of the crucibles received from the manufacturer do not meet specifications and are rejected.

A measurable difference between crucibles manufactured by the old and new methods occurs in the density profiles of the crucibles. Figure 19 shows the average density profiles of four old-type crucibles and the density profiles of two new-type crucibles. The points for the curves were obtained from densities of cross sections cut from the crucible walls and bottom. Crucibles made by the old method consistently developed cracks during the furnace heat cycle, while the new-type crucibles do not.

(b) Fume-trap Holder

A holder for the molded Fiberfrax* fume trap has been designed, built, and tested. The trap holder accommodates traps whose diameters vary between $9\frac{1}{2}$ and 10 inches. The allowance for variation in diameters of the traps is necessary because of the nature of trap manufacture. A single die is used to form all traps, but they come from the die in a wet, plastic condition. Later steps in the manufacturing process (impregnation and drying) result in distortion. Specifications of diameter limits have not been applied stringently in the past, yet most of the traps received were acceptable. Specifications will guide inspection of traps received in the future.

Figure 20 shows the trap holder and trap in position on the furnace when the furnace is tilted. Experiments have shown that a tight seal between the furnace top and the trap is not required.

*A product of the Carborundum Corporation. The stated composition of the fibers is aluminum oxide, 51.2 percent; silicon dioxide, 47.4 percent; boron oxide, 0.7 percent; and sodium oxide, 0.7 percent.

Figure 20

FUME TRAP WITH FURNACE IN TILTED POSITION

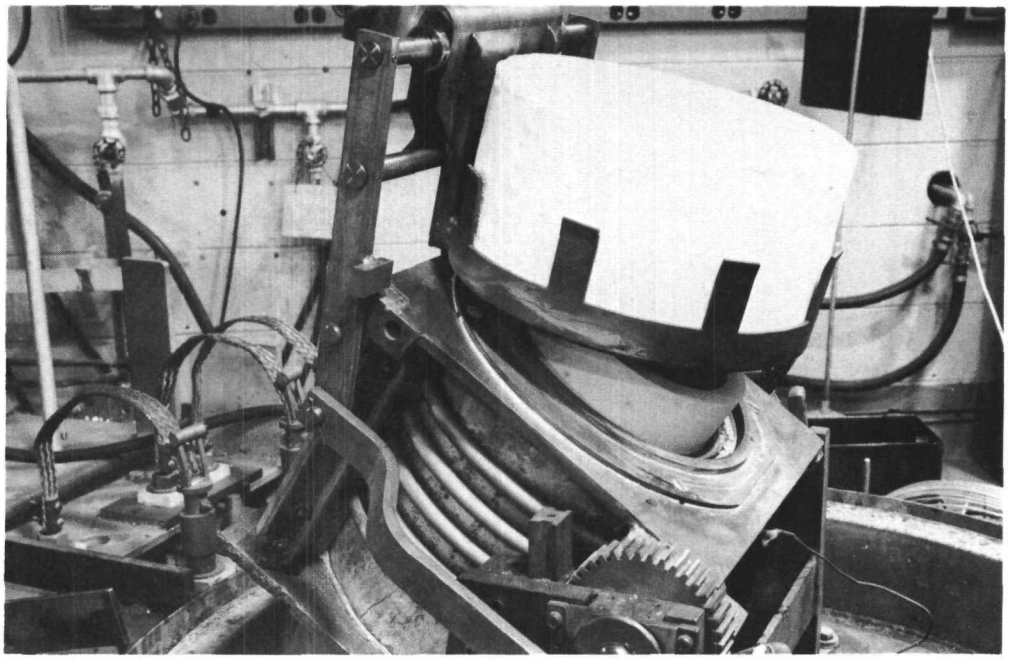

Sodium pickup by the traps was consistently 95 percent or greater with sodium charges of 80 grams or less, regardless of the condition of the seal. The walls of the trap are about $\frac{7}{8}$-inch thick. Evidently this wall thickness provides sufficient reactive surface at the junction of the furnace top and trap to enable vapor flowing through cracks to react prior to escaping into the bell jar.

The sorption efficiency of molded Fiberfrax traps for sodium was investigated as a function of the amount of sodium charged. It was found that the traps absorb 98 to 100 percent of the sodium charged, up to a sodium charge weight of 80 grams. Above this value sorption efficiency may be expressed by the empirical equation

$$E = 100 - \frac{\text{grams charged} - 80}{9.2} \quad .$$

It is estimated that a 10-kg batch of pins will contain about 40 grams of sodium. About 40 grams of condensable fission products will also be evolved from 10 kg of 2 percent burnup fuel. One run with a 145-gram sodium charge was made in which the heating rate was reduced to 50 percent of normal to determine if rate of heatup was a factor. The result of this run agreed with the previous runs made at the normal heating rate of 10 C/min; therefore, for the conditions of these experiments the rate of heating does not appear to be a factor. The relationship between the amount of sodium charged and the sorption efficiency, E, is shown in Figure 21.

FIGURE 21

VARIATION OF FUME TRAP EFFICIENCY WITH GRAMS OF SODIUM CHARGED

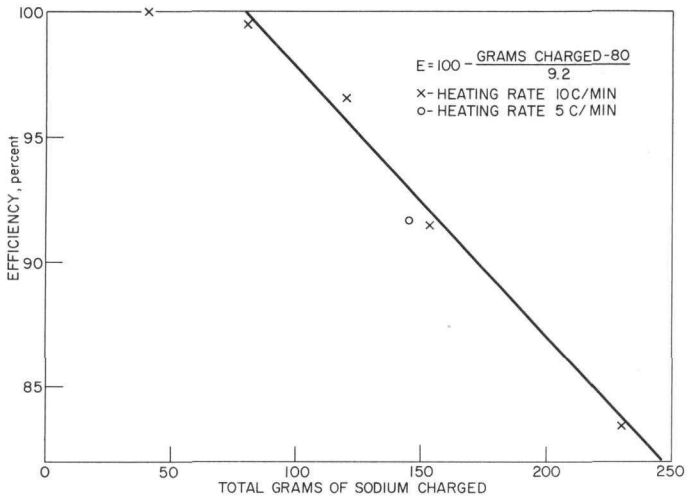

(c) Mark VI Furnace

The component parts and the assembled Mark VI Furnace are shown in Figures 22, 23, 24 and 25. The parts were made by Rock Island Arsenal from Argonne blueprints. The design encompasses all the changes which were made in previous models of the furnace and is the final design for the Idaho plant. The component parts were assembled into the complete unit. The unit was then placed in its supports on the furnace base plate by using the operating manipulator controlled from behind the shielding window. The furnace support bearings, the guide, and the pinion gear all engaged properly. The furnace was then put into operation and it has performed satisfactorily.

FIGURE 22

M-6 FURNACE COMPONENT PARTS

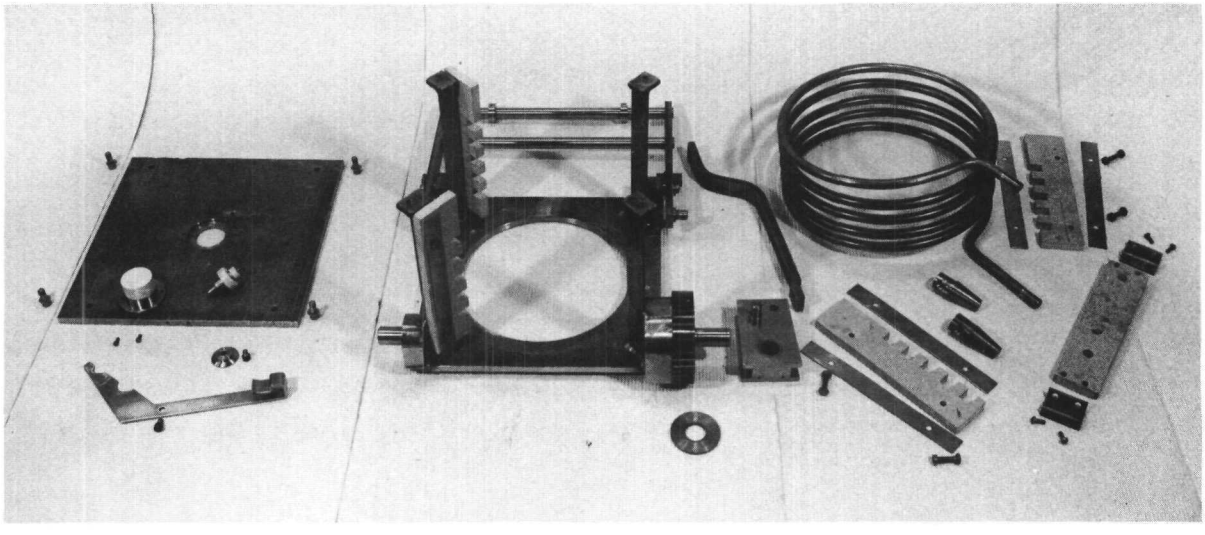

FIGURE 23

M-6 FURNACE COMPONENT PARTS

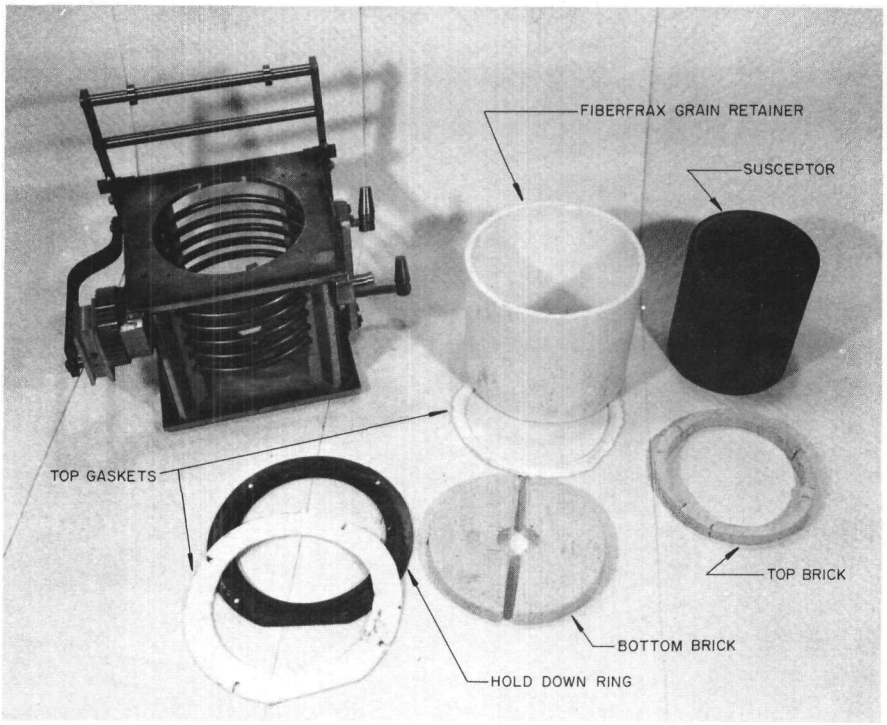

FIGURE 24

ASSEMBLED M-6 FURNACE

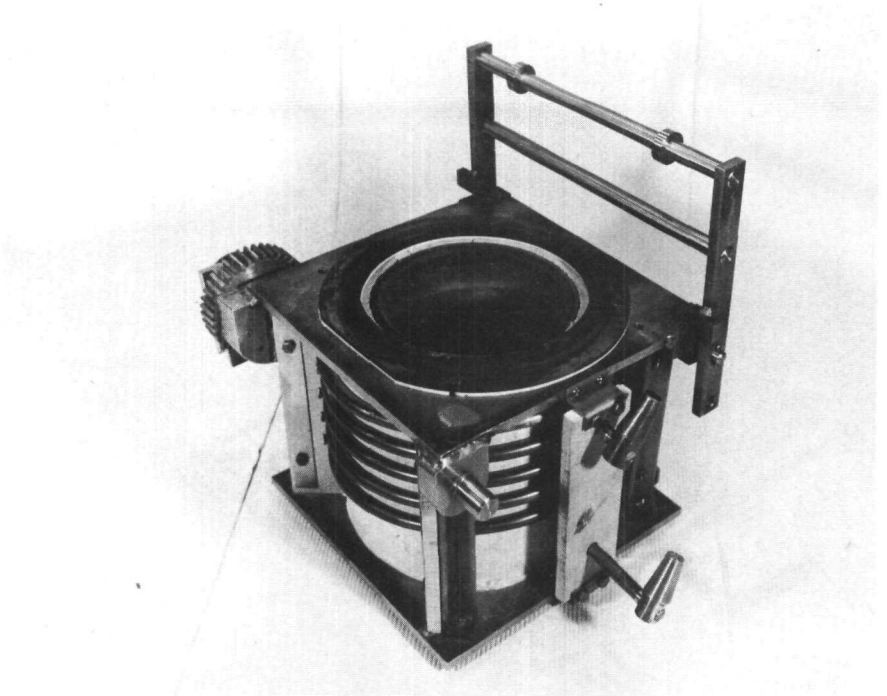

FIGURE 25

INVERTED VIEW OF THE ASSEMBLED M-6 FURNACE

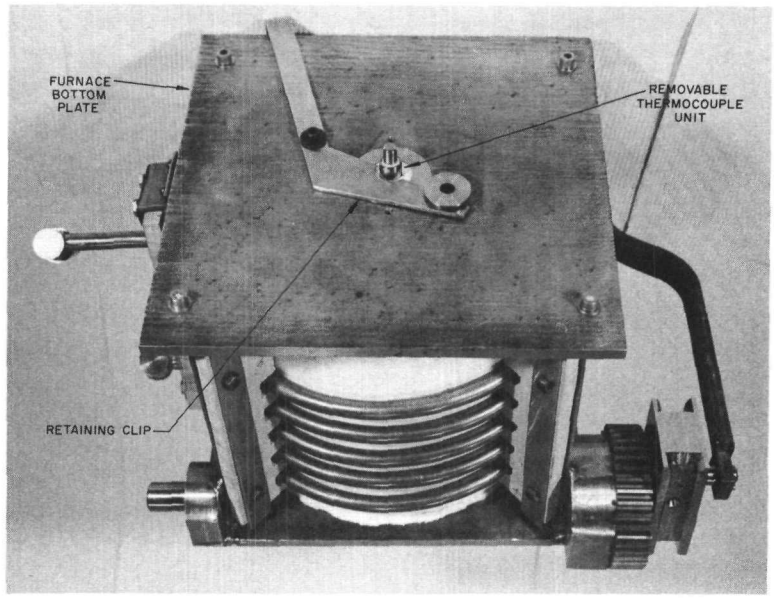

Figure 26 shows the furnace thermocouple. It can also be seen in Figures 22 and 25. The chromel and alumel cylinders make contact with clips on the furnace base plate when the furnace is in the run position.

FIGURE 26
FURNACE THERMOCOUPLE

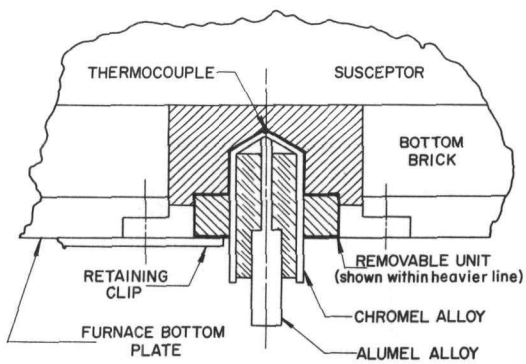

(2) EBR-II Fuel Alloy Production

Twenty-four ten-kilogram batches of enriched uranium pin scrap, generated during the manufacture of fuel pins for EBR-II, were received from Metallurgy. This scrap was melted down and poured into ingots using melt refining equipment. For the 24 runs the average yield was 92.3 percent, with the high yield being 95.4 and the low yield being 87.9 percent. Thirty-eight batches of pin scrap have been received and recast into ten-kilogram ingots to date.

C. Pyrometallurgical Research
(H. M. Feder)

1. Chemistry of Liquid Metal Solvents
(I. Johnson)

The chemistry of liquid metal systems is being investigated to provide basic concepts and data for the logical design of pyrometallurgical separations processes. The separations process under consideration consists of the dissolution of the spent reactor fuel in an appropriate volatile liquid, separation of the fission products and other extraneous elements by recrystallizations and/or extractions with immiscible liquids (either fused salts or other liquid metals), and, finally, recovery of the fissile metal(s) by evaporation of the solvent.

a. Solubilities in Liquid Metals

The solubilities of the elements whose separations are being attempted are of prime importance in the design of fuel reprocessing schemes. The dependence of solubilities on temperature and solvent composition needs to be known. The identity of the solid phase in equilibrium with the saturated solutions is useful when solubility trends are being investigated.

Solubility of Europium in Cadmium
(I. Johnson, K. E. Anderson and R. Claypool*)

The solubility of europium in liquid cadmium has been measured by means of the standard method discussed in ANL-6068, page 66. Two experiments were performed. In the first experiment, 16.2 grams of europium metal (99+ percent, Lindsey Chemical Company) and 440 grams of cadmium (99.99 percent, American Smelting and Refining Company) were heated together at 565 C in a high-purity alumina crucible for 16 hours. A porcelain thermocouple well and tantalum stirrer were used. Samples were taken with magnesium oxide-coated quartz sampling tubes fitted with grade 60 graphite filters. No evidence of reaction between samples and sampling tubes was observed at the temperature of these experiments. In the second experiment, 26.5 grams of europium metal (99+ percent, Michigan Chemical Company) and 404 grams of cadmium were used; the procedure was otherwise identical with that of the first experiment. The results of the two experiments are given in Table 22 and shown graphically in Figure 27.

---

* Student Aide, Summer 1960.

Table 22

SOLUBILITY OF EUROPIUM IN CADMIUM

Temp (C)	Europium (atom %)	Temp (C)	Europium (atom %)
502	4.25	367	0.287
478	2.57	361	0.251
462	2.18	353	0.203
422	1.095	345	0.192
421	0.995	328	0.107
403	0.677	328	0.105
389	0.542		

FIGURE 27
SOLUBILITY OF EUROPIUM, GADOLINIUM, DYSPROSIUM, AND ERBIUM IN LIQUID CADMIUM

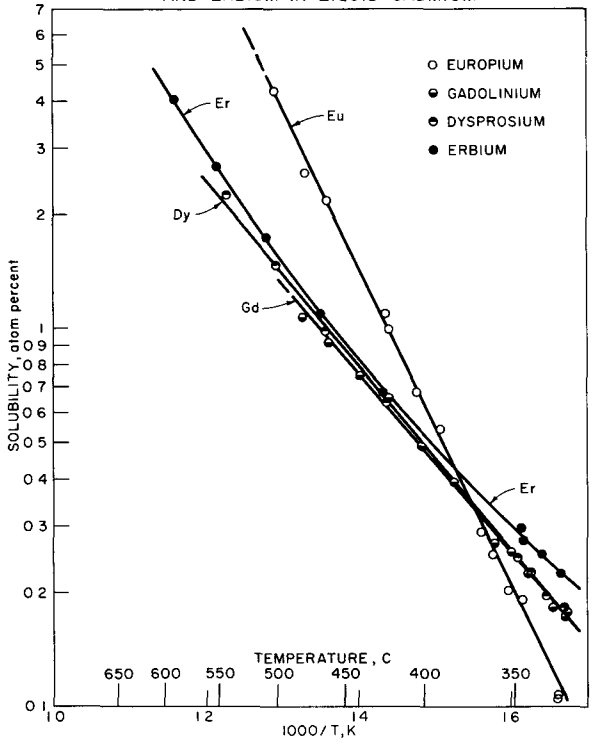

These data may be represented by the empirical equation

europium: $\log$ (atom percent) = $6.0627 - 4210.2T^{-1}$

to within ±8 percent over the temperature range from 330 to 500 C. The solid phase in equilibrium with the saturated solution was isolated from the ingot by the electrolytic etching method described by Martin (see

page 103). X-ray examination gave a pattern[10] which was similar to that which was reported for the tetragonal $BaCd_{11}$ intermetallic compound.[11] No europium-cadmium intermetallic phases have been reported in the literature. Chemical analysis and determinations of the density of the compound are being made.

Solubility of Gadolinium in Cadmium
(I. Johnson, R. Claypool* and K. E. Anderson)

The solubility of gadolinium in liquid cadmium was measured by means of the same procedure as previously described for europium. A sample of 8.4 grams of gadolinium metal (99+ percent, Michigan Chemical Company) and 410 grams of cadmium (99.99 percent, American Smelting and Refining Company) were held together at 510 C for 15 hours prior to sampling. During this heating period the mixture was stirred for seven hours. Samples were taken from 501 to 325 C.

The results are given in Table 23 and shown graphically in Figure 27. These data may be represented by the empirical equation

$$\text{gadolinium: } \log(\text{atom percent}) = 3.2172 - 2379.3\ T^{-1}$$

to within ± 3.5 percent.

Table 23

SOLUBILITY OF GADOLINIUM IN CADMIUM

Temp (C)	Gadolinium (atom %)	Temp (C)	Gadolinium (atom %)
480	1.13	360	0.269
460	0.917	351	0.256
439	0.749	343	0.225
420	0.652	330	0.183
401	0.486	325	0.174
381	0.391	324	0.177

The equilibrium solid phase was isolated from the ingot by the electrolytic etching method (see page 103). The X-ray diffraction pattern[10] obtained was similar to that reported by F. H. Ellinger[12] for the

[10]Schablaske, R., private communication.

[11]Sanderson, M. J. and Baenziger, N. C., Acta Cryst. 6, 627-631 (1953).

*Student Aide, Summer 1960.

[12]Ellinger, F. H., J. Phys. Chem. 64, 144 (1960).

cerium-cadmium intermetallic phase $CeCd_6$. The X-ray pattern of the cadmium-rich yttrium-cadmium intermetallic phase previously reported (ANL-6231, page 72) is also similar to the pattern obtained for $CeCd_6$.

Solubility of Dysprosium in Cadmium
(I. Johnson and K. E. Anderson)

The solubility of dysprosium in liquid cadmium was measured using the same procedure as described previously for europium. A sample of 16.1 grams of dysprosium metal (99.5 percent, Michigan Chemical Company) and 437 grams of cadmium (99.99 percent, American Smelting and Refining Company) were held together at 630 C for 22 hours prior to sampling. During the 22-hour heating period the mixture was stirred for 14 hours. Samples were taken from 634 to 325 C.

The results are given in Table 24 and shown graphically in Figure 27. These data may be represented by the empirical equation

$$\text{dysprosium: } \log (\text{atom percent}) = 3.3351 - 2446.6\ T^{-1}$$

to within ±3 percent.

Table 24

SOLUBILITY OF DYSPROSIUM IN CADMIUM

Temp (C)	Dysprosium (atom %)	Temp (C)	Dysprosium (atom %)
542	2.25	348	0.247
501	1.47	342	0.225
463	0.980	333	0.197
423	0.641	325	0.181
382	0.395		

The equilibrium solid phase was isolated from the ingot by the electrolytic etching method (see page 103). The X-ray diffraction pattern[10] obtained was similar to that found for the gadolinium-cadmium intermetallic phase and hence the equilibrium solid phase is presumably the intermetallic compound $DyCd_6$.

Solubility of Erbium in Cadmium
(I. Johnson and K. E. Anderson)

The solubility of erbium in liquid cadmium was measured using the same procedure as described previously for europium. A 30-gram sample of erbium metal (99+ percent, Michigan Chemical Company) and

451 grams of cadmium metal (99.99 percent, American Smelting and Refining Company) were held together at 630 C for 22 hours prior to sampling. The mixture was stirred for four hours during the heating period. Samples were taken from 628 to 327 C.

The results are given in Table 25 and shown graphically in Figure 27. These data may be represented by the empirical equation

$$\text{erbium: } \log(\text{atom percent}) = 6.3093 - 6644.0\ T^{-1} + 1.4847 \times 10^{6}\ T^{-2}$$

to within ± 2.6 percent.

Table 25

SOLUBILITY OF ERBIUM IN CADMIUM

Temp (C)	Erbium (atom %)	Temp (C)	Erbium (atom %)
589	4.01	386	0.604
551	2.70	346	0.298
508	1.74	345	0.277
467	1.09	336	0.252
425	0.676	327	0.223

The equilibrium solid phase was isolated from the ingot by the electrolytic etching method (see page 103). The X-ray diffraction pattern was similar to that found for the gadolinium-cadmium intermetallic phase and hence the equilibrium solid phase is presumably the compound $ErCd_6$.

Manganese-Cadmium System
(M. G. Chasanov and P. D. Hunt)

Preliminary results for the solubility of manganese in liquid cadmium were reported in ANL-6145, page 72. The results of a more comprehensive solubility determination using the same method are shown in Figure 28. The solubility data over the temperature range from 327 to 653 C may be represented by the empirical equation

$$\text{manganese: } \log(\text{atom percent}) = 3.263 - 3054\ T^{-1} + 0.4476 \times 10^{6}\ T^{-2}$$

The standard deviation, σ, was found to be 3.0 percent.

X-ray examination of compacts prepared from manganese and cadmium and annealed at 450 C gave no evidence of intermetallic formation; thermal analysis of charges containing 10, 20, and 30 weight percent of

manganese gave arrests only at the freezing point of cadmium and at temperatures corresponding to the $\alpha \rightarrow \beta$ transition of manganese. Similarly, Zwicker[13] has reported finding no alloys, even on heating manganese and cadmium to 1200 C.

FIGURE 28
SOLUBILITY OF MANGANESE IN LIQUID CADMIUM

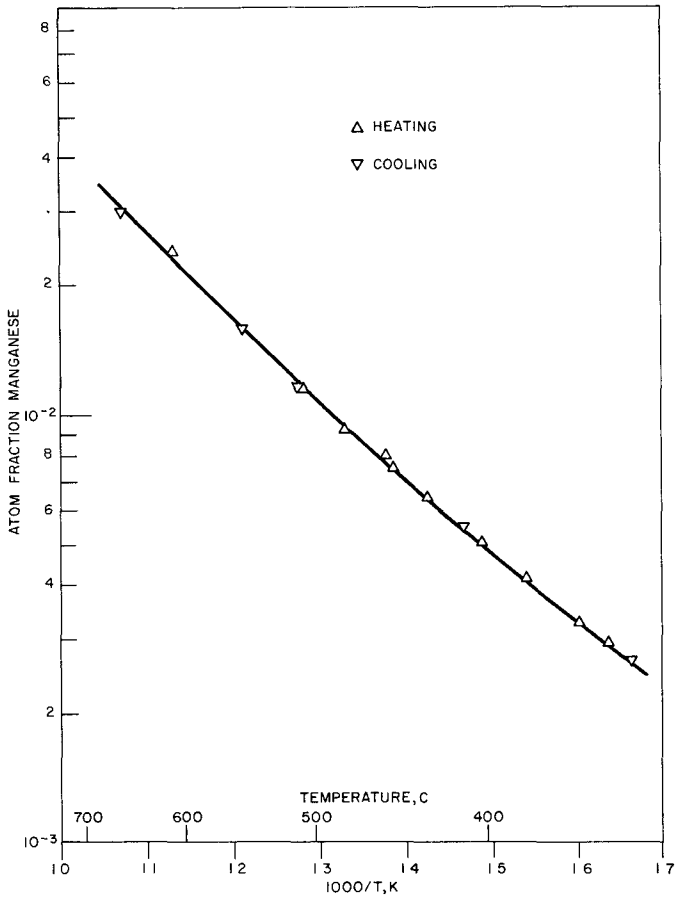

Nickel-Cadmium System

(M. G. Chasanov and P. D. Hunt)

The solubility of nickel in liquid cadmium was determined over the temperature range from 330 to 652 C by the same method used for the preliminary experiment reported in ANL-6145, page 73. Results are given in Figure 29. The upper line (from 509 to 650 C) may be represented by the empirical equation

$$\text{nickel: } \log (\text{atom percent}) = 1.954 - 740.8\ T^{-1} \quad .$$

The standard deviation, σ, was found to be 1.8 percent.

---

[13] Zwicker, U., Z., Metallkunde 41, 399 (1950).

FIGURE 29
SOLUBILITY OF NICKEL IN LIQUID CADMIUM

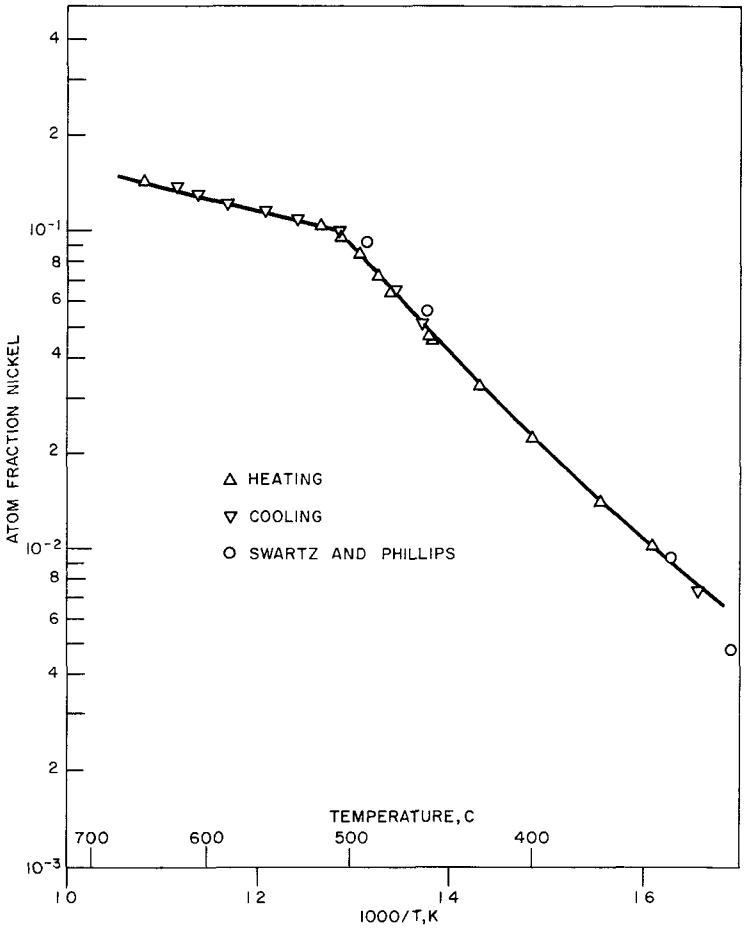

The lower curve (from 330 to 509 C) may be represented by the empirical equation

$$\text{nickel: } \log(\text{atom percent}) = 6.722 - 5628\ T^{-1} + 0.9045 \times 10^{6}\ T^{-2} \quad .$$

The standard deviation was found to be 1.6 percent.

The results of Swartz and Phillips,[14] obtained by thermal analysis, are also indicated in Figure 29; their values are in substantial agreement with our determinations.

The intersection of the curves in Figure 29 indicates a peritectic at 509.3 C; Voss[15] reported a peritectic at 502 C, whereas Swartz and Phillips found it at 490 C. All three values are in reasonable

---

[14] Swartz, C. E. and Phillips, A. J., Trans. AIME 111, 333 (1934).

[15] Voss, G., Z. anorg. Chem. 57, 69 (1908).

agreement, considering the uncertainty of peritectic determinations by thermal analysis or metallographic examination.

Zinc-Uranium System
(A. E. Martin and C. Wach)

Chiotti, Klepfer and Gill[16] found only one intermediate phase in the zinc-uranium system. This phase was originally identified as UZn_9 but was later shown by the crystal structure work of Makarov and Vinogradov[17] to correspond to the formula U_2Zn_{17}. In conformance with normal nomenclature of uranium binary systems, this phase will be referred to hereafter as the delta phase. It was found to have a congruent melting point in a condensed system at about 1050 C.[16]

Considerable evidence has been obtained in recent months at this laboratory for the existence of a second intermediate phase, referred to as the epsilon phase. The epsilon phase is richer in zinc than the delta phase and decomposes peritectically at about 840 C to form the delta phase and a uranium-saturated zinc melt. The evidence for the existence of the epsilon phase, its composition, peritectic decomposition temperature, and other properties is based on a wide variety of experiments, namely, effusion studies, thermal analysis, and diffusion tests, supported by X-ray and metallographic examinations and chemical analyses of products.

The effusion evidence was given in ANL-6183, pages 72 and 75, and is reported in more detail elsewhere in this report. Several exploratory thermal analysis experiments on zinc-uranium alloys containing about 20 percent uranium disclosed a peritectic thermal arrest at about 840 C. A more precise measurement of the arrest temperature was then made with a charge containing 22 percent uranium. The uranium was added as 20-mesh spheres. As a preliminary treatment the charge was held for 24 hours at 465 C. This procedure was known from previous experience to produce a bed of finely divided intermetallic particles. The charge was then heated to 800 C, and from this temperature the charge was heated to 900 C at the uniform rate of 0.8 C per minute. The peritectic temperature was established as 844 C by a substantial thermal arrest at this temperature.

The diffusion tests were carried out as follows. Uranium rods of $\frac{5}{16}$-inch diameter were heated in molten zinc in tantalum crucibles under helium atmospheres for various lengths of time at temperatures from 435 to 875 C. The melts were quenched to room temperature, the ingots were sectioned, and the interfaces between the uranium rods and the zinc were examined metallographically.

---

[16] Chiotti, P., Klepfer, H. H., and Gill, K. F., J. Metals, Trans. 9, 51-57 (1957).

[17] Makarov, E. S., and Vinogradov, S. I., Kristallografia 1, 634-643 (1956).

In tests made at 610, 710, 750, 800, and 875 C, well-defined annular rings of intermetallic were observed at the interfaces between the uranium and zinc. A single intermetallic layer had formed at 875 C, and it was identified by X-ray diffraction examination as the delta phase. A portion of this layer was separated mechanically and analyzed chemically. The results are given in Table 26. Two contiguous intermetallic layers were found from samples at 610, 710, 750, and 800 C. An X-ray diffraction examination of a sample of the outer layer obtained in the test at 710 C showed that it was the epsilon phase. Metallographic examination of all of these specimens indicated that the interior layer was the same as the single layer which had formed in the test at 875 C.

Table 26

ANALYSES OF ZINC-URANIUM INTERMETALLIC PHASES

Sample	Uranium (weight percent)	Zinc (weight percent)	Zinc: Uranium (atom ratio)
Delta layer formed on U rod at 875 C	28.3	72.0	9.26
Epsilon crystals,[a] Ingot No. 1,[b] +60 mesh	23.7	75.7	11.63
Epsilon crystals, Ingot No. 1, -60 +100 mesh	24.3	75.7	11.34
Epsilon crystals, Ingot No. 1, -100 mesh	23.9	75.8	11.55
Epsilon crystals, Ingot No. 2,[c] +60 mesh	24.6	75.5	11.18

[a] Recovered from ingots by electrolytic etching using an electrolyte of 200 g CrO_3, 1.5 g Na_2SO_4 and 1000 ml water. A current density of about 100 ma/sq cm and an emf of about 1.0 to 1.5 volts were used.

[b] Ingot No. 1 was prepared from a zinc-1.5 weight percent uranium melt by cooling from 725 C at a rate of 0.5 to 2 C/minute.

[c] Ingot No. 2 was prepared from a zinc-1.9 weight percent uranium-0.16 weight percent magnesium melt by cooling from 730 C at a rate of 0.3 to 0.8 C/minute.

The intermetallic layers were not as well defined in the specimens made at 435, 460, 500, and 550 C, especially at the first two temperatures, at which the reaction proceeded at a faster rate than at any higher temperature, with the formation of crystals of 1 micron diameter and smaller.

It did not prove feasible to separate a sample of the epsilon phase which had been formed in some of the diffusion experiments. However, since this was obviously the phase in equilibrium with liquid zinc at temperatures below the peritectic temperature, crystals of this phase were readily formed by cooling a zinc melt saturated with uranium. The crystals were separated from the zinc matrix by selective dissolution of the zinc by electrolytic etching. The analyses of samples recovered in this way from two different ingots are given in Table 26. In one case three different size fractions of crystals were analyzed to determine whether a trend existed in the zinc-uranium ratio with particle size. No trend was observed. Had there been one, it would have suggested that the electrolytic etching procedure was removing some zinc from the intermetallic crystals.

Additional evidence of the composition of the intermediate phases was obtained in two annealing experiments in which charges of 26.0 and 28.5 weight percent uranium (10.36 and 9.14 zinc:uranium atom ratios, respectively) were sealed in tantalum containers and, after an initial treatment at 455 C to form uniform beds of fine intermetallic particles, were held at 750 C for 27 days and quenched to room temperature. The only intermetallic phases found in these samples by X-ray diffraction examination were epsilon in the first sample and delta in the second.

The epsilon and delta phases were found to have different chemical and electrolytic etching rates. This facilitated the metallographic identification of these phases in samples which contained both phases, for example, samples from most of the diffusion tests and in all samples cooled slowly from above the peritectic temperature. In the latter samples, the epsilon phase was present as peritectic rims on the delta-phase particles.

Cadmium-Uranium System
(A. E. Martin and C. Wach)

The effect of cadmium on the alpha-beta transformation temperature of uranium was determined by thermal analysis. A cadmium-uranium charge containing 25 weight percent uranium in the form of 100-mesh spheres was first held for 18 hours at about 680 C to ensure saturation of the uranium particles with cadmium. The charge was cooled at 1 C/minute and an arrest was obtained at 644 C. After holding for 28 hours at about 630 C, the charge was heated at 1 C/minute and an arrest was obtained at 669 C. These transformation temperatures are, within experimental error, the same as those of pure uranium. Consequently, these data do not indicate an appreciable solubility of cadmium in uranium.

The effect of uranium on the lattice parameters of cadmium at 310 C was determined. A cadmium melt containing 2 percent uranium was frozen and held at 310 C for 23 hours and quenched to room temperature. The lattice parameters of the cadmium phase in the ingot were determined as $a_0 = 2.9790$ Å and $c_0 = 5.6181$ Å. Since these are, within experimental error, the same as those of pure cadmium, no appreciable solubility of uranium in cadmium at 310 C is indicated by these data.

The eutectic temperature was redetermined by thermal analysis. A sample of the melt, which contained 0.13 weight percent uranium, was withdrawn just before the determination to verify that the composition was optimum, namely, somewhat greater than the eutectic composition. (The latter was known to be about 0.06 weight percent uranium from solubility measurements.) The eutectic temperature was determined at a cooling rate of 1 C/minute as 0.26 C below the freezing point of cadmium. If the freezing point of cadmium is taken as 320.9, the eutectic temperature is 320.6 C.

b. Coprecipitation Studies

The degree of separation which may be achieved by recrystallization from metallic solvents is often limited, not by the lack of sufficient difference in solubility, but rather by the extent of coprecipitation. Thus, even though the solubility of an impurity is not exceeded when the temperature is lowered, a large fraction of the impurity present may crystallize with the fissile metal. For example, when the uranium-zinc intermetallic compound is crystallized from liquid zinc in the presence of small amounts of plutonium, it is found that the same fraction of plutonium and uranium are carried from the solution, and hence no separation is achieved. On the other hand, if sufficient magnesium is added to the solution to cause pure uranium metal to separate as the crystallizing phase, then the plutonium remains completely in solution and complete separation is theoretically possible.

Coprecipitation by $CeCd_{11}$ from Cadmium Solutions

(J. Moriarty*)

A fundamental study of the factors which determine the coprecipitation behavior of various metallic solutes by intermetallic compounds has been started. This is a continuation of previous work.[18]

Coprecipitation from metallic solutions is completely analogous to that found in aqueous solutions. The logarithmic distribution law of Doerner and Hoskins,[19] which may be expressed by the equation

$$\log\left(\frac{\text{tracer in solution}}{\text{total tracer}}\right) = \lambda \log\left(\frac{\text{carrier in solution}}{\text{total carrier}}\right) ,$$

is generally applicable (see ANL-5820, page 100). This relation may be ascribed to the existence of a dynamic equilibrium between the tracer in solution and each successive layer deposited on the crystals of the precipitating carrier. Diffusion within the solid host crystal is not able to equalize the tracer concentration during crystallization. The coprecipitation coefficient, λ, is a quantitative measure of the carrying characteristics of a specific tracer by a carrier.

Systematic measurements of the carrying characteristics of the cerium-cadmium intermetallic compound $CeCd_{11}$ (cubic, $BaHg_{11}$ type) are being made. Studies of the coprecipitation behavior of the following tracer elements are planned: cesium, rubidium, potassium, sodium, lithium, barium, strontium, magnesium, calcium, scandium, yttrium, lanthanum, samarium, europium, gadolinium, zirconium, uranium and thorium. These metals allow the influence of atomic size, metallic valence, and electronic configuration on coprecipitation behavior to be investigated.

The general experimental procedure has been described in ANL-5820, page 100. In the present experiments the system is allowed to reach equilibrium with respect to the crystallized $CeCd_{11}$ at each temperature before sampling the liquid phase. The standard sampling procedure described by Martin[20] is used. Filtered samples are taken at 30 C intervals from 550 to 350 C. The starting alloy composition for a typical experiment was 1.0 percent cerium, 0.01 to 0.1 percent tracer, with the remainder cadmium.

---

* Post Doctorate Fellow.

[18] Feder, H. M., and Teitel, R. J., Proc. Second International Conference on the Peaceful Uses of Atomic Energy, Geneva, Switzerland, (1958) Vol. 17, pp. 391-392.

[19] Doerner, H. and Hoskins, W., J. Am. Chem. Soc. 47, 662 (1925).

[20] Martin, A. E., Knighton, J. B., and Feder, H. M., J. Chem. and Eng. Data, to be published.

Values of coprecipitation coefficient, λ, were computed by fitting a logarithmic equation to the data using the least squares method. Results to date are reported in Table 27. Doerner-Hoskins graphs of the data are shown in Figure 31.

Table 27

COPRECIPITATION BY $CeCd_{11}$ FROM LIQUID CADMIUM

Tracer Element	Coprecipitation Coefficient λ	Tracer Element	Coprecipitation Coefficient λ
Sodium	0	Uranium	0.13 ± 0.04
Lithium	0	Strontium	0.10 ± 0.02
Potassium	0	Europium	0.099 ± 0.009
Yttrium	0	Zirconium	0.04 ± 0.01
Lanthanum	1.49 ± 0.11		

FIGURE 31
COPRECIPITATION BY $CeCd_{11}$ FROM LIQUID CADMIUM SOLUTION

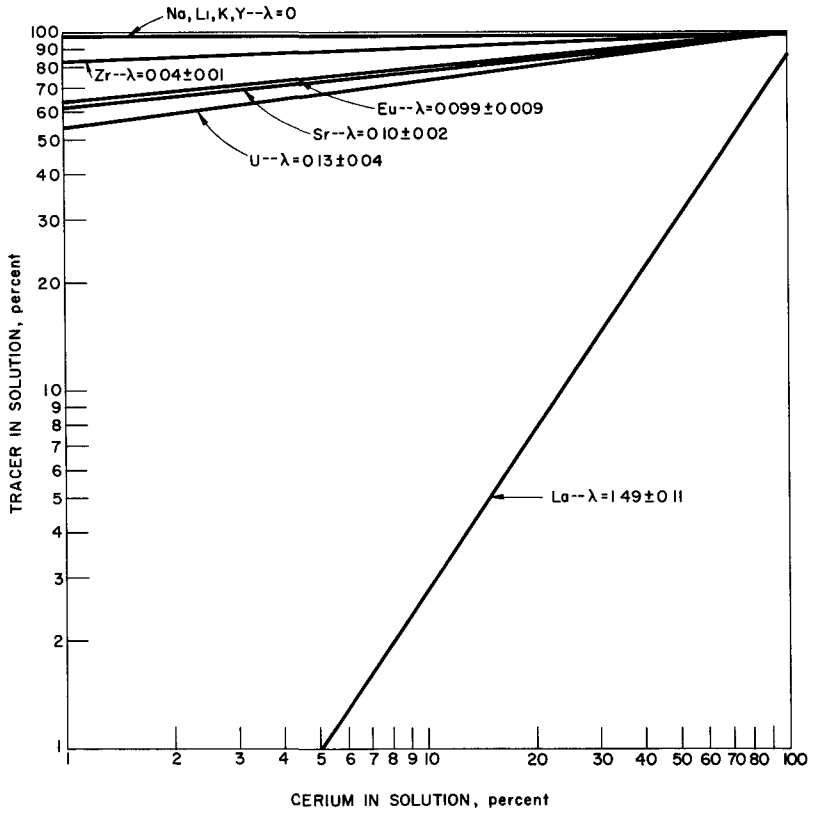

c. Liquid-Liquid Partition Studies
(F. Cafasso, R. Uhle and J. Vincenzi)

Partition of Palladium, Uranium, Cerium and Strontium between Bismuth and Zinc

The immiscible liquid pairs lead-zinc and bismuth-zinc are being examined as potential solvent systems for the separation of fissile elements from fission product elements by partition methods. Distribution coefficients for palladium, uranium, cerium, and strontium between lead and zinc were measured at approximately 730 C and were reported in ANL-6231, page 74. Similarly, the partition coefficients of these same four elements between bismuth and zinc have been measured in the range 547 to 549 C and are reported below.

The procedures which were used in the lead-zinc system were found to be applicable to the bismuth-zinc system. Bismuth, zinc, and the appropriate solute metal were placed in an alumina crucible and heated to approximately 550 C. The two-phase melt which resulted was stirred with a tantalum paddle for one hour and allowed to settle for two hours. Samples of both layers were then taken with magnesium oxide-coated quartz tubes fitted with graphite filters. Four samples of both layers of the melt were taken. In every case, it was found that equilibrium was established after the first hour of stirring.

Values of the distribution coefficient K, defined as the ratio of the weight percent (average) of the solute in the zinc layer to its weight percent (average) in the bismuth layer, are recorded in Table 28.

Table 28

COMPILATION OF DISTRIBUTION DATA FOR THE BISMUTH-ZINC SYSTEM

Temperature: 548 ± 1 C

Solute	Zinc Layer[a] (w/o, avg)	Bismuth Layer[b] (w/o, avg)	Distribution Coefficient, K (avg) = w/o in Zinc Layer / w/o in Bismuth Layer
Pd	1.5	4.5×10^{-2}	33.3
U	1×10^{-2}	6.5×10^{-2}	0.17
Ce	3×10^{-2}	5.7×10^{-1}	0.05
Sr	3×10^{-3}	3.9	7.7×10^{-4}

[a] The solubility of bismuth in zinc was found to be 12.6 w/o when uranium was the solute.

[b] The solubility of zinc in bismuth was found to be 37.0 w/o when uranium was the solute.

Only palladium concentrates preferentially in the zinc layer. A factor of about 64 separates the coefficients of strontium and cerium, whereas a factor of only 3.4 separates the coefficients of cerium and uranium.

The mutual solubilities of bismuth and zinc were measured only in the uranium system. At 549 C, the solubility of bismuth in zinc (containing 1×10^{-2} weight percent uranium) is 12.6 weight percent, whereas that of zinc in bismuth (containing 6×10^{-2} weight percent uranium) was 37.0 weight percent. These values are in reasonable agreement with the measurements made by Kleppa,[21] who reports values of 15 weight percent for the solubility of bismuth in zinc and 38.0 weight percent for the solubility of zinc in bismuth.

Temperature Dependence of the Uranium Distribution Coefficient in the Bismuth-Zinc System

In evaluating the utility of distribution methods in separations, three factors must be considered, namely, the solubilities of the solutes, their distribution coefficients, and the mutual solubilities of the solvents. All three factors are temperature dependent. Measurements of the distribution coefficient of uranium in the bismuth-zinc-uranium system were made at three temperatures: 447, 494, and 552 C. The distribution coefficient, defined as in the previous section, had values of 0.078 at 447 C, 0.10 at 494 C, and 0.168 at 552 C. These data are shown as a function of temperature in Figure 32.

FIGURE 32
EFFECT OF TEMPERATURE ON THE DISTRIBUTION OF URANIUM BETWEEN BISMUTH AND ZINC

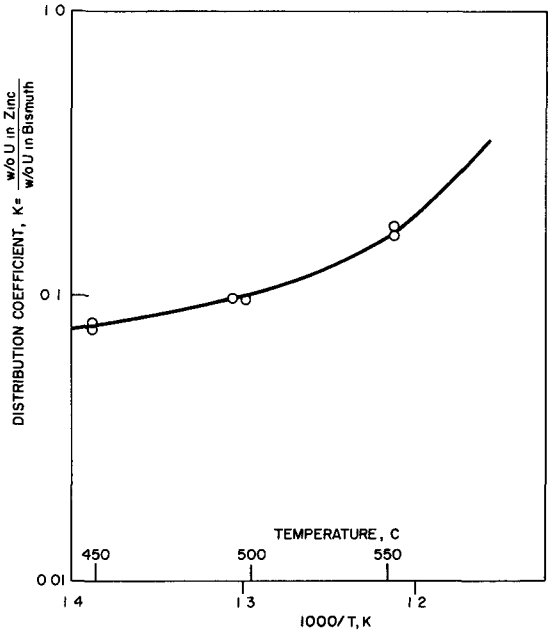

[21] Kleppa, O. J., J. Am. Chem. Soc., 74, 6052 (1952).

The value at 500 C is larger than that previously measured by other investigators.[22] Taking samples after the equilibrium melt had been quenched, Miles[22] obtained a value of 0.04 for the distribution coefficient of uranium at 500 C. The value at 500 C obtained in the present study by sampling liquid phases, which is considered to be the preferable sampling method, was 0.12. As the temperature is raised, the partition favors the zinc layer. For a 100 degree increase, the partition coefficient increases by a factor of two. This effect is much smaller than in the lead-zinc-uranium system (ANL-6231, page 75), in which it was found that an 80 degree rise caused a ninefold change of the coefficient in favor of the lead layer.

Comparison of Distribution in the Bismuth-Zinc and Lead-Zinc Systems

The distribution data for palladium, uranium, cerium, and strontium in both the lead-zinc system (ANL-6231, page 74) and the bismuth-zinc system have been compiled in Table 29 to allow a comparison. This comparison is made at two different temperatures, about 730 C for the lead system and about 550 C for the bismuth system. Each temperature is about 50 C below the consolute temperature of the respective system. Uranium, cerium, and palladium all favor the zinc phase in the lead-zinc system, whereas only palladium favors zinc in the bismuth-zinc system. In the lead-zinc system, the distribution coefficient of palladium is greater than that of uranium by a factor of six. Uranium, in turn, has a coefficient larger than cerium by a factor of six.

Table 29

COMPARISON OF DISTRIBUTION DATA FOR THE LEAD-ZINC AND BISMUTH-ZINC SYSTEMS

Solute	Distribution Coefficient,[a] $K = \frac{\text{w/o solute in Zinc Layer}}{\text{w/o solute in Lead Layer}}$	Distribution Coefficient,[b] $K = \frac{\text{w/o solute in Zinc Layer}}{\text{w/o solute in Bismuth Layer}}$
Palladium	150.0	33.3
Uranium	30.8	0.17
Cerium	3.7	0.05
Strontium	0.14	7.7×10^{-4}

[a] Temperature $\cong$ 730 C (reported in ANL-6231, page 74).

[b] Temperature $\cong$ 550 C.

[22] Miles, F. T., Progress Letter, BNL-2689 (December 1955).

In the bismuth-zinc system, a factor of 200 separates the coefficients of palladium and uranium. A factor of 3.4 separates the coefficients of uranium and cerium. Strontium appears to distribute in favor of the heavier phase in both systems, in lead in the lead-zinc system and in bismuth in the bismuth-zinc system.

Mutual Solubilities of Aluminum and Cadmium

The mutual solubilities of liquid aluminum and cadmium were measured as a function of temperature in the range 680 to 720 C and are shown in Figure 33. The solubility data may be represented by the empirical equations

$$\text{cadmium: } \log(\text{atom percent}) = 3.479 - 2944\ T^{-1} \text{ for cadmium in aluminum}$$

and

$$\text{aluminum: } \log(\text{atom percent}) = 3.702 - 2815\ T^{-1} \text{ for aluminum in cadmium.}$$

FIGURE 33
MUTUAL SOLUBILITIES OF ALUMINUM AND CADMIUM

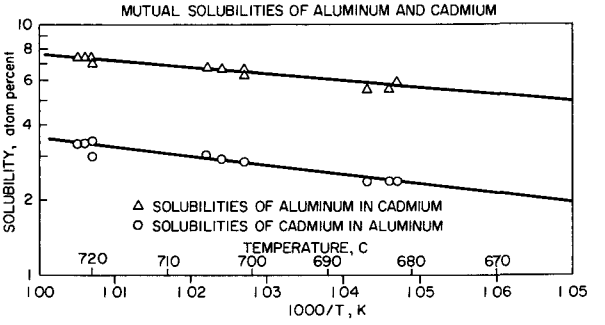

Extrapolation of the solubility curve of cadmium in aluminum to the monotectic temperature (649 C) gives a value of 1.7 atom percent. This value agrees well both with Hardy's[23] value of 1.6 atom percent, which he estimated from the maximum solid solubility at the monotectic temperature, and the value of 1.8 atom percent measured by Hansen and Blumenthal.[24]

At 686 C, the solubility of cadmium in an aluminum solution containing 4.8 weight percent uranium was found to be 8.0 weight percent (see ANL-6183, page 70). The solubility of aluminum in cadmium containing roughly 1×10^{-5} weight percent uranium was 1.5 weight percent

---

[23] Hardy, H. K., J. Inst. Metals, 80, 431 (1951-1952).

[24] Hansen, M. and Blumenthal, B., Metallwirtschaft, 10, 925 (1931).

at this same temperature. In a solute-free system, the mutual solubilities measured at 686 C were 9.2 weight percent cadmium in aluminum and 1.4 weight percent aluminum in cadmium. Apparently, the presence of roughly 5 weight percent uranium in aluminum lowered the solubility of cadmium in this solvent by 1.3 percent. The presence of trace amounts of uranium (1×10^{-5} weight percent) in cadmium had no effect on the solubility of aluminum in this solvent, as expected.

d. Thermodynamic Studies

Thermodynamic functions for key elements in liquid metal solvents and for the important solid intermetallic phases are being measured. Two methods are being used. Galvanic cells have proved to be especially useful for determining activities in liquid solutions and for measuring the free energy of formation of the equilibrium solid phase in two-phase systems. On the other hand, for systems containing several well-defined intermetallic phases, measurement of the decomposition pressure by the effusion method is proving to be most useful. The two methods supplement each other.

Thermodynamics of the Uranium-Zinc System
(E. Veleckis and N. Goetzinger)

A preliminary report on the phase relationships and thermodynamic properties of the uranium-zinc system (determined by measurement of the vapor pressure by the effusion method) was presented in ANL-6183, pages 72 to 75. Additional data have been obtained which permit a more precise computation of the thermodynamic properties. The phase relationships in this system are discussed elsewhere in this report (see page 102).

The apparatus used in these studies was described by C. L. Rosen in ANL-5959, page 125. Modification of the null-point detection, weighing, and recording parts of the apparatus have been made which significantly improve the reliability of the apparatus. The furnace which was used to heat the effusion cell has been replaced by a molten salt bath. This allows more accurate control and measurement of the temperature.

For binary systems containing a single volatile component, the vapor pressure of the volatile species is related to composition of alloy by the Knudsen equation,[25] which may be written as

$$P_{mm} = -17.1435 \frac{w_2 \sqrt{TM_1}}{M_2 KA} \frac{dr}{dt} \quad ,$$

[25] Knudsen, M., Ann. Physik, 28, 75 (1909); 28, 999 (1909); 29, 179 (1909).

where P_{mm} is the pressure of the gas in the cell in mm Hg; w_2 the weight of nonvolatile species in the sample in grams, M_1 and M_2 the molecular weights of volatile and nonvolatile species, respectively, T the absolute temperature, K the Clausing short channel correction factor,[26] A the area of the orifice in sq cm, r the atomic ratio n_1/n_2, and t the effusion time in seconds.

The Knudsen cells which were used for vapor pressure measurements were made of tantalum. Two holes were drilled opposite to each other in the cell wall. This placement of the holes prevented the lateral displacement of the cell during the experiment. The cells were calibrated with pure zinc, because reliable vapor pressure data are available for zinc and because it constitutes the volatile component in the system under study. A further advanage lies in the fact that, with zinc, the calibration temperatures are close to those of the actual runs, thus making the orifice expansion corrections unnecessary. The so-called effective orifice area, i.e., the product of the actual area A and Clausing correction factor K, for Cells B and C were found to be 1.718×10^{-3} sq cm and 5.173×10^{-3} sq cm, respectively.

In a typical experiment, approximately 300 mg of finely powdered uranium-zinc alloy was weighed and placed in the effusion cell. The cell was then suspended from the right-hand side of the balance beam. After evacuating the entire system, purified helium gas was introduced into the system to a pressure of about 300 mm Hg. The salt-bath, preheated to the desired temperature, was then raised around the tube in which the effusion cell was suspended. The helium in the system insured rapid heat transfer between the salt bath and the effusion cell, and prevented effusion during the heatup period. After thermal equilibrium was reached, the effusion was initiated by a rapid evacuation of the helium. Effusion was continued until there was no further change in weight, i.e., until all the zinc was evaporated. The cell was then cooled in a helium atmosphere and the uranium residue was weighed. Depending on temperature and cell orifice size, the experiments lasted from 5 to 36 hours. The vacuum maintained in the system during the experiment was 1×10^{-5} mm Hg or better.

Thirteen runs have been made in the temperature range from 420.8 to 504.0 C. The original data were obtained in the form of isothermal weight loss versus time curves. As shown previously (see ANL-6183, page 73), such curves exhibit three distinct segments; these were interpreted at that time as representing two-phase fields in the phase diagram.

---

[26] Clausing, P., Ann. Physik, 12, 961 (1932); Z. Physik, 66, 471 (1930).

A more satisfactory method of representing the effusion data is provided by isothermal zinc vapor pressure versus alloy composition curves that are obtained from the original plots by a graphical differentiation. Three typical isotherms are shown in Figure 34. Included in this figure is a graphical representation of the proposed phase diagram in the experimental temperature range.

FIGURE 34

VARIATION OF VAPOR PRESSURE OF ZINC WITH COMPOSITION OF THE ALLOY IN URANIUM - ZINC SYSTEM

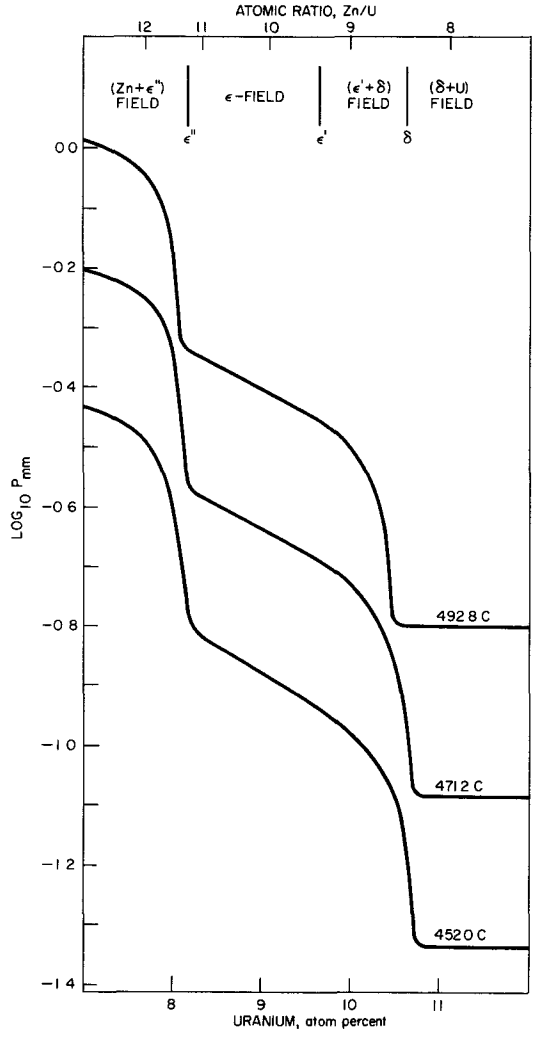

The sharp pressure decline at ϵ'' and at δ is a clear indication of phase boundaries existing at these compositions. The pressure descent at δ is followed by a well-developed pressure plateau which is indicative of formation of an intermetallic phase (designated by δ) of a very narrow homogeneity range at that composition. Between ϵ'' and ϵ' the vapor pressure of zinc decreases linearly with composition, suggesting the existence of a phase (designated by ϵ) with a wide homogeneity range between the boundaries ϵ'' and ϵ'. Extensive rounding-off in $(Zn + \epsilon'')$ and $(\epsilon' + \delta)$ fields is due to surface depletion of the sample as the concentration of the zinc-producing phase is rapidly falling off, thereby causing a premature pressure drop within the effusion cell. Similar depletion effects are observed in the uranium-rich side of the $(\delta + U)$ field. In calculating thermodynamic properties, the regions $(\epsilon' + \delta)$ and $(\delta + U)$ were regarded as pressure plateaus. The average compositions of the phase boundaries were found to be as follows: ϵ'' = 8.17 a/o uranium, $\epsilon' \cong$ 9.65 a/o uranium, and δ = 10.63 a/o uranium.

The logarithm of the vapor pressure of zinc at ϵ'' and in the $(\epsilon' + \delta)$ and $(\delta + U)$ regions, as well as that for pure zinc,[27] are shown as functions of the reciprocal absolute temperature in Figure 35.

---

[27] Barrow, R. F., Dodsworth, P. G., Downie, A. R., Jeffries, E. A., Pugh, A. C., Smith, F. I., Swinstead, J. M., Trans. Faraday Soc., 51, 1354 (1955).

FIGURE 35
VAPOR PRESSURE OF ZINC OVER δ AND ϵ
PHASES IN URANIUM-ZINC SYSTEM

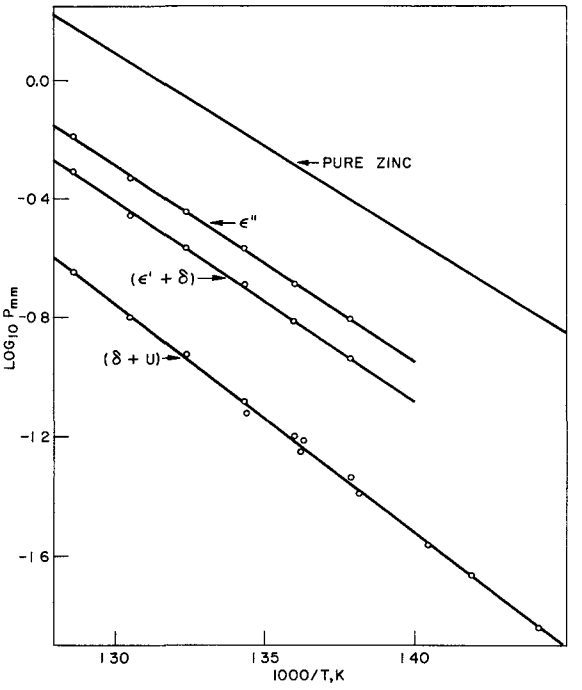

The straight lines shown may be represented by the empirical equations

$$\log P_{mm} = 8.329 - 6626\ T^{-1} \qquad \epsilon''$$

$$\log P_{mm} = 8.391 - 6766\ T^{-1} \qquad (\epsilon' + \delta) \text{ field}$$

$$\log P_{mm} = 9.290 - 7724\ T^{-1} \qquad (\delta + U) \text{ field.}$$

Combining these results with the expression for pure liquid zinc given by Barrow et al., the standard free energies of formation of ϵ-phase at the ϵ'' and ϵ' boundaries and of the δ phase may be represented by the following analytical expressions (see ANL-6183, page 73):

$$\Delta F^{\circ}_{\epsilon''} = -174.3 + 65.53\ T \log T - 40{,}850$$

$$\Delta F^{\circ}_{\epsilon'} = -139.2 + 54.57\ T \log T - 40{,}690$$

$$\Delta F^{\circ}_{\delta} = -122.8 + 49.56\ T \log T - 40{,}730.$$

As determined by effusion experiments, the average composition of the δ-phase boundary corresponds to the empirical formula $UZn_{8.41}$. In view of the structural evidence cited elsewhere in this report (see page 102), it seems plausible to assume that the δ-phase composition is U_2Zn_{17}. This latter composition value was, therefore, used in calculating $\Delta F^{\circ}_{\delta}$.

A summary of experimental data and standard free energies of formation are tabulated in Table 30. Except for the values of $\Delta F^{\circ}_{\delta}$, the free energies of formation were determined by direct integration of vapor pressure versus composition curves.

Table 30

EXPERIMENTAL DATA AND STANDARD FREE ENERGIES FOR THE SYSTEM URANIUM-ZINC

Run	Cell	Temperature (C)	Pressure (mm)			ΔF° (kcal/g atom U)		
			ϵ''	$\epsilon' + \delta$	$\delta + U$	ϵ''	ϵ'	δ [a]
V50	C [b]	420.8	-	-	0.0144	-	-	-28.26
V49	C	431.6	-	-	0.0214	-	-	-27.82
V48	C	438.8	-	-	0.0272	-	-	-27.75
V51	C	450.5	-	-	0.0406	-	-	-27.33
V67	B	452.0	0.157	0.115	0.0459	-30.53	-27.66	-26.37
V61 [c]	B	460.5	-	-	0.0608	-	-	-26.02
V52	C	460.8	-	-	0.0561	-	-	-27.18
V66	B	462.0	0.205	0.152	0.0632	-30.51	-27.50	-26.13
V53	C	470.6	-	-	0.0752	-	-	-27.10
V62	B	471.2	0.270	0.204	0.0818	-30.38	-27.49	-26.23
V63	B	482.0	0.358	0.272	0.1192	-29.67	-26.82	-25.37
V64	B	492.8	0.467	0.351	0.1586	-30.24	-27.07	-25.50
V65	B	504.0	0.647	0.491	0.2262	-27.92	-25.55	-24.75

[a] The values of ΔF° were calculated assuming r = 8.50 for the δ-phase boundary.

[b] The effective orifice areas (KA) for Cells C and B were 5.173×10^{-3} sq cm and 1.718×10^{-3} sq cm, respectively.

[c] Incomplete run.

Recently, Chiotti and Kilp[28] made vapor pressure measurements over the δ phase in the temperature range from 650 to 940 C and obtained the following equation:

$$\log P_{mm} = 9.21 - 7713\ T^{-1} \quad .$$

This equation compares favorably with the equation obtained in the present study:

$$\log P_{mm} = 9.290 - 7724\ T^{-1} \quad ,$$

over the temperature range from 420 to 504 C. The agreement of the two equations is noteworthy in view of the large temperature difference between the two studies.

[28] Chiotti, P. and Kilp, G. R., Trans. A.I.M.E., 218, 41 (1960).

Magnetic Studies

(F. Cafasso and D. Gruen*)

$CeCd_{11}$

The magnetic susceptibilities of a number of intermetallic compounds of the type AB_{11} where A may be some rare earth metal (e.g., cerium, praseodymium, neodymium, samarium) or some actinide element (e.g., uranium) are being studied in a joint effort of the Chemical Engineering Division and the Chemistry Division.

Susceptibility measurements were made by the Faraday method on roughly 100-mg powdered samples of the alloys, over the range from 4.2 K to room temperature. The assembly, consisting of a magnet, cryostat, balance, and sample suspension system, has been described in ANL-6145, page 81.

$CeCd_{11}$ was the first system studied. Earlier measurements made at room temperature (295.3 K) and at the normal boiling points of nitrogen (77.33 K) and helium (4.2 K) were reported in ANL-6145, page 83. Measurements at the nitrogen boiling point were repeated, and additional measurements at the boiling point of hydrogen (20.30 K), at the triple point of nitrogen (63.15 K), at 67.88 K (nitrogen under a fixed pressure of 210 mm Hg), and the boiling point of ethane (184.5 K) have been made. Values of the molar susceptibility of the compound $CeCd_{11}$ at each temperature are recorded in Table 31.

Table 31

MOLAR SUSCEPTIBILITY OF $CeCd_{11}$

Temp (K)	$M\chi_{CeCd_{11}} \times 10^3$	$M\chi_{Ce} \times 10^3$	$[M\chi_{Ce}]^{-1} \times 10^{-2}$
4.1_9	127.73	127.96	0.079
20.3_0	35.96_9	36.19_2	0.28
63.1_5	12.16_9	12.39_2	0.81
67.8_8	11.26_1	11.48_4	0.87
77.2_1	10.10_4	10.32_7	0.97
77.3_3	10.04_5	10.26_8	0.97
184.8_0	4.11_3	4.33_6	2.31
295.3_0	2.36_8	2.59_1	3.86_1

* Cooperating Chemist, Chemistry Division.

The molar susceptibility of cerium atoms in the alloy $[{}_M\chi_{Ce}]$, calculated by correcting for the diamagnetic contribution of the cadmium atoms per mole of alloy, is also tabulated in this table. The reciprocal of the molar susceptibility of cerium, $[{}_M\chi_{Ce}]^{-1}$, is plotted against temperature in Figure 36. A straight line was drawn through all the points obtained below room temperature. The system appears to obey a law of the Curie-Weiss type $\left[\chi = \frac{C}{(T-\Delta)}\right]$ with a value for Δ of -2 K. A least-squares treatment of the data yielded the following susceptibility-temperature relationship:

FIGURE 36

VARIATION OF $\chi^{-1}_{M\,Ce}$ WITH TEMPERATURE

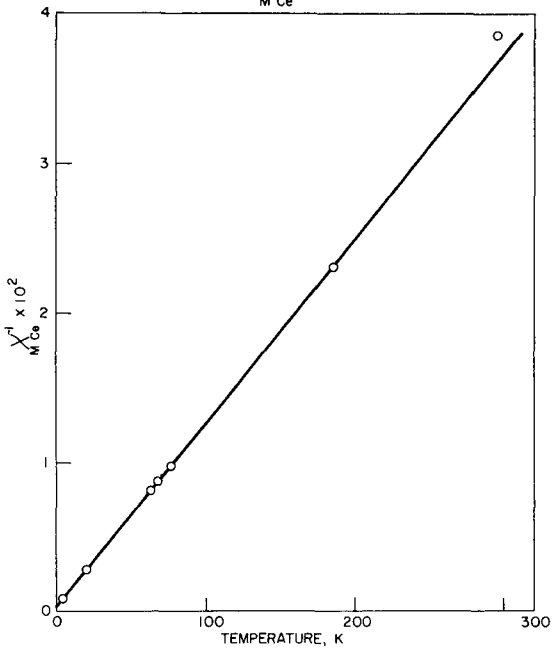

$$M\,\chi\,Ce = \frac{C}{T+2},$$

where C = 0.81. The effective number of Bohr magnetons (M_{eff}) for this system can be calculated from the relationship $M_{eff} = 2.84\sqrt{C}$. The constant C may be obtained from the slope of the line shown in Figure 36. A value of 2.55 is calculated for the experimental M_{eff} in this way. This value is in good agreement with the value of 2.56,[29] the theoretical value of the effective Bohr magneton number for a free gaseous cerium ion in a $^2F_{5/2}$ ground state.

The room-temperature susceptibility value is the only point which does not lie on the line. This can be attributed to the fact that the force experienced by the sample at this temperature is so small that the corrections for the diamagnetism of the container materials and for the cadmium atoms in the intermetallic (which constitute 90 percent of the sample) become significant. The latter value is not known with any degree of accuracy, so that the room temperature susceptibility value may be expected to be the least reliable. It is also possible that at room temperature the excited state of cerium $^2F_{7/2}$ is becoming populated. If this is so, some curvature would be introduced in a plot of $[{}_M\chi_{Ce}]^{-1}$ versus T.

---

[29] Van Vleck, J. H., The Theory of Electric and Magnetic Susceptibilities, Oxford University Press, London (1932), p. 243.

2. Calorimetry
(W. N. Hubbard)

Thermodynamic data are lacking for many compounds of interest in high-temperature chemistry because of the experimental difficulties involved in making the necessary measurements. A program has been undertaken to help fill this gap.

Part of the program consists of determinations of heats of formation at 25 C by oxygen bomb calorimetry. Because some of the compounds of interest are difficult to burn in oxygen and, consequently, cannot be studied by oxygen bomb calorimetry, the new technique of fluorine bomb calorimetry has been developed for their study. The accumulation of basic heat of formation data for fluorides is a necessary preliminary adjunct to fluorine bomb calorimetry and is a valuable program on its own merit.

The heats of formation at 25 C from oxygen or fluorine combustion calorimetry will be combined with the changes in enthalpy measured by a high-temperature enthalpy calorimeter to determine thermodynamic properties at high temperatures. A calorimetric system for measurements up to 1500 C has been designed and is now being fabricated. Design concepts for an electron beam furnace to operate up to 2500 C are being tested in the laboratory.

Some of the compounds of interest are borides, aluminides, carbides, silicides, nitrides, sulfides, and selenides of metals such as uranium, zirconium, molybdenum, and tungsten. Some of the compounds are being prepared for the program by Stanford Research Institute. Two compounds (the disulfides of molybdenum and tungsten) have been prepared here.

a. Combustion of Tungsten and Sulfur in Oxygen
(R. L. Nuttall and D. R. Fredrickson)

In a previous report (ANL-6183, page 117) results of measurements of the heat of combustion of tungsten disulfide in oxygen were reported. To derive the heat of formation of tungsten disulfide from these data, the heats of formation of other reactants and products of the combustion must be known. To reduce the effects of uncertainties associated with some of these values, comparative experiments were made. In these experiments, tungsten and sulfur, in the mole ratio of 1 to 2 correspond to tungsten disulfide, were burned under conditions which were, as nearly as practicable, the same as those prevailing for the tungsten disulfide combustions. A preliminary value, -2226.70 ± 0.88 cal per gram of tungsten and sulfur, was found for the energy change in the reaction

$$W(c) + 2S(c) + 9/2\ O_2(g) + 4\ NaOH(aq) \rightarrow WO_3(c) + 2\ Na_2SO_4(aq) + 2\ H_2O(aq) \quad . \qquad (1)$$

The combustions were carried out in a platinum-lined bomb, Pt-1, in a rotating bomb calorimeter, ANL-R1, under the following conditions: (1) the gas phase in the bomb consisted of 29 atmospheres oxygen and 1 atmosphere air; (2) tungsten and sulfur powders were contained in separate one-inch diameter quartz dishes; (3) a cotton thread fuse attached to a platinum ignition wire was used to ignite the sample; and (4) 10 ml of sodium hydroxide (4 N) was added to the bomb to dissolve the sulfur oxides formed.

The measured heat evolved has been corrected for (1) a small residue of tungsten and tungsten dioxide resulting from incomplete combustion, (2) incomplete oxidation of a very small amount of sulfur to sulfite, (3) the excess sulfur above the necessary stoichiometric quantity, (4) some dissolution of tungsten trioxide in the sodium hydroxide, and (5) the various energies added by rotation of the bomb, heating the ignition wire, and combustion of the cotton fuse.

Table 32 is a summary of the tungsten-sulfur combustions. The numbers in column (2) are the sum of the mass of tungsten burned and a corresponding mass of sulfur to give a mole ratio of one to two. The mass of tungsten burned was determined by subtracting the small mass of unburned metal found in the combustion products from the mass introduced before the combustion.

Column (3) lists the corrections applied to account for the incomplete combustion of a small part of the tungsten to the dioxide.

Column (4) lists the correction applied to account for the incomplete combustion of a small part of the sulfur to form sulfite in the final bomb solution.

Because the bomb was originally charged with a mole ratio of tungsten and sulfur slightly different from the exact ratio of 1:2, a correction was made for the excess sulfur. This correction appears in column (5).

Column (6) is a summation of minor corrections to the measured energy, which include heat effects due to dilution, vaporization, and compression.

The correction for the heat evolved by burning the cotton fuse appears in column (7).

Column (8) gives the measured energy evolved in each combustion for the isothermal bomb process. This value contains corrections for the heat capacity of the contents of the bomb, ignition energy, rotational energy, and heat of solution of tungsten trioxide in sodium hydroxide.

Table 32

STANDARD HEAT OF COMBUSTION OF TUNGSTEN AND SULFUR IN OXYGEN

(1)	(2)	(3)	(4)	(5)	(6)	(7)	(8)	(9)	(10)	(11)
Run	Corrected Mass of Tungsten and Sulfur Burned (g)	WO_2 Corrections (cal)	Sulfite Corrections (cal)	Excess Sulfur Corrections (cal)	Other Corrections (cal)	Fuse Corrections (cal)	Total Energy $(\Delta E_{IBP})^a$ (cal)	$n\Delta E_c$ (cal)	$\Delta E_c/M$ (cal/g)	ΔE_c (kcal/mole)
1	1.98735	-	-8.99	+25.87	-4.14	+10.98	-4456.93	-4433.21	-2230.71	-553.20
2	1.99572	-	-4.33	+14.17	-4.08	+11.10	-4462.67	-4445.81	-2227.67	-552.44
3	1.98601	-	-5.33	+31.31	-4.13	+12.61	-4463.55	-4429.09	-2230.14	-553.06
4	1.96735	-15.32	-5.0	+46.47	-4.12	+11.64	-4407.79	-4374.12	-2223.36	-551.38
6	1.96184	-12.93	-5.0	+61.96	-4.16	+11.17	-4419.07	-4368.03	-2226.50	-552.15
7	1.95425	-10.18	-5.0	+73.33	-4.12	+11.21	-4412.85	-4347.61	-2224.69	-551.71
8	1.97281	-4.94	-5.0	+37.90	-4.10	+11.29	-4421.71	-4386.55	-2223.50	-551.41
9	1.97072	-8.94	-5.0	+50.76	-4.12	+10.98	-4430.70	-4387.03	-2226.11	-552.06
10	1.98110	-5.94	-5.0	+32.63	-4.14	+12.18	-4442.92	-4413.19	-2227.65	-552.44
								Average	-2226.70	-552.21
								Std Dev of Mean	0.88	0.22
								or	0.04%	

[a] ΔE_{IBP} = energy evolved in each combustion for the isothermal bomb process.

A summation of columns (3), (4), (5), (6), (7), and (8) gives the standard change in internal energy due to combustion of the sample according to equation (1). Values of this quantity, $n\Delta E_c$, for each combustion are given in column (9).

Columns (10) and (11) give the energy change for one gram of the tungsten-sulfur mixture, and for one mole of tungsten plus two moles of sulfur, respectively.

The calorimetric system ANL-R1-Pt-1 was recalibrated for this work with combustions of benzoic acid, and a value of 3577.03 cal/deg was obtained for the energy equivalent of the system.

b. Combustions of Uranium Mononitride in Oxygen
(E. Rudzitis, D. R. Fredrickson, R. L. Nuttall)

Experiments are being made to determine the heat of combustion of a sample of uranium mononitride prepared by Stanford Research Institute. Conditions for carrying out the reaction

$$6\ UN(c) + 8\ O_2\ (g) \longrightarrow 2\ U_3O_8\ (c,\alpha) + 3\ N_2\ (g) \qquad (2)$$

in the bomb have been worked out, and calorimetric measurements of the heat evolved are being made. The reaction is easily initiated with an electrically heated platinum wire.

The primary problem encountered in the development of techniques for the measurements was that of directing the course of the reaction to U_3O_8. At first, an oxygen deficient product $U_3O_{(8-x)}$ was usually obtained. The evidence for this was gathered from careful observation of the weight change caused by the bomb reaction and by subsequent ignition of the reaction product in air at 900 C, as well as from X-ray diffraction studies of the oxygen-deficient product.

It was found that oxygen deficiency in the product was related to the reaction temperature. By spreading the sample over a relatively large area (~1 sq in.) on a platinum support plate and using only 5 atm oxygen pressure, a lowering of the temperature and, consequently, a smooth quantitative reaction to the desired end product, U_3O_8, were obtained.

To verify that the nitrogen product of the reaction was gaseous nitrogen rather than oxides of nitrogen, the product gases of the reaction were subjected to infrared analysis. No oxides of nitrogen were detected. The solution of these various problems has led to the development of a suitable technique for the combustion of uranium mononitride, and calorimetric combustions of this compound are now being carried out.

c. Trial Combustions of Zirconium Dihydride in Oxygen
(E. Rudzitis)

In the previous report (ANL-6231, page 81) some of the problems encountered in attempts to burn quantitatively zirconium dihydride in oxygen were discussed. The problems were mainly those of obtaining a satisfactory material balance. Further experimentation showed that the zirconium dihydride sample was contaminated with zirconium dioxide, which was undoubtedly formed when the sample was ground in the presence of air. It was also shown that significant amounts of zirconium dioxide powder were carried away from the support dish as a fine dust. Consideration of this new information has resolved the material balance discrepancies.

No further exploratory work is planned. When calorimetric measurements are made, the same low-temperature heat capacity calorimetric sample, which was prepared by the Chemistry Division, will be used; but it will be ground in an inert atmosphere to avoid oxygen contamination. Material balance studies will be carried out on the actual calorimetric runs.

d. Combustion of Boron in Fluorine
(S. Wise)

The experimental work on the combustion of boron in fluorine has been completed. An abstract of a paper entitled "The Heat of Formation of Boron Trifluoride by Fluorine Bomb Calorimetry" has been submitted for presentation at the March, 1961 American Chemical Society Meeting.

Table 33 is a summary of the results of the acceptable combustion experiments. The data are expressed in terms of the defined calorie equal to 4.1840 absolute joules. The mass of the boron was determined by subtracting the mass of the recovered boron from the mass of the original sample. The quantity ΔE_{IBP} is the actual energy released during a combustion corrected for deviation from isothermal conditions and for the ignition energy. The only significant contribution to the energy correction to standard state was from the hypothetical compression and expansion of the bomb gases. The coefficient $\left(\frac{\partial E}{\partial P}\right)_T$ necessary for this correction was estimated from the intermolecular force constants of the gases (fluorine, argon, and boron trifluoride). Impurity corrections were made on the assumptions that the metal impurities (such as silicon, manganese, magnesium, and iron) and hydrogen were present as the elements, and that carbon and oxygen existed in the sample as B_4C and B_2O_3, respectively. Correction for the loss in weight of nickel from the bomb and internal fittings was made on the basis of a loss of 1.3 mg nickel per run. It was assumed that nickel fluoride was formed during the boron combustion and was subsequently washed from the bomb surfaces after each run. The bomb was weighed before and

after a series of fifteen runs and was observed to have lost an average of 1.0 mg per run. A constant weight check was kept on the weights of the internal fittings. These lost 0.3 mg nickel per run. In the last column of Table 33, the corrected energy changes at 25 C per gram of boron are tabulated for the reaction

$$B(c) + 3/2\ F_2(g) = BF_3\ (g). \qquad (3)$$

Table 33

HEAT OF COMBUSTION OF BORON IN FLUORINE

(1)	(2)	(3)	(4)	(5)	(6)	(7)	(8)
Run	Mass of sample (g)	Total Energy (ΔE_{IBP})[a] (cal)	ΔE_{corr} to std state (cal)	ΔE_{corr} for fuse (cal)	ΔE_{corr} loss of Ni (cal)	ΔE_{corr} for impurities (cal)	$\Delta E_c^\circ/M$ (kcal/g)
21	0.17030	-4244.03	0.15	17.06	3.5	9.7	-24.896_7
22	0.17205	-4287.28	0.14	12.43	3.5	9.8	-24.923_0
23	0.16335	-4069.82	0.14	10.65	3.5	9.3	-24.924_8
25	0.16094	-4018.82	0.12	13.28	3.5	9.2	-24.963_5
26	0.16230	-4042.18	0.13	7.72	3.5	9.3	-24.933_0
27	0.16097	-4017.02	0.13	13.59	3.5	9.2	-24.945_6
28	0.16370	-4074.66	0.14	10.65	3.5	9.3	-24.901_3
29	0.16187	-4027.26	0.13	9.19	3.5	9.2	-24.897_9

Average $\Delta E_c^\circ/M = -24.923_2$ kcal/g.

Std Dev of Mean = 0.008_5 kcal/g.

or $0.03_4\%$

[a] ΔE_{IBP} = energy evolved in each combustion of isothermal bomb process.

The value of 10.82 g per gram atom as the atomic weight of boron leads to the value (subject to minor revisions) of -269.67 ± 0.32 kcal/mole for the energy of formation, ΔE_f°, of boron trifluoride. Application of the ΔnRT correction leads to the value for the standard heat of formation, ΔH_f°, of -269.97 ± 0.32 kcal/mole.

e. Combustion of Boron Nitride in Fluorine
(S. Wise)

Experimental work has started toward the determination of the heat of formation of boron nitride (BN) by combustion in fluorine. Because boron nitride burns spontaneously in fluorine, a method has

been devised for separating the two substances in the calorimeter until the calorimetric run begins. A nickel tank (0.25 liter), containing fluorine, forms a jacket around the outside of the evacuated nickel bomb, containing the boron nitride sample (see Figure 37). A valve, which is opened by the drive shaft of the calorimeter rotating mechanism, controls the flow of fluorine through a connecting nickel tube from the tank to the bomb during the calorimetric run. Preliminary runs with boron nitride indicate that the tank-bomb arrangement will be satisfactory for experiments involving many substances which react spontaneously with fluorine.

FIGURE 37
CALORIMETER FLUORINE TANK WITH TOGGLE VALVE CONNECTION TO COMBUSTION BOMB

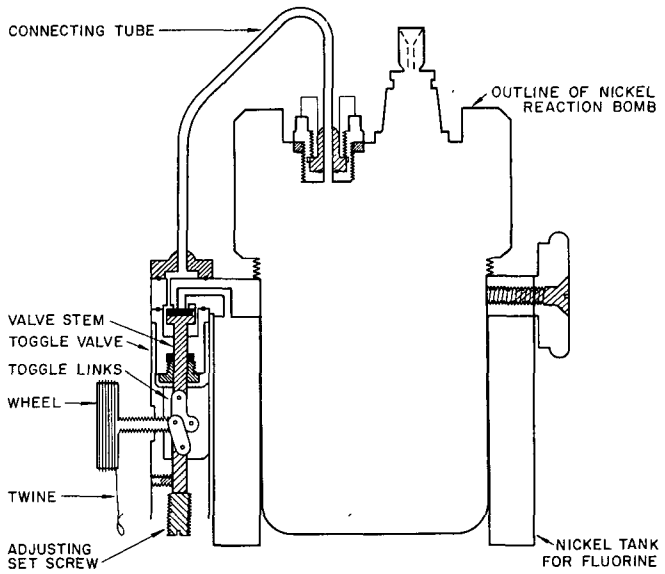

f. Combustion of Molybdenum in Fluorine
(J. Settle)

The experimental work has been completed for the study of the heat of formation of molybdenum hexafluoride. A value of -372.44 ± 0.05 kcal/mole was obtained for the standard heat of formation of molybdenum hexafluoride, MoF_6, (gas). A manuscript entitled "Fluorine Bomb Calorimetry: 2. The Heat of Formation of Molybdenum Hexafluoride," by J. L. Settle, H. M. Feder and W. N. Hubbard, is being prepared for journal publication.

g. Combustion of Uranium in Fluorine
(J. Settle)

Determination of the heat of formation of some of the uranium compounds prepared for the group by Stanford Research Institute would be a very difficult task by oxygen bomb or solution calorimetry because of the difficulty of obtaining well-defined reaction products. Typical of these compounds are the borides and silicides of uranium. To obtain the heats of formation of these compounds by fluorine combustion calorimetry, it is necessary to know the heats of formation of uranium hexafluoride (UF_6), boron trifluoride (BF_3), and silicon fluoride (SiF_4). The heat of formation of boron trifluoride has recently been determined in this laboratory (see page 124). The heat of formation of silicon fluoride has also recently been accurately measured.[30] The estimated uncertainty interval of the heat of formation of uranium hexafluoride[31,32] is, unfortunately, greater than 1 percent. It is evident that a more precise determination of the heat of formation of uranium hexafluoride is a desirable step in the proposed study of these uranium compounds.

Experiments have been initiated for the purpose of determining the necessary conditions for calorimetric combustions of uranium in fluorine according to the idealized reaction

$$U\,(c,\alpha) + 3\,F_2\,(g) \rightarrow UF_6\,(c) \quad . \qquad (4)$$

These combustions have been carried out in a glass bomb, using fluorine of 99.4 percent purity.

Three types of sample arrangements have been investigated in attempts to obtain the desired reaction. (1) The suspended foil technique described in ANL-6231, page 84, was tried. The uranium foil was burned in undiluted fluorine. (2) A short length of uranium rod was supported by a relatively massive nickel base. The uranium rod was burned in fluorine diluted with argon. (3) Small pieces of uranium metal were mixed with uranium tetrafluoride powder. The mixture was burned in undiluted fluorine.

The suspended foil technique offers the advantage that no inert support is required for the sample. The success of the method, however, depends upon the possibility of making the combustion proceed rapidly

---

[30] Vorobiev, A. F., Kolesov, V. P., and Skuratov, S. M., The Bulletin of Chemical Thermodynamics, 3, 23 (1960).

[31] The Chemistry of Uranium eds. Katz, J. J., and Rabinowitch, E., McGraw-Hill Co.; New York, N. Y. (1951), p. 412.

[32] Weinstock, B., and Christ, R. H., J. Chem. Phys. 16, 436 (1948).

enough to fluorinate the sample completely while it is still suspended. Experiments with uranium foil as thin as 0.0015 inch and fluorine pressures as high as 30 atmospheres indicated that the combustion did not proceed fast enough. These experiments invariably led to melting of the sample, with only a small fraction of the uranium being burned.

Several moderately successful experiments were achieved by using uranium rod about $\frac{1}{16}$-inch diameter by 1-inch long, supported vertically in a massive nickel base. The samples were ignited at the top with silver-clad uranium fuse wire and a small piece of uranium foil which acted as a kindler. With this sample arrangement, it was necessary to dilute the fluorine with an inert gas to reduce the temperature in the reaction zone and prevent melting of the uranium. When the gaseous mixture consisted of one atmosphere fluorine and sufficient argon to make the total pressure twelve atmospheres, there was no melting observed. The nickel base acted as a thermal sink which reduced the temperature of the lower portion of the uranium rod so that the burning uranium was supported by unreacted uranium. However, after the reaction has stopped, the surface of the unreacted uranium was covered with thin layers of lower uranium fluorides. If this type of reaction is carried out calorimetrically, a difficult chemical problem will arise. In order to define the reaction, the uncombined uranium must be quantitatively recovered and each of the reaction products must be defined quantitatively. A reasonably precise determination of the heat of formation of uranium hexafluoride can only be made if the amount of lower uranium fluorides formed is small compared to the amount of uranium hexafluoride formed.

The method of mixing uranium metal with uranium tetrafluoride is attractive for several reasons. No unreacted uranium metal is left after combustion. Moreover, it should be possible to limit the combustion products to uranium pentafluoride and uranium hexafluoride, with the uranium pentafluoride forming a small fraction of the total product. By varying the ratio of uranium metal to uranium tetrafluoride, the heats of formation of both uranium tetrafluoride and uranium hexafluoride could be derived from a single series of experiments. The estimated uncertainty of the literature values for the heat of formation of uranium tetrafluoride[33,34,35] is in excess of 0.5 percent; a substantial increase in the precision of that value would, therefore, be worth while. The main problem remaining with this method is to find a suitable container for uranium and uranium tetrafluoride.

---

[33] Domange, L. and Wohlhuter, M., Compt. Rend. 228, 1591 (1949).

[34] The Chemistry of Uranium, eds. Katz, J. J. and Rabinowitch, E., McGraw-Hill Co., New York, N. Y. (1951), pp. 367-371.

[35] Brewer, L., Bromley, LeR. A., Gilles, P. W., and Lofgren, N. L., The Chemistry of Uranium, Collected Papers, TID-5290 (1958), p.233.

Experiments by method (2) will be conducted in a calorimetric bomb so that the combustion reaction can be defined and preliminary data on the heat of combustion of uranium in fluorine can be obtained. The search for a suitable container for use in method (3) will be continued.

h. Combustion of Titanium, Hafnium, and Thorium in Fluorine (E. Greenberg)

Experiments were initiated to develop techniques for fluorine combustion calorimetry of titanium, hafnium, and thorium. Observation of these noncalorimetric combustions in a glass bomb indicated that titanium and hafnium can be burned in the same manner as zirconium, but the same technique is not satisfactory for thorium.

The titanium or hafnium sample, in the form of a rod approximately 0.1 x 0.1 x 1 inch, was supported vertically in a relatively massive nickel base. It was ignited electrically with a fuse wire threaded through a small piece of foil inserted in a slot at the top of the sample. To reduce the combustion temperature and thereby prevent the melting of the sample; the fluorine was diluted to about 20 percent with argon. As in the case of zirconium (see ANL-6183, page 79), the volatile tetrafluoride was sublimed away from the hot combustion zone until the latter stages of combustion, when a heavy coating built up on the sample rod. In each case the product of combustion was a uniform white solid. X-ray crystallographic identification of the products is being deferred until the calorimetric samples are available and the combustions are done in the nickel bomb. High-purity samples are in the process of being fabricated by the Metallurgy Division.

In the attempted thorium combustions, the sample rod became red hot at the top, but combustion could not be sustained. Combustion experiments with 5-mil foils in varying fluorine-argon mixtures resulted in melting of the sample. Additional experiments are in progress.

i. High-temperature Enthalpy Calorimetry (R. L. Nuttall and D. R. Fredrickson)

Progress is being made on the assembly of the 1500 C enthalpy calorimeter and the design of the furnace for a 2500 C calorimeter. For the latter a second mockup electron gun has been designed with the cooperation of the Electronics Division. Drawings have been made and construction will be started soon.

II. FUEL CYCLE APPLICATIONS OF VOLATILITY AND FLUIDIZATION TECHNIQUES

A direct fluorination volatility process has been proposed for the recovery of uranium and plutonium from irradiated nuclear reactor fuels. In this process advantage is taken of the volatilities of uranium and plutonium hexafluoride and of fluidization techniques. Attempts are being made to apply this process to uranium oxide and zirconium matrix fuels.

The proposed process for recovery of uranium and plutonium from spent uranium oxide, involves decladding by an appropriate reaction in a fluidized bed. Plutonium and uranium hexafluorides, which result from the reaction of the declad oxide fuel with fluorine, may be separated using a combination of the variability of the rates of fluorination of the plutonium and uranium compounds, and chemical reactivities of the hexafluorides.

The decladding step of the process for uranium dioxide fuels involves gas-metal reactions in the case of elements clad either with stainless steel or Zircaloy. The gas-metal reactions are carried out with the fuel elements submerged in an inert fluidized bed (calcium fluoride or alundum) which serves as a heat transfer medium. Dilute mixtures of hydrogen chloride in hydrogen fluoride or the separate gases have been successfully employed where zirconium decladding is necessary. In recent work chlorine has replaced the hydrogen chloride. In the case of stainless steel cladding, chlorine alone appears suitable as the decladding reagent based on results from pilot plant studies.

The cladding reactions (referred to as primary) are being carried out in a two-zone fluid-bed reactor. Volatilization of the clad or alloying material occurs in the lower zone during the chlorination reaction. The volatile materials pass upward into the upper zone where hydrogen fluoride is admitted, thus effecting conversion to solid fluorides. The two zones are separated by an inverted conical baffle (other types may also be suitable) which reduces back-mixing of the gases and prevents the formation of gas mixtures that have been shown to affect these reactions adversely. The two-zone scheme appears attractive for reacting the cladding or alloying agent as well as for the chlorination of the sintered oxide fuel itself.

In pilot-plant studies the reaction of 304 stainless steel tube sections with chlorine has been investigated in a $1\frac{1}{2}$-inch diameter, two-zone fluid-bed reactor. Penetration rates ranged from 6 mils/hr at 570 C to 10.6 mils/hr at 590 C using 100 percent chlorine as the primary (lower zone) reactant. Hydrogen fluoride was admitted to the upper reaction zone where the volatile ferric chloride is converted to the solid fluoride. The solid material deposits primarily on the surface of the bed particles, with a small fraction forming in the gas phase and remaining as fines. At 570 C, a three-hour experiment resulted in reaction of 75 percent of the 50-mil

thick specimen. Other halogenating agents tested for decladding included bromine, carbon tetrachloride, and a mixture of carbon tetrachloride and water vapor, but none of these showed any promise. An equimolar ratio of chlorine and carbon tetrachloride gave a slightly lower rate of reaction than chlorine alone, 7.3 and 3.4 mils/hr at 600 and 577 C as compared with about 9.0 and 5.5 mils/hr.

After decladding has been achieved, a subsequent fluorination step is expected to provide the necessary separation of the fissile elements. The direct fluorination of dense uranium dioxide pellets is being examined in fluid-bed pilot-plant studies. A six-inch deep bed of $\frac{1}{4}$-inch inert-fired pellets was completely reacted in 6.5 hr, with satisfactory reaction control at 500 C and 20 percent inlet fluorine. In preliminary runs with hydrogen-fired pellets, overall fluorination rates appear lower by a factor of about 3 than with inert-fired pellets. In three-inch deep beds satisfactory fluorinations were carried out at 500 C with up to 40 percent inlet fluorine concentration. Analysis of runs to date shows a substantial effect on reaction rate and fluorine efficiency of the concentration of intermediate uranyl fluoride fines in the fluid bed.

Heat transfer tests are being continued in mockup systems similar to those encountered in fluorinations of uranium dioxide pellets, that is, with a fluidized medium in the voids of a nonfixed bed of heated pellets. Film coefficients for heat transfer from a single heater to a fluidized medium in the pellet voids obtained for $\frac{3}{8}$-inch pellets were 75 percent of those for fluidization without pellets. Heat transfer for this case appeared as good or better than in a similar system with $\frac{1}{2}$-inch pellets. Tests are in progress to determine the effective radial thermal conductivity of packed, fluidized beds in a system with an axial heater and a cooled column wall. Preliminary results show a conductivity of the order of 10 Btu/(hr)(sq ft)(F/ft). This value is very close to that for stainless steel type 347.

Spent oxide reactor fuels will contain both plutonium and uranium. Laboratory investigations are in progress to examine the problems involved in the steps of the Direct Fluorination Volatility Process, including those encountered in the quantitative transport of plutonium hexafluoride.

Two experiments have been performed on the fluorination of multigram quantities of plutonium dioxide, and 99 and 97 percent of the plutonium was accounted for in the volatile effluent.

Experiments have been made to demonstrate that plutonium hexafluoride produced in a laboratory fluorinator can be passed through heated sections of pipe and through thermal gradients with very good recovery of the compound. Trap to trap transport through laboratory equipment has demonstrated that 98 to 100 percent of the plutonium hexafluoride volatilized could be recovered.

It has also been demonstrated that a 38-gram sample of plutonium hexafluoride could be held at 60 C for 25.5 hours with no more decomposition than could be attributed to alpha radiation decomposition.

The reaction of bromine with plutonium hexafluoride, with and without the presence of uranium hexafluoride, has been investigated. Bromine is a satisfactory reagent for the reduction of plutonium hexafluoride to plutonium tetrafluoride and can be used to separate uranium and plutonium.

The gamma-ray spectrum of plutonium tetrafluoride has been investigated up to 2.0 Mev. Fast neutron flux measurements have been made on samples of plutonium tetrafluoride to assay the hazards connected with the α-n reaction.

A combined chlorination-fluorination process (Direct Chlorination Process) has been proposed as an alternate to the fluorination step. Accordingly, work was begun on the chlorination of sintered uranium dioxide pellets using chlorine, carbon tetrachloride, and mixtures of the two. Initial experiments conducted in a tube furnace on single pellets of dioxide (prepared at Mallinckrodt Nuclear Corp., with a density nearly 95 percent of theoretical) attained reaction rates of 370 to 780 mg/(sq cm)(hr), based on pellet weight loss data and the original surface area of the pellet. The highest rate reflects about 25 percent consumption of a pellet in one hour at 600 C. The chlorine-carbon tetrachloride mixture ($\frac{1}{3}$ each and $\frac{1}{3}$ nitrogen) proved best in the range from 500 to 600 C, although the difference in rate between this mixture and carbon tetrachloride alone narrowed at the higher temperature. These chlorination results suggest a Direct Chlorination Process as an alternate to the Direct Fluorination Process now being developed. This process would have the advantages of less costly reagents and lower heat load (lower heats of reaction).

Supporting corrosion studies on typical materials of construction being carried out in a one-inch tube-furnace showed nickel and Inconel sustained similar corrosion rates, about 20 mils/mo at 600 C, in chlorine-nitrogen stream (equimolar quantities), whereas the rate for Hastelloy-C was somewhat lower, being 12 mils/mo. At 550 C, the rate for nickel and Inconel was about 6 mils/mo.

Application of the Direct Fluorination Volatility Process to highly enriched, low uranium-Zircaloy alloy plate-type fuels has been reported previously (ANL-6183, pages 101 to 106 and ANL-6145, page 119). Application of a Direct Chlorination Process has been examined in pilot-plant studies. Appreciably higher rates of attack on uranium-Zircaloy-2 alloy plate assemblies were achieved with chlorine as the primary reactant instead of hydrogen chloride in the lower zone of the six-inch diameter,

two-zone reactor; rates ranged from 274 to 417 g/hr of metal reacted as opposed to a maximum rate of 300 g/hr using hydrogen chloride at temperatures near 400 C. Also, much lower concentrations of chlorine were used, about 10 to 20 percent as compared with 60 to 90 percent hydrogen chloride. Analyses of several size fractions of the final bed indicate the uranium and zirconium are uniformly deposited on the particles in the upper zone during the course of the hydrofluorination reaction. No losses of these materials from the reactor have been experienced, as determined by analysis of the off-gas scrub solution, indicating that the two-zone scheme has high efficiency for "trapping" volatiles.

The reaction of chlorine and hydrogen fluoride with anhydrous ammonia in the gas phase followed by water scrubbing was found to be an effective method for efficient disposal of the excess reactants in these halogenation studies. Appreciable corrosion had been experienced previously in a recirculating caustic column. A three-inch diameter by three-foot long glass column (partially packed) was adequate for absorbing a combined flow of 12 mole/hr chlorine and 10 mole/hr hydrogen fluoride, using about 5 to 10 gal/hr water and 25 percent excess ammonia.

The conversion of uranium hexafluoride to uranium dioxide by a two-step fluid-bed process is currently being studied. The major problem in the first step, reaction of the hexafluoride with steam to form uranyl fluoride, continues to be one of control of particle size. A recycle stream of "seed" particles equivalent to about 15 percent of the feed is being employed. The present feed rate is equivalent to 174 lb uranium/(hr)(sq ft reactor cross section), and the column is being operated at 200 C.

An auxiliary three-inch reactor has been installed for work on the second step, reduction of the uranyl fluoride to dioxide with hydrogen or hydrogen-steam mixtures. The column has been designed so that both fluid and static or moving-bed experiments may be carried out. Preliminary data from runs at 600 and 650 C indicate that much better conversion is obtained with a hydrogen steam mixture than with hydrogen alone.

A. Laboratory Investigations of Fluoride Volatility Processes

1. Fluorine Chemistry and Fluoride Separation Studies
(J. Fischer)

a. Process Development - Plutonium Fluorination and Transport Studies
(L. Trevorrow, G. J. Vogel, L. Anastasia, H. Griffin, J. Riha, G. Redding, T. Gerding and T. D. Baker)

One aim of the current experimental program is to demonstrate steps in the Direct Fluorination Volatility Process preliminary to pilot-plant-scale operations. Problems involved in the quantitative

transport of plutonium hexafluoride are being investigated. Ten- to fifty-gram batches of plutonium hexafluoride are being used in these experiments.

Preparation of Plutonium Hexafluoride

Plutonium hexafluoride was prepared by reacting plutonium oxide with elemental fluorine, which had passed through a heated bed of sodium fluoride to remove hydrogen fluoride. An equipment flow diagram of the fluorination system is shown in Figure 38. Fluorine was preheated and, using a magnetic piston pump, circulated through the tube reactor, which contained a boat of weighed plutonium oxide. The plutonium hexafluoride was condensed in two cold traps (at -78 C) connected in series. The second of the two traps could be removed and weighed. The equipment had been conditioned with fluorine and had been used previously to fluorinate uranium oxide and fluoride.

FIGURE 38
SCHEMATIC FLOW DIAGRAM
OF PLUTONIUM FLUORINATION SYSTEM

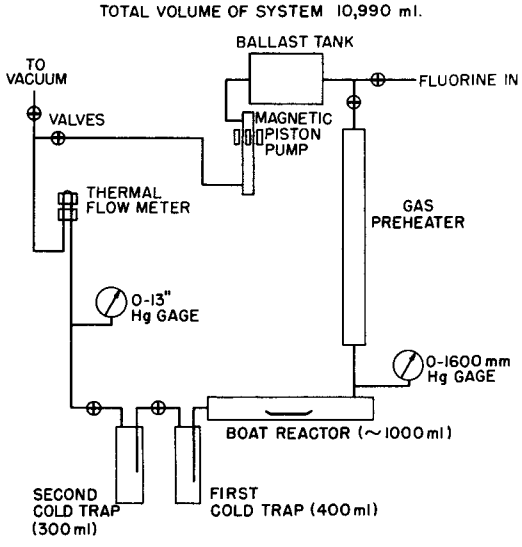

The plutonium oxide was dried in a flowing helium stream for 2½ hours at 400 C. The system was then evacuated and the ballast tank was filled with fluorine. Fluorine was then expanded into the rest of the system, which was at the operating temperature. Two fluorinations of plutonium dioxide samples were made. In the first fluorination, the experiment was interrupted twice to weigh the solid residue in the boat and the plutonium hexafluoride which had been collected in the traps. The second experiment was uninterrupted, weighings being made only at the completion of the experiment. In order to obtain a more accurate material balance for plutonium in the second experiment, the plutonium oxide, the boat residue, and the nonvolatile solid in the first cold trap (mainly plutonium tetrafluoride from the radiation decomposition of plutonium hexafluoride) were analyzed for plutonium. Fluorine was removed from the plutonium hexafluoride by evacuation of the vessel which was cooled to -78 C.

The plutonium material balance for Run 2, Table 34, shows that 97 percent of the plutonium in the original sample could be accounted for. In Run 1, 99 percent recovery was obtained, based on the assumption that the residue found in the cold trap and in the reactor was plutonium tetrafluoride.

Table 34

OPERATING TIMES, FLOW RATES AND PLUTONIUM MATERIAL BALANCE FOR THE FLUORINATION OF PLUTONIUM OXIDE

	Duration (hr)	Approximate Gas Flow (cc/min at 30 C)	Plutonium Material Balance (as Pu): Found in Reactor Boat (g)	Found in Cold Trap 2 (g)	Found in Cold Trap 1 (g)	Total Pu Found (g)	Initial Pu[a] in PuO_2 (g)	Material Balance (percent)
PuF_6 Prep 1: (Reactor Temp: 500 C)								
Part A	11.1	700	24.85[b]	18.27	-	-	-	-
Part B	10.0	900	7.99[b]	33.76	-	-	-	-
Part C	19.7	1200	0.36[b]	40.81	2.56[b]	43.73	44.16	99
PuF_6 Prep 2: (Reactor Temp: 550 C)								
	40.3	1200	0.072[c]	34.73	3.2	38.03	39.35	97

[a] PuO_2 analysis: 95.2 percent PuO_2.

[b] Assumed to be PuF_4.

[c] By analysis of residue.

A plot, Figure 39, of the pressure drop in the total system against time, indicative of the fluorine consumption rate, showed an initial rapid uptake of fluorine owing probably to the formation of the tetrafluoride. All of the sample was not converted, since inspection of the solid in the boat in the first run showed a brown, crusty top layer with some yellow-green plutonium oxide underneath. Steindler et al.,[36] showed that plutonium oxide is rapidly converted to plutonium tetrafluoride by fluorine above 300 C. If one assumes that the plutonium being fluorinated after the second hour is mainly tetrafluoride, it is possible, using the fluorine consumption rate and the efficiency, to calculate a rate of fluorination. The rate from the second to the twenty-third hours was 85 mg plutonium tetrafluoride/(sq cm)(hr) equivalent to 65 mg plutonium/(sq cm)(hr). The area used in the calculation was the top area of the powder in the hemicylindrical boat when fifty percent of the plutonium had been removed. This calculated rate is compared with rates of 420 and 650 mg plutonium tetrafluoride/(sq cm)(hr) calculated by Steindler et al., for Rocky Flats and Los Alamos plutonium tetrafluoride and with a rate of 100 mg plutonium/(sq cm)(hr) for plutonium dioxide.

FIGURE 39
CUMULATIVE PRESSURE DROP IN THE FLUORINATION SYSTEM DURING THE FLUORINATION OF PLUTONIUM OXIDE

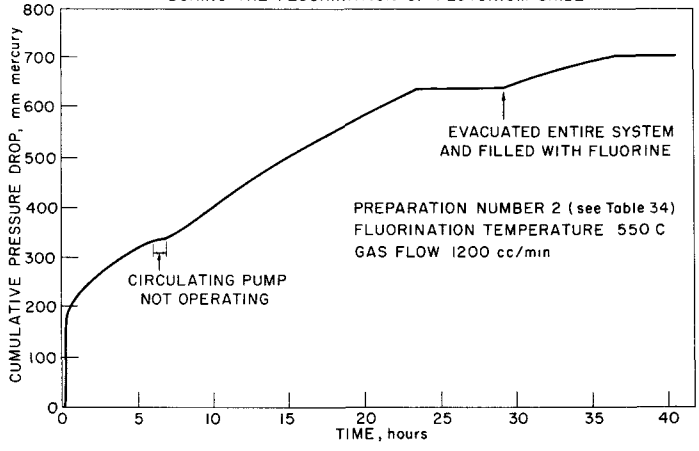

Pure Plutonium hexafluoride was obtained by evacuating the vessel containing the plutonium hexafluoride at a temperature of -78 C. The evacuation removed such volatiles as hydrogen fluoride, fluorine, and carbon tetrafluoride. The vapor pressure was 132 mm at 27 C after about one hour of evacuation compared to the literature value of 121 mm.[37] A vapor pressure agreeing with the literature value was attained after some of the plutonium hexafluoride had been distilled off.

---

[36]Steindler, M. J., Steidl, D. V. and Steunenberg, R. K., Nuclear Sci. and Eng. 6, 333 (1959).

[37]Weinstock, B., Weaver, E. E., and Malm, J. G., J. Inorg. and Nuclear Chem., 11, 104 (1959).

Recovery of Plutonium Hexafluoride from the Fluorination Reactor

The initial separation step in the fluoride separation process is one in which the declad oxide fuel element is to be fluorinated to remove most of the uranium. During the next step the complete fluorination of the uranium and plutonium remaining is to be accomplished. The resulting mixture of plutonium and uranium hexafluorides is removed from the off-gas stream of the reactor by condensation. At the exit of the reactor the ratio of plutonium hexafluoride to fluorine will be equal to or less than the equilibrium constant for the reaction

$$PuF_4(s) + F_2(g) \rightleftharpoons PuF_6(g)$$

at the temperature of the reactor. Thus no thermal decomposition should occur in the reactor. However, the equilibrium constant (PuF_6/F_2) decreases with temperature and, since the reactor exit gas passes through a thermal gradient on its way to the condenser, a driving force for decomposition will be present. The rate of approach to equilibrium also decreases with temperature, and the amount of decomposition can be reduced by cooling the gas quickly to a lower temperature where the decomposition rate is slower.

A schematic flowsheet of the equipment used to determine the plutonium hexafluoride recovery when the hexafluoride and fluorine were passed through a thermal gradient is shown in Figure 40. The experimental procedure was to volatilize plutonium hexafluoride into fluorine and circulate the mixture through a pipe heated to a maximum of 600 C and then through a nickel tube of $\frac{5}{16}$-inch inside diameter which provided the thermal gradient. The temperature drop in the 13-inch tube section was from about 500 C at the hot end to 45 C at the cold end, giving a thermal gradient of about 450 C. The plutonium hexafluoride passing through the gradient was condensed from the circulating stream by two cold traps in series. The recovery of plutonium hexafluoride was determined from the weighed amounts collected in the cold trap and the weight loss of the supply container.

FIGURE 40
TRANSFER OF PLUTONIUM HEXAFLUORIDE IN A FLUORINE STREAM THROUGH A THERMAL GRADIENT FLOW SYSTEM

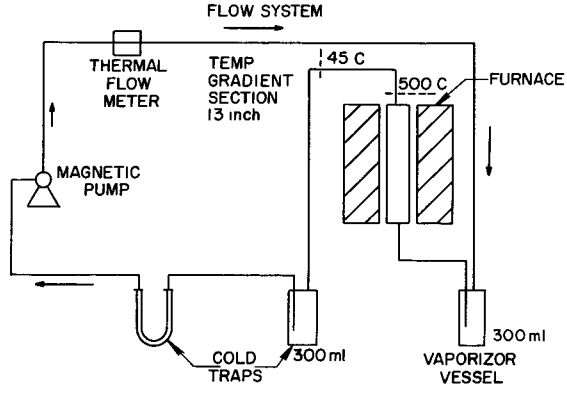

The results listed in Table 35 show that, in Runs 1 through 5, 98 to 100 percent of the plutonium hexafluoride sublimed into the gas stream was recovered in the cold traps. The ratio of plutonium hexafluoride to fluorine was less than the equilibrium ratio at the temperature (600 C) of the hot pipe, and thus no net decomposition of plutonium hexafluoride was expected to occur in the pipe. However, some decomposition might be expected in the thermal gradient tube. It was concluded on the basis of these results that satisfactory recovery of plutonium hexafluoride from the fluorination reactor appears feasible provided that sufficiently rapid cooling of the gas stream is possible. Further experiments are being carried out to provide a more severe test of the recovery. Plutonium tetrafluoride is being fluorinated and the off-gas from the reactor is being passed through a large vessel (to afford a long residence time) heated to a specified temperature.

An additional experiment (No. 6) was done in which the ratio of plutonium hexafluoride to fluorine was much higher than the equilibrium ratio at 600 C. As expected, some of the plutonium hexafluoride decomposed in the heated pipe. After this experiment, the thermal gradient tube was sectioned; only a reddish-brown, adherent film was found on the walls.

All weighings of plutonium hexafluoride plus container in the above experiments were corrected for the amount of fluorine lost because of radiation decomposition of the plutonium hexafluoride. This represents a minor correction and is a function of the residence time and the amount of plutonium hexafluoride in the container. Before all weighings, the plutonium hexafluoride was cooled to -78 C and the vessel evacuated. The loss of plutonium hexafluoride by radiation decomposition has been empirically established as two percent per day in the solid phase.

Transfer of Plutonium Hexafluoride

In the operation of a separations plant it may be necessary to transport plutonium hexafluoride from one vessel to another, either for further processing or for storage. Quantitative recovery is probably the most important requirement of a transfer of plutonium hexafluoride. Therefore, several experiments were carried out to determine how a quantitative transfer might be obtained.

The equipment used in these experiments was the same as that used in the experiments on decomposition of plutonium hexafluoride in the thermal gradient (see Figure 40). The vaporizer vessel was the source of plutonium hexafluoride. The hexafluoride was transferred by various techniques from this vessel through the lines to the cold traps where it was condensed.

Table 35

RECOVERY OF PLUTONIUM HEXAFLUORIDE FROM A FLUORINE STREAM AFTER PASSAGE THROUGH A FURNACE TUBE AND THERMAL GRADIENT

No.	Gradient Temperature: Hot Tube (C)	Gradient Temperature: Cold Exit (C)	Flow Time (hr)	Avg Flow Rate (cc/min)	Linear Flow Rate in $\frac{5}{16}$-in. ID Tube at 300 K (ft/sec)	Avg Mole Ratio[a] PuF_6/F_2	Avg F_2 Pressure (mm)	Wt PuF_6 Introduced to Stream (g)	Wt PuF_6 Condensed from Stream (g)	Recovery (percent)
1	551	49	18.33	640	0.71	0.0028	736	26.96 (0.22)[b]	26.94 (0.03)[b]	99.88
2	556	48	18.53	660	0.73	0.0020	780	21.59 (0.17)	21.64 (0.32)	100.25
3	577	46	16.75	430	0.48	0.0038	714	22.36 (0.14)	21.96 (0.05)	98.21
4	599	45	17.00	170	0.19	0.0062	695	14.18 (0.06)	13.95 (0.14)	98.38
5	553	43	25.17	160	0.18	0.0078	723	25.50 (0.10)	25.16 (0.04)	98.67
6	590	44	10.00	160	0.18	0.0210	720	22.20 (0.16)	20.08 (0.01)	90.50

[a]Moles PuF_6 calculated from total quantity of PuF_6 vaporized; moles F_2 calculated from total flow time, average pressure, and flow rate measured by thermal flow meter at about 300 K.

For comparison, the equilibrium constants for the reaction $PuF_4(s) + F_2(g) \rightleftharpoons PuF_6(g)$ are as follows:

Temp (C)	$K(PuF_6/F_2)$
600	0.017
500	0.010
400	0.0050
300	0.0027
100	0.0005

[b]Weight correction, grams, for amount of fluorine lost because of radiation decomposition of plutonium hexafluoride.

The vaporizer vessel was weighed before and after the transfer to determine the weight of plutonium hexafluoride vaporized. The cold traps were weighed before and after the transfer to determine the weight of plutonium hexafluoride recovered. In all of these experiments the cold traps and vessels were frozen and evacuated before weighing. Thus the fluorine formed by radiation decomposition of plutonium hexafluoride was removed, requiring a correction in the determination of the weight of plutonium hexafluoride in a vessel. These corrections were made by taking into account the weight of plutonium hexafluoride, its residence time in a vessel, and the rate of radiation decomposition. The rate used for these corrections was two percent per day for the condensed phase. Values of one to two percent per day have been reported by other workers, and a value of two percent per day has been found to be approximately correct in the present work.

The operating conditions and transfer efficiency data are presented in Table 36. In Experiments 9 and 10, helium was used as a carrier gas. The helium was circulated over the solid plutonium hexafluoride in the vaporizer vessel. In Experiment 9 the resulting mixture of plutonium hexafluoride vapor and helium gas was passed through the furnace tube (see Figure 40) at room temperature to the cold traps, where the plutonium hexafluoride was condensed. In Experiment 10 the furnace tube was bypassed, and the gas mixture flowed through about 4 ft of $\frac{5}{16}$-inch ID tubing and six Hoke No. 413 diaphragm valves to the cold trap. Samples of about 28 grams each were transferred in Experiments 9 and 10 with recoveries of 99.98 and 99.51 percent.

In Experiments 11 through 15, helium was again used as a carrier gas to transfer plutonium hexafluoride. In these experiments the flow path included the furnace tube. The temperature of the furnace tube in Experiments 11 through 15 was 70 C. This temperature was chosen to simulate conditions in a processing plant where the lines might be heated to prevent condensation of uranium or plutonium hexafluorides. In Experiments 11 through 15 transfers of 23 to 48 grams were carried out with recoveries of 99.31 to 99.96 percent. In Experiment 8, about 15 grams of plutonium hexafluoride was transferred using fluorine as the carrier gas. In this transfer the furnace tube was bypassed and the flow path was the same as that described for Experiment 10. The transfer in fluorine at room temperature was carried out with a recovery of 100.20 percent. In Experiment 14 the furnace tube was again bypassed, and a 45-gram sample of plutonium hexafluoride was transferred by a vacuum distillation with a recovery of 100.02 percent.

It was concluded from these experiments that large quantities of plutonium hexafluoride can be transferred almost quantitatively by carrier gas sublimation using helium or fluorine, or by vacuum distillation.

Table 36

RECOVERIES OBTAINED WHEN TRANSFERRING PLUTONIUM HEXAFLUORIDE IN A FLUORINE OR A HELIUM STREAM, OR BY VACUUM DISTILLATION

No.	Carrier Gas	Flow Time (hr)	Avg Flow Rate (cc/min)	PuF_6 Source Vessel Temp (C)	Avg Mole Ratio (PuF_6/carrier gas)[a]	System Pressure (mm)	Wt PuF_6 Introduced to Stream (g)	Wt PuF_6 Condensed from Stream (g)	Recovery (percent)
9	He	4.0	240	45	0.0395	775	28.43 (0.04)[b]	28.40 (0.05)[b]	99.98
10	He	4.0	400	35	0.0217	730	28.49 (0.04)	28.35 (0.01)	99.51
11	He[c]	4.0	350	39	0.0187	790	23.38 (0.05)	23.37 (0.08)	99.96
12	He[c]	4.0	155	55	0.0833	805	48.82 (0.05)	48.53 (0.00)	99.41
13	He[c]	3.5	350	56	0.0433	800	46.07 (0.02)	45.83 (0.01)	99.48
15	He[c]	4.0	450	55	0.0280	730	40.49 (0.03)	40.21 (0.01)	99.31
8	F_2	3.5	170	45	0.0210	720	14.90 (0.08)	14.93 (0.43)	100.20
14	(Vacuum)	1.6	-	-	-	-	44.80 (0.06)	44.81 (0.00)	100.02

[a]Moles PuF_6 calculated from total quantity of PuF_6 vaporized; moles carrier gas calculated from total flow time, average pressure, and flow rate measured by thermal flow meter at about 300 K.

[b]Weight correction, grams, for amount of fluorine lost due to radiation decomposition of plutonium hexafluoride.

[c]Carrier gas containing PuF_6 was passed through 70 C zone in these runs.

Plutonium hexafluoride may also be transported conveniently and rapidly in the liquid phase by gravity, or may be liquefied and transferred by flash distillation. Thermal decomposition of the plutonium hexafluoride at a temperature above its triple point (51.59 C)[38] might prohibit the use of these transfer mechanisms. To determine the loss of hexafluoride by thermal decomposition at a temperature slightly above its melting point, a 38-gram sample was heated to 60 C in a weighed container and held at this temperature for 25.5 hours. The upper part of the vessel was heated above 60 C to prevent condensation. At the end of the experiment the plutonium hexafluoride was completely distilled from the vessel and the vessel was reweighed. The gain in weight was due to the formation of the nonvolatile plutonium tetrafluoride, which was produced by two mechanisms - radiation decomposition and thermal decomposition of the plutonium hexafluoride. The weight gain of the vessel during the experiment was 0.66 gram. The amount that could accrue by radiation decomposition was calculated to be 0.70 gram. It was concluded that the total quantity of plutonium hexafluoride which will decompose at 60 C is about the same as the quantity which may be expected to decompose from radiation effects alone.

b. Reactions of Plutonium Hexafluoride
(M. Steindler, D. Steidl)

Reaction of Plutonium Hexafluoride and Bromine

The chemistry of plutonium hexafluoride is of direct interest to the Volatility Process for oxide fuels. Plutonium hexafluoride formed by the fluorination of the fuel at elevated temperatures will be collected with uranium hexafluoride and certain fission product fluorides. Separation of plutonium from uranium will probably be accomplished by selective reduction of the more reactive plutonium hexafluoride. It has been shown (ANL-6183, page 94; ANL-6231, page 96) that sulfur tetrafluoride will reduce plutonium hexafluoride quantitatively to the tetrafluoride with the formation of sulfur hexafluoride. The reduction of uranium hexafluoride does not take place under these conditions.

The reaction of bromine and plutonium hexafluoride has also been investigated as a means for accomplishing the selective reduction of plutonium hexafluoride. The experimental procedure employed was the same as described previously for reactions of sulfur tetrafluoride (ANL-6231, page 97) and consisted of mixing the reagents in a nickel vessel which was subsequently heated to the desired temperature. Initial experiments carried out at 30 C for 17 hours indicated that at this temperature the reaction proceeds quite slowly and incompletely. All experiments at 78 C were allowed to proceed for one hour, as indicated in the

---

[38] Weinstock, B., Weaver, E. E., and Malm, J. G., loc. cit.

data summarized in Table 37. A sample of the solid reaction product was analyzed for fluoride (pyrohydrolysis) and plutonium (amperometric titration). The sample showed a ratio of fluoride to plutonium of 4.11 in agreement with the expectation that the solid product of the reaction is plutonium tetrafluoride.

A number of equations may be written for this reaction depending on the bromine fluoride produced. Information on the stoichiometry of the reaction will probably be obtained.

Table 37

THE REACTION OF PLUTONIUM HEXAFLUORIDE AND BROMINE

PuF_6 (millimoles)	Br_2 (millimoles)	Temp (C)	Time (hr)	PuF_4 (millimoles)[a]	% Reacted[a]
0.226	0.072	30	17	0.11	49
0.214	0.066	30	17	0.15	70
0.211	0.292	78	1	0.212	100
0.088	0.651	78	1	0.084	96
0.279	0.079	78	1	0.251	90

[a]Based on weight gain of reaction vessel.

2. The Reaction of Mixtures of Uranium Hexafluoride and Plutonium Hexafluoride and Bromine

The reaction of bromine with mixtures of uranium and plutonium hexafluorides was carried out to determine the suitability of this reaction for separations process application. The reaction was carried out in the same manner as described for the reaction of bromine and plutonium hexafluoride. The results are shown in Table 38. It is believed that the discrepancies in the uranium and plutonium material balances are not significant and are due to experimental error. The lack of volatile plutonium together with the recovery of uranium hexafluoride indicates applicability of bromine as a selective reductant for plutonium hexafluoride in these mixtures.

Radiations from Plutonium Fluorides
(M. Steindler)

The radiation emitted by samples of plutonium fluorides is of importance to process development research not only because of its contribution to the existing hazard from alpha emitters and the general toxicity

of fluorides, but also because it influences decontamination requirements. The gamma-ray spectrum as well as data on the neutron emission of plutonium tetrafluoride are reported in an attempt to provide information for the above-mentioned considerations.

Table 38

THE REACTION OF BROMINE WITH MIXTURES OF URANIUM HEXAFLUORIDE AND PLUTONIUM HEXAFLUORIDE

Reaction Time: 2 hours

				Volatile Products[a]		Solid[b]
PuF_6 (millimoles)	UF_6 (millimoles)	Br_2 (millimoles)	Temp (C)	U (millimoles)	Pu (millimoles)	Product (millimoles)
0.611	7.69	0.668	80	8.0	0.006	0.72
0.324	2.83	0.403	94	2.8	0.008	0.35

[a]By analysis.

[b]Assumed to be tetrafluorides.

Owing to the importance of plutonium tetrafluoride in volatility processes, the gamma-ray spectrum of a small sample of plutonium tetrafluoride was determined. No detailed information appears available in the literature on the gamma-ray spectrum of plutonium tetrafluoride, but Helgeson[39] has stated that the gamma flux is composed of three effective energies of which a 680-kev gamma ray contributes 50 percent of the dose rate. We have been unable to confirm any major contribution at this energy. The results obtained in this brief investigation indicate a major contribution from gamma rays of 200 kev or less, particularly in light of the fact that nickel (absorber) was used as a sample holder.* The results obtained are shown in Table 39 and Figure 41.

The high specific activity of plutonium coupled with the presence of fluorine atoms in plutonium tetrafluoride produced appreciable quantities of neutrons by the reaction, F^{19} (α,n) Na^{22}. Although it is possible to calculate the rate of emission of neutrons from a sample of plutonium tetrafluoride from the yield of the reaction ($\sim$10 n/10^6 α for F^{19}), observed emission rates are considerably lower than those calculated, primarily owing to the degradation of the energy of alpha particles by nuclides other than fluorine. In order to determine the magnitude of the problem of handling relatively large quantities of plutonium tetrafluoride, the neutron fluxes from several samples of the tetrafluoride were measured under laboratory (not scatter-free) conditions.

[39]Helgeson, G. L., Surface Dosage Rate Studies of Task III Feed Materials, HW-31522 (1954); Declassified 1960.

*$\frac{3}{8}$-inch OD nickel tube (1.6-mm wall, $\sim$ 1400 mg Ni/sq cm)

Table 39

OBSERVED GAMMA SPECTRUM OF PLUTONIUM TETRAFLUORIDE

4 x 4-inch NaI(Tl) crystal, 256-channel analyzer, ~45% geometry, no absorber other than sample container.

E (kev)[a]	Relative Peak Height[b]	Comments
17	0.21	Highly attenuated, X-ray shoulder on 30-kev peak
30	0.8	Pu^{239} (37)[c]
60	4.7	Am^{241} (60), Pu^{239} (52)
100	1.00	U^{238} X-ray, F^{19} (109), Pu^{239} (120)
130	0.70	Shoulder of 100 kev
160	0.33	Shoulder of 100 kev
200	0.17	F^{19} (196)
380	0.07	Pu^{239} (380) broad
500	0.014	Na^{22} (511) annihil shoulder
850	0.002	-
1200	0.0003	Na^{22} (1276)
1700	0.0004	Na^{22} (1787)
1950	0.0001	-

[a] Approximate

[b] The 100-kev peak was arbitrarily chosen as unity.

[c] (37), etc = energy (kev) where element is expected to appear.

FIGURE 41
GAMMA SPECTRUM OF PLUTONIUM TETRAFLUORIDE

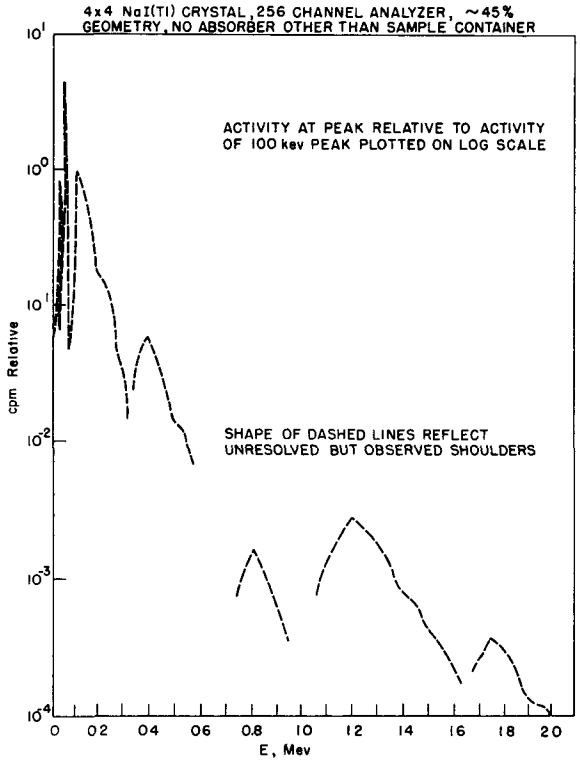

Samples of plutonium tetrafluoride contained in polyethylene bottles and enclosed in a 20-mil plastic bag were suspended 75 cm above the concrete floor of a small room. The detector, a standard unshielded Long Counter, was also suspended at the same height. The counter had been previously calibrated with a standard plutonium-beryllium source.* The results are shown in Table 40 and Figure 42.

A plot of the data (Figure 42) indicates a deviation from the familiar "inverse square" law. Deviation is not surprising,** and warrants recognition in monitoring the neutron flux from experimental equipment.

*We are indebted to Dr. L. Anderson, Industrial Hygiene and Safety Division, for helpful discussions and advice.

**For a discussion of the operation of Long Counters, including errors owing to scatter of neutrons and shift of effective center of the detector with neutron energy, see Fast Neutron Physics, Part I, J. B. Marion and J. L. Fowler (ed.) Interscience Publishers, Inc., New York (1960).

Table 40

FAST NEUTRON FLUX MEASUREMENTS WITH SAMPLES OF PLUTONIUM TETRAFLUORIDE

Samples: Powdered PuF_4.

Container: Polyethylene bottles surrounded by 20-mil PVC bag.

Detector: Moderated BF_3 counter, Sens = 56.7 cpm per unit of flux.

Distance: 75 cm above the floor. Sample to front of paraffin tub = D

D (cm)	Fast Neutron Flux [n/(sq cm)(sec)] for indicated wt PuF_4			
	10 g[a]	77 g	118 g	220 g[c]
10	12.8	-	-	-
11	-	-	186	-
12	-	91	-	-
14	-	-	-	290
20	5.6	49	81	170
30	2.8	27	44	91
60	1.1	8	15	34.2
90	0.6	4.8	8.2	19.8
β-(H + S) at 2 inch,[b] mr/hr	15	150	180	100
γ(H) at 2 inch,[b] mr/hr	-	60 mr/hr	90 mr/hr	65 mr/hr

[a]Sample contained in two glass jars (one inside the other). No polyethylene or PVC used.

[b]Measured with a "Juno" survey instrument. Hard only (H) total shielding = 700 mg/sq cm Al, (H + S) measurement through 0.01-inch Lucite (~30 mg/sq cm).

[c]In glass bottle enclosed in $\frac{1}{4}$-inch wall Lucite jar (6-inch diameter, 8-inch high) which was contained in a 20-mil PVC bag.

FIGURE 42
NEUTRON MEASUREMENTS ON
PLUTONIUM TETRAFLUORIDE

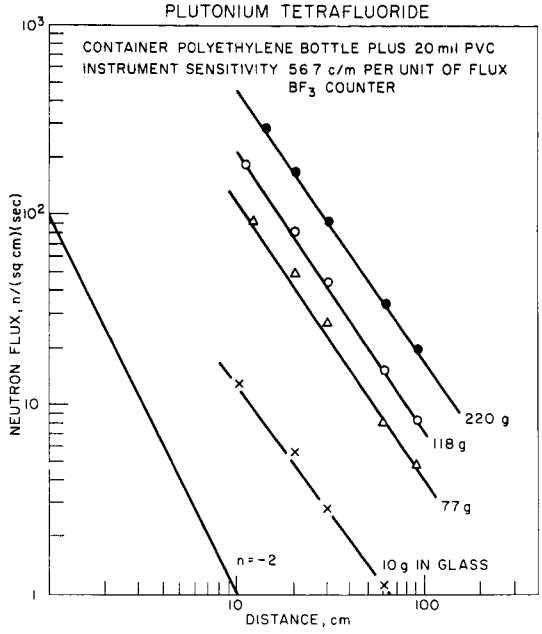

The data in Table 40 represent the only detailed information available on the neutron flux from samples of plutonium fluorides. The data may be used to estimate the biological hazard if the limitations of the Long Counter and the particular experimental conditions are recognized.* If an energy of 1 Mev is assumed for the neutrons from Pu-α-F, then 18 n_f/(sq cm)(sec) is equivalent to 100 mr/40 hour week or 1 n_f/(sq cm)(sec) = 0.14 mrem/hr.

B. Engineering-scale Development (A. A. Jonke)

The volatility of uranium and plutonium hexafluorides is the basis of a reprocessing scheme by which the fissionable elements can be separated and recovered from irradiated fuels for reuse in the nuclear fuel cycle. Such reprocessing schemes are intended to effect nearly complete removal of the radioactive fission products. Processes are under development for two types of nuclear fuels which are considered to be representative of the most important power reactor fuels, namely, ceramic fuels and zirconium-matrix fuels. Fluidization techniques are being used in these processes and also in preparation of uranium compounds.

1. Direct Fluorination of Uranium Dioxide Fuels (W. J. Mecham, J. D. Gabor, J. Gates, A. Rashinskas, J. Wehrle)

Direct fluorination is being studied as a process for the recovery of fissionable material from uranium dioxide reactor fuel, a type of fuel receiving emphasis in current reactor designs. Although dense pellets of the kind proposed for several nuclear reactors are too large to be fluidized directly, the use of an inert fluidizable material to cover and fill the void spaces of the packed bed of pellets has been studied to achieve some of the advantages of fluidization for gas-solid reactions, particularly with respect to heat transfer and temperature control.

a. Fluorination of Uranium Dioxide Pellets

Pilot-plant-scale work has been directed toward study of the means of controlling the highly exothermic reaction between fluorine and uranium dioxide. Earlier work on pellet fluorinations showed that

*See second footnote on page 145.

the reaction proceeded in two steps: (1) uranyl fluoride was produced first as fines, which spalled off the uranium dioxide pellet surface into the fluidized bed. (2) This uranyl fluoride was then fluorinated to form uranium hexafluoride vapor (see ANL-6145, page 103). Work with deeper pellet beds and lower temperatures tended to produce a larger amount of fines (see ANL-6183, page 98). The pellets used in these fluorinations were all of the same inert-fired type.

In the present period, fluorination of a six-inch bed of the inert-fired pellets was carried to completion. Other runs were made with pellets of a hydrogen-fired type, which exhibited a significantly lower reactivity than the inert-fired type. Fluorinations were carried out successfully with the hydrogen-fired pellets at temperatures up to 500 C and inlet fluorine concentrations up to 40 mole percent.

General Operability

In order to compare the behavior of the two different types of pellets studied, a summary of the most important runs made to date is presented in Table 41. All runs were made in a three-inch diameter fluid-bed reactor. Runs after UOF-20 were made in the new forced air-cooled reactor. In these runs all material charged and discharged was weighed. The uranium hexafluoride condenser was very efficient and overall material balances were better than 99.5 percent.

For temperatures of 500 C and below and for inlet fluorine concentrations of 40 percent or lower, temperature control and general operability have been good for runs reported in Table 41. In runs under other conditions and for pellet fluorinations following a Zircaloy decladding step, some difficulties have appeared with temperature control and bed caking.

Table 41

SUMMARY OF URANIUM DIOXIDE PELLET FLUORINATION RUNS

General Conditions 3 inch Diameter Fluid Bed Reactor
Pressure 1 atm Total gas rate 0 5 cu ft/min (STP)
60-200 mesh MgF_2 or CaF_2 Fluid Bed
Diluent gas nitrogen

Run UOF	Pellet Type	Pellet Charge (kg)	Pellet Bed Height (in)	Inert Fluid Bed Height (in)	Inlet F_2 Conc (m/o)	Temp (C)	Run Time (hr)	Avg UF_6 Prod Rate (g/hr)	Fluorine Efficiency			UO_2F_2 Fines		UF_6 Product (% charge)	Pellets Unreacted (% charge)
									To Form UF_6 (%)	To Form UO_2F_2[c] (%)	Total (%)	On Filters (g)	In Bed (g)		
6	Inert Fired	1 76	3	12	10	500	3 0	240	67	3 7	71[a]	6 5	101	31	63
7	Inert Fired	1 76	3	12	20	500	1 5	495	77	5 1	82[a]	4 0	128	32	60
9	Inert Fired	1 77	3	12	30	500	1 0	693	62	4 8	67[a]	6 5	135	30	61
12	Inert Fired	3 49	6	15	20	500	1 5	478	62	15	87[a](88[b])	74	394	16	70
11	Inert Fired	5 26	9	18	20	500	1 5	425	55	35	90[a](94[b])	210	872	9 3	70
14	Inert Fired	5 24	9	60	20	400	~1 5	76	21	58	79[a]	114	1384	3 0	69
20	Inert Fired	4 19	9	34	20	500	6 2	650	72	7 5	80[a]	471	Complete Fluor	78	0
22	Hydrogen Fired	1 91	3	32	20	400	4 0	192	21	10	31[a](35[b])	198	534	27	33
24A	Hydrogen Fired	1 81	3	30	20	500	3 0	194	20 3	1	21[a](30[b])	74	7	27	68
24B	Hydrogen Fired	-	3	30	40	500	0 5	248	28 4		29[a]				

[a]Total efficiency UF_6 efficiency + UO_2F_2 efficiency

[b]Total efficiency from exit F_2 analysis (average)

[c]Calculated from total fines

The inert-fired pellets have generally been easier to process than hydrogen-fired pellets. The former produces uranyl fluoride fines more readily. These fines offer high surface area and also distribute throughout the inert fluid bed, allowing for easier heat removal. A summary of information on the pellets is given in Table 42.

The earlier runs, including most of those with the inert-fired material, were made with a pellet bed support of nickel balls in the bottom of the reactor. However, because of temperature instabilities with hydrogen-fired pellets in an initial run (UOF-21), a modified bed support was installed to eliminate the possibility of the nickel balls contributing to poor heat transfer. The new bed support consisted of a nickel plate with a number of $\frac{3}{16}$-inch holes. This plate was placed about 10 inches up from the bottom of the fluidized bed and is believed capable of providing better heat transfer at the pellet bed inlet. A run made with hydrogen-fired pellets gave satisfactory temperature control at 40 m/o fluorine and 500 C with this new bed support.

Table 42

PROPERTIES OF PELLETS USED IN FLUORINATION RUNS

Type	Inert Fired	Hydrogen Fired
Manufacturer	No. 1	No. 2
Purity	Reactor Grade	Reactor Grade
Source	Ammonium Diuranate calcined at 770 C	Ammonium Diuranate plus recycled U_3O_8
Sintering	Fired in inert atmosphere at 1720 C	Fired in Dry Hydrogen at 1700 C for 4 hr
Density, g/cc	10.49	10.26
%Theoretical Density	95.6[a]	93.6[a]

[a]Based on a theoretical density of 10.97 g/cc.

Effect of Variables in Pellet Fluorinations

In Figure 43 are shown the variations in uranium hexafluoride product collection rate and in overall fluorine efficiency as the fluorination of a batch of $\frac{1}{4}$-inch inert-fired pellets was carried to completion (Run No. UOF-20). For reference, the theoretical maximum product collection rate is plotted corresponding to 100 percent utilization of inlet fluorine to form uranium hexafluoride by the reaction

$$UO_2 + 3F_2 \longrightarrow UF_6 + O_2 \quad .$$

Also shown is the cumulative fraction of uranium converted to hexafluoride during the course of the run.

FIGURE 43
URANIUM HEXAFLUORIDE COLLECTION RATE AND FLUORINE UTILIZATION EFFICIENCY DURING FLUORINATION OF URANIUM DIOXIDE PELLETS

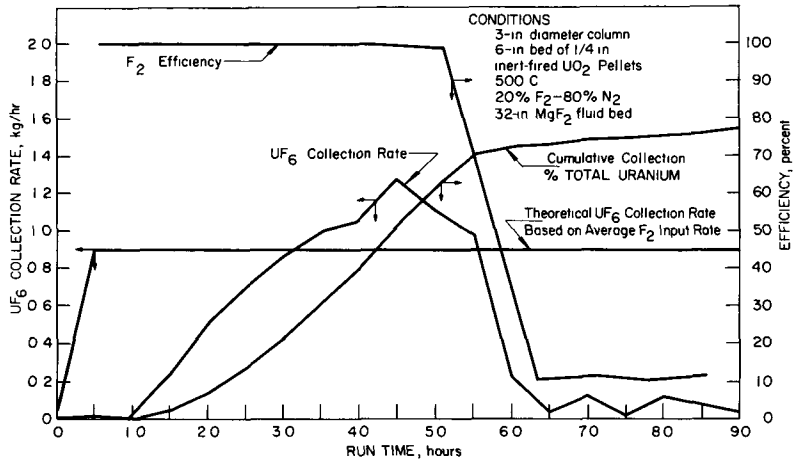

As shown in Figure 43, the rate of uranium hexafluoride product collection was very low for the first hour of the run, after which the rate increased to a maximum at about 4.5 hours. During this period the total fluorine consumption was very close to 100 percent. At 6.0 hours both the product collection rate and the fluorine efficiency dropped sharply to a low and nearly constant level for the remaining period of the run. The fraction of uranium in the charge that was converted to hexafluoride was nearly zero percent at 1.0 hr, 52 percent at 4.5 hr, 73 percent at 6.0 hr, and 78 percent at 9.0 hr.

Although fluorination in this run was complete in the sense that the reaction zone was well depleted of uranium, not all of the uranium was collected as hexafluoride product, because some uranium fines were carried out of the reaction zone and deposited in cooler parts of the system, namely, the disengaging and filter section. The amount of such material in this run was much larger than normal, because filter fines were intentionally not returned to the reactor during fluorination. This was done in order to determine the approximate amount of uranium fines entrained in the off-gas stream.

The most important information shown in Figure 43 for this run is the pattern of uranium hexafluoride collections. Low initial rates are due to fines formation (see ANL-6145, page 107), chiefly by the reaction

$$UO_2 + F_2 \longrightarrow UO_2F_2 \quad ,$$

which proceeds much faster than the reaction (see ANL-5959, page 22 and ANL-5924, pages 28 to 33)

$$UO_2F_2 + 2F_2 \longrightarrow UF_6 + O_2 \quad .$$

When the fines concentration has built up in the inert fluid bed, then uranium hexafluoride is produced at a rate corresponding to the fluorination of uranyl fluoride. Pellet fluorination was virtually complete under these conditions at 6 to 6.5 hours.

In runs where the rates of production of uranium hexafluoride were measured for partial fluorinations and under different conditions, the role of the intermediate fluoride fines was also significant. In Figure 44 is shown the effect of inlet fluorine concentration on the uranium hexafluoride production rate for two different types of pellets. The rates for the inert-fired pellets showed nearly linear dependence on fluorine concentration. Since the fluorine efficiencies in these three runs were nearly equal, a net first-order rate dependence on fluorine concentration is implied. The hydrogen-fired pellets fluorinated at about $\frac{1}{3}$ the rate of the inert-fired pellets. The correlation of fines concentration with fluorination rates is evident; that is, the high rates of production of hexafluoride are associated with high concentrations of uranyl fluoride fines in the bed.

FIGURE 44
EFFECT OF INLET FLUORINE CONCENTRATION ON RATE OF FLUORINATION OF URANIUM DIOXIDE PELLETS

3-In DIAMETER COLUMN
GAS RATE 0 5 cu ft/min
TEMPERATURE ; 500 C
1/2 - In UO_2 PELLETS
32 TO 40 % OF PELLETS REACTED
3-In PELLET-BED HEIGHT
12 TO 30 - In FLUID-BED HEIGHT

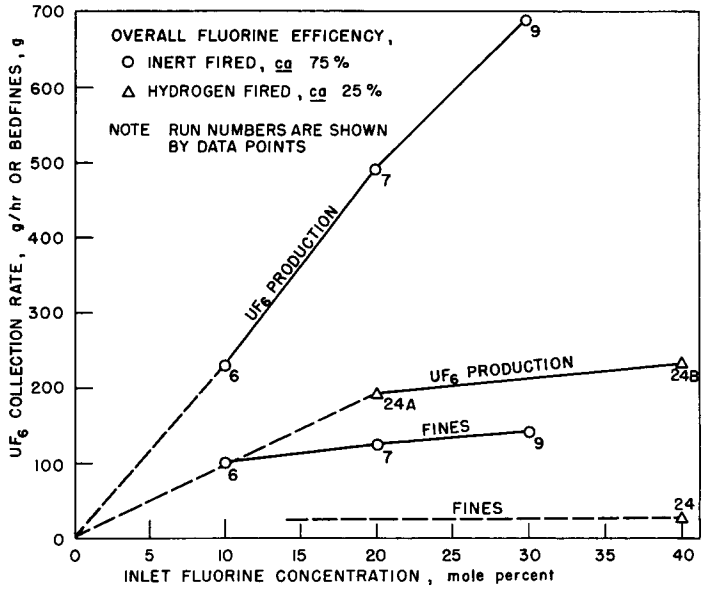

The variation of fluorine efficiency with pellet bed depth is shown in Figure 45. The runs were all partial bed fluorinations in which about $\frac{1}{3}$ of the uranium was converted to the hexafluoride. Because of the larger amount of uranium dioxide surface present in the deeper beds, a greater percentage of the fluorine was used for the formation of

uranyl fluoride, and in the deeper beds relatively less fluorine was available to form uranium hexafluoride during the initial phases of the batch fluorinations. As shown in Figure 45, the amount of uranyl fluoride fines in the bed increased with bed depth. The lower reactivity of the hydrogen-fired pellets is evident.

FIGURE 45
EFFECT OF PELLET BED HEIGHT ON FLUORINE EFFICIENCY DURING INCOMPLETE FLUORINATION OF URANIUM DIOXIDE PELLETS
GAS RATE 0.5 cu ft/min, PELLET DIAMETER 1/2 in
INLET FLUORINE CONC 20 m/o, COLUMN DIAMETER 3 in
TEMPERATURE 500 C, FLUID-BED HEIGHT, 12 to 30 in
PERCENT PELLETS REACTED 32 to 40, NOTE RUN NUMBERS ARE SHOWN BY DATA POINTS

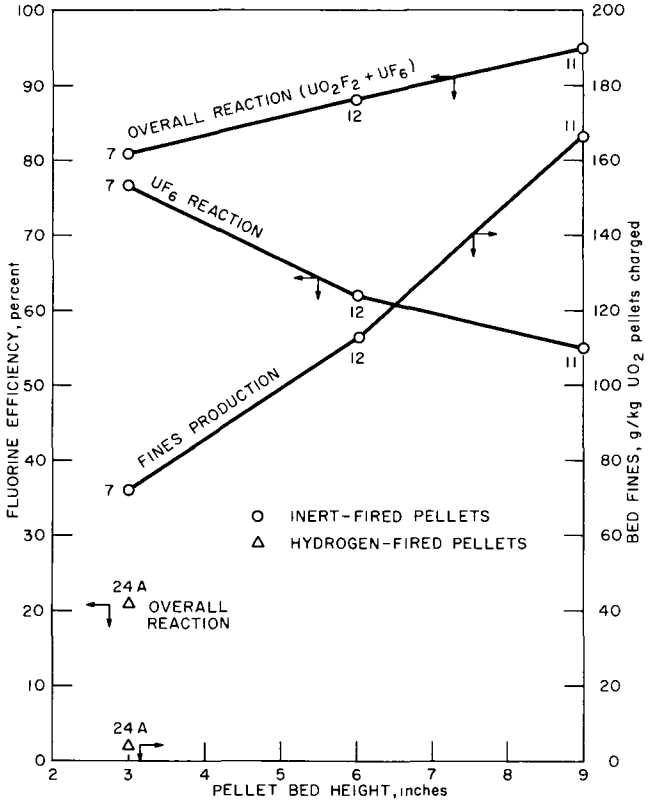

In Figure 46 is shown the effect of temperature on fines formation. More fines were produced at lower temperatures, indicating a relatively stronger dependence on temperature of the reaction of uranyl fluoride to form uranium hexafluoride.

Further work is to be done with deeper beds and with the hydrogen-fired pellets.

FIGURE 46
EFFECT OF TEMPERATURE ON CONCENTRATION ON FINES IN FLUID BED IN FLUORINATION OF URANIUM DIOXIDE PELLETS
COLUMN DIAMETER 3 in
INLET GAS 0.5 cu ft/min
INLET F_2 20 m/o
1/4-in UO_2 PELLETS
FLUID-BED HEIGHT 18-16 in

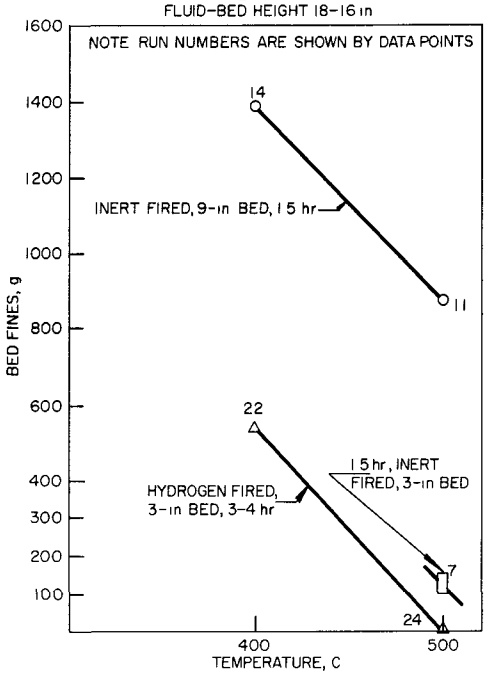

b. Heat Transfer Study in Packed Fluid Beds
(C. Bayens,* W. Murphy)

In the Direct Fluorination Process applied to uranium dioxide pellet fuel, a packed bed of pellets undergoes an exothermic reaction with fluorine gas, and inert material fluidized in the voids of the pellet bed is used to aid in heat removal and temperature control. Heat transfer tests on a mockup system are being made to assist analysis of temperature control in process runs.

In the previous report (see ANL-6231, page 113), values of the film coefficient h, determined as a function of gas velocity, were reported for a system consisting of $\frac{1}{2}$-inch diameter by $\frac{3}{4}$-inch long brass pellets with -140 +200 mesh copper shot, using air as the fluidizing gas in a brass column of 2.88-inch diameter. The coefficient h was measured for heat transfer from pellet-sized heaters to the fluidized material. Average results showed that as the gas velocity was increased, the value of h rose rapidly at incipient fluidization to a value approximately equal to that for open-tube fluidization. There was no appreciable effect of relative pellet-to-fluidized-bed height, provided the heater surface was submerged in the fluidized bed. On the other hand, apparently random variations were observed for h for individual heaters in different positions. These variations were most pronounced at a gas rate of about three times the minimum fluidization rate. A partial convergence (to within ±25 percent) of h-values was observed at gas rates of 10 times minimum fluidization. Average values of h for these cases were about 60 percent of maximum values observed in open-tube fluidization. These average values of h were also about 4 times those obtained for low gas rates in the same system without fluidization, and about 8 times those obtained for pellets without fluidizable material in the voids. These results indicate substantial improvement of film coefficients by the presence of fluidized material in the pellet voids. Further study of effects of variables such as pellet size and particle size of the fluid bed is contemplated.

In the present period, a series of tests was made of a 10-inch bed of $\frac{3}{8}$-inch x $\frac{3}{8}$-inch brass pellets with a single $\frac{3}{8}$-inch diameter by $1\frac{1}{2}$-inch long heater centrally located at the axis. Copper shot, -140 +200 mesh, was used with air as before. The chief purpose of this series

*Co-operative student from the University of Detroit.

of tests was to obtain data on heat transfer film coefficients with $\frac{3}{8}$-inch pellets; $\frac{1}{2}$-inch pellets had been used previously. Bed temperature gradients were measured by three vertically movable thermocouples located at three different radial positions: close to the heater, one-pellet distance and two-pellet distance from the heater. The thermocouples consisted of an unsheathed junction travelling inside a guide well of metal screen (16 mesh). Pressure drops and film coefficients in these tests are summarized in Figures 47 and 48, respectively. Although relative values of h are similar to previous ones (that is, about 70 percent of the value for unhindered fluidization), the absolute values of h were higher. This result is possibly due to the different technique of temperature measurement. The effect of the metal screen guide-well around the thermocouple will be determined to check this point. The dotted lines in Figures 47 and 48 are constructed on the basis of superficial gas velocities corrected for the reduction in column volume due to the presence of pellets. This allows a closer comparison with open-tube fluidization.

FIGURE 47
COMPARISON OF BED PRESSURE DROP FOR HINDERED AND UNHINDERED FLUIDIZATION
STATIC HEIGHT OF COPPER SHOT BED 10 in (no pellets), 12 in (with pellets),
HEIGHT OF 3/8 in × 3/8 in BRASS PELLET BED 10 in

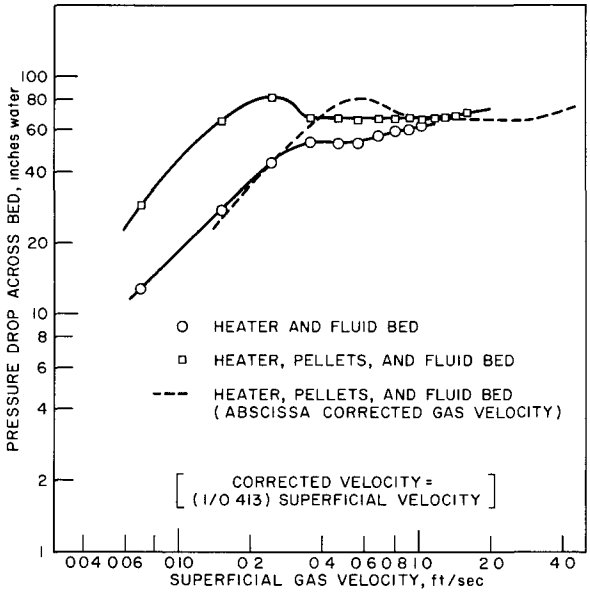

FIGURE 48
FILM COEFFICIENT OF A SMALL HEATER IN A FLUIDIZED BED AS A FUNCTION OF GAS VELOCITY
STATIC HEIGHT OF COPPER SHOT BED 10 in (no pellets), or 12 in (with pellets)
HEIGHT OF 3/8 in × 3/8 in BRASS PELLET BED 10 in

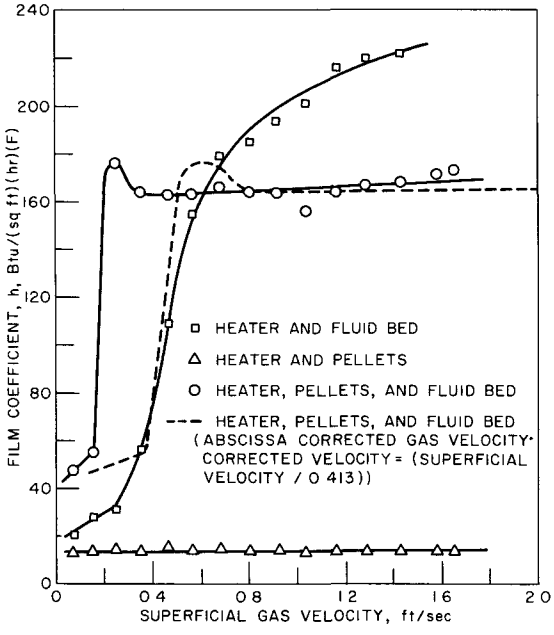

In the above series of runs, a complete set of bed temperature profiles was obtained at three radial positions. Significant temperature gradients in the bed were observed only for static bed cases; with fluidization, a zero temperature gradient was observed. However, the heat flux associated with these gradients was not measurable in these tests.

Another series of experiments was performed to examine the radial temperature gradients developed in a packed-fluidized bed. In order to obtain measurable heat fluxes through the bed, a different heat configuration was used. A $\frac{3}{8}$-inch diameter tubular heater with an active length of 27 inches was axially mounted in the 2.88-inch column with water-cooled walls and submerged in the bed to be tested. Heated air was introduced as fluidizing gas and the power of the heater was adjusted to equalize the temperature of the exit air to that of the inlet air. Thus the entire power of the heater (rated at 1500 watts) was conducted through the bed to the wall of the column.

A baseline run was made with this equipment under normal fluidization, that is, fluidization without fixed packing. The material fluidized was 80 percent 60-mesh, 20 percent 80-mesh glass beads, with an average diameter of 0.0110 inch. The minimum fluidization velocity of this material was 1.0 ft/sec as determined by the pressure-drop curve. Temperatures at various points were recorded during the runs. The bed temperature was measured at different elevations by a vertically moving thermocouple guided by a tubing well of 16 mesh screen. The radial position of the well was halfway between the heater and the wall. A schematic diagram of the equipment and the results obtained in a run at a superficial gas velocity of 1.5 ft/sec is given in Figure 49.

FIGURE 49
LONGITUDINAL TEMPERATURE GRADIENT IN A HEATED FLUIDIZED BED
GLASS BEADS 60 TO 80 MESH
SUPERFICIAL GAS VELOCITY 1.5 ft/sec
X-INDICATES THERMOCOUPLE POSITIONS

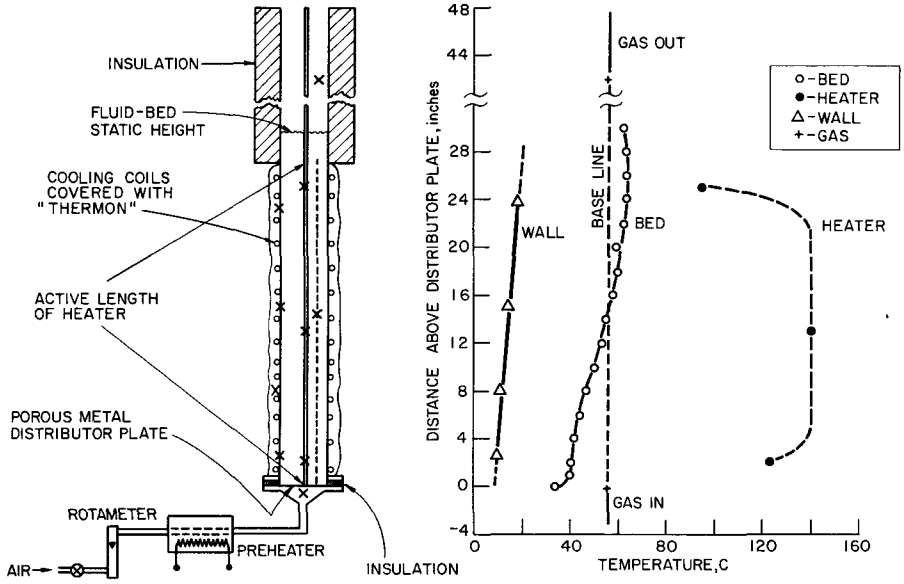

As seen from Figure 49, the bed temperature at the bottom was 15 to 20 C below that of the inlet gas and at the top was about 6 C above that of the exit gas. The temperature difference between the bed and the wall was 45 C at the top and 30 C at 2 inches above the bottom. Maximum

longitudinal temperature difference across the bed was 25 to 30 C. These gradients are considered to be the result of the particular patterns of heat flow and fluid-bed turbulence relative to the thermocouple locations. The fact that the exit gas temperature is 6 C below the top bed temperatures does not necessarily indicate a temperature difference of that magnitude between the gas temperature and the particle temperature at a common point, since the gas temperature above the bed is likely to be an average value for the whole cross section, whereas the bed temperature is at a particular point. The bed is subject to a rather high overall radial temperature gradient: 130 C over the 1.4-inch radius.

The average film coefficients obtained for the wall and heater surface calculated from the above temperatures of the bed were

$$h_{wall} = 24 \text{ Btu}/(\text{hr})(\text{sq ft})(\text{F})$$

$$h_{heater} = 79 \text{ Btu}/(\text{hr})(\text{sq ft})(\text{F}).$$

To make measurements of radial temperature gradients in a packed-fluid bed, a 12-inch high wire mesh basket containing pellets was positioned in the fluid bed 9 inches above the gas distributor plate. The basket was the full inside diameter of the column and fit closely. Temperatures at three different positions along a radius were measured by thermocouples mounted on adjacent pellets. Two such radial temperature distributions were measured in the pellet bed. A sketch of the configuration is given in Figure 50.

FIGURE 50
HEAT TRANSFER TEST THERMOCOUPLE LOCATIONS IN PACKED FLUID BED

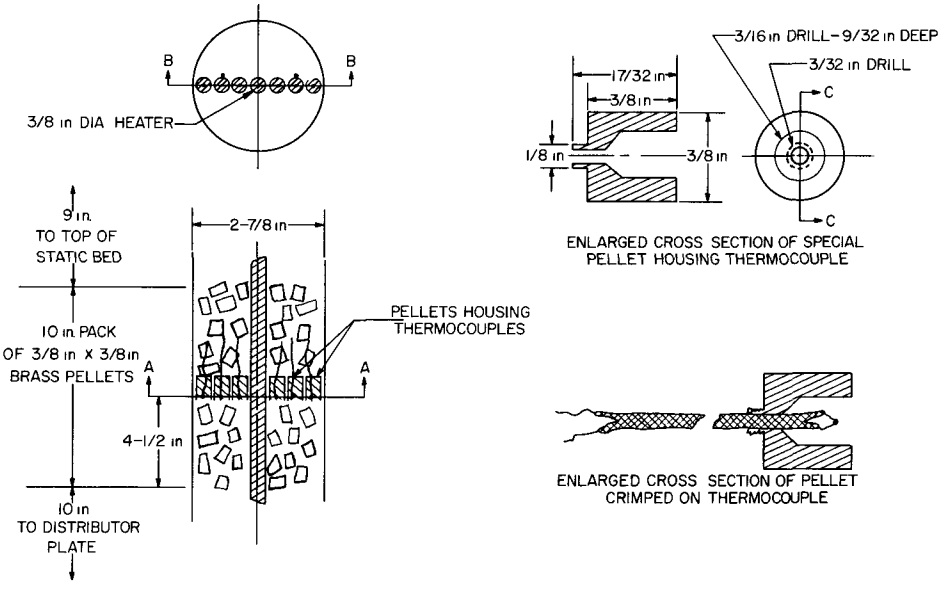

The radial thermal conductivity of the bed was based on the differential equation

$$q = kA \frac{dT}{dr} = k(2\pi rL) \frac{dT}{dr} \quad .$$

In integrated form,

$$k_{1,2} = \frac{q \ln (r_2/r_1)}{2\pi L \ \Delta T_{1,2}} \quad ,$$

where

q = heater power

k = thermal conductivity

A = cross-sectional area of heat flow

r = radius

T = temperature

L = height of zone.

Radial distances of the three thermocouples as measured from the heater surface were $\frac{3}{16}$, $\frac{9}{16}$ and $\frac{15}{16}$ inch, respectively. Averaged k values calculated in this way for runs to date are given in Table 43, together with pertinent operating conditions. In Run K-1 the two sets of radial temperatures were measured at two different elevations. In other runs, they were at the same elevation.

From values of k in Table 43 it appears that higher k's were obtained near the ends of the pellet zone than near the center. Averaged k's are reported for all data in each separate steady-state run; the maximum range in particular values of k in all runs was from 4 to 17 Btu/(hr)(sq ft)(F/ft). For comparison, the thermal conductivity of solid stainless steel (type 304 or 347) is 10.

Further experiments with other particle sizes are planned.

2. Halogenation of Reactor Fuels
(N. Levitz)

Reaction of halogen gases with metal may be used to declad power reactor fuels, for halogenation of uranium dioxide fuel, and for direct conversion of uranium-zirconium alloy fuels to solid fluorides. In connection with halogenation, an improved design of the off-gas scrub tower utilizing anhydrous ammonia was developed.

Table 43

RADIAL HEAT TRANSFER IN A PACKED FLUID BED

Conditions:
2.88-inch ID column
10-inch pellet bed submerged in 29-inch fluid bed
Fluid particles: glass beads 0.0110-inch diameter (avg)
Superficial gas velocity: 1.5 ft/sec
Corrected gas velocity:[a] 3.6 ft/sec

Run	K-1		K-2	K-3	K-4	K-5
Gas Inlet and Exit Temp, C[b]	90		48	97	97	51
Total Heater Power, watts	768		768	1836	1836	768
Heater Temp, C	147		182	247	249	147
Wall Temp, C	10 to 20		10 to 20	10 to 20	10 to 20	10 to 20
Thermocouple Position						
Above Bottom of Fluid Bed, inch	$17\frac{3}{4}$	$11\frac{1}{4}$	$15\frac{3}{4}$	$14\frac{1}{4}$	$14\frac{1}{2}$	$14\frac{1}{2}$
Relative to Pellet Zone	1 in. from top	$2\frac{1}{4}$ in. from bottom	5 in. from bottom	$4\frac{1}{4}$ in. from bottom	$4\frac{1}{2}$ in. from bottom	$4\frac{1}{2}$ in. from bottom
Effective Thermal Conductivity of Bed k avg, Btu/(hr)(sq ft)(F/ft)	10.8	17.2	4.2	8.6	8.0	6.8
Heater Film Coefficient h_H, Btu/(hr)(sq ft)(F)	67	60	57	110	107	74
Wall Film Coefficient, h_W Btu/(hr)(sq ft)(F)	31	41	30	41	36	28
Overall Coefficient, U Btu/(hr)(sq ft)(F)	4.2	6.3	1.9	3.7	3.4	2.9
Max Bed ΔT observed, C[d]	11	7	29/29[c]	30/-[c]	29/42[d]	25/14[c]

[a]Considering volume of pellets.

[b]Heater power adjusted so exit gas temperature equalled the inlet gas temperature.

[c]Measured at same elevation but at two different radii.

[d]Maximum difference between three temperatures measured at the same elevation but at three different radii.

a. Decladding Power Reactor Fuels
(J. T. Holmes, D. J. Raue)

Studies of a process for the recovery of fissile materials from sintered uranium dioxide-stainless steel clad fuels are in progress. The decladding step involving the reaction of chlorine and stainless steel is being studied in a two-zone, $1\frac{1}{2}$-inch diameter fluid-bed reactor. Experiments conducted previously in a horizontal tube furnace achieved penetration rates of 5.0 and 9.7 mils/hr at 570 and 600 C, respectively, using $\frac{1}{2}$-inch segments of $\frac{5}{8}$-inch OD tubing, 50 mils thick (see ANL-6231, page 56). Tube furnace experiments on the direct chlorination of sintered uranium dioxide pellets have been initiated.

(1) Process Studies

The reaction of stainless steel with chlorine gas was studied under fluid-bed conditions and found to proceed at a sufficient rate to be used as a decladding reaction. Other halogenating agents tried did not give high enough reaction rates to be considered further.

A corrosion study indicated that nickel or Inconel could be used as the material of construction for the chlorination reactions.

The reaction of uranium dioxide with chlorine and carbon tetrachloride was found to proceed fast enough to suggest that a chlorination and hydrofluorination followed by fluorination in a two-zone fluid-bed reactor could be used as a method for processing uranium dioxide fuels. This procedure would result in low fluorination costs, since hydrogen fluoride would be used as the initial fluorinating agent.

The reaction of anhydrous ammonia with chlorine and hydrogen fluoride followed by water scrubbing is being used for the disposal of the waste gases as an alternate to a recirculating caustic scrub tower.

Stainless Steel Decladding Reactions

The reaction of stainless steel with chlorine gas is being studied in the lower zone of a $1\frac{1}{2}$-inch diameter, two-zone, fluidized-bed reactor. The lower zone is 17 inches long and is separated from the 11-inch long upper zone by an inverted conical baffle. The baffle prevents back-mixing of gases from the upper zone where anhydrous hydrogen fluoride is admitted. One half-inch segments of $\frac{5}{8}$-inch diameter 304 stainless steel tubing were used as test specimens. The volatile and solid chlorides formed in the lower zone are converted to solid fluorides in the upper zone by the anhydrous hydrogen fluoride. The reaction rates were calculated from the weight loss of the stainless steel tube segments. A reaction rate of 5 to 10 mils/hr would be sufficient for decladding typical

stainless steel fuels now in use: The N. S. Savannah fuel has 32-mil 304 cladding on uranium dioxide pellets, and the APPR-1 and -1A and the OMRE are using 5-mil 304 cladding over cermet-type fuels.[40] The results of four two-zone fluid-bed experiments are shown in Table 44. The reaction rates are slightly higher than those measured in the one-inch diameter horizontal tube reactor experiments - 6.0 as opposed to 5.0 mils/hr at 570 C and 9.7 as opposed to 10.6 mils/hr achieved at temperatures near 600 C (see ANL-6231, page 124). The lower rates were thought to be caused by the smaller gas contact area resulting from resting the coupon on its side in the tube reactor.

Table 44

FLUID-BED REACTION OF 304 STAINLESS STEEL AND CHLORINE

Inlet superficial gas velocity: 0.4 ft/sec

Average flow rates: 8.3 to 9.3 moles/hr chlorine (lower zone)
5 to 6.6 moles/hr hydrogen fluoride (admitted in upper zone)

Lower Bed Temperature (C)	Run Time (min)	Reaction Rate - Penetration[a] (mils/hr)	Percent of Specimen Reacted
570	180	6.0	75
575	58	9.0	30
578	48	10.2	30
590	65	10.6	48

[a]Based on the initial surface area and weight loss of pellets.

The decladding operation will be studied further in a six-inch diameter, two-zone, fluid-bed reactor on bundles of 304 stainless steel tubing. Alundum will be used as the initial inert fluid-bed material.

The reaction rate of chlorine with a 304 stainless steel coupon, which had been autoclaved in demineralized water (to simulate reactor conditions) at 600 psi and 252 C for 6.5 days, was found to be the same as for the "as received" coupons. Oxidation due to reactor atmospheres does not appear to slow the chlorination reaction.

---

[40]Data Manual, Nucleonics, 18, 148 (November 1960).

The reaction of an equimolar mixture of chlorine and carbon tetrachloride with 304 stainless steel was found to be slightly slower than the reaction with pure chlorine. The reaction rates obtained from the one-inch tube furnace experiments were 7.3 and 3.4 mils/hr at 600 C and 577 C, respectively, compared to about 9.0 and 5.5 mils/hr using pure chlorine at these temperatures.

The corrosion of stainless steel by a carbon tetrachloride-water vapor mixture[41] and bromine[42] has been reported, but experiments conducted in the one-inch tube reactor with these reagents gave too low a rate to merit further investigation (see Table 45).

Table 45

REACTION OF 304 STAINLESS STEEL WITH BROMINE AND CARBON TETRACHLORIDE

Gas Composition	Total Flow Rate (moles/hr)	Temperature (C)	Reaction Rate (mil/hr)
31% Br_2, 69% N_2	2.9	490 to 495	0.05
33% Br_2, 67% N_2	3.0	600 to 605	0.80
33% CCl_4, 67% N_2	3.0	545 to 550	0.18
31% CCl_4, 18% H_2O, 51% N_2	3.9	540 to 550	0.02

(2) Corrosion of Construction Materials

The one-inch horizontal tube reactor was used to study the corrosion rates of nickel and Inconel in chlorine gas above 500 C. These two materials have almost identical corrosion properties as shown on Figure 51. The data are presented with those of Tseitlin[43] and Brown.[44] A value of 12 mils/mo was obtained for Hastelloy-C in chlorine at 600 C as compared with about 20 mils/mo for nickel and Inconel. The length of experiments varied from 2 to 19 hours and the flow rates of chlorine and nitrogen were both 2.0 moles/hr.

---

[41] Gladis, G. P., Chem. Eng. Prog. 56 No. 10, 43 (1960).

[42] Perry, J. H., Chemical Engineers Handbook, 3rd ed., McGraw-Hill Book Co., Inc., New York, N. Y. (1950), p. 1475.

[43] Tseitlin, Kh. L., J. Appl. Chem. (USSR), 27, 887 (1945).

[44] Brown, M. H., DeLong, W. B., and Auld, J. R., Ind. Eng. Chem., 39, 839 (1947).

FIGURE 51
CORROSION OF NICKEL AND INCONEL BY CHLORINE
(Tube-Furnace Experiments)
Duration - 2 to 19 hr

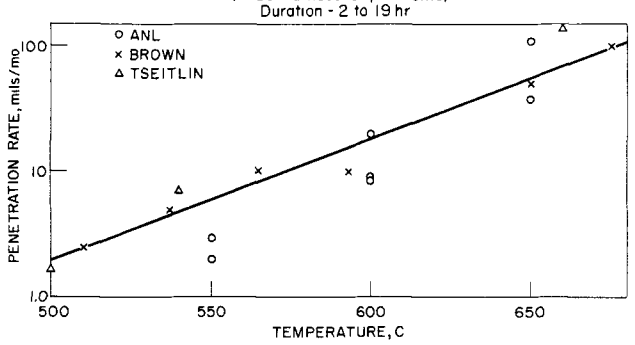

The corrosion rate of nickel, Inconel and other materials will be measured under fluid-bed conditions.

b. Halogenation of Uranium Dioxide Fuel

A series of experiments was made in the one-inch tube furnace reactor to determine the effect of the decladding agent, chlorine, on uranium dioxide and to investigate the possibility of complete chlorination of uranium dioxide fuels by reaction with carbon tetrachloride or a mixture of chlorine and carbon tetrachloride. The uranium dioxide used for this study was in the form of $\frac{5}{8}$-inch long by $\frac{5}{16}$-inch diameter pellets made by Mallinckrodt Nuclear Corporation. The dioxide powder was originally prepared in the fluid-bed process for converting uranium hexafluoride to uranium dioxide (see page 166). Pellets were formed at pressing pressures ranging from 50 to 90 tsi and they were fired for 8.0 hours at 1650 C, resulting in theoretical densities near 95 percent.

The results are reported as reaction rates based on weight changes of the pellets and the initial surface area. The flow rates of all reagents were 1.8 moles/hr. The run times were 2.0, 1.5 and 1.0 hours for experiments conducted at 500, 550 and 600 C, respectively.

The rates of pellet degradation were 370 to 780 mg/(sq cm)(hr) for the chlorine-carbon tetrachloride mixture and 94 to 720 mg/(sq cm)(hr) for carbon tetrachloride alone for this temperature range. The rates are similar in magnitude to those previously reported for the fluorine-uranium dioxide reaction (see ANL-6183, page 98). The remaining unreacted pellets were free of any scale, indicating that volatile species are probably formed, even at 500 C.

Experiments at 500 and 550 C with chlorine alone gave slight weight gains, one and three percent, respectively, whereas at a temperature of 600 C a weight loss [~200 mg/(sq cm)(hr)] was observed. These data suggest nonvolatile chlorides form at the lower temperature, and volatile species probably form at the higher temperature. The data are shown in Figure 52.

FIGURE 52
CHLORINATION OF URANIUM DIOXIDE PELLETS

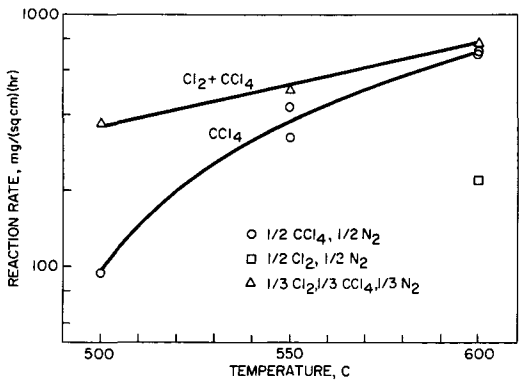

The chlorination results merit consideration of the complete chlorination of uranium dioxide as a means of reprocessing this type of fuel. The apparent advantage over direct fluorination of uranium dioxide with fluorine is the lower fluorination cost obtainable with hydrogen fluoride as the initial fluorinating agent as carried out in the upper zone of a two-zone reactor. Also, appreciably less heat is generated in the chlorination reactions, making the heat removal problem less severe. Complete uranium recovery would require the use of fluorine to oxidize the lower fluorides to uranium hexafluoride. The separation of uranium and plutonium would probably be carried out in a manner similar to that used in the Direct Fluorination Process (see page 147).

c. Direct Conversion of Uranium-Zirconium Alloy Fuels to Solid Fluorides

Work continued in a two-zone fluid-bed reactor on the first step of a Direct Fluorination Process for the recovery of uranium from low uranium-Zircaloy alloy plate-type fuels. The scheme is also applicable to Zircaloy or stainless steel-clad uranium dioxide fuel. In previous work, the metal, submerged in an inert bed, was reacted with hydrogen chloride in the lower zone. The resulting chlorides reacted with hydrogen fluoride in the upper zone, resulting in complete trapping of the volatile materials (primarily zirconium tetrachloride). The rate of dissolution was about 10 to 15 percent/hr of a 2-kg charge of two weight percent uranium-Zircaloy alloy at temperatures between 360 and 400 C and inlet hydrogen chloride concentrations of 60 to 90 percent in nitrogen (see ANL-6231, page 118).

Chlorination-Hydrofluorination Studies in a Two-zone Reactor

Work on the two-reaction zone scheme for processing low uranium-Zircaloy alloy fuels was continued in the six-inch diameter fluid-bed reactor. The initial step involving conversion of the metal to the chloride is carried out in the lower zone of the fluidized bed at temperatures above the sublimation point of the zirconium tetrachloride (331 C), thus forming a volatile component of the bulk constituent. In the upper zone, separated from the lower zone by a conical baffle, hydrogen fluoride is admitted to react with the volatile zirconium tetrachloride forming the solid tetrafluoride. The uranium is also converted to the tetrafluoride in

this step. Since chlorine is less expensive than hydrogen chloride (used previously) and may react to form a volatile uranium chloride, a series of three runs was made to ascertain its applicability to the process scheme.

Approximately three kilograms of metal consisting of several plates of five weight percent uranium-Zircaloy-2 alloy were reacted in dilute chlorine at bed temperatures ranging from 350 to 400 C. The plates were submerged in a bed of -40 +200 mesh alundum (abrasive grain aluminum oxide). Alundum has been found to be nonreactive in fluorine up to temperatures of 625 C, so no difficulties during the subsequent fluorination step were expected. Mixtures of chlorine and nitrogen containing from 10 to 25 volume percent chlorine were used as the primary reactant. Hydrogen fluoride, the secondary reactant, was admitted in the upper zone in a mole ratio of approximately two moles of fluoride per mole of chlorine gas. The inlet superficial gas velocity in the lower zone was 0.5 ft/sec. Three runs were made in sequence, using the final bed containing the residual unreacted metal as the starting material for the subsequent run.

Results (Table 46) showed that appreciably higher rates of attack were achieved with chlorine as the primary gas than with hydrogen chloride: 274 to 417 g/hr of metal reacted as opposed to a maximum rate of 300 g/hr for hydrogen chloride. Chlorine appears to be a much more effective reactant, since much lower concentrations were used. Physical examination of the metal specimen between chlorination runs showed severe scoring of the metal in contrast to the smooth surface observed during hydrochlorination.

Table 46

SUMMARY OF CHLORINATION-HYDROFLUORINATION RUNS - TWO-ZONE PROCESS

Equipment: 6-inch diameter Inconel reactor
Specimen: 5 w/o Uranium-Zircaloy-2 plates (unclad)
Bed: 21 kilograms type 38 Alundum Grain (Norton Co.)
Baffle: Stainless steel cone with $1\frac{1}{2}$-inch diameter opening
Inlet Superficial Gas Velocity: 0.50 ft/sec
Hydrogen Fluoride Rate: 1.1 scfm

Run Number	Bed Temperature (C)	Chlorine Concentration in Nitrogen (v/o)	Run Duration (hr)	Fuel Element Wt		Grams of Alloy Reacted Per Hour
				Initial (g)	Final (g)	
ZHF-26	350 to 400	10 to 20	2.0	2,965	2,245	360
ZHF-27	400	10 to 25	3.9	2,245	662	417
ZHF-28	395	15 to 20	1.8	662	169	274

At chlorine concentrations above 15 percent, sufficient heat of reaction was liberated to allow a considerable reduction in the column heat input and still maintain a bed temperature of 400 C. At higher chlorine concentrations (to 25 percent), some bed caking was evident in the vicinity of the metal plates. This indicates that operation with chlorine concentrations above 25 percent may require some equipment modifications to permit a greater rate of heat removal.

Results of X-ray spectral analyses and microscopic examination of separate size fractions of final bed samples showed that the zirconium and uranium fluorides were deposited as a coating of uniform thickness on the alundum bed particles, as they were previously during the experiments with hydrogen chloride and the calcium fluoride bed (see ANL-6231, page 121). No zirconium has been detected in the off-gas scrub streams, indicating the two-zone scheme to be of high efficiency for trapping volatile materials. This type of reactor may have a widespread applicability.

d. Waste Gas Disposal

Severe corrosion by the chloride-hydrogen fluoride off-gas stream in the nickel scrub-tower used in conjunction with the 1.5-inch diameter fluid-bed reactor resulted in repeated plugging of the system. The unit was three inches in diameter and three feet tall. Twenty five percent potassium hydroxide solution was circulated through the column; nevertheless, corrosive conditions existed, possibly due to hypochlorite (oxidizing agent) formation.

Tests were made with three solid absorbents in an attempt to eliminate liquid corrosion and plugging problems. Activated alumina and limestone were both ineffective in absorbing chlorine. Ascarite (sodium hydroxide on asbestos) was found to be very efficient, but it formed a hard cake which could not be removed from the trap, thus making its use impractical.

The reaction of chlorine and hydrogen fluoride with anhydrous ammonia in the gas phase was found to be an effective method for safe disposal of these gases. Solid ammonium fluoride and ammonium chloride are formed. A three-inch by three-foot long glass scrub column was constructed to study this reaction. The off-gas was introduced at the bottom of the column through the annular space of a two-fluid nozzle of the type used for the ADF work (see ANL-6068, page 94). The ammonia was introduced through the center tube of the nozzle. A free space of about 15 inches, below the $\frac{1}{2}$-inch carbon raschig ring packing which fills the upper part of the column, allowed sufficient time for the gas phase reaction to take place. Water was sprayed into the top of the column as the scrub solution. The solid ammonium chloride and fluoride are very soluble in water and were easily scrubbed from the gas stream. It was

found that submerging the gas-mixing nozzle under about $\frac{1}{2}$ inch of water eliminated the buildup of solids on the nozzle face. An excess of about 25 percent ammonia was sufficient to keep the aqueous solution basic and to react completely with chlorine and hydrogen fluoride with maximum off-gas flow rates from the 1.5-inch fluid-bed system (12 mole/hr chlorine and 10 mole/hr hydrogen fluoride combined flow). The water flow rate was 5 to 10 gal/hr.

C. Conversion of Uranium Hexafluoride to Uranium Dioxide

(I. Knudsen, H. Hootman,* N. Levitz, M. Jones, J. Kincinas)

The fluid-bed process for the preparation of ceramic-grade uranium dioxide from uranium hexafluoride is being studied for application to the production of nuclear fuel. Uranium hexafluoride is reacted with steam to form uranyl fluoride which is then reduced to uranium dioxide with hydrogen. High sintered densities have been obtained in pellet fabrication tests performed on powder made in previous experiments (ANL-6183, page 122, and ANL-6231, page 134). The reactions have been carried out simultaneously in a single reactor and in separate steps; conversion to solids is about 99.99 percent complete. The newly formed material deposits as a dense coating on the particles in the bed. Work is being concentrated on the two-step procedure because of greater flexibility in choice of reactor conditions and process control.

1. Steam Hydrolysis of Uranium Hexafluoride

Several uranium hexafluoride hydrolysis runs have been made previously at rates up to 205 lb uranium/(hr)(sq ft reactor cross section) for periods of $2\frac{1}{2}$ hours in the three-inch diameter Monel reactor (see ANL-6183, page 119). Continuous operation for longer periods of time requires seed particle recycle to offset normal particle growth. However, excessive addition of seed particles may increase the superficial velocity to minimum bed fluidizing velocity ratio above the limit beyond which fines have consistently been formed (see ANL-6145, page 127). About twenty-five hours of running time have been accumulated in a recent series of experiments, but each run was interrupted by the sudden formation of fines. The longest successful period was about four hours. Run conditions were held constant at 100 g/min uranium hexafluoride [174 lb uranium/(hr) (sq ft reactor cross section)], 250 percent steam excess, 200 C reactor temperature, 0.75 ft/sec steam superficial velocity, and 18-inch bed height. Feed rate of the seed particles, a -60 +200 mesh fraction, was varied from about 6 to 25 g/min; average bed particle size was 300 to 350 microns. Column operation was good except for particle size control. In view of these difficulties, a program has been initiated starting with short runs and gradually increasing the run duration in an attempt to isolate the factors causing the upsets.

*Resident Student Associate from Michigan College of Mining and Technology.

2. Reduction of Uranyl Fluoride

The advantages of a two-step operation in the reduction of uranium hexafluoride to uranium dioxide are considered to be higher throughput and greater flexibility in the operational parameters of the process. However, the second step, the reduction of uranyl fluoride to uranium dioxide, has been found to be the rate-controlling reaction of the process. Therefore, effort is being expended in the study of this reaction. Previous work (see ANL-6183, page 120) indicated that the reaction is highly temperature dependent.

Design and construction of a second three-inch Monel reactor was completed in order to facilitate additional pilot-plant studies. This reactor will be used for the reduction of uranyl fluoride in a two-step process, or it may be used for additional fluoride removal in a one-step process. The reactor (of three-inch diameter and 30 inches long) has been built to accommodate each of the three process options; fluid-, static-, or moving-bed experiments. Cooling coils and heaters cover the full length of the reactor for static- and moving-bed operation. The system offers rapid heatup time and good temperature control. Screw feeders will be used to insert feed and to withdraw product during continuous operation. Four high-pressure nitrogen inlets have been installed along the length of the reactor to break up solids held up in the moving bed option. Sintered Monel bayonet filters with automatic blowback were installed to reduce solids loss. A spray contact-absorber is used to remove the hydrogen fluoride from the off-gas. Provision has also been made for addition of steam to the reactant gas stream.

At the present time, batch fluid-bed operation is being used. Runs were made at 600 and 650 C with 100 percent hydrogen on uranyl fluoride feed material which was produced at 200 C. Preliminary results indicate that a mixture of steam and hydrogen markedly increases the conversion rate over that achieved with hydrogen alone. Thermobalance studies using hydrogen alone at 600 C achieved about 97 percent conversion in 85 minutes.

III. REACTOR SAFETY

The oxidation, ignition, and combustion processes of uranium, zirconium, and plutonium are being studied to provide information to aid in minimizing the hazards associated with handling these metals.

Studies of the ignition of uranium powders by the burning curve method are continuing. Results have shown that an increase in heating rate caused an increase in ignition temperature for a -80 +100 mesh (d = 149 microns) powder. An increased heating rate, however, decreased the critical height of powder required to yield a constant ignition temperature. The critical height was shown previously to be nearly independent of container diameter. The effects of heating rate were shown to be consistent with the Frank-Kamenetskii theory of thermal explosions and the Murray, Buddery and Taylor ignition equation. Both treatments apply when a linear oxidation rate law prevails.

The effect of pre-oxidation on the ignition temperature of a -140 +170 mesh (d = 88 microns) uranium powder was investigated. The ignition temperature decreased as much as 25 C when the surface of the particles appeared to be fully covered by oxide nodules (20 percent reaction). Further pre-oxidation caused the ignition temperature to increase.

Ignition temperatures of uranium and uranium carbide powders were measured in air and compared to values obtained in pure oxygen. Ignition temperatures of both materials in air were within 20 C of those in oxygen.

Studies of the rate of burning propagation along uranium and zirconium foil strips is continuing. Propagation rates did not increase significantly with uranium when the ambient air temperature was increased to 300 C. Propagation rates increased about 40 percent at most in experiments with zirconium when the ambient air temperature was increased to 400 C.

Previous work has shown that the presence of certain halogenated hydrocarbons in air decreases the burning propagation rate along metal foils. An investigation into the causes of the decreased rates was initiated. Studies of the cooling of a heated platinum foil by various mixtures of trifluorobromomethane and dichlorodifluoromethane with air and argon indicated that increased heat removal was not responsible for the decreased burning rates.

The experimental program to determine rates of reaction of molten reactor fuel and cladding metals with water is continuing. The principal laboratory-scale method involves the rapid melting and dispersion of metal wires in a water environment by a surge current from a bank of condensers.

A new high-pressure apparatus was described in the previous quarterly (see ANL-6231, page 155). The series of runs with 60-mil zirconium wires at pressures up to 1500 psi is continuing. More extensive and more rapid reaction was reported in the previous quarterly for runs in heated water. This trend was found to continue to higher metal temperatures. Up to 90 percent reaction occurred at an initial metal temperature of 2200 C.

A series of equations was derived to describe the behavior of heated metal spheres in a water environment. The derivations were similar to those reported in a previous quarterly (see ANL-6029, page 126), with the addition of equations to describe the gaseous diffusion process whereby water vapor diffuses through the hydrogen mantle surrounding reacting particles. Preliminary results of studies on the analog computer have led to a reasonable interpretation of the unusual pressure effect.

A second laboratory-scale method involves the rapid contact of steam with heated metal. In this method, the metal receives a "pressure pulse" of water vapor. A new apparatus was constructed which is entirely enclosed in a box heated to 105 C. Runs with one atmosphere of water vapor reacting with molten aluminum at 1000 C are reported. Preliminary results indicate that the oxide film is very protective at these temperatures.

A series of metal-water transient irradiation experiments in TREAT was made with uranium wires for which the rate of energy input was progressively changed. Ninety-three percent enriched uranium wires with diameters of 34 and 64 mils were used. Observation of the uranium after the reactor bursts indicated that, with an average energy of 44 megawatt-seconds (216 calories per gram uranium), a reactor period of 515 milliseconds did not melt the uranium. Reactor periods of 304 milliseconds or less resulted in melting of the wires. The uranium attained temperatures of about 1500 C and the process was accompanied by the extensive formation of particles. One run with a bundle of three uranium wires, resulted in 12.9 percent reaction, accompanied by the fusing together of the three wires with the production of some fine particles. A plot of the amount of uranium-water reaction versus the reactor period indicated that the extent of reaction decreased as the period increased.

Particle size measurements were made on uranium wire which had been melted and dispersed under water by the TREAT reactor bursts. The particles of most frequent occurrence had diameters in the range 2 to 16 mils; this is to be compared with the original diameter of 64 mils. However, the presence of larger globules resulted in Sauter mean diameters (see Table 56 for definition) ranging from 17 to 78 mils. A correlation was observed between the extent of uranium-water reaction and the change in specific surface area; as the ratio of final area to initial area increased from 1.0 to 5.4, the percent of metal-water reaction increased from 0.4 to 17.2 percent.

A. Metal Oxidation and Ignition Kinetics
(L. Baker)

1. Ignition Studies of Uranium Powder by the Burning Curve Method
(M. Tetenbaum, R. Wagner, and L. W. Mishler)

The burning curve procedure has been used extensively to provide reproducible data on the ignition characteristics of uranium. Massive blocks, wires, foils, and powders contained in crucibles have been studied. The sample, mounted on a thermocouple, is heated at a uniform rate (usually 10 deg per min) in a flowing oxidizing atmosphere. As the rate of reaction increases, the sample self-heats and finally ignites. A graphical intersection method is used to determine ignition temperature. The difference between furnace and sample temperature gives an indication of the rate of reaction over a wide temperature range. The burning curve method has been used to define the effects of varied specific area and sample geometry on ignition temperatures of uranium powder (see ANL-6183, page 130 and ANL-6231, page 138).

a. Effect of Heating Rate on Ignition Temperature

The effect of heating rate on the ignition temperature of uranium powder in oxygen was investigated during this quarter. The results are shown in Figure 53. It is seen from Figure 53 that ignition temperature increases with heating rate, confirming previous observations obtained with 8.5-mm uranium cubes (see ANL-5974, page 15). The ignition temperature values obtained with -80 +100 mesh spherical uranium are 235, 245, 270, and 285 C for heating rates of approximately 3, 6, 18, and 38 C per minute, respectively. It is important, therefore, when comparing ignition temperatures, to make sure that comparisons are made under similar heating rate conditions.

FIGURE 53

EFFECT OF HEATING RATE ON IGNITION TEMPERATURE OF -80 +100 MESH SPHERICAL URANIUM POWDER

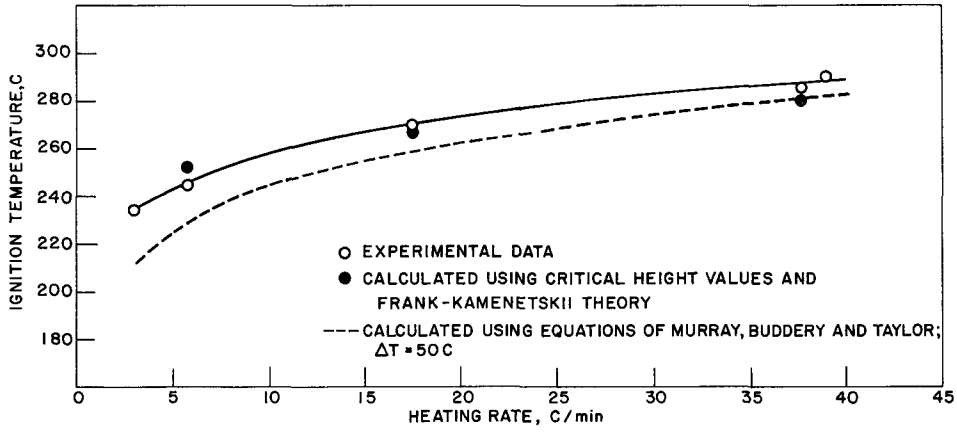

It is interesting that Fassel et al.[45] in their studies on the ignition of magnesium and magnesium alloys claim that ignition temperature is not influenced by rate of heating. On the other hand, Anderson and Belz[46] in their combustion studies with zirconium powder find a linear increase of ignition temperature with heating rate for large samples, and a linear decrease in ignition temperature for small samples.

Calculated values of ignition temperature are also indicated on Figure 53. The calculations are discussed in a later section.

b. Effect of Heating Rate on Critical Height Values

The term critical height was defined in the previous quarterly (see ANL-6231, page 143) as the minimum height of a given powder required to yield constant ignition temperature values practically independent of container size. It was anticipated on the basis of the Frank-Kamenetskii theory of explosions that the critical height values for a given powder mesh size should decrease with heating rate, if the use of critical height values for the significant geometrical dimension of the container was to account for the ignition behavior of uranium powder. The critical height values obtained in oxygen with -80 +100 mesh spherical uranium powder and the corresponding ignition temperatures calculated on the basis of Frank-Kamenetskii theory are shown in Table 47.

Table 47

EFFECT OF HEATING RATE ON CRITICAL HEIGHT VALUES OF -80 +100 MESH SPHERICAL URANIUM POWDER IN OXYGEN

Heating Rate (C/min)	Critical Height (mm)	Ignition Temperature (C)	
		Calculated (Frank-Kamenetskii)	Experimental
5.8	3.8	252	245
17.5	3	268	270
37.7	2.5	280	285

It is apparent from Table 47 that the measured critical height values fall in the expected direction. The calculated ignition temperatures using these critical height values are in good agreement with experimental values (see also Figure 53). This emphasizes the usefulness of the critical height concept as the significant geometrical dimension of the container in the application of the Frank-Kamenetskii theory of thermal explosions.

[45] Fassel, W. M., Gulbransen, L. B., Lewis, J. R., and Hamilton, J. H., J. Metals 3, 522 (1951).

[46] Anderson, H. C., and Belz, L. H., J. Electrochem. Soc. 100, 240 (1953).

c. Effect of Pre-oxidation on Ignition Behavior of Uranium Powder

This study presents the effects of pre-oxidation on the ignition temperature of uranium powder prior to burning curve ignition temperature measurements in pure oxygen. The samples were oxidized by heating -140 +170 mesh spherical uranium powder (spread as a thin layer in a dish) in air at approximately 150 C for varying lengths of time, then cooled and weighed. Microscopic examination of the powders revealed that the surface of the particles had become coated with black (oxide) nodules, the extent of coverage varying with heating time. Complete coverage of particles with nodules appeared to have occurred after fifteen hours of heating. The results are summarized in Table 48. The data show the ignition temperature decreasing, leveling off, and finally increasing with extent of pre-oxidation. These changes, particularly the decrease in ignition temperature, should be of considerable practical consequence, since it illustrates how important it is to know, among other things, the oxidation history of a sample of uranium if it is to be handled properly from the standpoint of ignition. It can be inferred upon examination of the data in Table 48 (without attempting at this time an explanation for the mechanism of oxidation of uranium) that the extent of nodule coverage and, therefore, the variation of effective specific area, rate of oxygen uptake, and ignition temperature are intimately related.

Table 48

EFFECT OF PRE-OXIDATION ON IGNITION TEMPERATURE BEHAVIOR OF -140 +170 MESH SPHERICAL URANIUM POWDER

Heating Time in Air at 150 C (hr)	Oxygen Uptake[a] (μg/sq cm)	% Reacted[b]	Incremental Oxidation Rate [μg/(sq cm)(min)]	Ignition Temperature (C)	Microscopic Observation after Pre-oxidation
0	-	-	-	260	Relatively smooth spheres some interference colors
1 05	3.06	0.08	0.05	255	Partial coverage with nodules
2 25	15.0	0 40	0 17	250	Partial coverage with nodules
5 50	61 1	1 7	0 24	240	Partial coverage with nodules
8 00	143	3.8	0 55	235	Partial coverage with nodules
14.8	720	19.2	1 41	235	Full coverage with nodules
20 0	1520	40.7	2 58	240	Full coverage with nodules
43 0	2950	79 5	1 04	250	Full coverage with nodules

[a]Oxygen content of batch as received was 500 μg/g sample (0 37% reacted)

[b]Oxide assumed to be UO_2.

d. Ignition Behavior of Uranium Powder in Air

The ignition behavior of spherical uranium powders of different mesh sizes was measured using air as the oxidizing atmosphere. The sample temperature was measured with a thermocouple in addition to the usual container probe (as in oxygen runs) in order to sense ignition. The results obtained both in air and in oxygen are shown below:

Mesh	Representative Particle Diameter (μ)	Ignition Temperature (C) In Air	Ignition Temperature (C) In Oxygen
- 20 + 25	710	285	305
- 80 +100	149	270	270
-140 +170	88	260	265
-270 +325	44	240	245

It is apparent that ignition temperatures obtained in air are about the same as in oxygen. This is reasonable, since reactions leading to ignition are not extensive or rapid enough to generate a diffusion barrier of nitrogen between the oxygen of the air and the metal. It should be pointed out, however, that the rise in temperature at ignition is less pronounced, and the flash of light considerably less intense than in oxygen.

e. Ignition Behavior of Uranium Carbide

Ignition temperature measurements were made both in air and in pure oxygen atmospheres on various mesh fractions of irregular uranium monocarbide. With runs in air, it was found necessary to probe the sample temperature with a thermocouple in order to sense the temperature rise at ignition. The results are summarized below:

Mesh	Representative Particle Size (μ)	Ignition Temperature (C) In Air	Ignition Temperature (C) In Oxygen
-20 + 25	710	320	320
-30 + 35	500	315	310
-50 + 60	250	300	300
-70 + 80	177	305	295
-80 +100	149	295	280

It is apparent that ignition temperature values obtained with various mesh size powders of irregular uranium monocarbide are almost identical in air and in oxygen. These values are approximately 15 degrees higher than the ignition temperatures obtained with corresponding mesh size spherical uranium powder.

f. Theory of Uranium Powder Ignitions

It was demonstrated in the previous quarterly (see ANL-6231, page 147) that the ignition behavior of uranium powder can be satisfactorily predicted on the basis of Frank-Kamenetskii theory of thermal explosions using critical height and estimated effective thermal conductivity values. The ignition behavior of uranium powder can also be described by converting isothermal expressions to a rising temperature basis (neglecting heat losses), according to the treatment of Murray, Buddery, and Taylor.[47] The equations are based on linear oxidation kinetics:

$$s\Delta T = \frac{6A\Delta H}{\rho d\phi}\ \psi \qquad (1)$$

where

$$\psi = e^{-\frac{E}{RT_0}\left\{\left(\frac{RT_0}{E}\right)^2 - 2\left(\frac{RT_0}{E}\right)^3\right\}} ,$$

and where s is the specific heat, ΔT the difference in temperature between sample and container (generally ΔT is assumed to be 50 C at ignition), T_0 the container temperature when ignition takes place, A the frequency factor in the Arrhenius equation, E the energy of activation, R the gas constant, ΔH the heat of reaction, ρ the density, d the diameter of the spherical powder particles, and ϕ the container heating rate.

Using Equation 1, ignition temperatures were calculated for a variety of specific area fractions on the basis of a heating rate of ϕ = 17.5 C per minute (experimental heating rates varied between 15 and 20 C per minute) and ΔT = 50. The results are shown in Table 49 and Figure 54. It is apparent from the data shown that the theoretical ignition temperature values calculated from Equation 1 are in reasonable agreement with experimental values.

---

[47] Murray, P., Buddery, J. H., and Taylor, J. F., (Mrs.), The Pyrophoric Nature of Metal Powders, A.E.R.E. M/R 1428 (1954).

Table 49

COMPARISON OF EXPERIMENTAL AND THEORETICAL IGNITION TEMPERATURES FOR URANIUM POWDER

Mesh	Representative Particle Diameter (μ)	Specific Area (sq cm/g)	Ignition Temperature (C) Calculated [a] Murray, Buddery, and Taylor	Calculated Frank-Kamenetskii	Calculated [b] Murray, Buddery, and Taylor	Experimental
-200 +230	62	51.2	236	253	227 (35 6)	255
-120 +140	105	30.2	249	263	240 (36 2)	260
- 80 +100	149	21.3	259	270	249 (37 7)	270
- 40 + 45	350	9.06	283	290	275 (41 1)	295
- 18 + 20	840	3.78	310	310	305 (43.5)	310
- 12 + 14	1410	2.25	328	325	323 (45.0)	320

[a] Calculated using ΔT = 50 C, ϕ = 17.5 C/min.

[b] Calculated using $\Delta T = 1.2\,RT_0^2/E$, ΔT values in parenthesis ϕ = 17 5 C/min.

Values calculated on the basis of the Frank-Kamenetskii theory of thermal explosions were also calculated for the powders and are also given in Table 49 and Figure 54. Details of the calculation were discussed in the previous quarterly (see ANL-6231, page 147). Experimental critical height values were used in the calculation. The finest powder (-270 +325 mesh) was estimated to have a thermal conductivity of 10^{-4} in cgs units (the conductivity of oxygen gas in the pores). A very coarse powder (-10 +12 mesh) was estimated to have a thermal conductivity of 10^{-3} in cgs units based on measurements with 2500-micron lead powder. Values for other particle sizes were interpolated. Ignition temperature values calculated in this way are shown to be in excellent agreement with the experimental data.

FIGURE 54

EXPERIMENTAL AND THEORETICAL IGNITION TEMPERATURES OF SPHERICAL URANIUM POWDER AS A FUNCTION OF SPECIFIC AREA

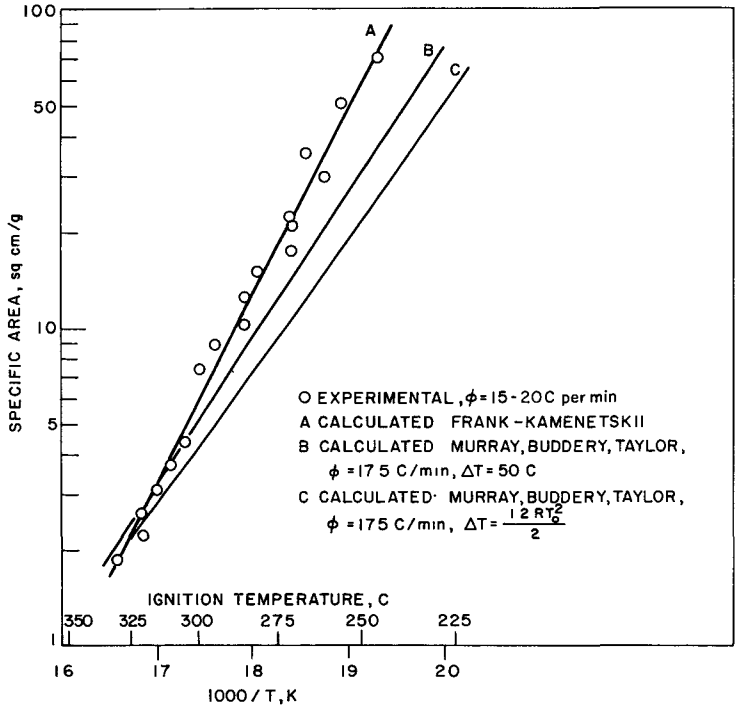

A further intercomparison can be made. Frank-Kamenetskii has shown that the critical temperature rise due to self-heating is given by

$$\Delta T = 1.2 R T_0^2 / E \quad . \qquad (2)$$

When this ΔT value is exceeded, the system becomes unstable, and accelerative self-heating leads to ignition. The critical temperature rise calculated from experimental ignition temperatures obtained with spherical uranium powder fractions is shown in parenthesis in Table 49. These ΔT values were then used to calculate ignition temperatures (ϕ = 17.5 C/minute) on the basis of the proposal of Murray, Buddery, and Taylor (Equation 1). The agreement with experimental ignition temperature values, shown in Table 49, is not particularly good for relatively small diameter particles, i.e., 62 to 250 microns. With particles of larger diameter, 840 to 1410 microns, the agreement becomes considerably better.

The Murray, Buddery, and Taylor treatment, which leads to Equation 1, can also be used to predict the effect of heating rate on the ignition temperature of uranium powder. A theoretical curve for -80 +100 mesh spherical uranium powder calculated on the basis of ΔT = 50 C was included in Figure 53. The two curves show the same trend, although calculated values are a little lower.

A generalized plot of the ignition temperatures of uranium powders as a function of specific area and heating rate is given in Figure 55.

FIGURE 55

THEORETICAL CURVES BASED ON EQUATIONS OF MURRAY, BUDDERY AND TAYLOR SHOWING EFFECT OF HEATING RATE ON IGNITION TEMPERATURE OF SPHERICAL URANIUM POWDER (ΔT = 50C)

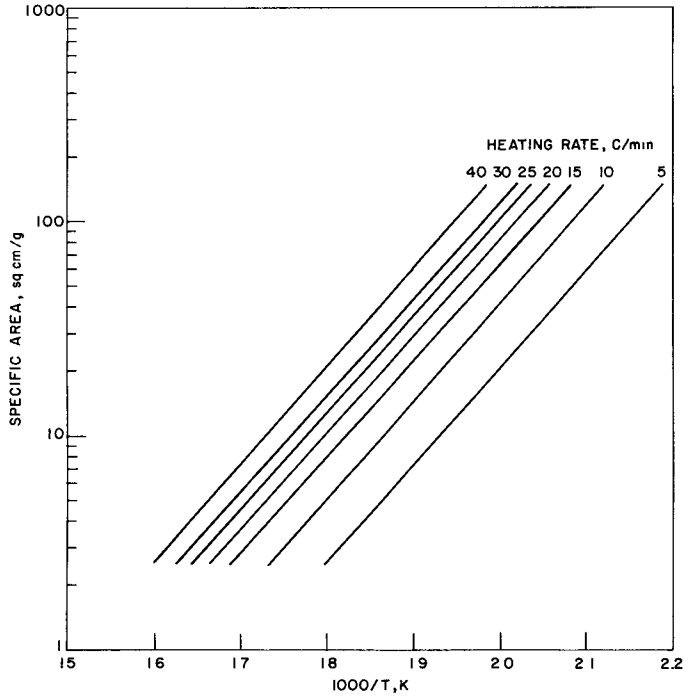

We may summarize the principal results of uranium powder ignition studies as follows: (1) The ignition behavior of uranium powder has been found to be dependent on specific area of powder fraction, degree of oxidation, rate of heating, and geometry of sample; (2) On the basis of the Frank-Kamenetskii theory of thermal explosions, the ignition behavior of uranium powder can be predicted using critical height values obtained from sample geometry studies as the significant geometrical dimension of the container; (3) The ignition behavior of uranium powder can be adequately described by converting isothermal expressions to a rising temperature basis according to the treatment of Murray, Buddery, and Taylor.

2. Burning Propagation Studies

(L. Leibowitz, J. G. Schnizlein, and L. W. Mishler)

The burning propagation rate, i.e., the rate of advance of a combustion zone along a foil or wire, has been a useful, reproducible quantity for studying the nature of burning metal as well as for judging the influence of various factors on the combustion process.

The metal is ignited at one end by an electrically heated platinum wire and a motion picture record is made of the process. Linear propagation rates are readily obtained from these motion pictures. The effect of sample size and geometry, gas composition, pressure, and ambient temperature are being examined for zirconium, uranium, and plutonium.

a. Burning Propagation at Elevated Ambient Temperatures

Most of the work carried out on burning propagation has been with the surrounding atmosphere at room temperature, the only source of heat being the metal combustion itself. Since in many practical cases there may be considerable heating of the atmosphere, it seemed of interest to explore, on a laboratory scale, the effect of this additional variable.

An apparatus suitable for these measurements has been constructed (see ANL-6231, page 151). It consists simply of a glass tube surrounded by a furnace containing openings for photographing the event. The metal samples are brought to the desired temperature in an argon atmosphere and the propagation carried out in air. With zirconium, linear air flow velocities between 0.25 and 11.0 cm/sec were employed, and for uranium velocities of 1.5 and 3.5 cm/sec were used. No notable effect of this variable was observed. All the data currently available are presented in Table 50. The listed values of propagation rate are averages for several air velocities flowing both with and against the propagation. Agreement with previous values at room temperature is generally good. The greatest effect found was for the 0.13 x 0.6-mm zirconium foil with air at 400 C; the rate increased about 40 percent.

Table 50

BURNING PROPAGATION STUDIES AT ELEVATED AMBIENT TEMPERATURES

(Foils burned in air)

Foil Material	Thickness x Width (mm)	Ambient Temperature (C)	Burning Zone Length (cm)	Burning Propagation Rate (cm/sec)
Uranium	0.13 x 3.0	24[a]	-	0.56 ± 0.02[b]
	0.13 x 3.0	24[a]	-	0.52 ± 0.05
	0.13 x 3.0	150	-	0.52 ± 0.03
	0.13 x 3.0	300	-	0.58 ± 0.06
	0.01 x 1.0	24[a]	-	3.4[b]
	0.01 x 1.0	24[a]	-	2.5 ± 0.2
	0.01 x 1.0	300	-	3.6 ± 0.4
Zirconium	0.13 x 0.6	24[a]	1.3 ± 0.1[b]	0.46 ± 0.03[b]
	0.13 x 0.6	24[a]	1.7 ± 0.2	0.59 ± 0.06
	0.13 x 0.6	400	2.7 ± 0.3	0.83 ± 0.10
	0.02 x 5.0	24[a]	3.7[b]	1.5[b]
	0.02 x 5.0	24[a]	3.6 ± 0.2	1.5 ± 0.2
	0.02 x 5.0	150	4.1 ± 0.3	1.5 ± 0.2
	0.02 x 5.0	400	5.6 ± 0.4	2.0 ± 0.3

[a]average room temperature.

[b]previous base-line value.

In addition to these experiments, several attempts were made to burn 60-mil (1.58 mm) diameter uranium wire and 0.13 x 1.0-mm zirconium foil strips at an ambient temperature of 400 C. Neither of these two samples would burn in air with the surroundings at room temperature, although 30-mil uranium wire and 0.13 x 0.6-mm zirconium foil will burn in room temperature air. Heating the surroundings to 400 C, however, would not produce a self-sustaining combustion.

Higher temperatures cannot be explored with uranium since the foil will ignite spontaneously as soon as air is introduced. It is possible to use higher temperatures with zirconium, however, and such experiments are planned.

b. The Effect of Halogenated Hydrocarbons on Burning Propagation

It has been observed that the presence in air of various halogenated hydrocarbons will significantly lower the burning propagation rate of uranium, zirconium, and plutonium foil strips (see ANL-6145, pages 137 and 142 and ANL-6231, page 152). These compounds may operate simply by removing heat from the burning metal by a reaction such as

$$RX \longrightarrow R^{\cdot} + X \quad , \tag{3}$$

or perhaps with (1) followed by

$$R^{\cdot} + O_2 \longrightarrow RO_2^{\cdot} \quad . \tag{4}$$

Reaction (4) might in effect decrease the net diffusion of oxygen to the burning metal.

Several experiments have been carried out using an electrically heated 3-mil platinum foil 3.0 mm wide. Provision was made to measure foil temperature, current, and voltage. The voltage was measured between two points on the foil 3.3 cm apart. The current and voltage measurements were used to compute power. The entire platinum assembly was enclosed in a glass tube through which the desired gas mixture was passed. With a flow rate of 1000 cc/min (2 cm/sec) and constant power input, foil temperatures were measured with and without addition of 5 percent by volume of either trifluorobromomethane or difluorodichloromethane. The values obtained using both air and argon are listed in Table 51.

Table 51

INFLUENCE OF HALOGENATED HYDROCARBONS ON THE TEMPERATURE OF AN ELECTRICALLY HEATED PLATINUM FOIL

	Pt Temperature (C)			Pt Temperature (C)		
Power (watts)	Pure Argon	Argon with 5% Halocarbon	Difference (C)	Air	Air with 5% Halocarbon	Difference (C)
with CF_3Br						
3.9	612	571	41	529	508	21
7.7	834	796	38	758	742	16
12.7	1006	917	89	944	930	14
with CF_2Cl_2						
5.1	685	648	37	606	586	20
7.4	815	773	42	737	719	18
12.3	1002	886	116	938	926	12

The large cooling effect of the hydrocarbons in argon at the highest temperatures may be due to a deposit of some pyrolysis product (possible carbon) which was visible only at those temperatures. The addition of 0.1 percent oxygen to the argon was sufficient to reduce this effect to that seen at the other temperatures. At a 12.0-watt power level, the foil temperature was 1000 C in argon and 956 C in argon + 5 percent difluorodibromomethane + 0.1 percent oxygen. Steady temperatures were achieved within a few minutes with the oxygen, whereas over thirty minutes were required in the absence of oxygen.

Insofar as these measurements reflect the situation with burning metal, they indicate that the hydrocarbons do not operate simply by removing heat. The observed cooling effect in air is much too small. If simple cooling were the predominant factor, the effect would be the same in argon and air. The difference found may be attributed to heat evolved in reaction (4). The tendency of the hydrocarbons to supress burning may be by oxygen removal (reaction 4) in the zone near the hot surface.

Work in this area will continue with some attention being given to the effect of these halogenated hydrocarbons on the ignition behavior of the metals being studied.

B. Metal-Water Reactions
(L. Baker)

1. Laboratory Studies: Condenser Method
(L. Baker, R. Warchal)

The condenser discharge experiment is an attempt to obtain fundamental rate data under experimental conditions similar to those encountered during a serious accident in a nuclear reactor. Either a nuclear runaway or a sudden loss of coolant during operation of a water-cooled reactor could result in contact between very hot fuel and cladding metals with water or steam and might involve fine particles. The condenser discharge experiment simulates the limiting case of a nuclear incident in that the heating time is very short and very fine metal particles are produced.

In the condenser discharge experiment, metal wires are rapidly melted and dispersed in a water-filled cell by a surge current from a bank of condensers. The energy input to the wire is used to calculate the initial reaction temperature. The transient pressure measures reaction rate, the amount of hydrogen generated gives the extent of reaction, and the particle size of the residue indicates the surface area exposed to reaction.

Analysis of the results is based on one of the usual laws of metal oxidation (parabolic rate law) and on the laws of gaseous diffusion and heat transfer. In this way an attempt is made to interpret experimental work as it proceeds.

a. Zirconium Runs at High Pressure

The series of runs with 60-mil zirconium wires in the new high-pressure reaction cell is continuing. First results were reported in the previous quarterly. Since then it was discovered that the thermocouple used to measure water temperature and hence saturated vapor pressure was giving incorrect indications. It was possible, however, to correct the data. The corrected data along with the recent results are given in Table 52 and plotted in Figure 56.

Table 52

ZIRCONIUM-WATER REACTION DATA FROM HIGH-PRESSURE CONDENSER DISCHARGE APPARATUS

(Zirconium used: 60-mil wires)

Run	Calc Metal Temp (C) and Physical State	Saturated Vapor Pressure (psia) and Temp (C) of Ambient Water	Percent Reaction	Appearance of Residue
194	1800, Solid	10 (90)	8.6	Distorted Wire
191	1800, Solid	32 (124)	7.8	Distorted Wire
195	1840, Solid	215 (198)	9.0	Distorted Wire
190	1840, 10% Liq	225 (200)	8.5	Distorted Wire
216	1800, Solid	1500 (313)	11.4	Distorted Wire
189	1840, 20% Liq	205 (196)	14.5	Some Particles
213	1840, 60% Liq	900 (278)	25.9	Some Fines
196	1840, 80% Liq	16 (103)	31.5	Some Fines
206	1840, 80% Liq	26[a] (117)	37.6	Some Fines
203	1840, 80% Liq	50 (138)	55.2	Some Fines
188	1840, 80% Liq	155 (183)	30.7	Some Fines
200	1840, 100% Liq	19 (108)	51.7	Some Fines
217	2200, Liquid	19 (108)	90.3	Powder
218	2300, Liquid	79 (155)	52.0	Fines
219	2600, Liquid	16 (103)	82.9	Powder
220	2600, Liquid	150 (181)	73.8	Fines

[a]Argon gas added (20 psi)

The data obtained with room temperature water are included in Figure 56 and show the striking effect of water temperature or vapor pressure on the results. Two regimes are apparent: reaction with water at room temperature increases gradually, reaching 20 percent at an initial metal temperature of 2600 C; reaction with water heated to 90 to 310 C (vapor pressure 10 to 1500 psi) reaches over 50 percent for fully melted metal at the melting point.

FIGURE 56

RESULTS OF CONDENSER DISCHARGE RUNS WITH 60-MIL ZIRCONIUM WIRES

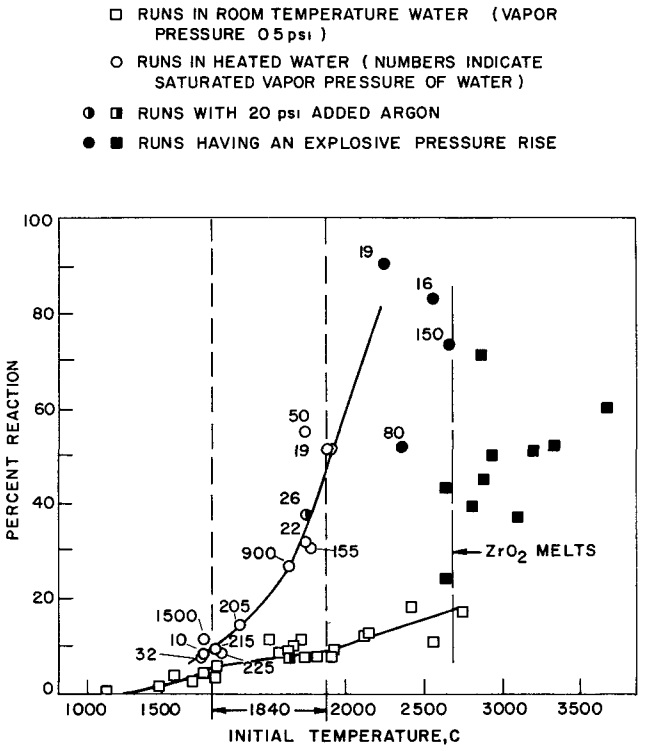

Pressure traces from zirconium runs in the high-pressure regime indicated that the transition from slow pressure rise rates to explosive rates occurred in the region between the melting point of zirconium, 1840 C, and 2200 C. Runs with fully melted metal at the melting point required up to 0.1 second to reach a final value. Reactions with fully liquefied metal at 2200 C were essentially completed in several milliseconds. Residue from runs giving 50 percent reaction or more had significantly finer particles.

b. Theory of the Reaction Process

The unusual effects of pressure on the extent of the zirconium-water reaction has emphasized the need to consider a gaseous diffusion step in the process. A mathematical analysis based solely on

the parabolic rate law was presented in a previous quarterly (see ANL-6029, page 126). Only limited agreement with the data was obtained. The method was extended to include a step involving the diffusion of water vapor through the hydrogen barrier surrounding the metal particles.

The previous method required an empirical heat transfer coefficient. The present treatment utilizes the fact that the Nusselt number for diffusion or heat transfer has a minimum value of 2 for spherical particles. It is, therefore, possible to calculate directly minimum diffusion and heat loss rates without any further numerical assumptions. The theoretical minimum Nusselt number is approached accurately for small spherical particles unless extreme turbulence or very rapid particle motion occurs.

FIGURE 57
DIAGRAM OF HOT METAL SPHERE REACTING WITH LIQUID WATER

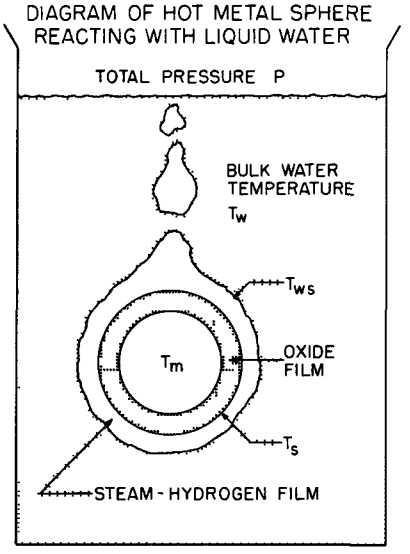

The rate of diffusion of water vapor through a spherical hydrogen film (see Figure 57) can be formulated as a mass transfer coefficient (h_d) times the area of a sphere ($4\pi r_0^2$) times the concentration difference ($\Delta P_w/RT_f$) as follows (symbols are defined in Table 53):

$$\text{moles } H_2O/\text{sec} = h_d\,(4\pi r_0^2)\,(\Delta P_w/RT_f) \quad . \qquad (5)$$

The mass transfer coefficient can be expressed in the Nusselt form $Nu = h_d(2r_0/D)$ and the mean film temperature can be arbitrarily taken as an average between metal surface temperature and the bulk water temperature $T_f = (T_s + T_w)/2$. Values of the diffusion coefficient, D, for the hydrogen-water system were calculated by Furman [48] His results can be represented approximately as follows:

$$D = (D_0/P)(T_f)^{1.68} \quad , \qquad (6)$$

where $D_0 = 6\ 53 \times 10^{-5}$ (sq cm)(atm)/(sec)($K^{1\ 68}$). The molar diffusion rate (5) can readily be expressed as the rate at which the oxide front advances into unreacted metal when reaction is controlled by gaseous diffusion

$$\frac{\text{moles } H_2O}{\text{sec}} = 4\pi r^2 \left(\frac{dr}{dt}\right)_d \frac{\rho_m{}^n}{M_m} \quad . \qquad (7)$$

The diffusion-controlled reaction rate is then obtained by combining equations 5 through 7 as follows:

$$-\left(\frac{dr}{dt}\right)_{\text{diffusion}} = \frac{NuD_0M_m}{2\rho_m nR}\,\frac{r_0}{r^2}\left(\frac{T_s + T_w}{2}\right)^{0.68}\frac{\Delta P_w}{P} \qquad (8)$$

---

[48] Furman, S. C., Metal-Water Reactions: V, GEAP-3208 (July 1959)

If the reaction is controlled by solid state processes, the parabolic rate law is used to represent the rate as follows:

$$-\left(\frac{dr}{dt}\right)_{kinetic} = \frac{A}{2\rho_m^2 (r_0 - r)} \exp\left(-\frac{\Delta E}{RT_s}\right) \quad . \tag{9}$$

Table 53

DEFINITION OF SYMBOLS USED IN EQUATIONS (5) THROUGH (9)

A	is pre-exponential factor in parabolic rate law, $g^2/(cm^4)(sec)$
C_p	is specific heat, cal/(mole)(K) or cal/(g)(K)
D	is diffusion coefficient, sq cm/sec
ΔE	is activation energy, kcal/mole
ϵ	is total emissivity of oxide surface
F	is fraction of original metal in liquid state
h	is heat transfer coefficient, cal/(sec)(sq cm)(K)
h_d	is mass transfer coefficient, cm/sec
k	is thermal conductivity, cal/(sec)(cm)(K)
L	is heat of fusion, cal/mole
M	is molecular weight, g/mole
n	is moles of hydrogen generated per atom of metal reacted
Nu	is Nusselt number
ΔP_w	is partial pressure of water vapor driving diffusion, atm
P	is total pressure, atm
r	is radius of unreacted metal, liquid or solid, cm
r_0	is original radius of unreacted metal, cm
R	is gas constant, (cc)(atm)/(mole)(K)
ρ	is density, g/cc
σ	is Stefan Boltzmann constant, cal/(sec)(sq cm)(K^4)
t	is time, sec
T	is temperature, K

Table 53 (cont'd.)

Subscripts:

f refers to the diffusion film

m refers to the metal

ox refers to the oxide

s refers to the oxide surface

w refers to the bulk of the water

The reaction must be controlled by the slowest step in the overall process. When the two expressions 8 and 9 have similar values, the proper combining law depends upon the effect of pressure on the parabolic rate law. It was tentatively assumed that pressure has no effect on the kinetic rate law (9). The equation, 8 or 9, used in computation is then the one giving the lowest rate.

Both the diffusion and the kinetic rates depend on temperature. A detailed heat balance is, therefore, required to complete consideration of the problem. Heated metal spheres cool by two processes: convection (or conduction) and radiation. Convection heat loss can also be formulated in terms of a Nusselt number $Nu = h\ 2\ r_0/k_f$. The thermal conductivity refers to a hydrogen-water vapor mixture at the mean film temperature. There are no experimental data over the temperature range of interest. Only approximate methods of direct calculation are available in the literature. A very useful procedure exists, however, to relate rates of heat transfer and diffusion when they occur simultaneously. The reaction is called the Lewis equation[49] and has the following form:

$$h_d = \frac{h}{\rho_f C_{pf}} \text{ if } D = \frac{k_f}{\rho_f C_{pf}} \quad . \tag{10}$$

The diffusion coefficient and the thermal diffusivity of many gases and gas mixtures are numerically equal. An estimate of the value of thermal diffusivity for an equimolar hydrogen-water vapor mixture at 1600 K was made by methods given by Hirschfelder.[50] The calculated value is compared to the value of diffusion coefficient given by Equation 6 as follows:

$$D \text{ (Equation 6)} = \frac{15.8}{P} \text{ sq cm/sec; } \frac{k_f}{\rho_f C_{pf}} \text{ (calc)} = \frac{12.1}{P} \text{ sq cm/sec} \quad ,$$

---

[49] Eckert, E.R.G., Introduction to the Transfer of Heat and Mass, McGraw-Hill Book Co. (1950), page 251 ff.

[50] Hirschfelder, J. O., Curtiss, C. F., and Bird, R. B., Molecular Theory of Gases and Liquids, John Wiley and Sons, Inc., New York (1954).

and was considered sufficiently close to justify use of the Lewis relation to calculate convective heat loss rates. The Lewis relation has the advantage that it applies for turbulent exchange whether numerical equality obtains or not.

The density of vapor to be used in Equation 10 was obtained from the gas laws, and an average specific heat of hydrogen-water vapor mixtures was approximated as follows:

$$C_{pf} = C_{pf0} \left(\frac{T_s + T_w}{2} \right)^{0.20} , \tag{11}$$

where $C_{pf0} = 2.22$ cal/(mole)($K^{1.2}$). The rate of heat loss from particles was expressed by Newton's Law of cooling:

$$H_{conv} = h\,(4\pi r_0^2)(T_s - T_w) . \tag{12}$$

Substituting for h yields the following:

$$H_{conv} = Nu \frac{2\pi D_0 C_{pf0}}{R} r_0 \left(\frac{T_s + T_w}{2} \right)^{0.88} (T_s - T_w) . \tag{13}$$

The radiation heat loss is expressed as follows:

$$H_{rad} = \epsilon\sigma\,(4\pi r_0^2)\,T_s^4 . \tag{14}$$

Heat generated by reaction must also be included in the heat balance. Heat generation is proportional to reaction rate and can be expressed as follows:

$$H_{reac} = Q\rho_m\,(4\pi r^2) \left(-\frac{dr}{dt} \right) . \tag{15}$$

Two temperatures were defined in order to include the insulating effect of the oxide film. The surface temperature, T_s, was taken to represent the temperature at the outer surface of oxide. The inner surface, adjacent to unreacted metal, was assumed to have a temperature T_m. The metal temperature T_m was assumed to be constant throughout the unreacted metal because of the high thermal conductivity of metal and because small particles are considered. The metal temperature is influenced by heat generation and by heat losses as follows:

$$Cp_m \rho_m \left(\frac{4}{3} \pi r_0^3 \right) \frac{dT_m}{dt} = H_{reac} - H_{conv} - H_{rad} . \tag{16}$$

The heat balance contains no provision for external heating. The assumption is made that heating by condenser discharge occurs instantaneously. Analysis of in-pile data or studies of reactor accidents would require a term to express fission or decay heating as a function of time.

Equation 16 does not apply when the metal temperature passes through the melting point of the metal. At that point heat is absorbed or evolved without a change in metal temperature. Allowance for this effect was made by using the following expression at the melting point:

$$L\rho_m \left(\frac{4}{3}\pi r_0^3\right) \frac{dF}{dt} = H_{reac} - H_{conv} - H_{rad} \quad . \tag{17}$$

The temperature drop across the oxide film ($T_m - T_s$) is estimated by the equation governing steady-state conduction through a spherical shell:

$$4\pi k_{ox} \left(\frac{r_0 r}{r_0 - r}\right) (T_m - T_s) = H_{conv} + H_{rad} \quad . \tag{18}$$

Equations 8, 9, 13, 14, 15, 16, 17 and 18 were programmed on the Pace Analog Computer by Mr. L. Just of the Applied Mathematics Division.

c. Preliminary Results of Computer Study

The Nusselt number was fixed at a value of 2 and the emissivity at a value of 1 for the preliminary work. It was initially assumed that the term $\Delta P_w/P$ in the diffusion rate, equation 8, was unity when diffusion was controlling. This implied that the water surface temperature (indicated in Figure 57 as T_{ws}) remained at the boiling point determined by the external pressure P. The water vapor pressure driving diffusion, ΔP_w, was, therefore, equal to the total pressure P. The result would be that diffusion rates are independent of pressure. This conclusion may not be consistent with the experimental discovery of a profound effect of the water vapor pressure on the reaction.

The possibility of a sensitivity of the parabolic rate law to pressure was investigated on the computer. Increased pressure gave increased reaction indefinitely; no tendency could be found toward a limiting reaction at increased pressure as required by the experimental results. Inert gas pressure should yield the same effect experimentally as increased steam pressure if the pressure were affecting processes at the solid surfaces or within the oxide film. Inert gas pressure was found experimentally, however, to have little or no effect.

It appeared that the effective water surface temperature does not reach the boiling point. The factor $\Delta P_w/P$ might, therefore, become considerably less than unity. Hydrogen generated by reaction in runs with room-temperature water increases the total pressure and, therefore, the boiling point so that diffusion rates are suppressed. Hydrogen generated by runs in heated water and accumulated in the reaction cell does

not greatly change the boiling point, so that diffusion rates remain near a maximum value. Further increases in water temperature would cause no further increase in diffusion rate.

A typical set of computed results is shown in Figure 58, in which the extent of reaction, the metal temperature, and the reaction rates are plotted as a function of time.

FIGURE 58
COMPUTED ZIRCONIUM-WATER REACTION
(INITIAL METAL TEMPERATURE 2125 K, SOLID)
(SPHERE DIAMETER 2 1 mm)

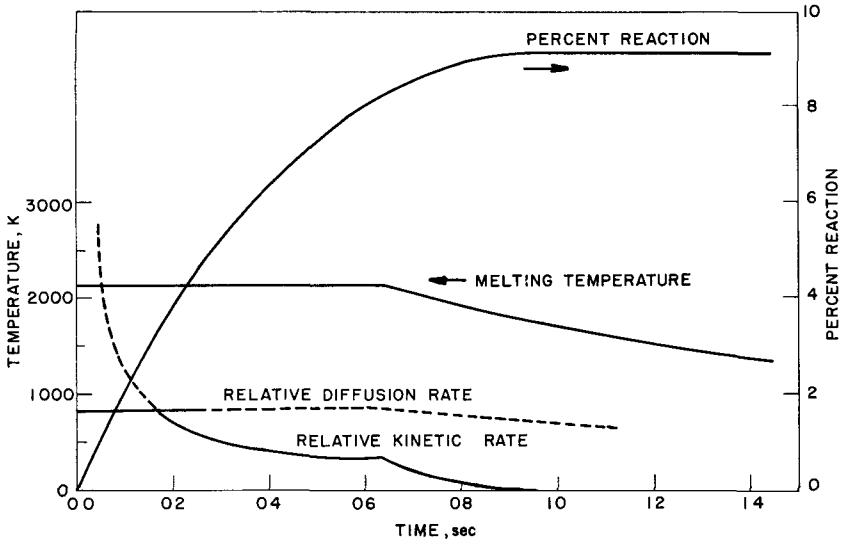

The factor $\Delta P_w/P$ had the value of 1; the run therefore corresponds to one in the high-pressure region. The only unknown constants were the rate constant A and the activation energy ΔE. The activation energy was taken to be 55 kcal/mole and the constant A adjusted to produce a fit to the experimental data under the same conditions. The results show that the metal, initially heated to the melting point, did not exceed the melting temperature. The tendency to release heat was taken up by the latent heat of fusion, Equation 17.

Two computed runs are shown in Figure 59. The runs were at an initial temperature of 2125 K, the melting point with 50 percent of the metal melted. The run with a particle diameter of 2.1 mm does not become fully melted when 10.7 percent reaction occurred. An identical run with an 1.05-mm particle diameter does become fully melted and self-heats to a temperature of 3100 K. The buildup of oxide decreases the kinetic rate resulting in a reversal of the self-heating tendency followed by rapid quenching; 47.6 percent reaction occurred. The maximum temperature, 3100 K, is above the melting point of zirconia (2900 K), so that it is unlikely that the kinetic rate would effectively stop the reaction. It is interesting, however, that preliminary calculations predict this kind of an "ignition" in the melting point region corresponding to the very steep region of Figure 56.

FIGURE 59
COMPUTED ZIRCONIUM RUNS
(INITIAL METAL TEMPERATURE 2125 K, 50% MELTED)
(INITIAL SPHERE DIAMETER AS INDICATED)

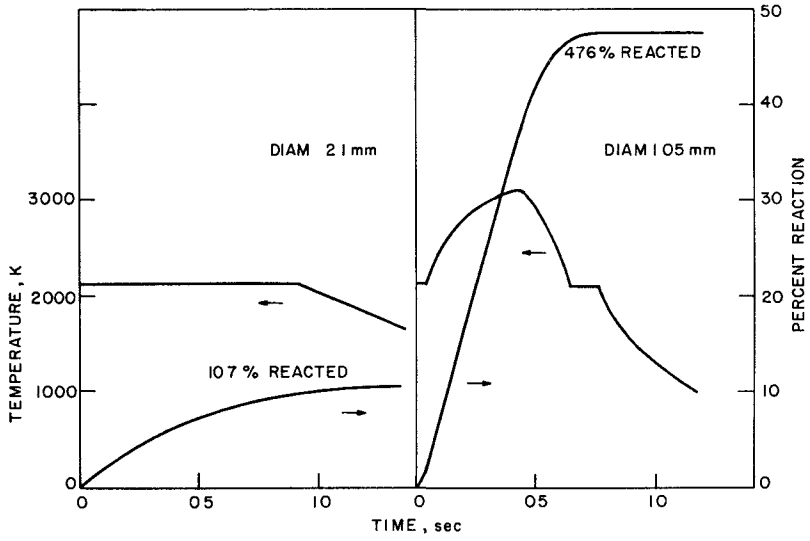

The rates of pressure rise indicated in Figures 58 and 59 are somewhat slower than observed rates. This results from using the minimum Nusselt number of 2. An increased Nusselt number will result in a faster reaction. It is expected, however, that the final extent of reaction will not be greatly different.

2. Laboratory Studies: Pressure-pulse Method
(D. Mason, P. Martin)

The pressure-pulse method was developed to study the reaction of molten metals with water vapor under conditions as nearly isothermal as possible. The results obtained from this method are to be used as an aid in analyzing the data obtained from other metal-water studies. The pressure-pulse method should give the best determination of the form of the rate law.

The basic operation of the equipment has remained the same since the original construction. However, many changes have been made in details of construction and the pressure range has been extended to about one atmosphere. The apparatus and procedure of operation described apply specifically to aluminum. Minor changes made it applicable to other metals.

The aluminum is heated under about three millimeters pressure of argon. The argon is present to reduce the vaporization of aluminum. Heating is accomplished by an induction heater. When the desired temperature is attained, electronically controlled valves are operated in sequence to permit contact water vapor of known pressure with the molten

metal for a specified period of time. The apparatus and procedure of operation were described in a previous report (see ANL-6068, page 153). They are presented here with the modifications which have been made.

A series of runs with aluminum has been completed. Liquid aluminum samples at 1000 C have been reacted with water vapor at 500 millimeters pressure.

a. Apparatus and Procedure

A diagram of the apparatus is shown in Figure 60. The metal sample (aluminum), contained in a crucible (alumina), is heated in a high-vacuum glass cell, C, to a temperature somewhat above the melting point (700 to 750 C for aluminum). At this time, argon is introduced from bulb F to suppress vaporization encountered at higher temperatures. The sample is now heated to at least 1200 C. This has the effect of causing the aluminum to wet the alumina crucible and alumina thermocouple tube, producing a flat uniform liquid surface. The sample is then cooled to just above the melting point and the system is evacuated to remove any evolved gases.

FIGURE 60
DIAGRAM OF PRESENT PRESSURE-PULSE SYSTEM

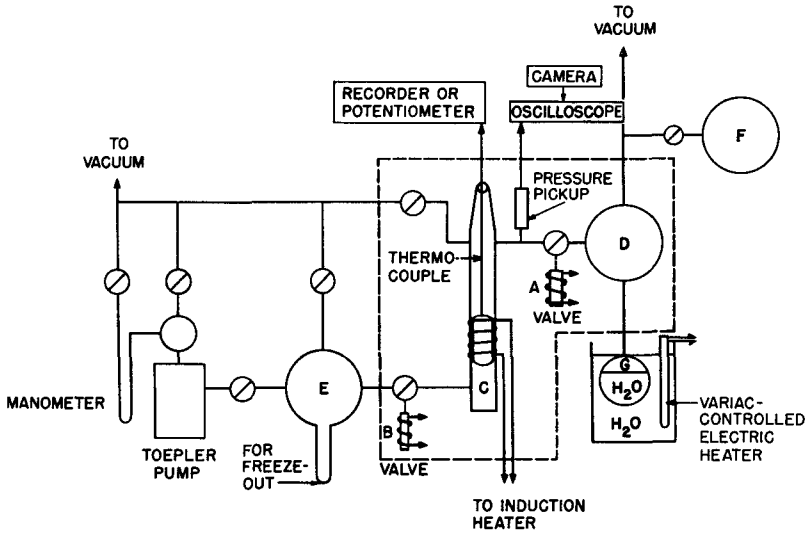

Argon is again admitted and the sample is heated to the desired temperature by the induction heater. Solenoid valve A is then opened and closed rapidly to allow water vapor from the reservoir, D, to contact the sample in C. Following a preset delay, valve B is opened and closed rapidly to expand the water vapor, argon, and product hydrogen from the cell into the large evacuated bulb, E. Water vapor is condensed in the cold trap and the hydrogen and argon transferred from bulb E to a manifold of calibrated volume by the Toepler pump. The quantity of gas is thus

determined by a pressure measurement using a mercury manometer. Mass spectrometric analysis of the sample is used to determine the quantity of hydrogen formed and to detect air leaks.

The entire apparatus within the dotted line is thermostated at about 105 C to avoid condensation of the steam. The liquid water vessel, G, is heated by a boiling water thermostat and is consequently maintained at 99.7 ± 0.2 C.

b. Instrumentation

The operations of valves A and B are controlled automatically by an electronic timer. Condensers are discharged through the solenoids of the valves by the sequenced firing of thyratrons. The time interval between valve firings is variable in steps from 0.1 second to 20 seconds and can be extended indefinitely by manual operation.

A rapid-response pressure pickup located in the reaction cell records the pressure pulse on an oscilloscope camera. The oscillogram is a record of both contact time and the pressure.

Temperature measurements are made with a platinum-(platinum-10 percent rhodium) thermocouple located in the sample and protected by an alumina protection tube. The thermocouple emf is measured by a potentiometer or potentiometer-type recorder. To check the accuracy of temperature measurement, cooling curves were run with various metals in the crucible in cell C.

Pressure-pulse oscillograms show that product gas recovery is at least 95 percent. This is considerably better than would be estimated from a consideration of volume ratio alone. It is believed to be caused by the sweeping out of other gases by the water vapor, which is rapidly condensing on the cold trap while valve B is open.

c. Aluminum Runs

Table 54 and Figure 61 show the results of the aluminum runs obtained to date. Since the data are incomplete, it is not possible to draw definite conclusions about the rate law at this time. More data will be taken at 1000 C (including extension to 100 seconds) to enable better analysis. It is also planned to make runs at 800 C and 1200 C to determine the effect of temperature.

It is appropriate to mention, briefly, possible sources of error in the data. There are at least two main reasons for inconsistent results. If any vaporized aluminum condenses on other parts of the cell, high yields of hydrogen result. Vaporization is largely suppressed by the addition of argon. It may be impossible to prevent vaporization completely,

with the result that aluminum tends to deposit on the inside walls of the quartz cell; this requires the discard of the data. The effect of an aluminum deposit on the crucible walls is less definite and hard to evaluate.

Table 54

RESULTS OF THE REACTION OF ALUMINUM AT 1000 C WITH STEAM AT 500 mm BY THE PRESSURE-PULSE METHOD

Run	Reaction Time (sec)	Volume H_2 Evolved (cc STP)	Area (sq cm)	Volume H_2 Per Unit Area (cc STP/sq cm)
17	0.11	0.095	3.0	0.032
6	0.11	0.098	2.8	0.035
10	0.11	0.17	3.1	0.056
11	0.11	0.18	3.0	0.061
5	1.04	0.28	3.0	0.091
4	1.04	0.27	2.9	0.092
2	1.04	0.29	3.0	0.098
1	1.04	0.34	3.2	0.105
12	9.2	0.48	3.0	0.16
16	9.2	0.52	3.1	0.17
24	9.2	0.61	3.1	0.20
22	9.2	0.68	3.2	0.21
13	9.2	0.78	3.0	0.26

An oxide film on the aluminum before the run starts would probably cause low results. If this is the case, the effect would be the greatest for short runs.

FIGURE 61

REACTION BETWEEN ALUMINUM AT 1000C AND STEAM, 500 mm Hg PRESSURE

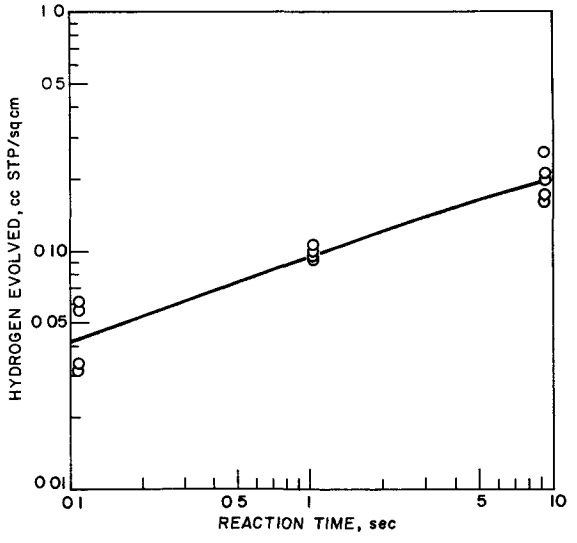

3. Engineering Studies: In-pile Testing in the TREAT Reactor*

(R. C. Liimatainen, R. O. Ivins, M. Deerwester, F. Testa)

In a runaway of a water-cooled nuclear reactor it is possible that the core materials may become molten. If the hot metal then reacts chemically with the water, the exothermic heat of reaction can be a significant part of the total energy release. As an example, a reactor burst having a specific fission energy input equivalent to 200 calories per gram of uranium metal can give rise to a 20 percent metal-water reaction. With a heat of reaction of 500 calories per gram of uranium, this corresponds to a chemical energy release of 100 calories per gram of uranium. Thus, in this case, the chemical energy is equivalent to one-half the fission energy.

The in-pile work is being conducted to approximate such reactor incidents in a realistic manner. The method of investigation is to subject reactor core materials, in a water environment, to a short intense burst of neutrons in TREAT.[51,52] The experiment is contained within the stainless steel autoclave shown in Figure 62. The autoclave, in turn, is located at the center of an eight-foot long, stainless steel, dummy, TREAT fuel can with graphite reflector blocks at the bottom and top (see Figure 63). Connections to the leads from the pressure pickup and thermocouples are made through an Amphenol fitting. The signals are amplified and recorded on an oscillograph in the reactor control building.

During this quarter, transients were made on enriched uranium wires for later comparison and correlation with the condenser discharge data. Figure 64 shows a record of one of the bursts which resulted in melting and fragmentation of the uranium wire; as indicated by the time scale and the integrated power trace, the transient heating took place in about 0.3 second. The somewhat jagged temperature trace in Figure 64 is caused by momentary loss of contact between the thermocouple and the specimen which is breaking apart. A summary of the primary data obtained from the runs with uranium wires is shown in Table 55. The extent of reaction was based on the reaction $U + 2H_2O \longrightarrow UO_2 + 2H_2$ and the hydrogen evolution as measured by a mass spectrometer.

---

*The cooperation of the TREAT operations group of the Idaho Division is gratefully acknowledged.

[51] Freund, G. A., Elias, P., MacFarlane, D. R., Gier, J. D., Boland, J. F., Design Summary Report on the Transient Reactor Test Facility, TREAT, ANL-6034 (1960).

[52] Kirn, F., Boland, J., Lawroski, H., Cook, R., Reactor Physics Measurements in TREAT, ANL-6173 (1960).

FIGURE 62

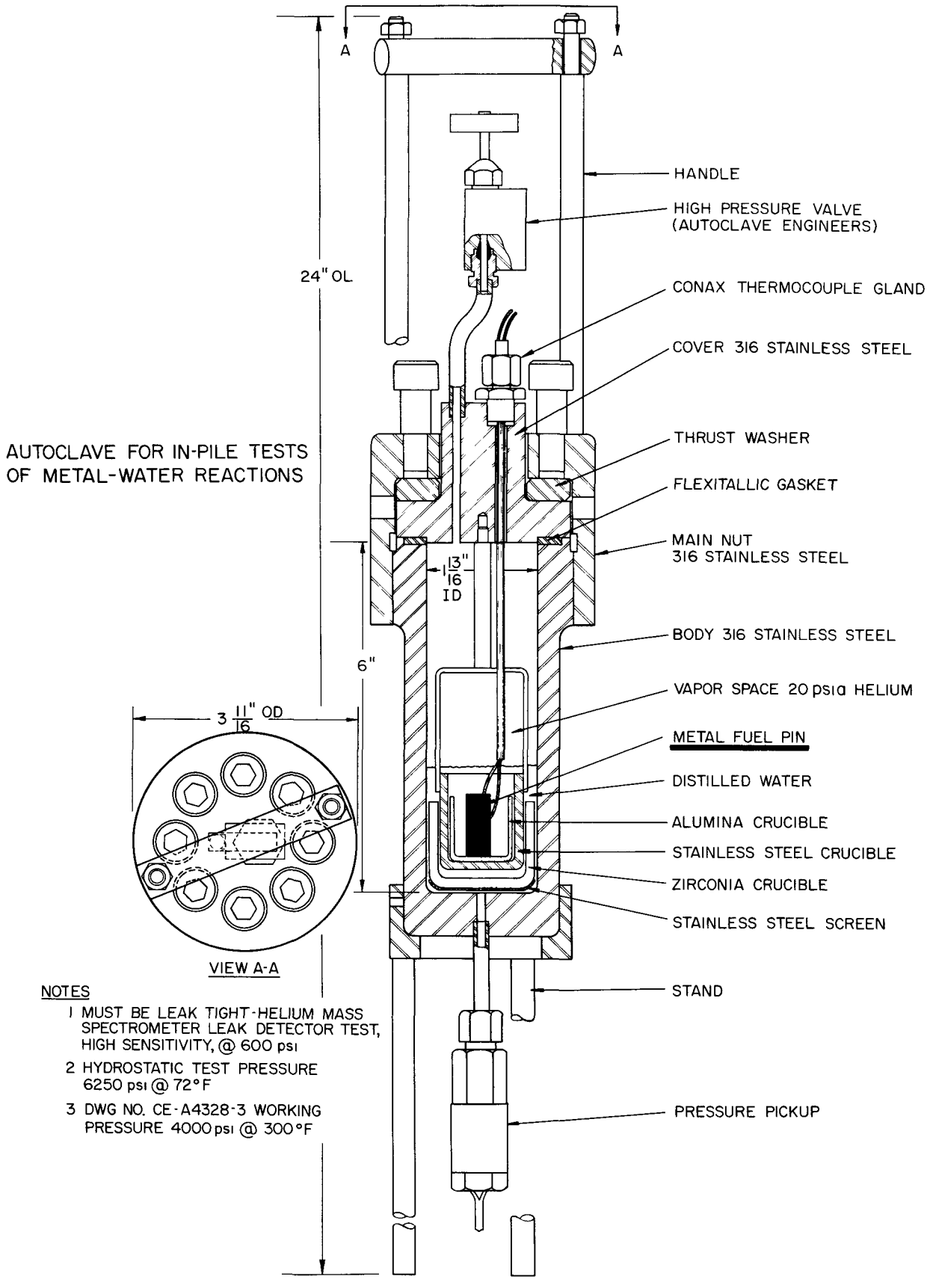
AUTOCLAVE FOR IN-PILE TESTS
OF METAL-WATER REACTIONS
A
A
24" OL
HANDLE
HIGH PRESSURE VALVE
(AUTOCLAVE ENGINEERS)
CONAX THERMOCOUPLE GLAND
COVER 316 STAINLESS STEEL
THRUST WASHER
FLEXITALLIC GASKET
MAIN NUT
316 STAINLESS STEEL
1 13/16" ID
BODY 316 STAINLESS STEEL
6"
VAPOR SPACE 20 psia HELIUM
3 11/16" OD
METAL FUEL PIN
DISTILLED WATER
ALUMINA CRUCIBLE
STAINLESS STEEL CRUCIBLE
ZIRCONIA CRUCIBLE
STAINLESS STEEL SCREEN
VIEW A-A
STAND
PRESSURE PICKUP
NOTES
1 MUST BE LEAK TIGHT-HELIUM MASS SPECTROMETER LEAK DETECTOR TEST, HIGH SENSITIVITY, @ 600 psi
2 HYDROSTATIC TEST PRESSURE 6250 psi @ 72°F
3 DWG NO. CE-A4328-3 WORKING PRESSURE 4000 psi @ 300°F

FIGURE 63

METAL-WATER REACTIONS TREAT TEST ASSEMBLY

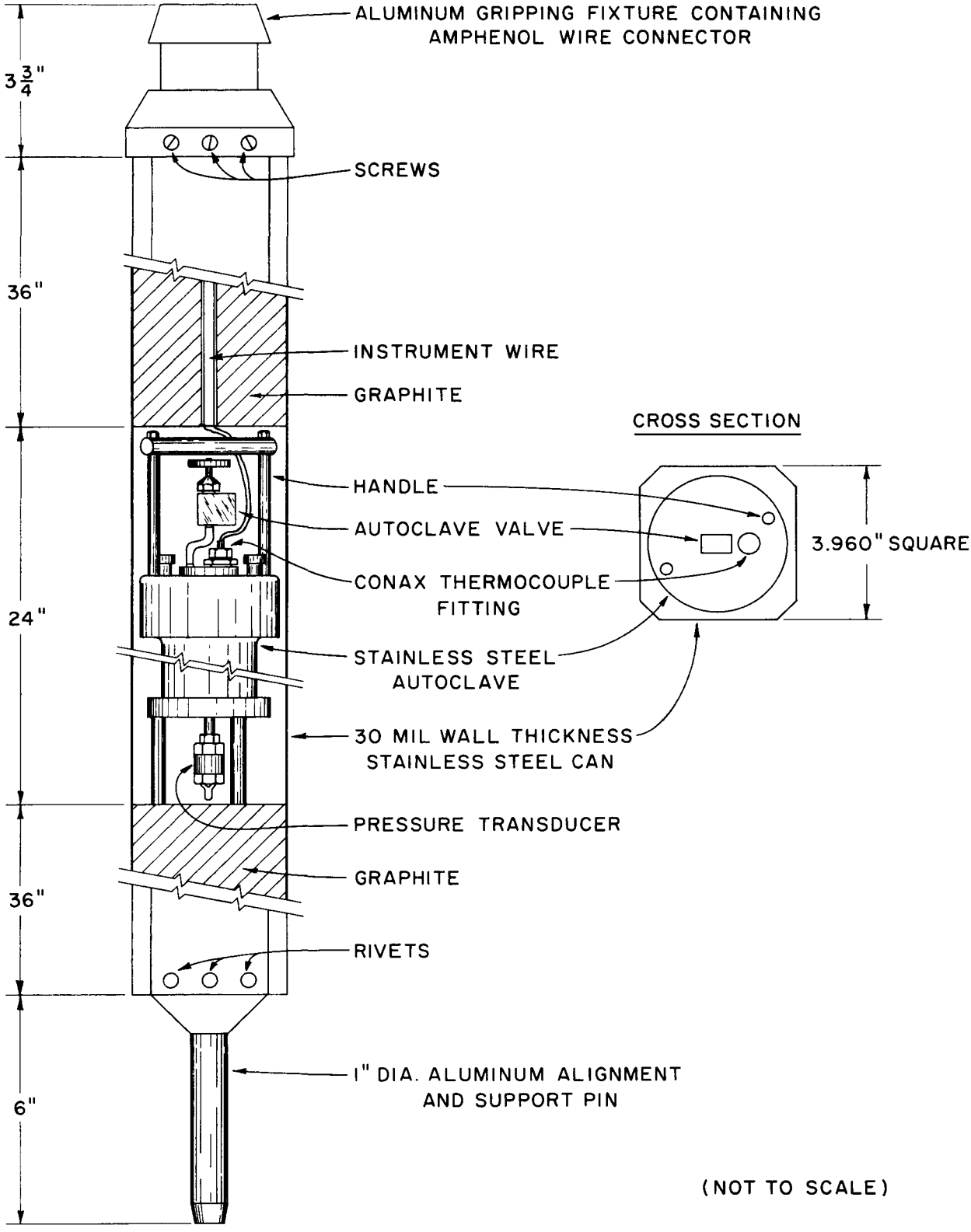

FIGURE 64

OSCILLOGRAPH RECORD
FROM TRANSIENT CEN-46

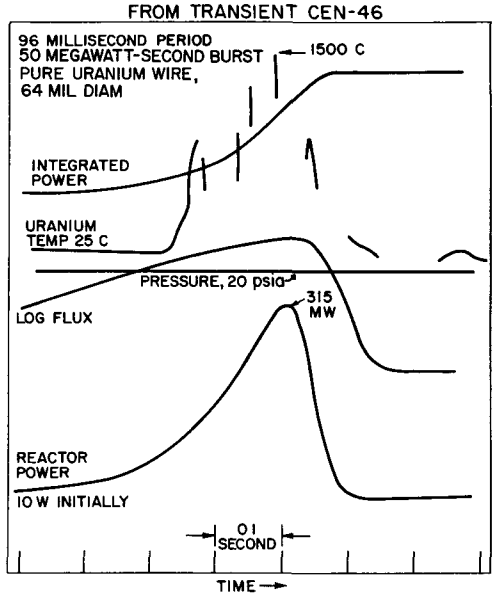

Table 55

RESULTS FROM NINTH SERIES OF TREAT, METAL-WATER EXPERIMENTS

CEN Transient No	43	44	42	45	41	46
Uranium Wire[a]						
diameter of wire, mils	64	64	64	64	64	34
number of wires	1	1	1	1	1	3
Reactor Characteristics						
burst energy, Mw-sec	32	43	43	44	54	50
peak power, Mw	30	79	92	137	331	315
period, ms	515	304	267	205	96	96
Thermal Neutron Dose nvt by gold foil	0.56×10^{14}	0.48×10^{14}	0.56×10^{14}	0.50×10^{14}	0.76×10^{14}	0.70×10^{14}
Fission Energy Input cal/gram by Mo-99	-	-	216	-	-	-
Peak Metal Temp[b], C	~100	~1500	>970	>1500	>1500	>1500
Appearance of Metal after transient	not melted, no change	two large globules plus particles	one large fragment plus particles	fragments and particles	fine particles, some powder-like	lump plus fine particles, some powder-like
Percent Reaction of U	0.4	8.1	7.5	9.3	17.2	12.9

[a]The uranium wire was 93 percent enriched, all wires were submerged in water. The wires were 0.75 inch long.

[b]Peak pressure rise was 0 psi in Experiment 41 through 46

For a given reactor burst, there are two factors which are of importance with regard to the metal-water problem: the total energy of the transient and the reactor period. For these uranium wire tests, the burst energy (megawatt-seconds) was held as constant as possible and the reactor period (milliseconds) was progressively changed. In this manner the rate of change of energy input was varied. Figure 65 gives

FIGURE 65

IN-PILE URANIUM-WATER REACTIONS

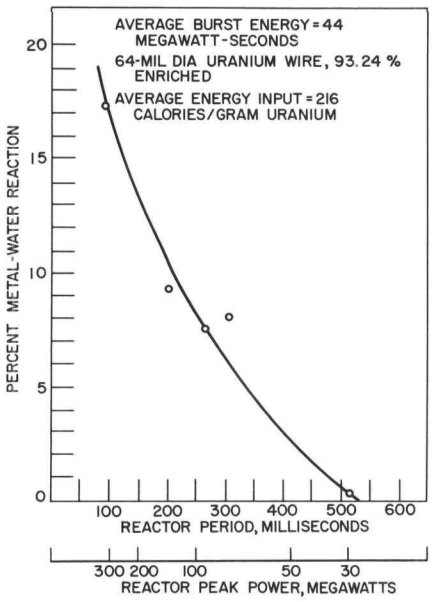

the correlation obtained for the single-wire runs; the result is attributed primarily to heat transfer characteristics. For a transient on a short period, the fission heat is added quickly, thus reducing heat losses and causing higher temperatures and more reaction. Conversely, a transient on a long period permits much heat loss, with lower temperatures, and hence less reaction.

One of the functions of the in-pile, metal-water work is to establish the changes in geometry that take place when the fuel specimen is subjected to a reactor burst of sufficient intensity to melt the metal partially or completely. For each of the runs with uranium wires, from 100 to 400 particles were counted and measured. The results in the form of size-frequency distribution plots are shown in Figures 66 through 69. From these distributions, it is evident that the largest number of particles occur in the size range of about 2 to 16 mils. However, when the Sauter mean diameter is computed, the large particles and globules exert a major influence, so that the mean surface to volume diameter is considerably larger than the geometric mean. These calculations are summarized in Table 56. The increase in the extent of reaction with the surface area change is shown in Figure 70. A photograph showing the change in geometry that took place for the three wire bundle is shown in Figure 71.

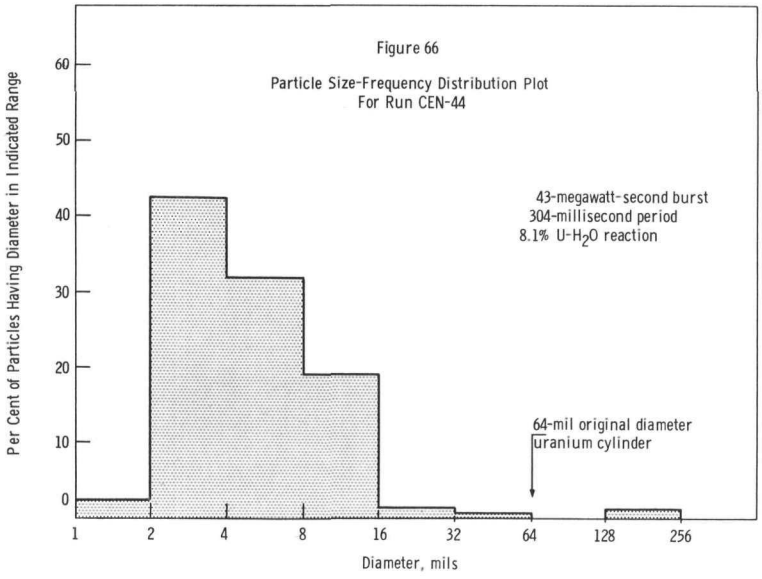

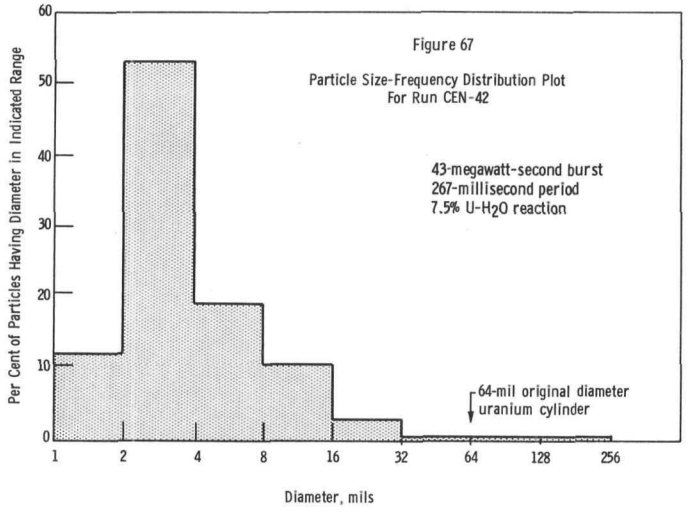
Figure 67
Particle Size-Frequency Distribution Plot
For Run CEN-42
43-megawatt-second burst
267-millisecond period
7.5% U-H2O reaction
64-mil original diameter
uranium cylinder
Per Cent of Particles Having Diameter in Indicated Range
Diameter, mils
0
10
20
30
40
50
60
1
2
4
8
16
32
64
128
256

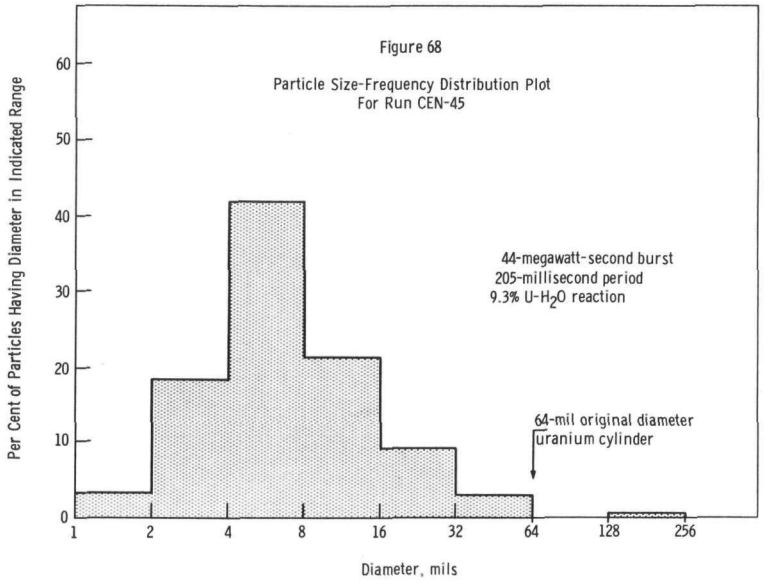
Figure 68
Particle Size-Frequency Distribution Plot
For Run CEN-45
44-megawatt-second burst
205-millisecond period
9.3% U-H2O reaction
64-mil original diameter
uranium cylinder
Per Cent of Particles Having Diameter in Indicated Range
Diameter, mils
0
10
20
30
40
50
60
1
2
4
8
16
32
64
128
256

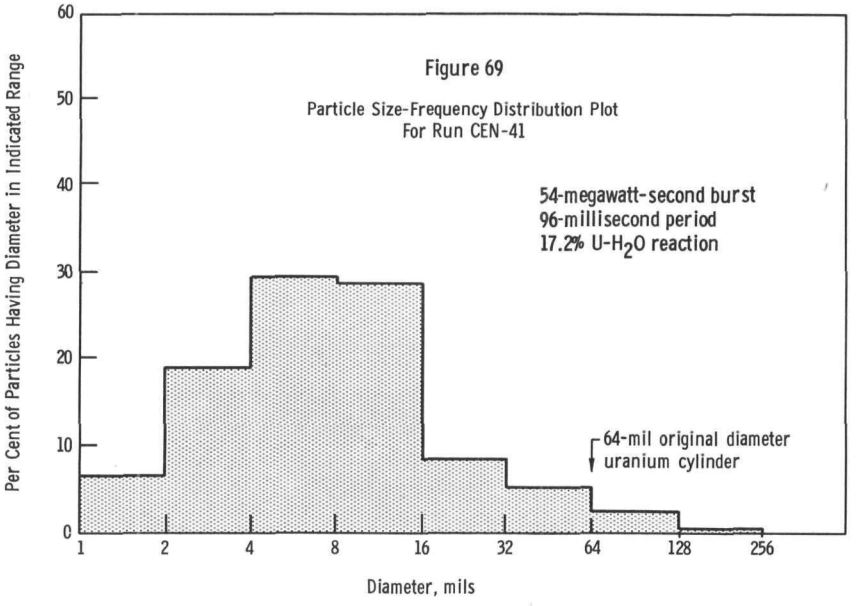
Figure 69
Particle Size-Frequency Distribution Plot
For Run CEN-41
54-megawatt-second burst
96-millisecond period
17.2% U-H2O reaction
64-mil original diameter
uranium cylinder
Per Cent of Particles Having Diameter in Indicated Range
Diameter, mils
0
10
20
30
40
50
60
1
2
4
8
16
32
64
128
256

Table 56

PARTICLE SIZE DATA FROM URANIUM WIRE-WATER TRANSIENTS

Original diameter of wire = 64 mils;
original specific surface area = 65 $\frac{\text{sq in.}}{\text{cu in.}}$

	CEN Transient Number				
	43	44	42	45	41
Wire melted	no	yes	yes	yes	yes
Reactor period, milliseconds	515	304	267	205	96
% U-H_2O reaction	0.4	8.1	7.5	9.3	17.2
dsv, diameter, mils	96[a]	78	32	33	17
A_s, specific surface area, $\frac{\text{sq. in.}}{\text{cu. in.}}$	65	77	188	182	353
A_r, area increase ratio	1.0	1.2	2.9	2.8	5.4

[a] Diameter of an equivalent sphere that has same surface to volume ratio as original wire

dsv = Sauter mean diameter = $\frac{6 \times \text{volume}}{\text{surface area}}$

$A_s = \frac{6}{\text{dsv}}$

$A_r = \frac{\text{specific surface area after transient}}{\text{specific surface area before transient}} = \frac{A_s}{A_0}$

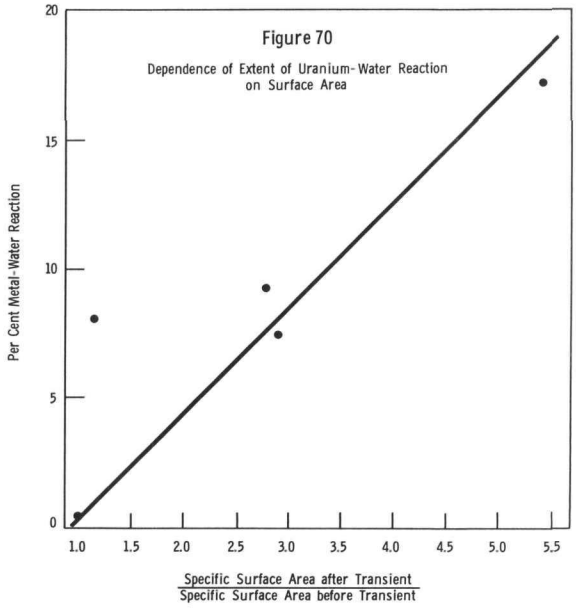

Figure 71

View of Uranium Wire Fuel Cluster before and after Metal-water Transient CEN-46

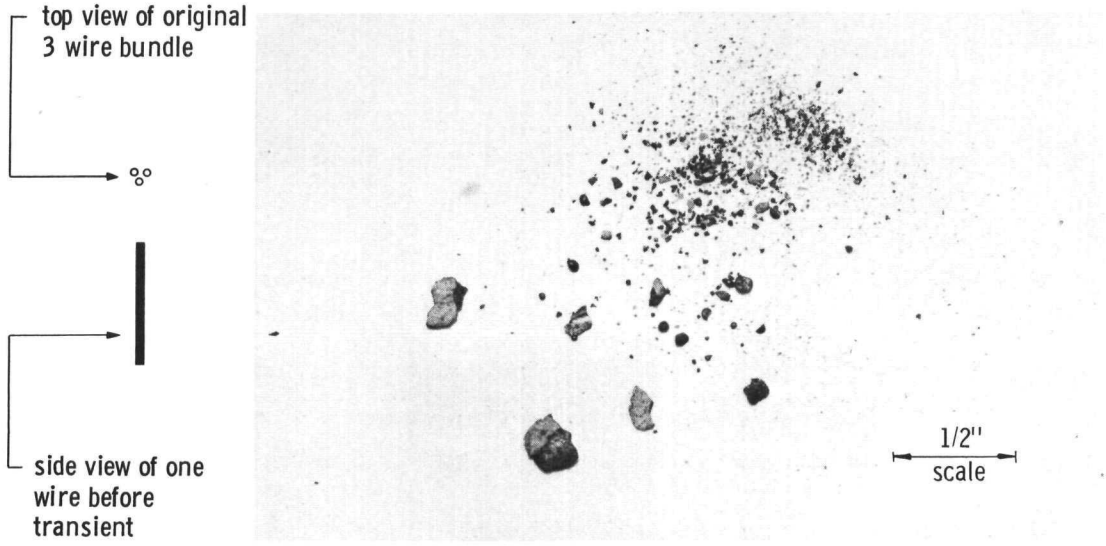

Consistent with the purpose of this program to simulate nuclear accidents closely, plans are in progress for extending the work to preirradiated fuel specimens and to water at high pressure. To date, two experiments have been conducted with a high-burnup uranium-zirconium alloy plate; however, the bursts were not energetic enough to achieve melting. These transients will be repeated at higher integrated powers. Some preliminary out-of-pile work has been done preparatory to conduction runs at elevated pressures. Consideration is also being given to testing multiplate fuel assemblies to approximate clusters present in actual reactor cores.

IV. REACTOR CHEMISTRY

The neutron capture cross sections of uranium-236 have been determined at neutron energies ranging from 0.36 to 1.73 Mev. The cross sections varied from 0.27 barn at 0.36 Mev to <0.1 barn at 1.73 Mev, going through a maximum of 0.32 barn at 0.97 Mev and a minimum of 0.25 barn at 0.47 Mev. Work has begun on the determination of the fast neutron capture cross sections of neptunium-237 for monoenergetic neutrons in the range from 0.4 to 1.7 Mev.

The Reactor Decontamination Program has two principal objectives: 1) to determine experimentally in pilot-plant equipment the degree of contamination to be expected in the steam phases of a boiling water reactor system in the event of fuel cladding failure, and 2) to find suitable methods of removing deposited activity from internal surfaces, should it be necessary because of excessive radiation levels. The pilot-plant equipment used for the first objective consists of a stainless steel type 304 loop that simulates the action of a boiling water reactor. Fuel ruptures are simulated by inserting tracer activities or irradiated metallic uranium. In a parallel effort, studies are being made in the laboratory to find suitable means of removing deposited activities.

In laboratory studies, scouting experiments indicated that oxalic or dilute sulfuric acids in conjunction with hydrogen peroxide have promising decontamination capabilities for stainless steel type 304 surfaces. Modifications of the second step of the alkaline permanganate-citrate decontamination procedure to reduce the corrosiveness on low alloy steels did not impair the ability to decontaminate stainless steel. The modifications consisted of upward pH adjustments or the addition of inhibitors. Citric acid alone was not very effective as a decontaminant; peroxide additions improved the results obtained. The addition of Delchem 2128A as a third step in conjunction with the alkaline permanganate-citrate procedure yielded somewhat improved decontamination over the conventional two-step procedure.

Two series of reproducibility runs were made with the stainless steel type 304 pilot plant loop. In the first series of three runs, stainless steel type 304 sample strips were used, whereas SAE type 1018 mild steel strips were used in the second. Results are not yet available.

A. Determination of Nuclear Constants
(C. E. Crouthamel)

1. Fast Neutron Cross Sections
(D. C. Stupegia, E. Dewell, and G. H. McCloud)

Uranium-236

Fast neutron capture cross sections have been determined for uranium-236 as a function of neutron energy. This nuclide is a product which accumulates in uranium-fueled reactors by the neutron capture of uranium-235. Its nuclear properties are therefore useful in various reactor calculations. The values obtained are plotted in Figure 72. The errors quoted are standard deviations. A report of this work has been submitted for publication in the Journal of Nuclear Energy.

FIGURE 72
NEUTRON CAPTURE CROSS SECTION OF URANIUM 236
AS A FUNCTION OF NEUTRON ENERGY

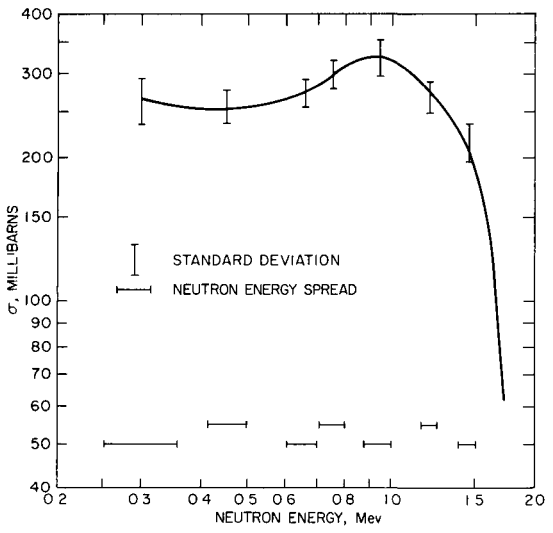

Neptunium-237

Work has begun on the determination of the fast neutron capture cross sections of neptunium-237 for monoenergetic neutrons. This is a buildup product in reactors by way of the neutron capture of uranium-236 and the (n,2n) reaction of uranium-238. The neutron source is the reaction $Li(p,n)Be^7$, using protons from the Van de Graaff accelerator. The neutron energy range available extends between about 0.4 and 1.7 Mev. The cross sections will be determined by measuring the absolute activity of neptunium-238 produced in a known mass of neptunium-237 by a known flux of neutrons. Approximately 1 gram of neptunium-237 is available for this work. The absolute activity of the 2.1-day beta and gamma emitter, neptunium-238, will be determined by 4π beta counting, and the gamma-ray scintillation spectrometer will be calibrated against this assay. Neutron flux will be measured using a fission chamber, which counts fissions in a thin sample of enriched uranium.

2. Capture and Fission in EBR-I, Mark III
(C. E. Crouthamel and R. R. Heinrich)

Samples of uranium-233, uranium-235, uranium-238, plutonium-239, and plutonium-240 have been irradiated in the fast breeder reactor EBR-I, Mark III, for a total of 800,000 kilowatt-hours. Ten core

and blanket rods containing 56 samples and the outer blanket brick containing 6 samples have arrived from the Idaho site. Scheduling for the removal of samples from the rods and brick has been completed with the Remote Control Division and removal should commence in approximately three weeks.

B. Reactor Decontamination
(W. B. Seefeldt)

1. Laboratory Investigations
(S. Vogler, H. Tyler)

The principal objective of the laboratory investigations is to study and modify existing decontaminations or film removal procedures that have been developed by either industry or other AEC contractors. In general, developed procedures are applicable to the primary circuits of pressurized water reactors, and modifications are directed toward use in the vapor spaces of boiling water reactors.

Current laboratory work has been concerned with the investigation of several new solutions as decontaminating reagents and the effect of modification of the alkaline permanganate-citrate procedure on the decontamination obtained. The new reagents are solutions of oxalic acid and hydrogen peroxide and a proprietary material developed industrially. The oxalic acid-hydrogen peroxide reagent-based decontamination procedure is under study at Oak Ridge National Laboratory for potential application in the Gas Cooled Reactor. The alkaline permanganate method is under development at Westinghouse-Bettis and Hanford.

a. Scouting Experiments

The decontamination experiments were performed with samples of stainless steel type 304 from a loop run. Samples were used from both the vapor and liquid portions of the loop. The experiments were performed by placing the contaminated metal ($\frac{1}{2}$ inch x $\frac{1}{2}$ inch) in the indicated solution (see Table 57) for a given period of time. The solution was stirred by means of a plastic-coated stirring bar and a commercial magnetic stirring unit. The results are summarized in Table 57. The data indicate good decontamination results for oxalic acid containing hydrogen peroxide, and for dilute sulfuric acid containing both hydrogen peroxide and fluoride ion. These preliminary data require further corroboration. It will also be necessary to evaluate the corrosion resistance of typical reactor materials of construction to these reagents.

Table 57

DECONTAMINATION OF STAINLESS STEEL TYPE 304

Activity Level: Vapor Samples ~5 x 10^3 cpm
Liquid Samples ~10^5 cpm

Reagent	Temperature (C)	Time (hr)	Decontamination Factor	
			Liquid	Vapor
3 M HNO_3	~100	1	6	24
0.5% $KMnO_4$, 1% NaOH } Step 1	~25	4	9	44
10% ammonium citrate } Step 2	85	0.25		
0.25 M Na_2CO_3, 0.25 M $NaHCO_3$, 0.5 M H_2O_2	75	1	3	2
0.5 M $Na_2C_2O_4$, 0.5 M H_2O_2	75	1	6	9
0.3 N H_2SO_4	95	0.5		27
0.3 N H_2SO_4, 1 M H_2O_2	95	0.5		33
0.3 N H_2SO_4, 1 M H_2O_2, 0.12 M NaF	95	0.5		>200
0.16 M $H_2C_2O_4$, 1 M H_2O_2	95	0.5		>200

b. Modifications of the Alkaline Permanganate-Citrate Procedure

The unmodified two-step alkaline permanganate-citrate procedure for decontamination of metallic surfaces consists of the application of a sodium hydroxide-potassium permanganate reagent followed by either ammonium citrate or citric acid. Corrosion experiments indicated that 10 percent citric acid or ammonium citrate at normal acidity (pH 4.8) was corrosive to 1 percent chromium-0.5 percent molybdenum-iron alloy. This alloy is a material of construction in the Experimental Boiling Water Reactor and is considered reasonably typical of low alloy steels used in other reactors. These tests indicated that by either raising the pH of the citrate solution or using corrosion inhibitors a decrease of the corrosion rate to an acceptable level resulted. The effect of these changes in the procedure was noted by measuring the decontamination of loop-produced stainless steel samples from the vapor section of the loop. The data assembled in Table 58 indicate no detrimental effects on decontamination of raising the pH of the citrate solution or adding the indicated corrosion inhibitor.

Table 58

DECONTAMINATION OF STAINLESS STEEL TYPE 304 BY THE ALKALINE PERMANGANATE-CITRATE PROCEDURE

Samples: Stainless Steel from Loop Vapor Space

Sample Activity: $\sim 1 \times 10^4$ gamma cpm

First Decontamination Step: 0.5 percent potassium permanganate and 1.0 percent sodium hydroxide for 4 hours at 25 C.

Second Decontamination Step: 85 C with the indicated reagents, first for a 15-minute exposure and then a 45-minute exposure.

Reagent	Decontamination Factor	
	15 Minutes	1 Hour
10% ammonium citrate	17	34
10% sodium citrate (pH 10)	34	50
10% ammonium citrate $1\frac{1}{4}$% Rhodine 130	50	100
10% sodium citrate $1\frac{1}{4}$% Rhodine 130	33	33

Examination of the residual activity indicated that slight amounts of zirconium were present in most specimens. Occasionally ruthenium was identified.

c. Citric Acid as Decontaminating Reagent

Several experiments were performed to determine the efficiency of citric acid alone as a decontaminating reagent. The solutions used and the decontaminations obtained are indicated in Table 59. These preliminary results indicate that citric acid alone was not an exceptional decontaminating reagent. A marked improvement in the decontamination was observed upon the addition of hydrogen peroxide.

Table 59

DECONTAMINATION OF STAINLESS STEEL
TYPE 304 WITH CITRIC ACID

Samples: Stainless Steel type 304 from Loop Vapor Space

Activity: $\sim 5 \times 10^3$ cpm

Time: 1 Hour

Temperature: 85 C

Reagent	Decontamination Factor
10% citric acid	8
10% citric acid 3% H_2O_2	41
10% sodium citrate (pH 10) $1\frac{1}{4}$% Rhodine 130	10

d. Evaluation of Delchem 2128A*

Delchem 2128A is a newly developed and released proprietary material for decontamination of stainless steel surfaces. A procedure was tested to determine its suitability for use in boiling water reactors. The suggested procedure called for the following sequence of reagents: Delchem 2128A at 126 C for one hour, alkaline permanganate at 90 C for one hour, and finally 25 percent nitric acid at room temperature for one-half hour. Water rinses were used between reagents. With a loop contaminated stainless steel type 304 sample, a decontamination factor of 360 was obtained. When the test was repeated minus the proprietary reagent a decontamination factor of 110 was obtained. In a third test similar to the second, substitution of ammonium citrate at 85 C for the nitric acid produced a decontamination factor of 90. A final test consisting of the proprietary solution at 126 C followed by nitric acid at room temperature yielded a decontamination factor of 13.

These results indicated that the proprietary solution yielded a slight increase in metal decontamination when used in conjunction with alkaline permanganate, but when used without alkaline permanganate the proprietary solution showed no increase in metal decontamination.

* Proprietary compound manufactured by Pennsylvania Salt Manufacturing Company.

2. Loop Studies
(D. Grosvenor, C. Bally)

A stainless steel type 304 loop which simulates the action of a boiling water reactor has been installed in a shielded cell in order to study the effects of fuel ruptures. It is of interest to know the amount and the kinds of fission products that will be distributed through the system in order to ascertain the degree to which maintenance might be impaired in a practical system should fuel cladding failure occur.

Fuel ruptures are simulated in the loop by introducing irradiated metallic uranium. Fission products are released by the uranium as it corrodes in the circulating water. Deposition of activity in the steam disengaging space is monitored by inserting a metallic sample strip into the loop; this is removed following a run, cut into convenient lengths, and counted in a 256-channel gamma scintillation spectrometer. This is correlated with similar information obtained from liquid and condensed steam samples.

Loop runs previously reported have been made with stainless steel sample strips at an operating pressure of 200 psi, and steam velocities of 0.8 ft/sec. Both tracer and mixed fission product activities have been used. Current efforts are directed at determining the reproducibility of data obtained from the loop. A series of three runs (Runs U3B, U3C, U3D) was made under identical conditions: (1) stainless steel type 304 sample strip, (2) 200 psi pressure, (3) 0.8 ft/sec steam velocity, (4) liquid level of 17 to 20 inches above reference, and (5) run time of 68 hours. Irradiated uranium was the source of fission product activity. A fresh sample strip was placed in the loop for every 68-hour experiment. Results are not yet available.

A second series of two runs (U3E and U3F) was made in which operating conditions were identical to those above except for the substitution of mild steel sample strips (SAE 1018) for the stainless steel. Results from these experiments are also unavailable.

V. ROUTINE OPERATIONS
(H. G. Swope)

A. Waste Processing
(H. G. Swope, J. Harast, K. Bremer, B. Kullen and R. Jarrett)

The total volume of liquid radioactive wastes processed from October 1 through December 31, 1960 was 20,659 gallons. The methods used and volumes of each were as follows:

Process	Gallons
Evaporation and Concentration	20,130
Neutralization of HF Wastes	325
Absorption on Vermiculite	204
Total	20,659

A summary of the amount of wastes processed in 1960 by various methods is shown in Table 60.

Table 60

SUMMARY OF LIQUID RADIOACTIVE WASTES PROCESSED DURING THE YEAR 1960

Gallons of Waste Treated as Shown

1960 Quarterly Period	Struthers-Wells Evaporator									30-Gallon Concentrator			Ion-Exchange Cation (HCR-H+) RT	Filtration	Flocculation	Absorption on Vermiculite	HF Wastes Neutralized	Decay	Totals
	Retention Tanks	Decon Soln	Misc Aqueous	GIF Pool Water[a]	Cim-Cool	Floc	D-34 Sludge	Regen Soln	Adams Filter Cake	Evap Bottoms	Misc Aq	Misc Org							
Jan - Mar	2,320	10,210	1,226	700	2,100	-	1,320	-	890	953	-	440	1 900	2 800	1 640	75	110	-	26,684
Apr - June	2,320	10,120	1,536	260	935	510	4,805	-	1,275	1,638	-	242	400	7,220	1,360	446	-	4,680	37,747
July - Sept	1,540	7,875	1,025	360	1,290	-	2 630	2,860	2,013	1,373	-	1,108	4,240	4,240	-	756	105	-	31 415
Oct - Dec	500	8,547	1,811	300	1,345	-	2,980	2,180	1,049	1,387	31	-	-	-	-	204	325	-	20,659
Totals	6,680	36,752	5,598	1,620	5,670	510	11,735	5,040	5,227	5,351	31	1 790	6 540	14,260	3,000	1,481	540	4,680	116,505

[a] Includes water from fuel rod carrier.

Abbreviations
GIF = High-level Gamma-irradiation Facility
RT = Retention Tanks
HF = Hydrofluoric acid wastes
EBWR = Experimental Boiling Water Reactor Wastes

B. High-level Gamma-irradiation Facility
(H. G. Swope, J. Harast, N. Ondracek, R. Juvinall, G. Teats and V. Lemke)

The year 1960 was the fifth full year of operation of the Argonne High-level Gamma-irradiation Facility. Table 61 summarizes 1960 work in Rack M-1. There were 9,300 samples (equivalent to a No. 2 sized can) irradiated in calendar year 1960 as compared to 8109 in 1959; day units were 17,063 and 13,787, and total night units were 28,203 and 29,351 in 1960 and 1959, respectively. In addition 4,134 special dosimetry samples were run during the year.

Table 61

ARGONNE HIGH-LEVEL GAMMA IRRADIATION FACILITY

Summary of Irradiations Performed in Rack M 1 During 1960

1960	No of Samples[a]				Total Day Units in Rads[b]				Total Night Units in Rads[b]			
	QMC	Industry	Educ Inst	ANL	QMC	Industry	Educ Inst	ANL	QMC	Industry	Educ Inst	ANL
January	455	0	40	18	613	0	30	158	21	0	0	1 700
February	694	13	0	13	977	13	0	120	0	77	0	2 088
March	1 223	6	0	46	1 855	11	0	506	192	3	0	2 651
April	557	0	80	41	899	0	73	339	0	0	0	2 119
May	1 027	0	10	30	1 575	0	7	276	0	0	134	1 738
June	929	28	24	34	1 080	24	12	604	29	181	0	2 991
July	462	39	7	51	630	71	14	525	87	581	73	2 811
August	796	21	203	41	1 175	12	286	212	219	0	0	1 873
September	886	72	0	25	1 186	77	0	349	0	431	0	2 036
October	303	29	0	24	484	80	0	373	0	1 100	0	1 466
November	561	27	2	26	858	54	7	414	78	431	0	1 062
December	408	9	16	24	581	20	32	351	8	256	0	1 767
Totals	8 301	244	382	373	11 913	362	461	4 327	634	3 060	207	24 302

[a]Equivalent to a No 2 sized can (3 7/16-in diameter x 4 9/16 in high)

[b]Includes loadings and reimmersions One unit 2×10^6 rad

In addition to the work done in Rack M-1, a second rack, M-2 (20-inch circular rack), was occasionally used.